

APPLICATIONS OF NANOPARTICLES IN WATER TREATMENT: REACTION KINETICS AND PATHWAYS

A THESIS SUBMITTED TO



**VISVESVARAYA TECHNOLOGICAL UNIVERSITY,
BELAGAVI**

For the award of the degree of

Doctor of Philosophy in General Science

(CHEMISTRY)

By

RAMESH S.MALLADI

(USN: 2GI10PGM02) M.Sc.



Research Guide

Dr. RAVIRAJ M. KULKARNI

Professor and Head,
Department of Chemistry

K.L.S Gogte Institute of Technology,
Udyambag, BELAGAVI- 590008, Karnataka, INDIA

JUNE 2017

**Karnatak Law Society's,
GOGTE INSTITUTE OF TECHNOLOGY,
Udyambag, BELAGAVI-590 008, Karnataka, India.
DEPARTMENT OF CHEMISTRY**

CERTIFICATE

This is to certify that **Shri. Ramesh S. Malladi** has worked under my supervision for his doctoral thesis titled, **“Applications of nanoparticles in water treatment: Reaction kinetics and pathways”**. I also certify that the work is original and has not been submitted to any other University wholly or in part for any other degree.

Dr. Raviraj M. Kulkarni
Research Supervisor
Professor and Head
Department of Chemistry,
KLS Gogte Institute of Technology,
Udyambag, Belagavi-590 008
Karnataka, India.

Karnatak Law Society's,
GOGTE INSTITUTE OF TECHNOLOGY,
Udyambag, BELAGAVI-590 008, Karnataka, India.
DEPARTMENT OF CHEMISTRY

DECLARATION

I hereby declare that the entire work embodied in this doctoral thesis has been carried out by me at **Research Center, Department of Chemistry, KLS Gogte Institute of Technology, Belagavi** under the supervision of **Dr. Raviraj M. Kulkarni, Professor and Head, Department of Chemistry, KLS Gogte Institute of Technology, Belagavi.** This thesis has not been submitted in part or full for the award of any diploma or degree of this or any other University.

Ramesh S. Malladi
Research Scholar
Department of Chemistry,
KLS Gogte Institute of Technology,
Udyambag, Belagavi-590 008
Karnataka, India.

ACKNOWLEDGMENTS

I humbly seek the blessings of his Holiness Shri Siddeshwar swamiji, Mallikarjun ashram, Vijayapur.

There are no words to express my deep sense of gratitude to my supervisor and Head of Chemistry Department, Dr. Raviraj M. Kulkarni for his persistent guidance, scholarly suggestions and constant encouragement throughout the period of my study which enabled me to complete this work. He has greatly enriched my knowledge with valuable suggestions and continuous encouragement and had spared valuable hours to supervise this thesis.

I am grateful to Dr. A. S. Deshpande, Principal, K.L.S Gogte Institute of Technology, Belagavi for his inspiration and kind permission to make use of college facilities. I thank the Members of Karnataka Law Society for their support in my endeavor.

I would like to express my sincere thanks to Honorable President Dr. M.B. Patil and Esteemed Board of Management, B.L.D.E. Association vijayapur, Karnataka and also to the Principal Dr. V. P. Huggi. I would like to express my gratitude to my H.O.D. Dr. Swastika N. Das and my colleagues of B.L.D.E.A's C.E.T. Vijayapur for extending their kind co-operation during the span of my research work.

I find words inadequate in offering my thanks to Dr. M. S. Hanagadakar, Mr. V. S. Bhamare, Dr. S. V. Divekar. Dr. K. A. Thabaj, Dr. S. A. Malladi, J. M. Karekar, and to whom I am deeply grateful for their constant cooperation, I would like to thank all non-teaching staff of department for their support.

I feel it a privilege to express my sincere thanks to Mrs. Deepti R. Kulkarni for their encouragement and moral support during my research work.

This research work would not have been completed successfully without my parent's blessings of Mrs. Hubai S. Malladi. And wishes of my brother Rajashekhhar S. Malladi. I am indeed indebted to my wife Preeti R. Malladi and my daughter Khushi R. Malladi their immense cooperation at all levels with moral and social support, due to which I could accomplish this research work.

Ramesh S. Malladi

Dedicated to my mother

Mrs. Hubai S. Malladi

&

My wife

Preeti R. Malladi

& my daughter

Khushi R. Malladi

ABSTRACT

A wide variety of organic contaminants have been detected in the aquatic environment, which are discharged through municipal waste-water, industrial effluents, commercial operations, runoff from agricultural lands, chemical spills etc. The conventional water treatment methods, such as, coagulation, flocculation, adsorption biological treatment techniques and chlorination etc. have not been able to get rid of these persistent organic contaminants from the environment. However, these techniques may produce potentially harmful by-products during the water treatment process. Hence, advanced oxidation process is considered to be best method for treatment of recalcitrant organic contaminants present in waste-water, industrial effluent etc. using semiconductor as photocatalyst to completely degrade toxic organic contaminant to CO₂ and H₂O.

Kinetic investigations related to water treatment are drawing much attention in the recent years, as they provide insight into the detailed reaction mechanisms. The transformation of organic contaminants will not take place if the reaction is slow with the oxidants used in the process, on the other hand, if reaction is fast then the transformation or degradation of the organic contaminant takes place. Therefore, it becomes necessary for researchers to understand the factors controlling the rates.

In the proposed research, we intend to study degradation kinetics and mechanism of some of the reactions involving organic contaminants using advanced oxidation processes. Advanced oxidation processes (AOPs) have been successfully employed for the degradation of many hazardous organic contaminants in aqueous environment with some acceptable levels, without generating harmful by-products. AOPs depend on in-situ generation of reactive hydroxyl radicals (OH[·]) using light or chemical energy. The so formed OH[·] radicals are used to decompose indiscriminately a variety of organic contaminants present in water and waste waters. The AOP process involves a semiconductor stimulated by UV or visible light to destruction of environmental contaminants is called photo catalysis which results in complete or partial demineralization of the organic molecules.

Titanium dioxide (TiO₂) is an excellent metal oxide semiconductor photocatalyst, due to its chemical and thermal stability and it is relatively inexpensive, biocompatible and non toxic. It is characterized by a band gap ranging from 3 to 3.2 eV, which allows UV light to pump the electrons from the valence bond to conduction band leading to the formation of electron hole pair. Thus generated electron-hole pair facilitates the formation

of OH[•] radicals leading to the degradation of organic contaminants. The high rate of electron-hole recombination in TiO₂, however, limits the efficiency of the photo catalyst, which can be prevented, to some extent, by doping with noble metals such as silver, ruthenium, copper, gold, platinum etc.

In order to improve the efficacy of photocatalyst and inhibit the electron-hole recombination metal oxide semiconductors are doped with rare earth metals. Metal oxides and metal doped metal oxides have been used for the degradation of many organic contaminants. In the present thesis we report synthesis and characterization of doped and undoped metal oxide semiconductors and their application in the photocatalytic degradation of some organic contaminants.

Chapter 1: General Introduction

This chapter gives general introduction about advanced oxidation processes (AOP's), methods of synthesis of metal oxide nanoparticles, mechanism of photosensitization of TiO₂ under UV, photocatalytic degradation and literature of various types of toxic contaminants present in water and waste water, have been summarized in this chapter.

Chapter 2: The photocatalytic activity of silver doped TiO₂ (Ag-TiO₂) nanoparticles was studied by photocatalytic degradation of lomefloxacin (LMF) using a photo-reactor with a mercury lamp (PHILIPS, TUV 8W T5, E_{max} =254 nm). The 1% and 2% Silver doped TiO₂ nanoparticles were synthesized by Liquid Impregnation (LI) method. The resulting nanoparticles were characterized by surface analytical methods such as X-ray diffraction (XRD), scanning electron micrographs (SEM), Energy dispersive X-ray Analysis (EDX) and Transmission Electron Microscopy (TEM). The study shows 2% Ag-TiO₂ nanoparticles exhibited better results (95% degradation) in 1 hour for the degradation of lomefloxacin compared to 1% Ag-TiO₂ and pure TiO₂. XRD analysis indicated that the crystallite size of TiO₂ was 17.00 nm, while the crystallite size of 1% Ag-TiO₂ and 2% Ag-TiO₂ was 13.07 nm to 14.17 nm. TEM images show the particle size of Ag-TiO₂ nanoparticles were in the range 40.00-45.00 nm in length and 10.00-15.00 nm in breadth. Pseudo-first order rate constants were found to decrease with increase in pH. The effect of UV intensity, catalyst dosage and initial concentration of LMF on the degradation rate were also studied and elaborately discussed.

Chapter 3: Ruthenium doped Titanium dioxide (Ru-TiO₂) nanoparticles were investigated as photo-catalyst in the photo-catalytic degradation of a common dye

bromothymol blue (BTB) in an aqueous suspension using UVC (254 nm) for a pH range of 4.0 to 8.0. The liquid impregnation method was used to synthesize 0.2%, 0.4% and 0.8% ruthenium doped TiO₂ (Ru-TiO₂) nanoparticles. The prepared nanoparticles framework substitution of Ru in TiO₂ were done using X-ray powder diffraction (XRD), Scanning Electron Microscopy equipped with energy dispersive X-ray (SEM-EDX), Fourier Transform Infrared Spectroscopy (FTIR), Transmission Electron Microscopy (TEM), Diffuse Reflectance Spectra analysis. The average crystallite sizes of doped and undoped nanoparticles were calculated from X-ray diffraction spectra using Scherrer equation. The average crystallite size of anatase phase of undoped TiO₂ was found to be 17.00 nm, whereas the crystallite sizes of 0.2%, 0.4% and 0.8% Ru-TiO₂ were 16.67 nm, 15.70 nm and 14.40 nm respectively. The TEM images confirm the particle sizes to be 10.00 to 40.00 nm. The band gap of 0.2, 0.4 and 0.8% Ru-TiO₂ was found to be 3.10, 3.04 and 2.96 eV respectively. Pseudo-first order rate constants (k_{obs}) determined were found to increase with decrease in pH. The effect of BTB Initial concentration, catalyst loading, a percentage of doping of photo catalyst, pH and UV light intensity of BTB on the degradation rate were also discussed.

Chapter 4: Pure and 5% barium doped zinc oxide nano-particles were synthesized by inexpensive chemical precipitation method. The prepared nano-particles were characterized by X-ray powder diffraction (XRD), Energy Dispersive X-ray Spectroscopy (EDX), scanning electron microscope (SEM), Ultraviolet-visible absorption spectroscopy and Transmission electron microscope (TEM) analysis. Scherrer equation was used to calculate the particle size of the prepared doped and un-doped nano-particles. The photocatalytic action of 5% barium doped zinc oxide is checked with photo-degradation of chloramphenicol (CLP) under UVC (254 nm) irradiation in aqueous suspension. Pseudo-first order rate constants (k_{obs}) were found to increase with decrease in pH. The effect of initial concentration, catalyst loading, light intensity, the effect of pH on the degradation rate were also studied and elaborately discussed. The results shows barium doped zinc oxide is more potential than un-doped zinc oxide. The HPLC and LC/MS were used to identify degradation products.

Chapter 5: The efficacy of color removal from aqueous methyl orange (M.O.) solution has been studied in presence of synthesized copper doped zinc oxide nanocrystals, irradiated with UV-C light. Simple non expensive chemical precipitation method was used to synthesis zinc oxide and 2% Cu-ZnO nanoparticles. Phase composition of Cu doped ZnO was examined by X-ray Diffraction powder technique (XRD), scanning

electron Microscopy equipped with Energy Dispersive X-ray (SEM-EDX) and UV-visible spectrophotometer. The degradation kinetics was studied under different conditions such as pH, catalyst concentration, substrate concentration, intensity of light etc.

Chapter 6: The photocatalytic degradation of sparfloxacin under UV-C (254 nm) using silver doped Titania first time investigated at pH 4.0 to 9.0. The simple Liquid impregnation method is used to prepare Ag-TiO₂ nanoparticles. In order to analyze their structural, optical, electronic and morphological characteristics. The synthesized nanoparticles were analysed by X-ray diffraction, (XRD). From the XRD data, the lattice parameters namely mean crystallite size, phase identification is done. The morphological characterization was done by SEM and TEM by analyzing the images in detail. EDAX analysis was done along with SEM to confirm the composition of the nanomaterials. Pseudo-first order rate constants were found to decrease with increase in pH. The effect of UV light intensity, catalyst loading and initial concentration of sparfloxacin on the degradation rate were also studied and reported.

Chapter 7: The un-catalyzed and Pd²⁺catalyzed oxidation of Lomefloxacin (LMF) with permanganate in acidic medium was examined. The oxidation product was identified by Agilent 6130 Series Quadrupole LC/MS. The reaction exhibit be 2:1 stichiometry, that is, 2 mol manganese (VII) reacted with 1 mol of lomefloxacin. Orders with respect to [LMF], [H⁺] and [Pd²⁺] were found to be fractional and less than unity. The oxidation reaction proceeds formation of complex with Pd²⁺ via a permanganic acid species, that forms an intermediate complex with lomefloxacin and then complex decomposes to give the final product. The rate of reaction was found to decrease with decrease in the dielectric constant. The effect of temperature on the rate of the reaction was studied at different temperatures and rate constants were found to increase with increase in temperature and the thermodynamic activation parameters with respect to slow step of the mechanism (E_a , ΔH^\ddagger , ΔS^\ddagger and ΔG^\ddagger)

List of Publications and Presentations by the candidate Mr. Ramesh S. Malladi
(USN: 2GI10PGM02)

Journal Publications:

1. “*Ag-TiO₂ nanoparticles for photocatalytic degradation of lomefloxacin*”, Raviraj M. Kulkarni, **Ramesh S. Malladi**, Manjunath S. Hanagadakar, Mrityunjay R. Doddamani, Udaya K. Bhat, *Desalination and water treatment*. Vol. 57 (34), **2016**, pp. 16111-16118.
2. “*Ru-TiO₂ Semiconducting Nanoparticles for the Photocatalytic Degradation of Bromothymol blue*” Raviraj M. Kulkarni, **Ramesh S. Malladi**, Manjunath S. Hanagadakar, Mrityunjay R. Doddamani, Santhakumari, Sanjay. D. Kulkarni, *Journal of Materials Science: Materials in Electronics*. Vol. 27, **2016**, pp. 13065–13074.
3. “*Ba-ZnO nano particles for photocatalytic degradation of Chloramphenicol*”, Raviraj M. Kulkarni, **Ramesh S. Malladi**, Manjunath S. Hanagadakar, Mrityunjay R. Doddamani, Udaya K. Bhat, *Environmental Chemistry Letters*. (2017) (communicated).
4. “*Cu-ZnO nanoparticles for photocatalytic degradation of methyl orange*” Raviraj M. Kulkarni, **Ramesh S. Malladi**, Manjunath S. Hanagadakar, *Advanced Materials Proceedings*, (2017) (communicated).
5. “*Ag-TiO₂ nanoparticles for photocatalytic degradation of sparfloxacin*”, Raviraj M. Kulkarni, **Ramesh S. Malladi**, Manjunath S. Hanagadakar, Mrityunjay R. Doddamani, Udaya K. Bhat, *Advanced Materials Proceedings*. (2017) (To be communicated).
6. “*Kinetics and Mechanism of Uncatalysed and Palladium (II)-Catalysed Oxidation of Lomefloxacin by Permanganate in Acidic Medium*”, Raviraj M. Kulkarni, **Ramesh S. Malladi**, Manjunath S. Hanagadakar, *Desalination and water treatment*. (2017) (communicated).
7. “*Transformation of Levofloxacin during Chlorination process: Kinetics and pathways*”, Mahadev S. Gudaganatti, Manjunath S. Hanagadakar, Raviraj M. Kulkarni, **Ramesh S. Malladi** and Rajaram K. Nagarale, *Progress in Reaction Kinetics and Mechanism*. Vol. 37, **2012**, pp. 366–382.
8. “*Silver (I) catalyzed and uncatalyzed oxidation of levofloxacin with aqueous chlorine: A comparative kinetic and mechanistic approach*” Raviraj M. Kulkarni,

- Manjunath S. Hanagadakar and **Ramesh S. Malladi**, Asian Journal Research in Chemistry. Vol. 6 (12), **2013**, pp. 1124-1132.
9. “Transformation of Linezolid during water treatment with chlorine-A kinetic study” Raviraj M Kulkarni, Manjunath S Hanagadakar, **Ramesh S Malladi**, Mahadev S Gudaganatti, Himansu S Biswal and Sharanappa T Nandibewoor, Indian Journal of Chemical Technology. Vol. 21, **2014**, pp. 38-43.
 10. “Experimental and theoretical studies on the oxidation of lomefloxacin by alkaline permanganate” Raviraj M. Kulkarni, Manjunath S. Hanagadakar, **Ramesh S. Malladi**, Sanjaykumar V. Divekar, Himansu S. Biswal, Eduardo M. Cuerda-Correa, Desalination and Water Treatment. Vol. 57, **2016**, pp. 10826-10838.
 11. “Oxidation of linezolid by permanganate in acidic medium: Pd (II) catalysis, kinetics and pathways”, Raviraj M. Kulkarni, Manjunath S. Hanagadakar, **Ramesh S. Malladi**, B. Santhakumari, Sharanappa T. Nandibewoor. Progress in Reaction Kinetics and Mechanism. Vol. 41(3), **2016**, 245-257.
 12. “Ag (I) catalyzed chlorination of linezolid during water treatment: Kinetics, mechanism”, Raviraj M. Kulkarni, Manjunath S. Hanagadakar, **Ramesh S. Malladi**. Journal of Environmental Chemical Engineering. (**2017**) (**communicated**)

Paper presentations in International Conferences:

1. Presented a research paper entitled “Photocatalytic Degradation of Bromothymol blue with doped Ru-TiO₂ nano particles: Kinetics and Mechanism” in Second International Conference on Advanced Oxidation Processes on October 5-8th, **Kottayam, Kerala, India, 2012**.
2. Presented a research paper entitled “Photocatalytic Decolorization of Bromothymol blue with doped Ag-TiO₂ nano particles: Kinetics and Mechanism”, in “International conference on emerging innovative technologies for a sustainable world – 2013 (ICEITSW-2013)”. Organized by Shridevi Institute of Technology, **Tumkur, Karnataka**. (India) held on 7th and 8th October 2013.
3. A research paper “Photocatalytic Degradation of sparfloxacin using Silver doped Titania” presented in “International conference on nanomaterials and nanotechnology”. Organized by International Association of Advanced Materials (IAAM) in collaboration with VBRI Press AB, Sweden during 01 - 03 March, 2017 at Vinoba Bhave Research Institute, **Allahabad, India**.

Paper presentations in National Conferences:

1. Presented a research paper entitled "*Photocatalytic Degradation of lomefloxacin using Ag-TiO₂ nano particles*" in 31st Annual conference of Indian Council of Chemists held at Department of Chemistry, **Sourashtra University, Rajkot, Gujarat**, on 26th -28th December, **2012**.
2. Presented a research paper entitled "*Photocatalytic Degradation of Methylene Blue using copper doped zinc oxide nano particles: Kinetics and Mechanism*". 1st National conference on present scenario of chemical sciences and its technological perspectives-2014" held at **Karnataka science college, Dharwad, Karnataka**. On 10th and 11th October, **2014**.
3. Presented a research paper entitled "*Photocatalytic Degradation of Methyl Orange using undoped and copper doped zinc oxide nano particles: Kinetics and Mechanism,*" In 1st National Conference on Emerging Trends in Chemistry And Material Science (ETCM-2014) ,Organized by Department of Chemistry, **KLS Gogte Institute of Technology, Belagavi, Karnataka** on 13th October 2014.
4. Presented a research paper entitled "*Photocatalytic Degradation of chloramphenicol using barium doped and undoped nanoparticles*" in 34st Annual conference of Indian Council of Chemists held at Department of Chemistry, **Tarsadia University, Surat, Gujarat**, on 26th -28th December, **2015**.

Table of Contents

Certificates	i
Declaration	ii
Acknowledgements	iii
Dedication	iv
Abstract	v-viii
List of Publications and Presentations	ix-xi
Table of Contents	xii-xii

CHAPTER	PAGE NO.
1. Introduction	1 - 33
1.1 Chemical kinetics.	1
1.2 Oxidation.....	2
1.3 Quality of drinking water.....	2
1.4 Emerging contaminants	2
1.5 Pharmaceuticals (PhAcs) in environment.....	2
1.6 Dyes in environment.....	6
1.7 Advanced oxidation processes (AOPs).....	7
1.8 Semiconductor nanoparticles.....	10
1.9 Doping of Titania.....	14
1.10 Synthesis of metal oxide nanoparticles.....	15
1.11 Factors influencing Titania and Zinc oxide nanoparticles.....	18
1.12 Review of literature and Literature Survey	20
1.13 Objectives of the work.....	24
References	25
2. Ag-TiO₂ nanoparticles for photocatalytic degradation of lomefloxacin	34 – 67
2.1 Introduction	34
2.2 Experimental	35
2.3 Results and Discussion.....	41
2.4 Conclusion	65
References	66

3. Semiconducting nanoparticles for the photocatalytic degradation of Ru-TiO₂ bromothymol blue	68 – 101
3.1 Introduction	68
3.2 Experimental	69
3.3 Results and Discussion	71
3.4 Conclusion	98
References	99
4. Ba-ZnO nanoparticles for photocatalytic degradation of chloramphenicol	102 – 128
4.1 Introduction	102
4.2 Experimental	103
4.3 Results and Discussion	106
4.4 Conclusion	126
References	127
5. Cu-ZnO nanoparticles for photocatalytic degradation of methyl orange	129 – 151
5.1 Introduction	129
5.2 Experimental	130
5.3 Results and Discussion.....	131
5.4 Conclusion	149
References	150
6. Ag-TiO₂ nanoparticles for photocatalytic degradation of sparfloxacin	152 – 176
6.1 Introduction	152
6.2 Experimental	153
6.3 Results and Discussion.....	154
6.4 Conclusion	172
References	175
7. Kinetics and mechanism of uncatalysed and palladium (II)-catalysed oxidation of lomefloxacin by permanganate in acidic Medium	177-206
7.1 Introduction	177
7.2 Experimental.....	178
7.3 Results and Discussion.....	181
7.4 Conclusion	202
References	203
Publications.....	

Chapter 1

Introduction

1.1 Chemical kinetics

The central goal of chemistry is to understand the molecular change. Chemical kinetics is a tool to understand the reaction mechanism involved in various processes. The kinetic study provides valuable information about the rate and mechanism of chemical reaction, which helps out in running a chemical reaction successfully by selecting optimum reaction conditions.

The knowledge of kinetics of reaction has many practical applications. Kinetic study helps in optimizing reaction conditions for industrial processes, in understanding the complex dynamics of the environmental problems complicated biochemical reactions that are the basis of life. Generally, reactions involving organic reactants have several plausible mechanisms. Kinetic study of atmospheric reactions helps us to understand demineralisation of pollutants released in the atmosphere. At a more fundamental level, we want to understand what happens to the molecules in a chemical reaction. By understanding this concept we can develop the theories, which can be used to predict the outcome and rate of reactions.

1.1.1 Applications of kinetics

The chemist uses kinetics to plan modern and superior routes for accomplishing aimed chemical reactions. This may be associated with increasing the yield of end products or use of a catalyst. The mathematical models, which are used by chemists and chemical engineers to predict chemical kinetics, provide information to understand and describe chemical processes such as ozone depletion, waste water treatment, decaying of food and vegetables, micro organism growth. The mathematical models may be applied in the designing and fabricating the chemical reactors to get a good yield, better separation of products, and to remove environmentally hazardous side products.

Kinetics has many applications in the field of medicine. For example, the mechanisms for the controlled/sustained release of drugs are based on the half life time of the substances used and sometimes the pH of the biological fluid as well. Half life time and pH have an effect on the method in which dosages are determined and prescribed. The reaction rates and the conditions in which the reactions take place are essential for determining certain aspects of environmental protection.

1.2 Oxidation

All living organisms have chemically reactive systems and depend on the continuance of oxidation and reduction reactions. For example, plants use solar energy to reduce CO₂ into sugar molecules and release the oxygen, while in another reaction glucose and other compounds are oxidized to produce carbon dioxide, water, and releases chemical energy which is utilized by animals for living. Hence, it is the job of chemists to understand and provide clear information about redox reactions taking place in simple molecules to help biologists. In turn biologists can have strong basis to understand the behaviour of complex organisms. Though, the term oxidation equally well known in both organic and inorganic chemistry, the present work has major concentration on oxidation of various organic substrates [1].

1.3 Quality of drinking water

Water is the most important component of our physiology. So, both quantity of water and quality of water is vital for human consumption. Drinking water should always be clean and free of toxic contaminants. Good quality of drinking water is required for maintaining good health for human beings.

1.4 Emerging Contaminants

The compounds like Pharmaceuticals (PhAcs), Dyes, Nutraceuticals, Plasticizers, Fragrances, Lotions, Shampoos, Flame retardants, Soaps, Pesticides, Detergents, Sunscreens and Cosmetics etc. are used in day today life. Complete demineralization of these compounds takes an important role in during water treatment process. These compounds form different types of products during water and waste water treatment and are released to water or aquatic environment. The product formed may be benign or hazardous.

This thesis emphasizes on the importance of degradation of such micro contaminants by taking some antibacterial agents and dyes as model compounds during water treatment process and their kinetic study.

1.5 PhAcs in environment

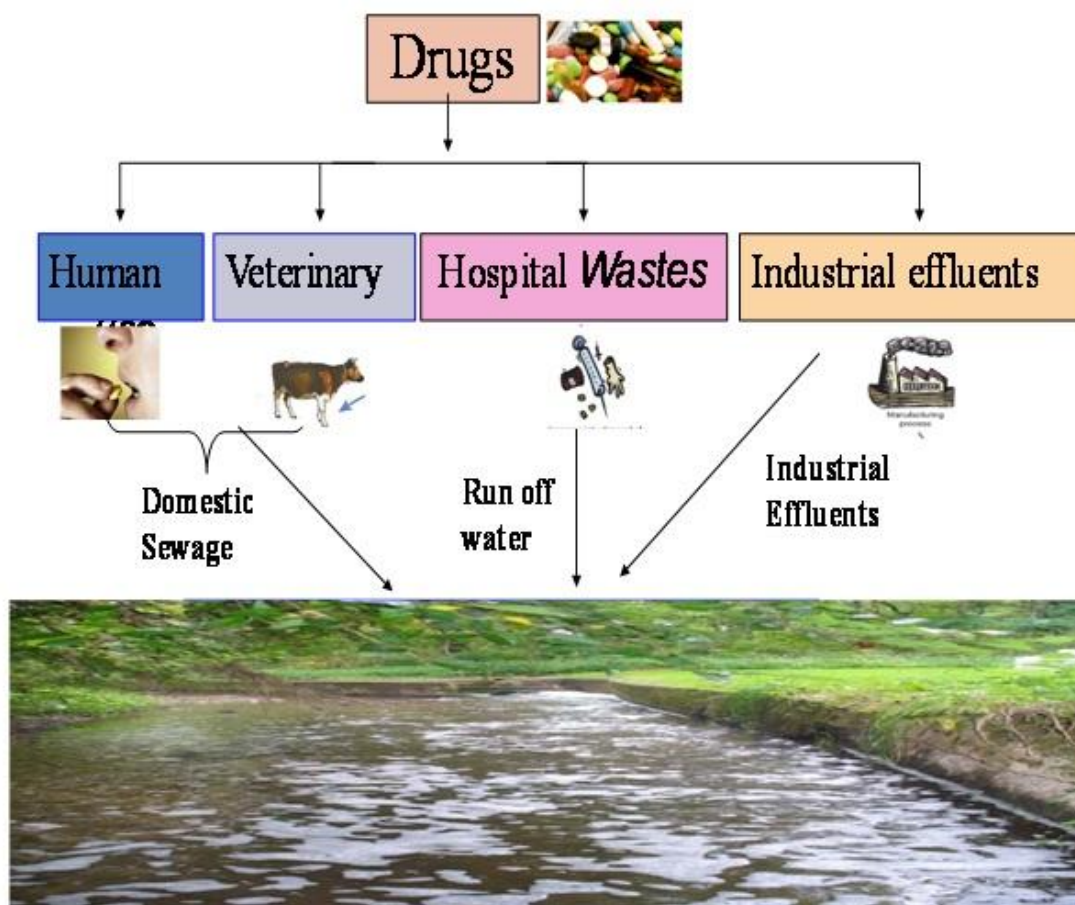
Numerous kinds of molecules detected in runoff and ground water. These PhAcs compounds concentration is found to be ng dm⁻³ to µg dm⁻³. So, they are also called as micro contaminants [2-4].

“Pollutants (biotic and abiotic), which are presently not considered in routine monitoring programs, possibly aspirant for future guideline, depending on the research on their eco-toxicity, possible health effects, the public awareness, and existence in the various ecological compartments. The emerging contaminants may not be new chemicals. The contaminants that have been often present in the environment, but whose presence and influences are now made cleared”. (Adapted from the EU NORMAN project: www.Norman-network.com as of 9/13/2006).

Emerging contaminants are chemical compounds or material substances of attention that are distinctly characterized by: A readily perceived or really cause damage to environment or to the human health. Decrease in the publicity health standards or an evolving standard. A pollutant may be "emerging" because of the invention of a new discharge matrix, a novel route to humans, or original discovery method or technology [5- 6].

PhAcs are the chemical compounds used for the treatment of various diseases. PhAcs consist of effective constituents that have been premeditated to boast pharmacological cause and give significant profits to the world. The major portion of medically recommended antibiotic dose is released into public waste water streams due to incomplete metabolism of antibiotics within the human body. (Rain) Runoff water carries the hospital wastes to rivers and contaminates the river water (nanograms to micrograms per litre) has been extensively reported in previous studies [7-9] as shown in Fig 1.1. The research on emerging contaminants got boost up, due to the advances in analytical and instrumental techniques. Many investigations and survey have reported the existence of PhAcs even in treated municipal water and effluents. Regular monitoring plan to check drinking water for PhAcs has not been enabled.

Fig. 1.1 Routes of pharmaceuticals entering in to the environment



1.5.1 Fluoroquinolones and Tetracycline.

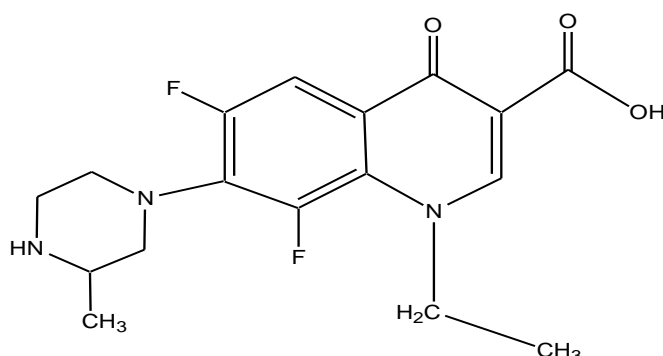
Fluoroquinolones are extensively used for treatment of various infectious diseases [10]. Lomefloxacin, levofloxacin ciprofloxacin, ofloxacin, enrofloxacin, and gatifloxacin are some of commonly used fluoroquinolones. The fluoroquinolones have higher renal clearance and hence they are released to the environment through excretion.

Fluoroquinolones may go in to the aquatic life through various routes such as house hold waste, municipal and effluent from wastewater plants. The current report shows that about 50 ng dm^{-3} undetectable concentrations of fluoroquinolones present in the surface water in various parts of the world [11].

In 1940's Tetracyclines were discovered. They are broad spectrum antibacterial agents. They are active against wide variety of gram positive and gram negative microorganisms. The better antimicrobial properties of these agents and the absence of

major undesirable side effects has led to their wide use in the therapy of human and animal diseases.

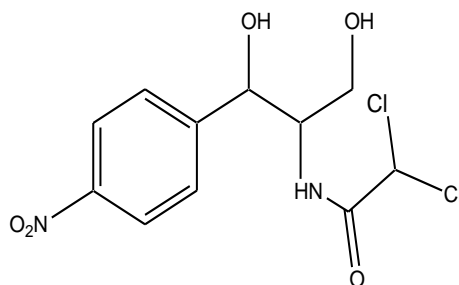
1.5.2 Lomefloxacin (LMF)



Structure of Lomefloxacin

Lomefloxacin is also a class of fluoroquinolones antibacterial agent. It is mainly used for cure broad range of bacterial diseases, such as urinary tract and bronchitis infections etc. LMF is used to treat the diseases. LMF is connected with phototoxicity and C.N.S. (central nervous system) undesirable effects [12].

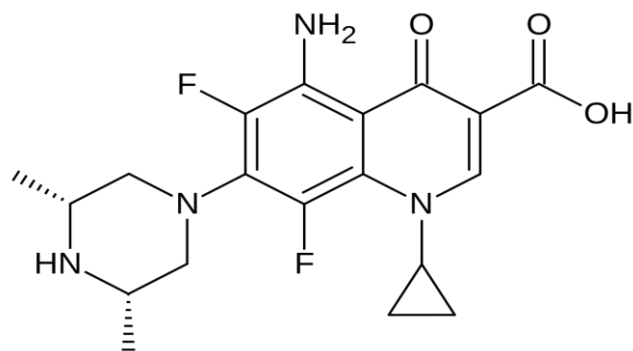
1.5.3 Chloramphenicol (CLP)



Structure of Chloramphenicol

Chloramphenicol (CLP) belongs to tetracycline family and is commonly known as chloromycetin [13]. It is a powerful antibiotic used for the many bacterial diseases [14]. It is used in the treatment of plague, cholera and typhoid fever. CLP is believed to be proto typical wide range spectrum antibacterial agent. Hence, its photocatalytic degradation and kinetics investigation is much important to know the mechanistic profile in the environment. From the application point of view, a regular study of photodegradation of CLP with Ba-ZnO is investigated.

1.5.4 Sparfloxacin (SPF)



Structure of Sparfloxacin

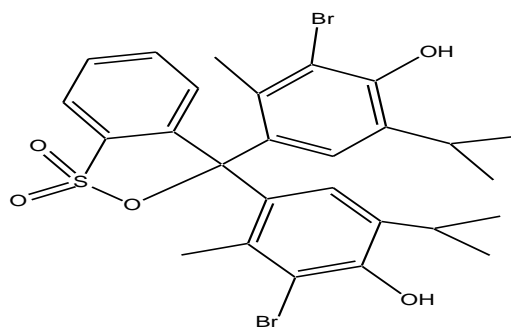
Sparfloxacin belongs to fluoroquinolone homologous series. It is a powerful, 3rd generation wide spectrum antibacterial fluoroquinolone derivative. The metabolic rate of SPF in human body is slow due to its solubility issues. Its removal from the healthy human body takes about one day after consumption of drug [15]. The mucous membrane, epithelial tissues fluid, alveoli etc of human body absorbs SPF in high concentrations [16-17].

1.6 Dyes in environment

We use colours for various applications such as painting, colouring the clothes, hairs, skins etc. Dyes are widely used in the textile industries, during the dyeing method the dye molecules enter into the aquatic environment as effluents. Most of the manufactures use dyes for printing, fabrics, plastics, cosmetics, etc. It is estimated that more than one lakh dyes are available and industries produce about 7×10^5 tonnes of dye stuff every year. The discharge of these dyes into the aquatic system by industries causes harmful effect on the environment. The aquatic animals are the first species to get the brunt. The dyes present in the environment decreases the light diffusion in the water bodies and reduce the photosynthetic activity [18].

There are various biological and conventional methods are available to treat these dyes. These methods include simple techniques like coagulation, filtration, adsorption, microbial treatments, etc. All these methods are proven to be efficient but they generate huge quantity of solid waste in to the environment. Hence, these methods are moreover unsuccessful to achieve complete mineralization of organic contaminants or create huge quantity of carcinogenic mud causing removal problem [19-20].

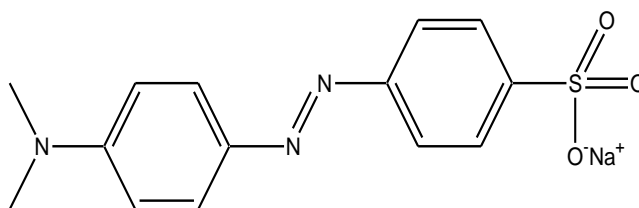
1.6.1 Bromothymol blue (BTB)



Structure of Bromothymol blue

Bromothymol blue (BTB) is an acid base indicator. It is also known as bromothymol sulfone phthalein. BTB commonly sold as sodium salt of the acid indicator in solid form. BTB may be used for examine photosynthetic performance, and as an inhaling indicator (it changes to yellow when CO₂ is added) [21-22].

1.6.2 Methyl Orange (MO)



Structure of Methyl orange

Methyl orange (MO) is an anionic azo dye and it is an important synthetic dye. It has been extensively utilized in fabrics, food stuffs, newspaper, and leather productions. The discharge of MO and its derivatives cause harmful effects on the aquatic environment. Human exposure may cause eye or skin irritation, or breathing may lead to gastro intestinal irritation with nausea, vomiting, and diarrhea etc [23].

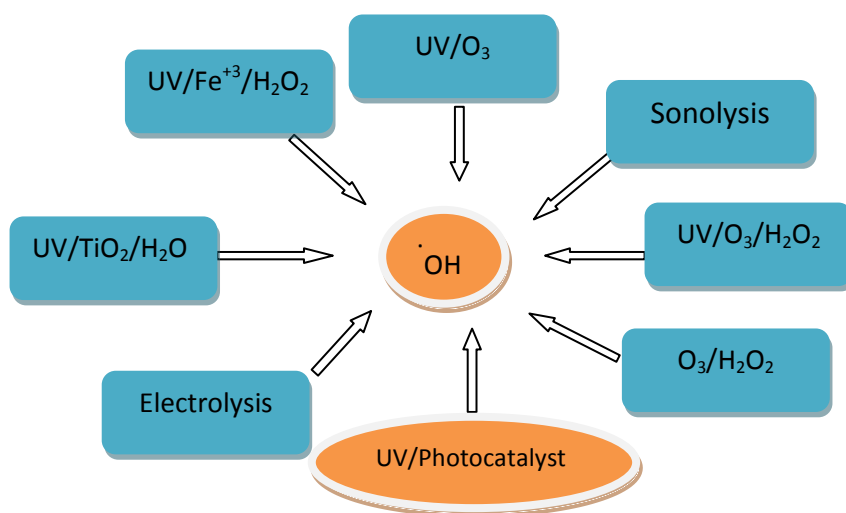
1.7 Advanced Oxidation Processes (AOP's)

“Advanced Oxidation Processes (AOPs) were defined by Glaze *et al.* (1987) as near ambient temperature and pressure water treatment processes which involve the generation of highly reactive radicals (specially hydroxyl radicals) in sufficient quantity to effect water purification” [24-25].

Many hazardous and carcinogenic organic contaminants are decomposed effectively to permissible levels without adding any harmful by-products. In these processes highly reactive ·OH radicals degrade the organic contaminants present in water

[26-28]. The most important characteristic of hydroxyl radicals is its non selective attack on organic contaminants. The product of reaction of hydroxyl radicals with organic contaminants is usually CO_2 and H_2O . The demineralization reaction is due to attack of OH^\cdot to organic contaminants through abstraction of hydrogen, radical radical reaction, and electrophilic addition.

There are many homogenous and heterogeneous techniques to generate hydroxyl free radicals as shown in Fig.1.2.



Most of the above techniques employed for UV - Spectrum for demineralization of organic contaminants. UV - Spectrum is randomly classified into three groups namely, 1) UV-A 2) UV-B and 3) UV-C. UV-A and UV-C is commonly applied in generation of OH^\cdot radicals. UV-A = Near UV, UV-C = Far UV.

Advantages of AOP's

- 1) Fast rate of reaction.
- 2) Minute footprint.
- 3) Powerful to decrease carcinogenicity and probably complete degradation of organic contaminants
- 4) Doesn't use membranes for other management with organic contaminants.
- 5) Doesn't produce stuff.

Disadvantages of AOP's

- 1) Central motivation.
- 2) Complicated chemistry knowledge must be adapted for particular appliances.
- 3) For various appliances extra peroxide is needed.

AOP involving UV can be widely divided into two categories:

- a) Homogeneous photo-oxidation.
- b) Heterogeneous photo-oxidation: Photocatalysis.

1.7.1 Homogeneous photo-oxidation

“Homogeneous photo-oxidation is the photo-reactions in a gas or liquid phase system, without the addition of any solid”. The homogeneous photodegradation involves the use of an oxidant for the production of free $\cdot\text{OH}$ radicals, which react with contaminants to initiate the oxidation process.

The following are the photochemical methods employed in the homogeneous photo degradation methods:

1. UV with H_2O_2 .
2. UV with O_3 .
3. UV with O_3 and H_2O_2 .
4. Photo-Fenton process.

Many of the AOP's use H_2O_2 in the production of OH radicals for oxidation (Table 1.1). The use of UV enhances the oxidizing strength of hydrogen peroxide as the radiation increases number of OH free radicals.

Table 1.1. Different homogeneous AOPs

Method	Reaction	Limitations
UV / H_2O_2	$\text{H}_2\text{O}_2 + h\nu \longrightarrow 2\cdot\text{OH}$	1) Absorb $\lambda < 300$ nm, a lesser component in solar radiation. 2) pH dependence.
UV / O_3	$\text{O}_3 + \text{H}_2\text{O} + h\nu \longrightarrow \text{O}_2 + \text{H}_2\text{O}_2$ $\text{O}_3 + \text{H}_2\text{O}_2 \longrightarrow \cdot\text{OH} + \cdot\text{O}_2\text{H} + \text{O}_2$	1) Absorb $\lambda < 300$ nm, a Lesser component in solar radiation. 2) pH dependence 3) Continuous supply of chemicals are required.
UV / O_3 / H_2O_2	$\text{O}_3 + \text{H}_2\text{O}_2 \longrightarrow \cdot\text{OH} + \cdot\text{O}_2\text{H} + \text{O}_2$	1) Absorb $\lambda < 300$ nm, a lesser component in solar radiaton. 2) Applicable over a wider pH range.
Fe^{3+} / H_2O_2 (Photo Fenton)	$\text{H}_2\text{O}_2 + \text{Fe}^{2+} \longrightarrow \text{Fe}^{3+} + \cdot\text{OH} + \cdot\text{OH}$ $\text{Fe}^{3+} + \text{H}_2\text{O} + h\nu \longrightarrow \text{Fe}^{2+} + \cdot\text{OH} + \text{H}^+$	1) Sludge disposal problem formed during the process. 2) Continuous supply of chemicals is required. 3) Process is expensive

1.7.2 Heterogeneous photocatalysis

Nowadays, most effective water treatment method used is heterogeneous photocatalysis [29-33]. In “heterogeneous photocatalysis the photocatalyst and reacting molecules (contaminants) are present in different phases”. The principle behind the photocatalysis is excitation of a semiconductor by UV/Vis light. A light of energy greater than the band gap of photocatalysts excites the electrons from valence band (VB) to conduction band (CB), leaving behind holes (h^+) in the VB and electron (e^-) in the CB. These so formed e^- and h^+ are responsible for reduction and oxidation processes. The h^+ are strong oxidants which are efficient for oxidizing all organic contaminants including water, results in the generation of OH free radicals [34-38].

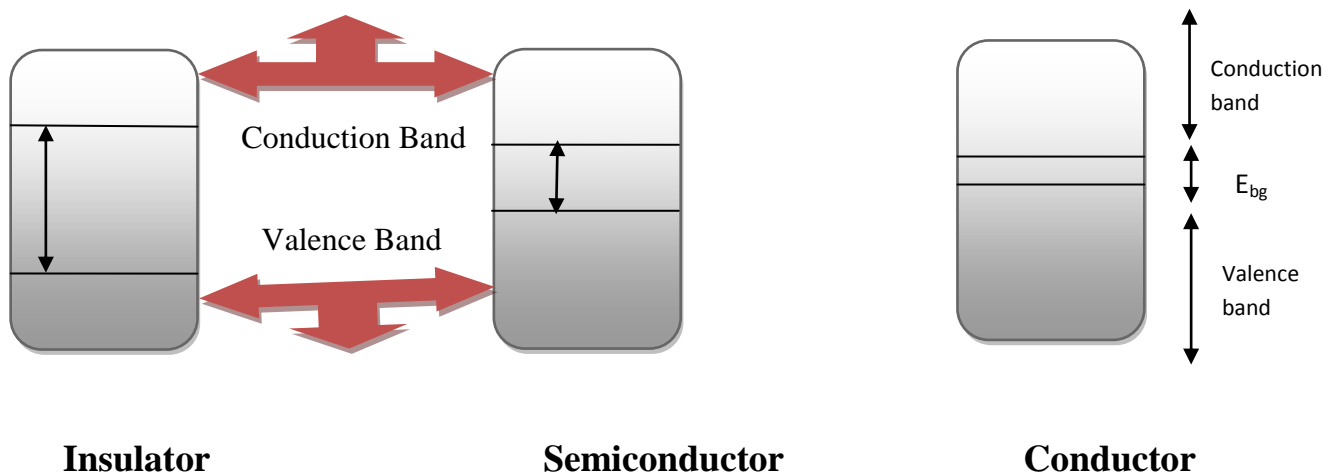
1.8 Semiconductor nanoparticles

These are material contains electronic arrangement with a filled VB and an unfilled CB. The difference between energies of the excited state of the CB and ground state of the VB is termed as energy gap/band gap. When an illuminate photon having a energy ($h\nu$) equivalent or $>$ than energy gap attain the semiconductor surface, when e^- is jumped from VB to CB leaving a h^+ [39-41]. **Fig. 1.3.** Illustrate that the energy gap is the prime factor that make out whether the material is conductor, semiconductor or an insulator. Semiconductor surface having e^- and h^+ oxidize oxygen, water, and hydroxide ions in to $\cdot OH$ radicals and other free radicals. Direct light activated holes can oxidize the organic contaminant present in water. Many types of UV semiconductor methods are applied for the photocatalytic demineralization of effluent. Most of the metal oxides including TiO_2 , ZnO , WO_3 , CdS and Fe_2O_3 were having photocatalytic properties [42-45]. **Table. 1.2.** gives the information regarding commonly used semiconductors as photocatalysts, The energy gap (E_{bg}) and individual wavelength of all the semiconductors listed in below **Table.** Titanium dioxide is having the maximum photocatalytic efficiency with a higher range of environmental applications.

Table1.2: Band gap energy and corresponding wavelength of semiconductors

Semiconductor	E_{bg} (eV)	λ (nm)
TiO₂ (anatase)	3.2	388
TiO ₂ (rutile)	3.0	413
ZnO	3.3	375
Fe ₂ O ₃	2.3	539
WO ₃	2.8	443
CdS	2.4	516
ZnS	3.5	354
InSb	0.17	7294
MoO ₃	3.06	405
V ₂ O ₅	1.74	712
CdSe	1.84	674
CdTe	1.61	770
GaSb	0.81	1530
InP	1.42	873
InAs	0.36	3444

Fig.1.3. Configuration of the electronic bands of conductor, semiconductor and insulator materials. Conduction Band Valence Band

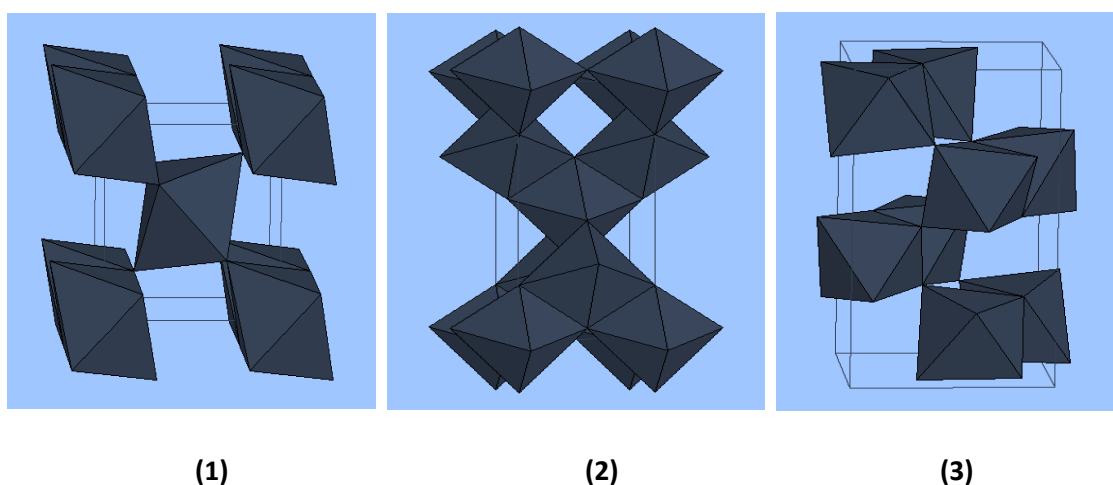


1.8.1 Titanium Dioxide (TiO₂) Photocatalyst

In the earth shell Titanium (Ti) is the 9th rich element consists of 0.62% of the earth shell. Titanium dioxide is the only one oxide of Titanium. Photocatalysis is a phenomenon where the reaction takes place in presence of light absorbed by a catalyst [46]. (B.A. Kennedy, surface mining, 2nd edition). TiO₂ is an apparent white amorphous powder, commonly used to produce products like paper, plastic, cosmetics, tooth-paste, and clinical drugs [47]. However, 10 to 50 nm TiO₂ nanosized particles widely used for self cleaning window glass, air and water sanitization processes. Fujishima et.al. (1972), invented the split of H₂O on TiO₂ electrodes photocatalytically. It led to a rigorous investigation of increasing the photocatalytic efficiency of TiO₂. Currently, environmental cleanup has been one of the very important applications of heterogeneous photocatalysis. TiO₂-mediated photocatalysts have the possible application of the total demineralization of organic contaminants in polluted water [48-49].

High degradation efficiency, chemical stability, low carcinogenicity, and low cost make TiO₂ a better photocatalyst for degradation of organic compounds [50-51]. “**Anatase (tetragonal), rutile (tetragonal), and brookite (orthorhombic)**” are the 3 different polymorph forms of the TiO₂ [52] as shown in Fig 1.4. Among these anatase and rutile polymorphs of TiO₂ are regularly used in photocatalysis, while, brookite form of TiO₂ is photo inactive. Usually, anatase form of TiO₂ is preferred for photocatalysis because it has high surface area, surface density of active sites for adsorption [53]. Electronic properties of Titanium dioxide such as band gap play an important rule for a semiconductor photocatalyst.

Fig.1.4. Polymorphs of TiO₂ 1) rutile, 2) anatase, 3) brookite



1.8.2 UV/TiO₂ photocatalysis process.

The heterogeneous photocatalytic reactions takes place in five steps [54]:

- I. Dispersion of reactants towards the photocatalyst surface (TiO₂).
- II. Adsorption of reactant molecules on Titania surface.
- III. Reaction with adsorbed reactant molecules with Titania.
- IV. Desorption of reaction products.
- V. Dispersion of products from photocatalytic surface in to solution.

Movement of reactant molecules and products, step (I) and step (V) respectively depend on the concentration of reactant-product, loading of photocatalyst and size of the particle. (II), (III), and (IV) Steps depends on the active centers on photocatalyst and also chemical affinity between reactant and product fragments.

When Ultra Violet radiation falls on photocatalyst titania (TiO₂), it will generate pair of electron (e⁻) and holes (h⁺). This is shown in Fig 1.5. The difference energy between CB and VB is termed as energy gap (Band Gap). The wavelength required for photo excitation is 388 nm.

The h⁺ of VB of titania decompose water molecule to produce H₂ gas and OH radical and e⁻ in CB reacts with O₂ molecule to produce ·O₂⁻ anion.

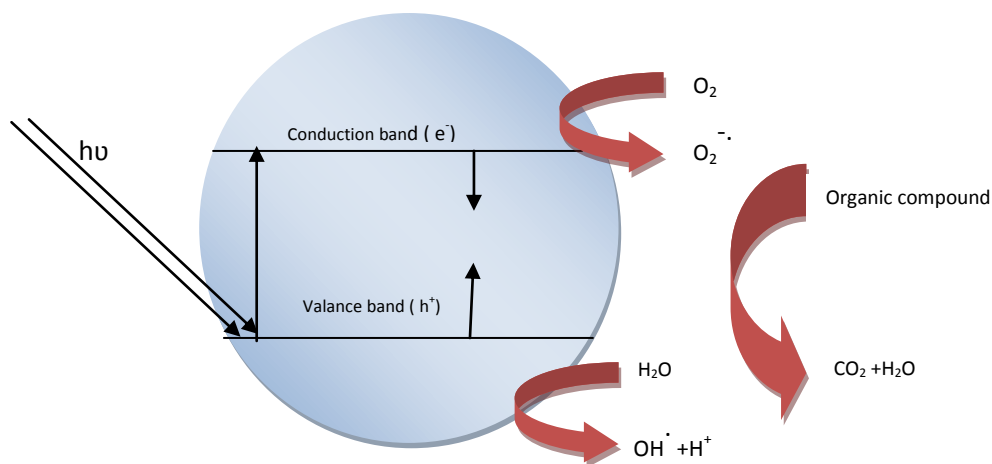
Reactions at valence band

- $\text{TiO}_2 + h\nu \rightarrow \text{TiO}_2 \quad (e^- + h^+)$
- $h^+ + \text{H}_2\text{O} \rightarrow \text{H}^+ + \cdot\text{OH}$
- $h^+ + \text{OH}^- \rightarrow \cdot\text{OH}$
- $\text{Organics} + \cdot\text{OH} \rightarrow \text{Degradation Products}$

Reactions at Conduction band

- $e^- + \text{O}_2 \rightarrow \cdot\text{O}_2^-$
- $\cdot\text{O}_2^- + \text{H}^+ \rightarrow \text{HO}_2\cdot$
- $\text{HO}_2\cdot + e^- \rightarrow \text{HO}_2^-$
- $\text{HO}_2^- + \text{H}^+ \rightarrow \text{H}_2\text{O}_2$
- $\text{H}_2\text{O}_2 + e^- \rightarrow \cdot\text{OH} + \cdot\text{OH}$

Fig.1.5. Excitation of e^- from Valence band to Conduction band in TiO_2



1.8.3 Zinc Oxide (ZnO) Photocatalyst

Zinc oxide (ZnO) has come out to be most effective photocatalyst. ZnO produces H_2O_2 more efficiently in water treatment processes [55], ZnO contains plenty of active centres with high surface reactivity, low cost, high stability [56]. Hence, it has high mineralization rates [57]. However, ZnO is believed to be an appropriate substitution of TiO_2 (3.2 eV), due to their broad energy gap (3.3 eV). ZnO has been showed as a superior photocatalyst as related to commercialized TiO_2 based on the basis of higher initiative rates [58], and absorption efficiency of solar radiations [59]. Defects, cracks, facets and area play vital role in deciding photocatalytic efficiency of photocatalyst. For this reason, the modification of surface of metal oxide is significant to increase the surface defects [60].

1.9 Doping of Titania

Titania has been considered to be most promising photocatalyst, however, titania having some limitations i.e. broad energy gap and fast re-combination rate of electron-hole ($e^- - h^+$) pairs [61]. Therefore, now a day's scientist interest is centred on the modification of the catalytic surface behaviour of titania through doping with various metal ions [62-63], these metal ions are either doped into crystal lattice or deposit on the surface of titania as islands or single nuclear composite [64-65]. The main objective of the doping is to reduce the energy gap or to create energy levels inside the forbidden band gap and decrease the re-combination by establishing traps for e^- and/or h^+ [66]. However, one of the major limitations of using titania as a photocatalyst is that its energy gap exists close to UV range of the solar spectrum. As a consequence, it allows only UV light to

generate $e^- - h^+$ pairs and start the photocatalytic oxidation. However, solar spectrum consists of less than 5% of UV light. Hence, the researchers continue their effort in reducing band gap, so that visible light is sufficient to generate $e^- - h^+$ pairs in TiO_2 . In order to achieve this photocatalytic activity of TiO_2 in the visible range, TiO_2 is doped with transition metals with Ru, Ag, Fe, Zn, Cu, Ni and V [67-69]. Doping of these metals in the TiO_2 lattice reduces the band gap of TiO_2 , as well as reduces the $e^- - h^+$ recombination.

1.10 Synthesis of Metal Oxide Nanoparticles

To synthesize nanomaterials extensively two methods are used. “**A) Top-down** **B) Bottom-up methods**”. In top-down method is a physical-method, where, a large matter is chopped into small pieces till we get required dimension. Any how this method is efficient only up to micro-meter level. Lithographic processes, laser-induced chemical etching and ball-milling fall in to this group. However, these processes are efficient only down to the micro-meter range. Getting nano-meter size is practically difficult and expensive.

The bottom-up methods primarily include chemical and biological techniques to prepare nanoparticles. It involves self-condensation of solute particles that is produced while a reaction. To control the growth led to the development of fragments with required dimension and shape. Even though the synthesis of nanoparticles with same dimension and shape is crucial. Hence, preparation of large scale nano materials remains a difficult task.

The advancement of predictable reviews for the availability of metal oxide nanoparticles is a present test and essential. The combination procedures may be sorted in two critical streams endless supply of progress.

The synthesis techniques may be categorised in two major streams depending on nature of transformation 1) liquid-solid 2) gas-solid usually liquid-Solid transformations are used to control topography of nano-materials. The number of popular synthesis of nanomaterials methods have been established, among these some methods are discussed below.

1.10.1 Hydrothermal Method

Hydrothermal method is a procedure to prepare nanoparticles in aqueous medium at high temperature and pressure. The process is carried out by heating the metal salts along with water in an autoclave at a specified temperature and pressure for about 24 hrs-48 hrs [70-73].

Advantages of Hydrothermal Method

- a. Purity of metal oxides produced is enhanced.
- b. Powder morphology can be controlled.
- c. Several unnecessary steps like calcination, mixing, and milling can be avoided or reduced.
- c. It is economical.

1.10.2 Solution combustion method

In this method, metal salts like metal nitrates/metal acetates/metal chlorides and fuel like urea/PEG/Glycine are subjected combustion at ≈ 350 °C. It is a gas producing exothermic reaction and is self purifying process giving ample nano sized particles of metal oxides in a short time. It is usually carried out in muffle furnaces [74-75].

Advantages of the Method

- a. Gives way to ultra fine/nano sized particles with large surface area.
- b. The Particle size can be controlled by using fuel/Metal salts
- c. The method is simple, fast and efficient one.
- d. The stoichiometry, homogeneity and purity of the resulting materials can be controlled.

1.10.3 Sol-Gel Synthesis

It is a wet chemical method involving several steps. At the time of gel formation there is sudden increase in viscosity [76].

Steps in sol-gel synthesis are

- 1. Hydrolysis:** Reaction of a metal alkoxide with water in a solvent (typically in alcohol).
- 2. Polymerisation:** Condensation of neighbouring molecules, removal of water and solvent, development of metal oxide linkage (polymeric networks).
- 3. Gelation:** Formation of Gel.
- 4. Drying:** Remaining water and solvent are removed at sensible temperature (<470 K), giving a hydroxylated metal oxide with organic residue.
- 5. Dehydration:** Removal of organic content and chemically bound water at $670-1070$ K.
- 6. Densification:** Temperature of the order of 1270 K is applied to get the dense metal oxide product.

Advantages of the Sol-Gel Method

- a. Better homogeneity and High Purity of the nano metal oxides.
- b. Lower processing temperature
- c. Size and morphology can be controlled easily.
- d. Easy preparation of thin films and coatings

1.10.4 Liquid-Liquid Interface Method

It's an innovative method to obtain metal oxide and metal chalcogenide using aqueous organic interface. In this method metal precursors are introduced in the organic layer which in contact with the aqueous layer. A suitable reagent is then added for hydrolysis. The reaction takes place at the interface and product is formed also at the interface [77].

Advantages of the Method

- a. Simple Method.
- b. It is economical.

1.10.5 Vapour-Phase Synthesis

In this technique the atoms and molecules are condensed in vapour /gas phase to achieve the formation of nano metal oxides. This is also known as Gas Condensation synthesis. This method was predominantly used in industries. The technique involves the hydrolysis of metal chloride in gas phase. The reaction is exothermic and provides the necessary high temperature for the reaction. So formed products of the reaction were recycled as per the requirement [78].

Advantages of the Vapor-Phase Synthesis Method

- a. Efficient method.
- b. The nanomaterials will have relatively high surface area.

1.10.6 Chemical Vapour Deposition Method

This method is used to obtain high purity, high efficiency nanomaterials. In this technique, the substrate in the form of wafer is taken on the surface of which, the volatile precursors are allowed to react. The metal oxides are accumulated on the substrate surface after the reaction. The by-products if any are removed by a purging the gas. It finds applications in the production of many microcrystalline, polycrystalline substances such as SiO₂, nanofibres, graphene etc [79-81].

Advantages of the Chemical Vapour Deposition Method

- a. The method is versatile.
- b. High performance nanomaterials can be produced.
- c. The properties of resulting materials can be controlled and varied as per the requirement.

1.10.7 Co-Precipitation Method (CPT)

This CPT involves dissolution of a metal nitrates or metal sulphate in deionised water or any solvent to form ionic solution. Then, oxo-hydroxide precipitate is formed by

adding a base. Especially, to control the particle size of the nanoparticles some surfactants are used [82-84].

Advantages of Co-Precipitation Method

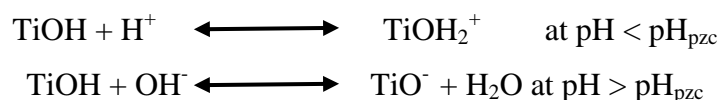
- a. This method reduces the reaction temperature when the reactant precipitates.
- b. Simple, in expensive method to synthesize fine metal-oxide powders.

1.11 Factors Influencing Titania and Zinc oxide Semiconductor

Some factors which influence the photocatalytic activity of TiO₂ and ZnO are listed below.

1.11.1 Effect of pH

pH is an significant factor, which decides the adsorption behavior of adsorbent and adsorbate [85-86]. At higher pH values the holes are less active in conduction band, whereas, electrons are more active in valence band. Similarly, in amphoteric solution the TiO₂ photocatalyst alters the surface charge properties with change in pH of the medium [87-88]. The following equation indicates shows the surface charge on TiO₂.



The commercial TiO₂ (Degussa) P-25 having point of zero-charge from 5.7 to 5.9. The influence of pH affects the mineralization of the contaminants. Since, at lower pH, the holes are believed to be dominant, whereas, in basic as well as neutral medium hydroxyl radicals are believed to be prominent [89-90].

pH of the medium not only influence the efficiency of the TiO₂, but also alters the behavior of contaminant moiety [91]. For illustration, the pK_a value of phenol is 9.95. The phenol moiety can be charged + ve ly or – ve ly by adding different pH solution. i.e., the action of phenol and TiO₂ changes when the pH of the media changes. So, pH of the media plays a vital behavior in photocatalytic mineralization and also influences the adsorption behavior of contaminant and photocatalyst surface [92].

Previous literature revealed that the photocatalytic mineralization of most of the organic contaminant depends upon pH of the medium. The photocatalytic mineralization of Orange G rate was two times more at pH=3, compared with pH=7. In lower pH (< 6) the higher mineralization of methyl orange is investigated in presence of TiO₂. This behavior may be due to strong interaction between methyl orange and positively charged TiO₂ [93].

1.11.2 Effect of Substrate

An earlier study shows that, when concentration of contaminants increases, most of the contaminant molecules accumulate on the photocatalyst surface, Hence, it affects the rate of mineralization of pollutant [94]. In 2009 Mahalakshmi *et al.*, reported that above 200 ppm propoxur concentration the rate of photo degradation will decrease. It is due to fact that above 200 ppm of propoxur solution the formation of $\bullet\text{OH}$ radicals will be constant when same quantity of photocatalyst was used. The degradation and mineralization of homologous series of an-ionic azo dyes increasing with decreases in substrate concentration when the concentration of dye increased from 0.125 mili molar to 0.75 mili molar, initially, when substrate concentration increased, the rate of reaction also increased up to 0.75 mili molar. Above limiting value (0.75 mili molar) increase in the substrate concentration, reduces the photocatalytic rate of reaction. This behavior is due to increase in substrate concentration, enhances the turbidity of the solution. Hence, color becomes more and more turbid, which reduces the light reaching the semiconductor [95]. The activity of photocatalytic reaction is reduced when the dye concentration increases. This is due to increase in dye concentration, reduces the generation of $\bullet\text{OH}$ radicals. Since, active centers of photocatalyst decreases by masking the dye ions [96-98]. One more probable reason is the UV- masking effect at higher concentration of dye, a major portion of UV-light cannot reach the photocatalyst surface. Therefore, it decreases the photocatalyst efficiency.

1.11.3 Effect of Light intensity

Illumination of light on photocatalyst plays vital role in all photocatalytic reactions. It also decides the amount of electron-hole pairs generated. Therefore, higher the intensity of light higher the rate of photons. Consequently, the rate of photocatalytic reactions will increase. Elementary reactions undergo charge/carrier formation, recombination, reduction- oxidation, it is easily stated that at lower intensity of light, lower is the carrier formation; hence, the rate of mineralization of an organic contaminants is directly proportional to light intensity. This implies that increases in the intensity of light increases the amount of photons and activates the active centers of the photocatalyst surface and increases the photocatalytic rate of reaction.

The photodegradation of propoxur was studied in different UV intensity of light. They found that as the light intensity increases, the possibility of stimulation of e^- also increases; hence, the degradation rate of propoxur also increases [99]. It is reported that

the influence of intensity of light on the photodegradation of MB (Methylene-Blue). It had been found that 50% of photodegradation of MB (40 ml/L) takes place in 15.2 minute using 1.5 mW cm^{-2} light intensity, while; only 11.0 minute was required for photodegradation of MB when light intensity was increase to 5.0 mW/cm^2 . The photodegradation of phenol with TiO_2 and light intensity (20-400 W) they got best linear co-relation b/n light intensity and rate constant [100].

1.11.4 Effect of photocatalyst dosage

It is well reported in the literature. The rate of reaction is directly proportional to the amount of photocatalyst (m) [101-103]. Wherever, the amount of photocatalyst increases, the surface area of photocatalyst also increases. Consequently, the number of active centers on the photocatalyst increases, hence, the rate of photocatalytic mineralization increases. The rate of photocatalytic reaction above the limiting value of dosage starts decreasing. When dosage of titania was increased above limiting value the number of active centers on the surface of titania remained constant. It is due to masking effect of light by the accumulated particles [104-105]. Further, Kabir *et al.*, observed that Phenol mineralization decreases with increase in the optimum loading of TiO_2 photocatalyst. The optimal photo-catalyst loading or efficient light penetration length, under given conditions, is important in designing a slurry reactor for efficient use of the photocatalyst and the reactor volume [106].

1.12 Review of Literature and Literature Survey

In the last two decades the research activities committed to environment protection has been recorded as a consequence of the special attention paid to the environment [107].

1. Blackburn and Waldo in 1995, T.A Ternes in 1998, R. Hirsch, et al in 1999, G. G. Ying, et al in 2002, S. Jobling, et al in 2002 reported the existence of the pharmaceutical molecules in the environment and D.W. Kolpin et al in 2002 mentioned about the rising concern of pharmaceutical molecules in the environment .
2. J.C. Hoff and E. E. Geldrich in 1981, R.L Wolfe et al in 1984, J.C Morris in 1986, G. A Burlingame, et al in 1992, J. Hoigne, in 1998, C. Gottschalk., et al in 2000, Von – Gunten et al in 2003, B. Legube in 2003, A. Bruchet and J.P. Duguet, in 2000 used various disinfectants like ozone, chlorine, chloramines, permanganates for oxidation of micro pollutants and elimination odour and taste control.

3. Some reports by B. Cancho, et al in 2000, S.D. Richardson et al in 2003, M. J. Plewa et al in 2004, S.W. Krasner et al in 2006, Y. Bichsel, and U.von Gunten in 2000, suggest that there is a possibility of formation of hazardous disinfection by products.
4. AOPs to be appropriate processes for decomposition of organic compounds present in the water such as halo compounds and inorganic contaminants.
5. Hussain et al reported that, in presence of Titania photocatalyst, organic effluents can be mineralized in to CO₂, H₂O and mineral acids at lower temperature and UV-light.
6. Oppenländer et.al., in 2002 reported that in presence of UV-light hydroxyl (.OH) radicals are formed, they are potential, non-selective oxidants, It can be applied for those compounds which are not photo sensitive. This can be oxidised by these hydroxyl groups.
7. Cooper et al., (2008). Studied that the AOPs are more suitable and broadly employed in water analysis.
8. Zhang et.al. In 1998 reported, the photo-catalytic mineralization of organic contaminant has shown as a potential tool for mineralizing various types of dyes in untreated water. A various investigators have shown the photo-catalytic of this class of compounds in presence of UV/A or visible light with encouraging data.
9. Wang, (2000) reported the photo-catalytic mineralization of 8 industrial available dyes having various moieties with substitute groups using Titania as a semiconductor catalyst in aqueous medium in visible light.
10. Qamar et al., (2005) studied the Chromotrope 2B and Amido Black 10B dyes in water medium using titania as a photocatalyst in various conditions by photocatalysis.
11. Xie and Yuan, (2003) investigated that titania colloidal nano-particles have enhanced interfacial adsorption ability and superior photo efficiency than P25 titania in water system and can be used to recover several times while keeping high photoactivity on X-3B degradation reaction.
12. Konstantinou et al., 2002 reported that wide use of titania is un-economical for big range of water management; hence, it is curiosity to investigate alternative photocatalyst to titania. A number of efforts have been made to investigate photocatalytic efficiency of various photocatalysts viz. SnO₂, ZrO₂, CdS, Fe₂O₃, WO₃ and ZnO.
13. Roselin et al., (2002) studied the photo-catalytic mineralization of RR 22 (Reactive Red 22) dye in the presence of a thin film of ZnO photocatalyst using a thin film flat bed flow photo-reactor under visible light.

14. Chakrabarti and Dutta, (2004) studied the photo mineralization of Methylene blue and Eosin Y, using ZnO semiconductor photo-catalyst. The dependence of parameters such as photocatalyst loading, effect of substrate, air flow rate, UV illumination, intensity of light and pH on the degree of photo-mineralization have been reported.
15. Pandurangan et al., (2001) reported, the photocatalytic mineralization of fabric dye, Basic Yellow and Auramine O with ZnO as the semiconductor in a batch reactor using visible light as an illuminant. In addition to de-colorization of dye solution, the COD was also decreased signifying that the side products formed from the dye was degraded.
16. Chen et al., 2005 studied that the restrictions of a reticular photocatalyst for particular appliances can be conquered by converting the surface of the photocatalyst. One important method to modify surface properties of titania is doping. Titania can be doped with noble metals or d-block elements or coupled with other metal oxide photocatalysts.
17. According to Hussain et al., TiO₂ may be a perfect semiconductor in numerous ways. It is expensive, chemically stable, and commercially available. Furthermore, its photo-generated holes are highly oxidizing, and the photo-generated electrons are reducing enough to produce superoxide from dioxygen.
18. Yu et al., investigated that Titania photocatalyst used in the removal of organic contaminant present in waste water. These appliances have been restricted by the huge energy band gap (3.2 eV), which can absorb only < 3% of the light in solar spectrum ($\lambda < 388$ nm) additionally by the quick re-combination of photo-generated e⁻ - h⁺ pairs.
19. Cantarella et. al., reported that in recent years nanomaterials are representing a definite solution to answer many of the present problems related to water quality, though several limitations. That is primarily efficient their recovery after water treatment, impact on human health and ecosystems. By these demerits polymeric composites may overcome these problems. Therefore, TiO₂ nanostructures in poly methyl acrylate (PMMA) were designed and these materials need not recover from water after treatment. These polymeric nanoparticles are low cost and more active towards microorganism.
20. Shet et. al., studied the Ag-TiO₂ nanoparticles were synthesized using a one pot reaction followed by calcinations at 450 °C for 3 h and were tested for their photocatalytic efficacy in degradation of phenol both in free and immobilized form under solar light irradiation through batch experiments. Results showed that Ag-TiO₂

nanoparticles were found to be effective in solar photocatalytic degradation of phenols.

21. Camposeco et.al., in 2016 investigated that Nanotubes, nanofibers and nanowires were prepared by TiO₂ surface modification using different concentration of NaOH. The prepared samples surface area, pore volume and pore size of the TiO₂ changed with NaOH treatment. These nanoparticles shows enhanced activity towards degradation of methylene blue and methyl orange in basic and acid conditions.
22. Duran-Alvarez et.al. reported in 2016. Heterogeneous photocatalysis with TiO₂ can effectively remove antibiotics from water using UV light, but it was significantly decreased under sunlight irradiation. Therefore, to increase the effectiveness of TiO₂, the studies were carried by using a metallic nanoparticle such as Au, Ag and Cu deposition on TiO₂. Result shows more effective removal of antibiotic with less toxic by products within the visible spectrum.

1.12 Objectives of the Work

The main objective of the research is to study the degradation of waste-water containing pharmaceuticals and dyes which are not easily mineralized by biological and conventional treatment methods employed in the industry. In this thesis an attempt has been made to improve the degradation efficiency of photocatalysts.

To study the

- a. Degradation rate of photocatalytic reaction**
- b. Effect of UV irradiation on rate of photocatalytic reaction.**
- c. Effect of dosage on rate of photocatalytic reaction.**
- d. Effect of substrate on rate of photocatalytic reaction.**
- e. Effect of pH rate on of photocatalytic reaction.**
- f. Effect of light intensity on rate of photocatalytic reaction.**

References

1. D.A. Bryant and N.U. Frigaard, "Prokaryotic photosynthesis and phototrophy illuminated" *Trends in Microbial.* Vol.14, 2006, pp. 488-496.
2. D.W. Kolpin, E.T. Furlong, M.T. Meyer, E.M. Thurman, S.D. Zaugg, L.B. Barber and H.T. Buxton, "Pharmaceuticals, hormones, and other organic wastewater contaminants in U.S. streams, 1999-2000: a national reconnaissance", *Environ Sci Technol.* Vol. 36 (6), 2002, pp. 1202-1211.
3. P.J. Squillace, J.C. Scott, M.J. Moran, B.T. Nolan, and D. Kolpin, "VOCs, pesticides, nitrate, and their mixtures in groundwater used for drinking water in the United States". *Environ. Sci. Technol.* Vol. 36, 2002, pp. 1923-1930.
4. K. Kummerer, "Pharmaceuticals in the Environment", *Annual Review of Environment and Resources.* Vol. 35, 2010, pp. 57-75.
5. B. Halling-Sorensen, S. Nors-Nielsen, P.F. Lansky, F. Ingerslev, H.C. Holten Lutzhoft, and S.E. Jorgensen, "Occurrence, Fate, and Effects of Pharmaceutical Substances in the Environment- a Review", *Chemosphere.* Vol. 36 (2), 1998, pp. 357-393.
6. K. Kummerer, "Resistance in the environment", *J. Antimicrob Chemother.* Vol. 54 (2), 2004, pp. 311-320.
7. T.A. Ternes, M. Meisenheimer, D. McDowell, F. Sacher, H.J. Brauch, B. Haist-Gulde, G. Preuss, U. Wilme and N. Zulei-Seibert, "Removal of pharmaceuticals during drinking water treatment". *Env. Sci. Tech.* Vol. 36, 2002, pp. 3855-3863.
8. D. Kolpin, E. Furlong, M. Meyer, E. Thurman, S. Zaugg, L. Barber, and H. Buxton "Pharmaceuticals, hormones, and other organic wastewater contaminants in U.S. streams, 1999-2000: a national reconnaissance". *Env. Sci. Tech.* Vol. 36, 2002, pp. 1202-1211.
9. T. Ternes, "Occurrence of drugs in German sewage treatment plants and rivers". *Wat. Res.* Vol. 32, 1998, pp. 3245-3260.
10. P.C. Sharma, A. Jain and S. Jain, "Fluoroquinolone antibacterial: a review on chemistry, Microbiology and therapeutic prospects", *Acta Poloniae Pharmaceutica-Drug Res.* Vol. 66, 2009, pp. 587-604.
11. P. Wang, Y.L. He and C.H. Huang, "Oxidation of fluoroquinolone antibiotics and structurally related amines by chlorine dioxide: Reaction kinetics, product and pathway", *Eval. Water. res.* Vol. 44, 2010, pp. 5989-5998.

12. E. Rubinstein, "History of quinolones and their side effects." *Chemotherapy*. Vol. 47, 2001, pp. 3-8.
13. J.W. Verhoeven. "Glossary of Terms Used in Photochemistry", *Pure and Applied Chemistry*. Vol. 68, 1996, pp. 2223-2286.
14. The American Society of Health-System Pharmacists. Retrieved Aug 1, 2015.
15. T. Shimada, Y. Nogita and Ishifashi, "Clinical pharmacokinetics of sparfloxacin", *Clin. pharmacokinet.* Vol. 25, 1993, pp. 358-369.
16. G. Montay, "Pharmacokinetics of sparfloxacin in healthy volunteers and patients: a review", *J. Antimicrob. Chemother.* Vol. 37, 1996, pp. 27-39.
17. R. Wise, D. Honeybourne, "A review of the penetration of sparfloxacin into the lower respiratory tract and sinuses", *J. Antimicrob. Chemother.* Vol. 37, 1996, pp. 57-63.
18. J.H. Weisburger, "Comments on the history and importance of aromatic and heterocyclic amines in public health", *Mutat. Res.* Vol. 506-507, 2002, pp. 9-20.
19. D. Beydoun, R. Amal, G. Low and S. McEvoy, "Role of nanoparticles in photocatalysis". *J. Nano. Res.* Vol. 1, 1999, pp. 439-458.
20. R. Matthews, "Photocatalysis in Water Purification: Possibilities, Problems and Prospects, Ollis D.F. and Al-Ekabi H. eds. *Photocatalytic Purification and Treatment of Water and Air*", (New York), Elsevier Science Publishers, (1993) pp. 121-139.
21. R.W. Sabnis, "Handbook of Acid-Base Indicators". CRC Press. (2007). ISBN 0-8493-8218-1.
22. R.W. Sabnis, "Handbook of Biological Dyes and Stains: Synthesis and Industrial Applications (1st ed.)". Wiley. (2010). ISBN 0-470-40753-0.
23. C.R. Foden and J. L. Weddell, *Hazardous Materials: Emergency Action Data*, CRS Press.
24. S. Malato, J. Blanco, A. Vidal, and C. Richter, "Photocatalysis with solar energy at a pilot-plant scale: an overview", *App. Cat. B: Env.* Vol. 37, 2002, pp. 1-15.
25. M.I. Maldonado, P.C. Passarinho and I. Oller, "Photocatalytic degradation of EU priority substances: a comparison between TiO₂ and fenton plus photo-fenton in a solar pilot plant" *J. Photochem. Photobio. A.* Vol. 185 (2-3), 2007, pp. 354-363.
26. F. Akbal and A.N. Onar, "Photocatalytic degradation of phenol", *Env. Monit. Ass.* Vol. 83, 2003, pp. 295-302.
27. W.Y. Han, W.P. Zhu, P.Y. Zhang, Y. Zhang and L.S. Li, "Photocatalytic degradation of phenol in aqueous solution under irradiation of 254 and 185 nm UV light", *Cat. Today.* Vol. 90, 2004, pp. 319-324.

28. M. Qamar, M. Muneer and D. Bahnemann, "Heterogeneous photocatalysed degradation of two selected pesticide derivatives, triclopyr and daminozid in aqueous suspensions of titanium dioxide". *J. Env. Manage.* Vol. 80, 2006, pp. 99-106.
29. M.P. Titus, V.G. Molina, M.A. Banos, J. Gimenez and S. Esplugas, "Degradation of chlorophenols by means of advanced oxidation processes: a general review", *Appl. Catal. B.* Vol. 47, 2004, pp. 219-256.
30. N.M. Mahmoodi, M. Arami, N.Y. Limaee, and N.S. Tabrizi, "Kinetics of heterogeneous photocatalytic degradation of reactive dyes in an immobilized TiO₂ photocatalytic reactor". *J. Colloid. Interface Sci.* Vol. 295, 2006, pp. 159-164.
31. A. Vohra, D.Y. Goswami, D.A. Deshpande, and S. Block, "Enhanced photocatalytic disinfection of indoor air", *Appl. Catal. B: Environ.* Vol. 25, 2006, pp. 57-65.
32. A. Fujishima, X. Zhang and D.A. Tryk, "Heterogeneous photocatalysis: from water photolysis to applications in environmental cleanup", *Int. J. Hydrogen Energy.* Vol. 32 (14), 2007, pp. 2664-2672.
33. J.P. Wang, Y.Z. Chen, H.M. Feng, S.J. Zhang and H.Q. Yu, "Removal of 2,4-dichlorophenol from aqueous solution by static-air-activated carbon fibers", *J. Colloid Interface Sci.* Vol. 313, 2007, pp. 80-85.
34. J.M. Herrmann, J. Matos, J. Disdier, C. Guillard, J. Laine, S. Malato and J. Blanco, "Solar photocatalytic degradation of 4-chlorophenol using the synergistic effect between titania and activated carbon in aqueous suspension", *Catal. Today.* Vol. 54, 1999, pp. 255-265.
35. S. Malato, J. Blanco, A. Vidal, and C. Richter, "Photocatalysis with solar energy: at a pilot-plant scale: an overview", *App. Cat. B: Env.* Vol. 37 (1): 2002, pp. 1-15.
36. B. Detlef, "Photocatalytic water treatment: solar energy applications", *Solar energy.* Vol. 77, 2004, pp. 445-459.
37. J.M. Herrmann, C. Duchamp, M. Karkmaz, B.T. Hoia, H. Lachheb, E. Puzenat and C. Guillard, "Environmental green chemistry as defined by photocatalysis", *J. Hazard. Mater.* Vol. 146 (3), 2007, pp. 624-629.
38. A. Mills and M. McFarlane, "Current and possible future methods of assessing the activities of photocatalyst films", *Catal. Today.* Vol. 129 (1-2), 2007, pp. 22-28.
39. M. Anne, Fox and M.T. Dulay, "Heterogeneous photocatalysis", *Chem. Rev.* Vol. 93(1), 1993, pp. 341-357.
40. M.R. Hoffmann, S.T. Martin, W. Choi, and D.W. Bahnemann, "Environmental applications of semiconductor photocatalysis", *Chem. Rev.* Vol. 95(1): 1995, pp. 69 - 96.

41. N. Serpone, "Brief introductory remarks on heterogeneous photocatalysis", *Sol. Energy Mat. Sol. Cell.* Vol. 38(1-4), 1995, pp. 369-379.
42. E. Bessa, G.L. Sant'Anna Jr, and M. Dezotti, "Photocatalytic/H₂O₂ treatment of oil field produced waters", *Appl. Catal. B: Env.* Vol. 29, 2001, pp. 125-134.
43. I. Salem, "Recent studies on the catalytic activity of titanium, zirconium, and hafnium oxides", *Catal. Rev.* Vol. 45, 2003, pp. 205-296.
44. K. Byrappa, A.K. Subramani, A. S. Ananda, K M L Rai and R. Dinesh M. Yoshimura "Photocatalytic degradation of Rhodamine B dye using hydrothermally synthesized ZnO", *Bullet. Mat. Sci.* Vol. 29, 2006, pp. 433-438.
45. J.A. Rodri'guez and M. Ferna'ndez-Garci'a, "Synthesis, Properties and Application of Oxide Nanoparticles", Wiley, USA. 2007
46. J.W. Verhoeven, "Glossary of Terms Used in Photochemistry", *Pure & Appl. Chem.* Vol. 68, 1996, pp. 2223-2286.
47. L. Frazer, "Titanium Dioxide: Environmental White Knight", *Environ. Health. Perspect.* Vol. 109, 2001, pp. A-174 - A-177.
48. A. Fujishima, T.N. Rao, and D.A. Tryk, "Titanium Dioxide Photocatalysis", *J. Photochem. Photobio. C: Photochem. Rev.* Vol. 1, 2000, pp. 1-21.
49. D.A. Tryk, A. Fujishima, and K. Honda "Recent Topics in Photoelectrochemistry: Achievements and Future Prospects", *Electrochimica Acta.* Vol. 45, 2000, pp. 2363-2376.
50. Y. Li, X. Li, J. Li, and J. Yin, "Photocatalytic degradation of methyl orange by TiO₂-coated activated carbon and kinetic study", *Water Res.* Vol. 40, 2006, pp. 1119-1126.
51. Z. Zheng, H. Liu, J. Ye, J. Zhao, E.R. Waclawik, and H. Zhu, "Structure and contribution to photocatalytic activity of the interfaces in nanofibers with mixed anatase and TiO₂ (B) phases", *J. Mol. Catal. A: Chemical.* Vol. 316, 2010, pp. 75-82.
52. S. Bakardjieva, V. Stengl, L. Szatmary, J. Subrt, J. Lukac, N. Murafa, D. Niznansky, K. Cizek, J. Jirkovsky and N. Petrova, "Transformation of brookite type TiO₂ nanocrystal to rutile, Correlation between microstructure and photoactivity", *J. Mater. Chem.* Vol. 16, 2006, pp. 1709-1716.
53. J.P. Wang, Y.Z. Chen, H.M. Feng, S.J. Zhang and H.Q. Yu. Removal of 2, 4-dichlorophenol from aqueous solution by static-air-activated carbon fibers. *J. Colloid Interface Sci.* Vol. 313, 2007, pp. 80-85.

54. J.M. Herrmann, J. Matos, J. Disdier, C. Guillard, J. Laine, S. Malato, and J. Blanco “Solar photocatalytic degradation of 4-chlorophenol using the synergistic effect between titania and activated carbon in aqueous suspension”, *Catal.Today*. Vol. 54, 1999, pp. 255-265.
55. E. R. Carraway, A. J. Hoffman and M. R. Hoffmann, “Photocatalytic oxidation of organic acids on quantum-sized semiconductor colloids”, *Env. Sci. Tech*. Vol. 28, 1994, pp. 786-793.
56. B. Pal and M. Sharon, “Enhanced photocatalytic activity of highly porous ZnO thin film, prepared by Sol-Gel process”. *Mater. Chem and Phys*. Vol. 76, 2002, pp. 82-87.
57. I. Poullos, D. Makri and X. Prohaska, “Photocatalytic treatment of olive milling waste water: oxidation of protocatechuic acid”, *Global Nest: The Int. J*. Vol. 1, 1999 pp. 55-62.
58. K.Y. Jung, Y.C. Kang and S.B. Park, “Photodegradation of trichloroethylene using nanometre-sized ZnO particles prepared by spray pyrolysis” *J. Mat. Sci. Lett*. Vol. 16, 1997, pp. 1848-1849.
59. S. Sakthivel, B. Neppolian, M. V. Shankar, B. Arabindoo, M. Palanichamy and V. Murugesan, “Solar photocatalytic degradation of azo dye: comparison of photocatalytic efficiency of ZnO and TiO₂”, *Sol. Energ. Mat. Sol. Cells*. Vol. 77, 2003, pp. 65-82.
60. R. Wang, J.H. Xin, Y. Yang, H. Liu, L. Xu and J. Hu, “The Characteristics and Photocatalytic Activities of Silver Doped ZnO Nanocrystallites”, *Appl. Surf. Sci*. Vol. 227, 2004, pp. 312-317.
61. J. Wang, W. Sun, Z. Zhang, Z. Jiang, X. Wang, R. Xu, R. Li and X. Zhang, “Preparation of Fe-doped mixed crystal TiO₂ catalyst and investigation of its sonocatalytic activity during degradation of azo fuchsine under ultrasonic irradiation”, *J. Colloid Interface Sci*. Vol. 320 (1), 2008, pp. 202-209.
62. S. Liao, H. Donggen, D. Yu, Y. Su, and G. Yuan, “Preparation and characterization of ZnO/TiO₂, SO₄/ZnO/TiO₂ photocatalyst and their photocatalysis”, *J. Photochem. Photobiol. A*. Vol. 168, 2004, pp. 7-13.
63. C. Chen, Z. Wang, S. Ruan, B. Zou, M. Zhao and F. Wu, “Photocatalytic degradation of C.I. acid orange 52 in the presence of Zn-doped TiO₂ prepared by a stearic acid gel method”, *Dyes Pigments*. Vol. 77, 2008, pp. 204-209.

64. T. Tong, J. Zhang, B. Tian, F. Chen and D. He, "Preparation of Fe³⁺-doped TiO₂ catalysts by controlled hydrolysis of titanium alkoxide and study on their photocatalytic activity for methyl orange degradation", *J. Hazard. Mater.* Vol. 155 (3), 2008, pp. 572-579.
65. L. Deng, S. Wang, D. Liu, B. Zhu, W. Huang, S. Wu and S. Zhang, "Synthesis, Characterization of Fe-doped TiO₂ Nanotubes with High Photocatalytic Activity", *Catal. Lett.* Vol. 129 (3-4), 2009, pp. 513-518.
66. Y.L. Pang and A.Z. Abdullah, "Effect of Low Fe³⁺ Doping on Characteristics, Sonocatalytic Activity and Reusability of TiO₂ Nanotubes Catalysts for Removal of Rhodamine B From Water", *J. Hazard. Mater.* Vol. 235-236, 2012, pp. 326-335.
67. S. Penner, "Steps toward the hydrogen economy" *Energy.* Vol. 31, 2006, pp. 33-43.
68. H.J. Choi, M. Kang, "Hydrogen production from methanol/water decomposition in a liquid photosystem using the anatase structure of Cu loaded TiO₂," *Int. J. Hydrogen Energy.* Vol. 32, 2007, pp. 3841-3848.
69. L.S. Yoong, F.K. Chong and B.K. Dutta, "Development of copper-doped TiO₂ photocatalyst for hydrogen production under visible light", *Energy.* Vol. 34 (10), 2009, pp. 1652-1661.
70. H.M. Wu, J. P. Tu, Y. F. Yuan, X. T. Chen, J. Y. Xiang, X. B. Zhao, and S. Cao, "One-step synthesis LiMn₂O₄ cathode by a hydrothermal method", *J Power Sources.* Vol. 161, 2006, pp. 1260-1263.
71. S.T. Myung, S. Komaba and N. Kumagai, "Hydrothermal synthesis and electrochemical behavior of orthorhombic LiMnO₂", *Electrochim. Acta.* Vol. 47, 2002, pp. 3287-3295.
72. G. Meligrana, C. Gerbaldi, A. Tuelb, S. Bodoardo and N. Penazzi, "Hydrothermal synthesis of high surface LiFePO₄ powders as cathode for Li-ion cells", *J. Power Sources.* Vol. 160, 2006, pp. 516-522.
73. T. Zhang, C. G. Jin, T. Qian, X. L. Lu, J. M. Baia and X. G. Li, "Hydrothermal synthesis of single-crystalline La_{0.5}Ca_{0.5}MnO₃ nanowires at low temperature", *J. Mater. Chem.* Vol. 14, 2004, pp. 2787-2789.
74. T.M. Tritt, H. Böttner, and L.D. Chen, "Thermoelectrics: direct solar thermal energy conversion", *MRS Bull.* Vol. 33, 2008, pp. 366-368.
75. A.G. Merzhanov, and I.P. Borovinskaya, "Self-propagated high-temperature synthesis of refractory inorganic compounds", *Doklady Akademii Nauk SSSR.* Vol. 204, 1972, pp. 366-369.

76. C.J. Brinker and G.W. Scherer, "Sol - gel science: The Physics and the chemistry of sol gel processing", Academic Press, Inc. London, (1990).
77. Y. Lin, H. Skaff, T. Emrick, A.D. Dinsmore, and T.P. Russell, "Nanoparticle Assembly and Transport at Liquid-Liquid Interfaces" *Science*. Vol. 299, 2003, pp. 226-229.
78. H. Haun, "Gas phase synthesis of nanocrystalline materials", *Nanostruct. Mater.* Vol. 9 (1-8), 1997, pp. 3-12.
79. W. Chang, G. Skandan, H. Hahn, S.C. Danforth, and B.H. Kear," Chemical vapor condensation of nanostructured ceramic powders", *Nanostructured Materials*. Vol. 4(3), 1994, pp. 345-351.
80. A. Konrad, U. Herr, R. Tidecks, and F. Samwer," Luminescence of bulk and nanocrystalline cubic yttria" *J. of Appl. Phys.* Vol. 90 (7), 2001, pp. 3516-3523.
81. M. Winterer, H. Hahn, and Z. Metallkd, "Chemical Vapor Synthesis of Nanocrystalline Powders ", *Nanoceramics by Chemical Vapor Synthesis*. Vol. 94, 2003, pp. 1084-1090.
82. A. Konrad, U. Herr, R. Tidecks, and F. Samwer, " Luminescence of bulk and nanocrystalline cubic yttria" *J. of Appl. Phys.* Vol. 90 (7), 2001, pp. 3516-3523.
83. A.A. Rostislav, "The synthesis and properties of nanocrystalline refractory compounds" *Russ. Chem. Rev.* Vol. 63, 1994, pp. 411-427.
84. A.B. Sharma, M. Sharma, and R.K. Pandey, "Synthesis, Properties and Potential Applications of Semiconductor Quantum Particles" *Asian Journal of Chemistry*. Vol. 21(10), 2009, pp S033-038.
85. M.V. Shankar, S. Anandan, N. Venkatachalam, B. Arabindoo and V. Murugesan, "Novel thin-film reactor for photocatalytic degradation of pesticides in aqueous solutions", *J. Chem. Technol. Biotechnol.* Vol. 79, 2004, pp. 1279-1285.
86. M.V. Shankar, K.K. Cheralathan, B. Arabindoo, M. Palanichamy and V. Murugesan "Enhanced photocatalytic activity for the destruction of monocrotophos pesticide by TiO₂/H". *J. Mol. Catal.* Vol. 223, 2004, pp.195-200.
87. A.Piscopo, D. Robert, and J.V. Weber, "Influence of pH and chloride on the photocatalytic degradation of organic compounds. I. Effect on the benzamide and parahydroxybenzoic acid in TiO₂ aqueous solution". *Appl.Catal. B: Environ.* Vol. 35, 2001, pp. 117-124.
88. G. Marci, V. Augugliaro, A. B. Prevot, C. Baiocchi, E. Garcia-Lopez, V. Loddo, L. Palmisano, E. Pramauro, M. Schiavello, "Photocatalytic Oxidation of Methyl-Orange

- in Aqueous Suspension: Comparison of the Performance of Different Polycrystalline Titanium Dioxide”, *Annali di Chimica*. Vol. 93, 2003, pp. 639-648.
89. V. Augugliaro, C. Baiocchi, A. Bianco-Prevot, E. Garcia-Lopez, V. Loddo, S. Malato, G. Marci, L. Palmisano, M. Pazzi, E. Pramauro, Azo-dyes Photocatalytic Degradation in Aqueous Suspension of TiO₂ under Solar Irradiation, *Chemosphere*. Vol. 49, 2002, pp. 1223-1230.
90. Lachheb H., Puzenat E., A. Houas, M. Ksibi, E. Elaloui, C. Guillard and J.M. Herrmann, “Photocatalytic degradation of various types of dyes (Alizarin S, Crocein Orange G, Methyl Red, Congo Red, Methylene Blue) in water by UV-irradiated titania”, *Appl. Catal. B. Environ.* Vol. 39, 2002, pp.75-90.
91. A. Piscopo, D. Robert, J.V. Weber, Influence of pH and chloride anion on the photocatalytic degradation of organic compounds. Part I. Effect on the benzamide and para hydroxybenzoic acid in TiO₂ aqueous solution. *Appl. Catal. B: Environ.* Vol. 21, 2001, pp. 1-8.
92. K. Naeem and O. Feng, “Parameters effect on heterogeneous photocatalysed degradation of phenol in aqueous dispersion of TiO₂”, *J. Environ. Sci.* Vol. 21, 2009, pp. 527-533.
93. N. Guettaï, H.A. Amar, “Photocatalytic oxidation of methyl orange in presence of titanium dioxide in aqueous suspension. Part I: Parametric study”, *Desalin.* Vol. 185: 2005, pp. 427-437.
94. G. Pecchi, P. Reyes, P. Sanhueza and J. Villasenor, “Photocatalytic degradation of pentachlorophenol on TiO₂ sol-gel catalysts”, *Chemosphere*. Vol. 43, 2001, pp. 141-146.
95. T.G. Sauer, C. Neto, H.J. José, R.F.P.M. Moreira, “Kinetics of photocatalytic degradation of reactive dyes in a TiO₂ slurry reactor”, *J. Photochem. Photobiol. A Chem.* Vol. 149 (1-3), 2002, pp. 147-154.
96. C. Zhu, L. Wang, L. Kong, X. Yang, S. Zheng, F. Chen, F. Maizhi, and H. Zong, “Photocatalytic degradation of azo dyes by supported TiO₂/UV in aqueous solution”. *Chemosphere*. Vol. 41, 2000, pp. 303-309.
97. G.A. Epling, and C. Lin, “Photoassisted bleaching of dyes utilizing TiO₂ and visible light”, *Chemosphere*. Vol. 46, 2002, pp. 561-570.
98. I.K. Konstantinou and T.A. Albanis, “TiO₂-Assisted Photocatalytic Degradation of Azo Dyes in Aqueous Solution: Kinetic and Mechanistic Investigations,” *Appl. Catal. B Environ.* Vol. 49, 2004, pp. 1-14.

99. M. Mahalakshmi, S.V. Priya, B. Arabindoo, M. Palanichamy and V. Murugesan, "Photocatalytic degradation of aqueous propoxur solution using TiO₂ and H₂Zeolite-supported TiO₂", *J. Hazard. Mater.* Vol. 161, 2009, pp. 336-343.
100. C. Chiou, C. Wu, R. Juang, "Influence of operating parameters on photocatalytic degradation of phenol in UV/TiO₂ process", *Chem. Eng. J.* Vol. 139 (2), 2008, pp. 322-329.
101. P.D. Vaidya, and V.V. Mahajani, Insight into heterogeneous catalytic wet oxidation of phenol over a Ru/TiO₂ catalyst. *Chem. Eng. J.* Vol. 87, 2002, pp. 403-416.
102. S. Rabindranathan, D.P. Suja, S. Yesodharan, "Photocatalytic degradation of phosphamidon on semiconductor oxides", *J. Hazard. Mater. B*, Vol. 102, 2003, pp. 217- 229.
103. S. Lathasree, A.N. Rao, B. SivaSankar, V. Sadasivam and K. Rengaraj, "Heterogeneous photocatalytic mineralization of phenols in aqueous solutions", *J. Mol. Catal.A: Chem.* Vol. 223, 2004, pp. 101-105.
104. A. Burns, W. Li, C. Baker and S.I. Shah, "Sol-gel synthesis and characterization of neodymium-ion doped nanostructured titania thin film", *Mater. Res. Soc. Symp. Proc.* Vol.703, 2002, pp.193-198.
105. S.F. Chen and Y.Z. Liu, "Study on the photocatalytic degradation of glyphosate by TiO₂ photocatalyst", *Chemosphere.* Vol. 67 (5), 2007, pp. 1010-1017.
106. M.F. Kabir, E. Vaisman, C.H. Langford and A. Kantzas, "Effects of hydrogen peroxide in a fluidized bed photocatalytic reactor for wastewater purification", *Chem. Eng. J.* Vol. 118, 2006, pp. 207-212.
107. O. Legrini, E. Oliveros, and A.M. Braun, "Photochemical process for water treatment", *Chem.Rev.* Vol. 93, 1993, pp. 671-698.

Chapter 2

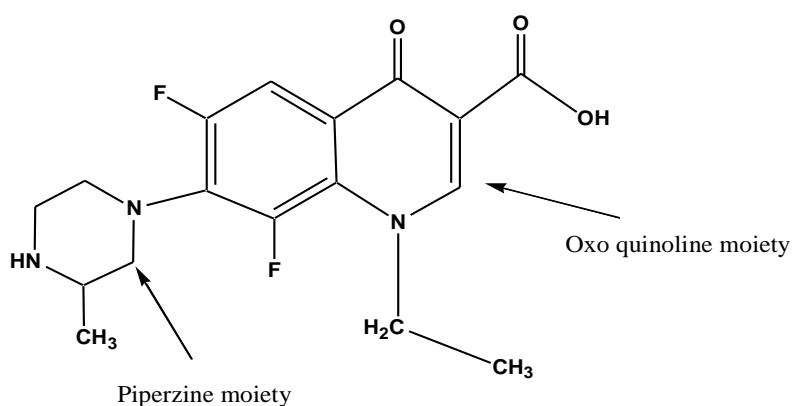
Ag-TiO₂ nanoparticles for photocatalytic degradation of lomefloxacin

2.1 Introduction

Advanced oxidation processes (AOPs) are most widely used for the treatment of toxic persistent organic contaminants present in aqueous environment. The conventional and biological methods are not efficient in the treatment of persistent organic contaminants and may produce hazardous by-products. AOPs involve direct formation of hydroxyl (OH[•]) radical, that decompose a plenty of organic contaminants without discrimination [1-3] using chemical or light energy. The AOPs generally involve a semiconductor photocatalyst illuminated by UV or visible light resulting in incomplete or complete mineralization of the organic molecules [4-5]. There are a number of studies associated with use of TiO₂ in the photo mineralization of pharmaceutical compounds [6-7].

The general importance of Titanium dioxide (TiO₂) discussed in chapter 1 (p.12-13).

Lomefloxacin (LMF) is a broad spectrum antibacterial agent of fluoroquinolone family. Fluoroquinolones have been used in large quantity to treat diseases and also for animal feeds. They enter into the environment through excretion of human beings and animals [8].



Chemical Structure of Lomefloxacin (LMF)

There are no reports in the literature related to detailed degradation kinetics of LMF. Hence, the present investigation was taken up to study the photocatalytic degradation of LMF by Ag-TiO₂ nanoparticles in aqueous medium. Ag-TiO₂ nanoparticles were synthesized by Liquid Impregnation (LI) technique. The prepared Ag-TiO₂ nanoparticles were characterized by X-ray diffraction (XRD), Scanning Electron Microscopy (SEM), Energy dispersive X-ray Analysis (EDX) and Transmission Electron Microscopy (TEM). Factors affecting the photocatalytic process viz. pH, LMF concentration and Ag-TiO₂ dosage, intensity of UV light were also studied and discussed.

2.2 Experimental

2.2.1 Materials and Methods

A stock solution of LMF (Gift sample from Dr. Reddy's laboratories) was prepared by dissolving known quantity of sample in deionised water. The TiO₂ (Anatase) sample was procured from Sisco Research Pvt. Ltd. Mumbai. India. AgNO₃ was procured from HIMEDIA. The analar grade chemicals were used to prepare acetate (pH 4.0-5.0), phosphate (pH 6.0-8.5) and borate (pH 9.0) buffers.

Instruments Used

- 1) For kinetic measurements, a CARY 50 Bio UV-Vis Spectrophotometer (Varian BV, The Netherlands) with temperature controller and HPLC system (Agilent 1100 series, USA) were used.



- 2) For degradation study, a photo-reactor with mercury lamp (PHILIPS, TUV 8W T5, $E_{\max} = 254 \text{ nm}$) was used. The typical light intensity illuminated on the surface of reaction mixture was 4 mW/cm^2 .



- 3) For measurements of UV light intensity an optical power meter (Newport 2936 – C) were used.



- 4) pH measurements, Elico pH meter models LI 120 were used.



- 5) For characterization of nanoparticles, a Siemens X-ray Diffractometer (Cu source) (XRD) AXS D5005 was used to identify the particle size of the doped TiO_2 . Shivaji University Kolhapur, Maharashtra (INDIA).



6) The surface morphologies were examined using a Scanning electron microscope (SEM) JEOL JSM 6360 Shivaji University Kolhapur, Maharashtra (INDIA).



7) The topography and particle size of Ag-TiO₂ was measured using JEOL JEM-2010 transmission electron microscopy (TEM) National Institute of Technology Surathkal, Karnataka (INDIA).



2.2.2 Photocatalyst preparation

Ag-TiO₂ (anatase) nanoparticles were prepared by LI method. Slurry of TiO₂ was prepared by adding 500 mg TiO₂ in 100 ml double distilled water. The silver nitrate solution of 1% and 2 % (molar ratio) was added to the slurry. The resulting slurry was thoroughly mixed by vigorous stirring and allowed to settle at room temperature over night. The liquid so obtained was dried in an oven at 100 °C for 12 hrs to get rid of any remaining moisture. The nanoparticles resulting from this step was calcined at 500 °C for 3 hrs in a muffle furnace to get silver doped TiO₂ nanoparticles [9-10].

2.2.3 The Photocatalysis Process

The photocatalysis study was carried out in a photoreactor equipped with 8W UV light source (Phillips) with maximum wavelength at 254 nm. The optical power reaching the surface of photocatalyst was kept at 4 mW/cm². A dose of 0.10 g dm⁻³ of 2% Ag-TiO₂ nanoparticles were added to LMF and buffer solution. Then, it was placed in the photoreactor with continuous stirring. After every 15 minutes interval the solution was taken out and centrifuged at 5000 rpm for 5 min. The decrease in the concentration of LMF was measured at 287 nm ($\epsilon = 27209 \text{ dm}^3 \text{ mol}^{-1} \text{ cm}^{-1}$) using a UV-Vis as shown in Fig. 2.1.

2.3 Results and discussion

2.3.1 Effect of silver doping

Effect of silver doping on anatase TiO₂ was studied by changing the percentage of silver from 1% to 2% (mole ratio) an increase in the content of silver leads to decrease in the particle size and increase in the photocatalytic activity as shown in Fig. 2.2. Smaller particle size increases surface area and higher content silver may also favour separating charge carriers efficiently, inhibiting the recombination of electron-hole pairs, and thus increasing the photocatalytic activity [11]. The rates of photocatalytic degradation of LMF by prepared photocatalysts were compared and it was observed that the degradation effect of LMF treatment with UV/2% Ag-TiO₂ was more efficient than other three treatments namely UV, UV/TiO₂ and UV/1% Ag-TiO₂. The % degradation efficiency of LMF was studied under same conditions with UV, UV/TiO₂, UV/1% Ag-TiO₂ and UV/2% Ag-TiO₂ and % adsorption in dark was also determined. The % degradation efficiency of LMF was found to be 45%, 59%, 77%, and 95% with UV, UV/TiO₂, UV/1% Ag-TiO₂ and UV/2% Ag-TiO₂ respectively within 100 minute as shown in as shown in Fig. 2.3. The photodegradation rate was highest with 2% Ag-TiO₂, hence, further studies were carried out with 2% Ag-TiO₂.

Fig. 2.1. UV–visible spectral changes during the degradation of lomefloxacin at $25 \pm 0.2^\circ\text{C}$, $[\text{LMF}] = 20.00 \times 10^{-5} \text{ mol dm}^{-3}$, $\text{pH} = 4.0$, $2\% \text{ Ag-TiO}_2 = 0.10 \text{ g dm}^{-3}$ and light intensity 4 mW/cm^2 .

Time (1) 00.00 min (2) 15.00 min (3) 30.00 min (4) 45.00 min
(5) 60.00 min

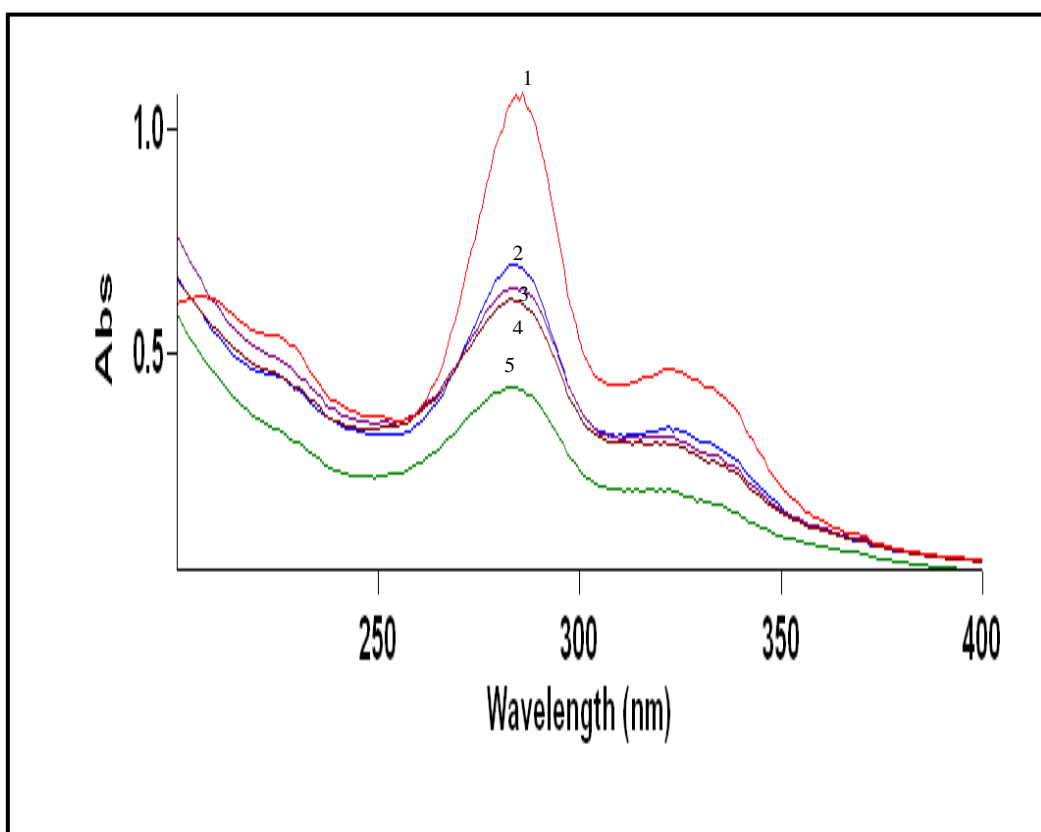


Fig. 2.2. Rate constants for the Photocatalytic degradation of LMF by various treatments $25 \pm 0.2^\circ\text{C}$, $[\text{LMF}] = 20.00 \times 10^{-5} \text{ mol dm}^{-3}$, $\text{pH} = 4.0$, $2\% \text{ Ag-TiO}_2 = 0.10 \text{ g dm}^{-3}$ and light intensity 4 mW/cm^2 .

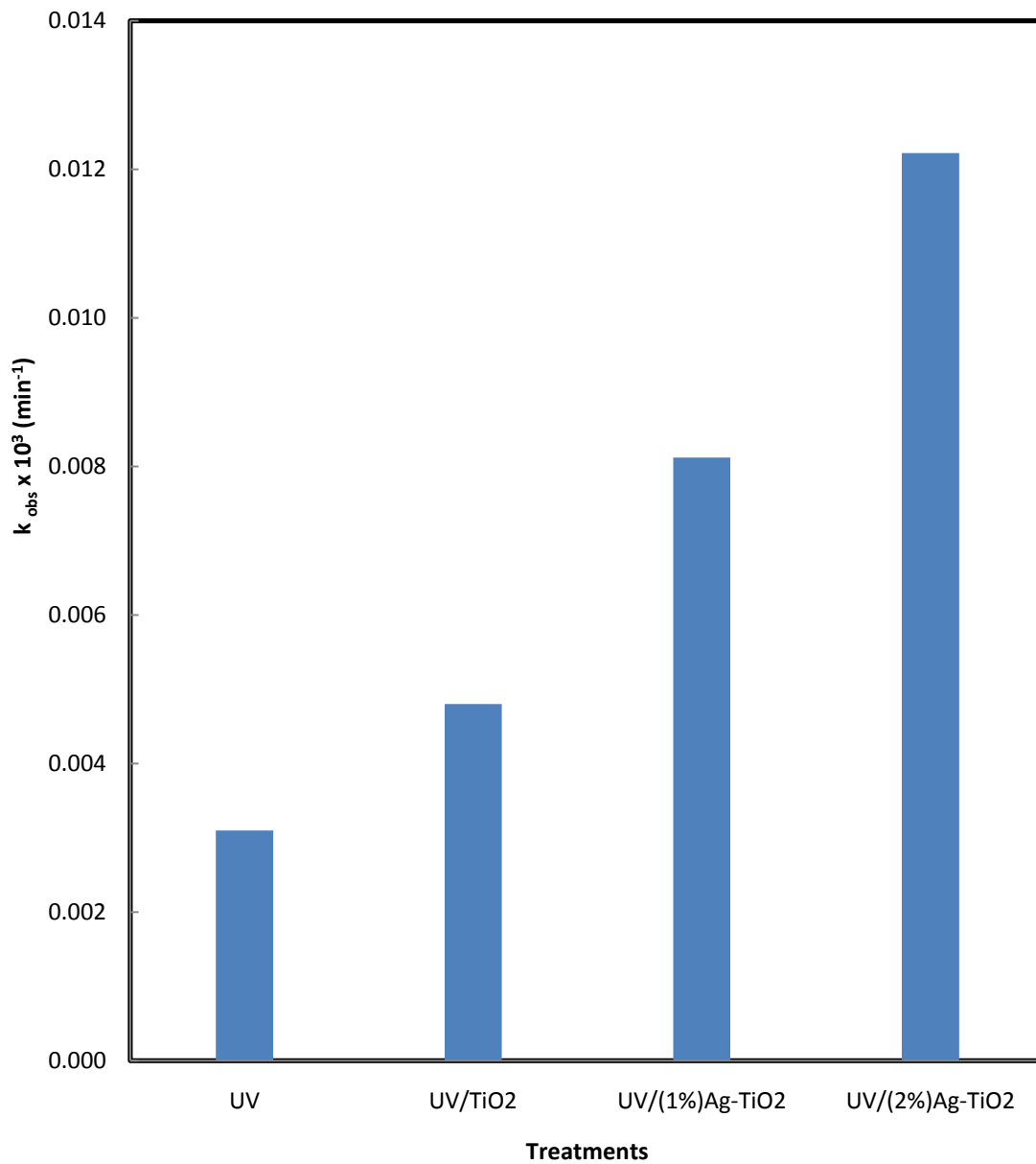
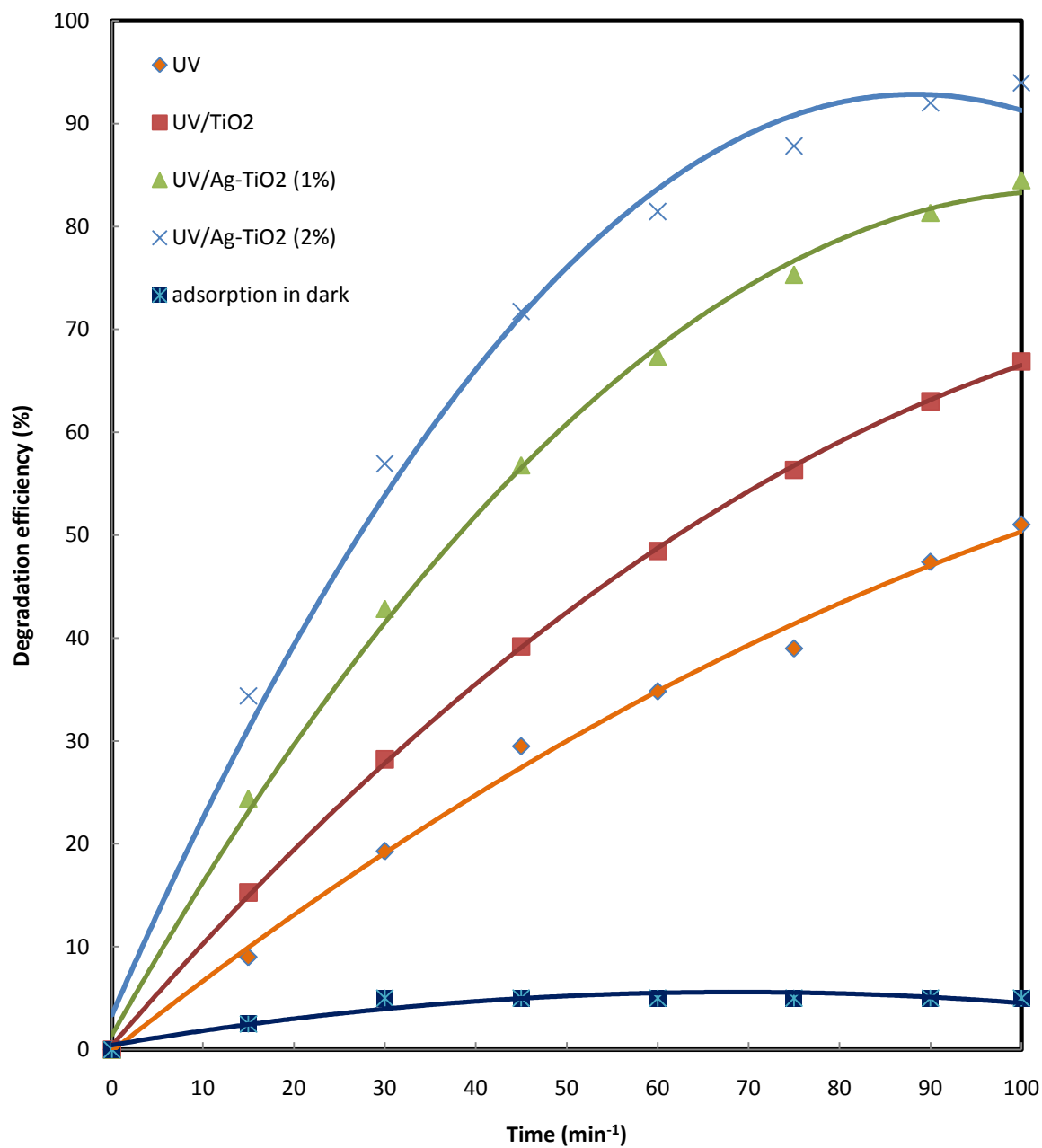


Fig. 2.3. % degradation efficiencies of various treatment methods with time at 25 °C.

[Photocatalyst] = 0.10 g dm⁻³, [LMF] = 20.00 x 10⁻⁵ mol dm⁻³ at pH 4.0 and light intensity 4 mW/ cm².



2.3.2 Characterization of TiO₂ and Ag-TiO₂

2.3.2.1 X-ray Diffraction Studies (XRD)

Identification of crystal phase of prepared nanoparticles was done using X-ray diffractometer (Fig. 2.4.a). The 2θ values indicate that the major phase of all the synthesized nanoparticles is anatase. Scherrer equation was applied to anatase main peak to calculate the average crystallite size of synthesized nanoparticles as shown in Table 2.1. The crystallite size of TiO₂ is of 17.00 nm while the crystallite size of 1% Ag-TiO₂ is 14.17 nm, 2% Ag-TiO₂ 13.07. Our results are in agreement with earlier work [7], where 15.00 nm to 37.00 nm of Ag-TiO₂ nanoparticles sizes were reported.

Calculation of particle size using X-ray diffraction plots

After plotting the XRD plots, particle-size of synthesized nanoparticles were calculated using Scherrer formula.

$$\text{i.e., } D_p = \frac{0.94\lambda}{\beta_{1/2} \cos \theta}$$

Where, D_p = average size of the ordered crystalline.

- k = dimensionless shape factor.
- λ = X-ray wavelength.
- β = line broadening at half the max-intensity (FWHM).
- θ = Bragg angle.

For this equation the maximum peak was considered from the plots and was magnified and re-plotted. In this peak the maximum intensity was found out and at half of that maximum intensity the width of the curve was calculated. This gave us the FWHM. (Width of the rectangle). Maximum angle θ at the maximum intensity was noted down. k was the dimensionless shape factor and is always assumed to be 0.94 the wavelength of the X-rays was found to be 0.154×10^{-9} m (Fig. 2.4.b).

Fig. 2.4 (a). XRD patterns of (a) Undoped TiO_2 , (b) 1% and (c) 2% Ag- TiO_2

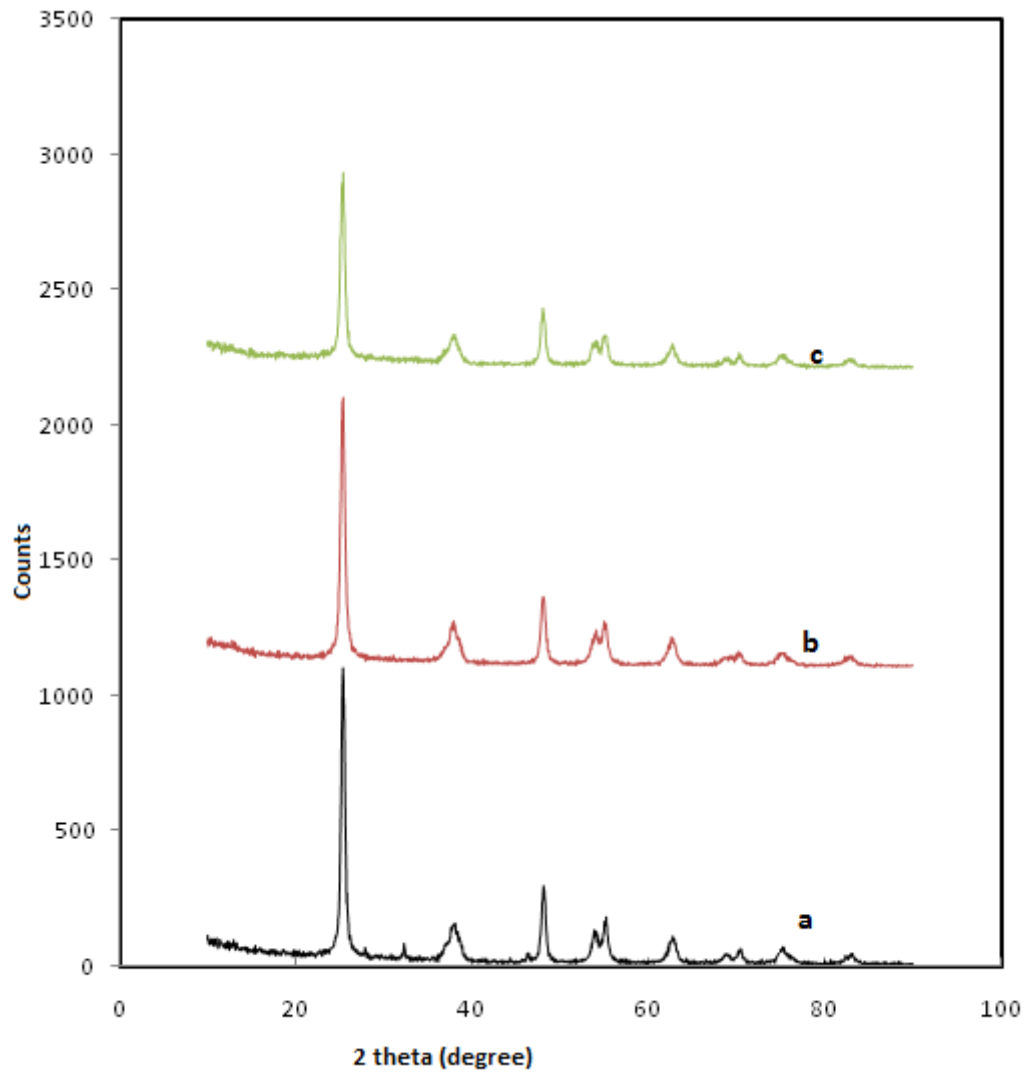
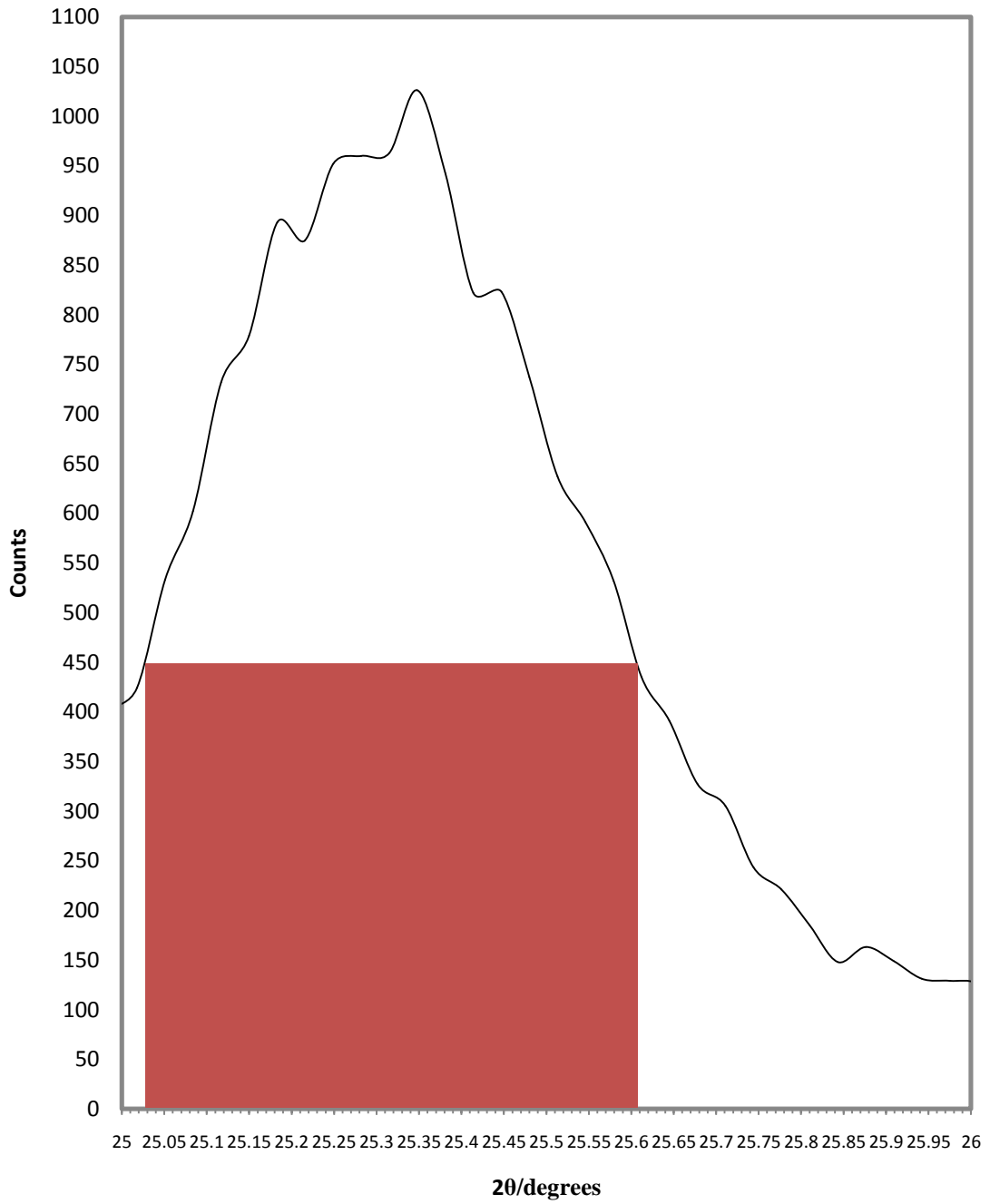


Table 2.1. Crystal size of undoped and Ag doped TiO₂ nanoparticles from Scherrer equation.

Sr. No	Particles	Particle size (nm)
1	Un doped TiO ₂	17.00
2	1% Ag-TiO ₂	14.17
3	2% Ag-TiO ₂	13.07

Fig. 2.4 (b) Calculation of particle size using XRDRD



Substituting the values the calculations were preceded as follows-

$$\lambda = 0.154 \times 10^{-9} \text{ m}$$

$$k = 0.94$$

$$\text{Intensity at maximum peak} = 1024 \text{ cps}$$

$$\text{Angle at the peak } 2\theta = 25.4^\circ$$

$$\text{Half of the intensity} = 512 \text{ cps}$$

$$\text{Full length at half maximum } \beta = 25.6 - 25.05 = 0.5500^\circ$$

$$= 8.727 \times 10^{-3} \text{ radians}$$

$$D_P = \frac{0.94 \times 0.154 \times 10^{-9}}{8.727 \times 10^{-3} \times 0.9956} = 17.00 \text{ nm for TiO}_2$$

Similarly we calculated for 1% Ag-TiO₂ and 2% Ag-TiO₂.

2.3.2.2 Scanning Electron Microscope (SEM)

The SEM images of synthesized Ag-TiO₂ nanoparticles (Fig. 2.5 (a) Fig. 2.5 (b) and Fig. 2.5 (c)) were used to characterize the surface morphology of nanoparticle aggregates. It is evident that the aggregates of the Ag-TiO₂ nanoparticles are heterogeneous and of irregular shape, which results in a high surface area [12].

2.3.2.3 Transmission Electron Microscope (TEM)

TEM images show the heterogeneously dispersed aggregates of Ag-TiO₂ nanoparticles having cylindrical in shape crystalline structures which can be clearly observed in (Fig. 2.6 (a) and Fig. 2.6 (b)). Tiny dark dots seen in TEM were recognized as Ag particles dispersed on TiO₂ nanoparticles with a particle size of approximately 10.00-15.00nm in breadth and 40.00-45.00nm in length. The crystallite size of the synthesized nanoparticles observed in TEM image was close to the values obtained from Scherrer equation.

2.3.2.4 Energy Dispersive X-ray spectroscopy (EDX)

The elemental analysis of synthesized nanoparticles was done using EDX. EDX spectra (Fig. 2.7 (a) and Fig. 2.7 (b)) show that the prepared nanoparticles contains Ti, O and Ag. Ag L peak was found but peak of Ag K cannot be detected because low electron accelerating voltage was applied [13]. The peaks from the spectrum reveal the presence of Ti, O and Ag at 4.508, 0.525 and 2.983 keV respectively. The atomic % of Ti, O and Ag is 77.51, 20.49 and 2.00 respectively. This composition of Ti, O and trace amount of Ag, which leads to better photocatalytic activity.

Fig. 2.5. SEM micrographs of a) Undoped TiO₂, b) 1% Ag - TiO₂ and c) 2% Ag - TiO₂

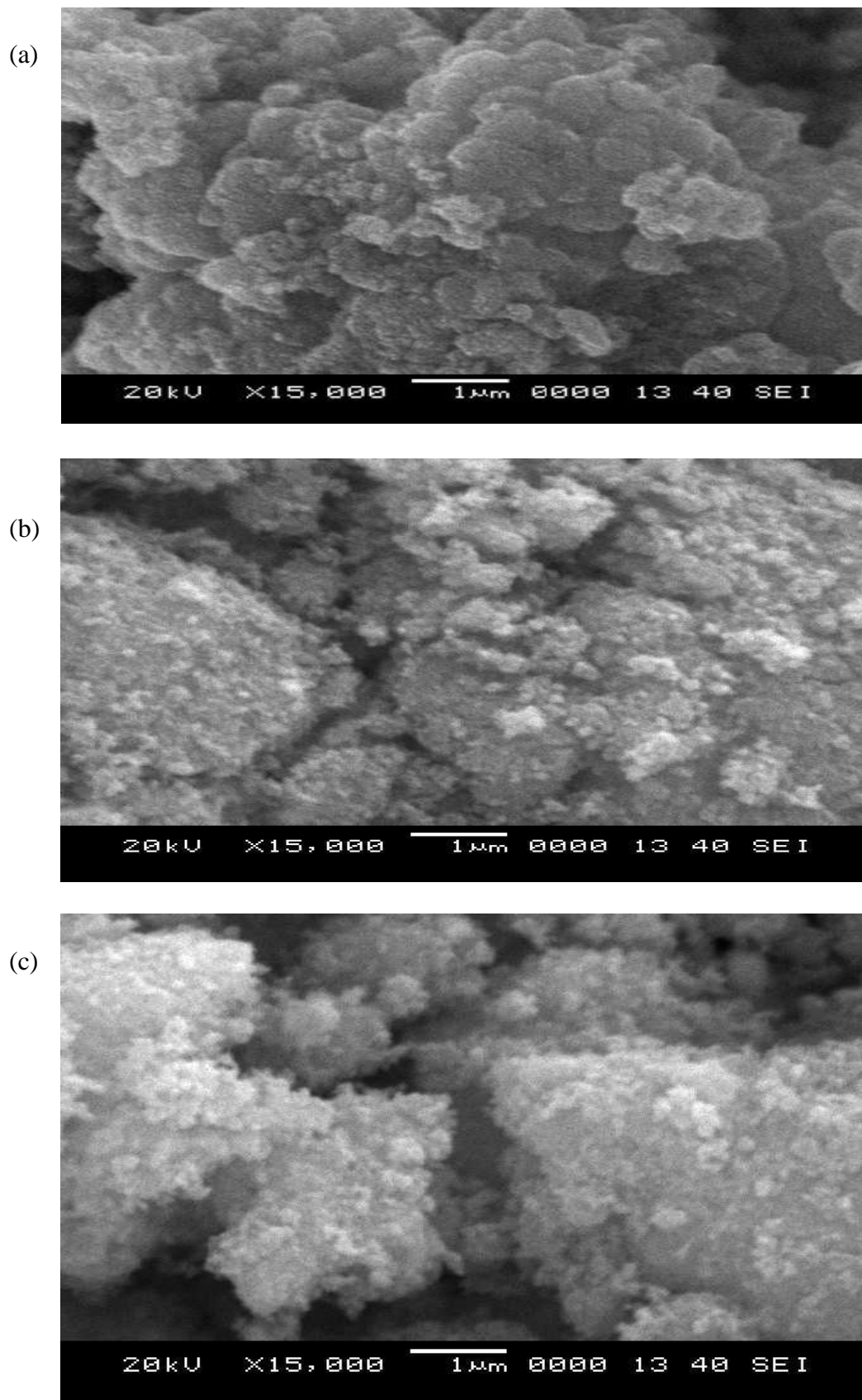
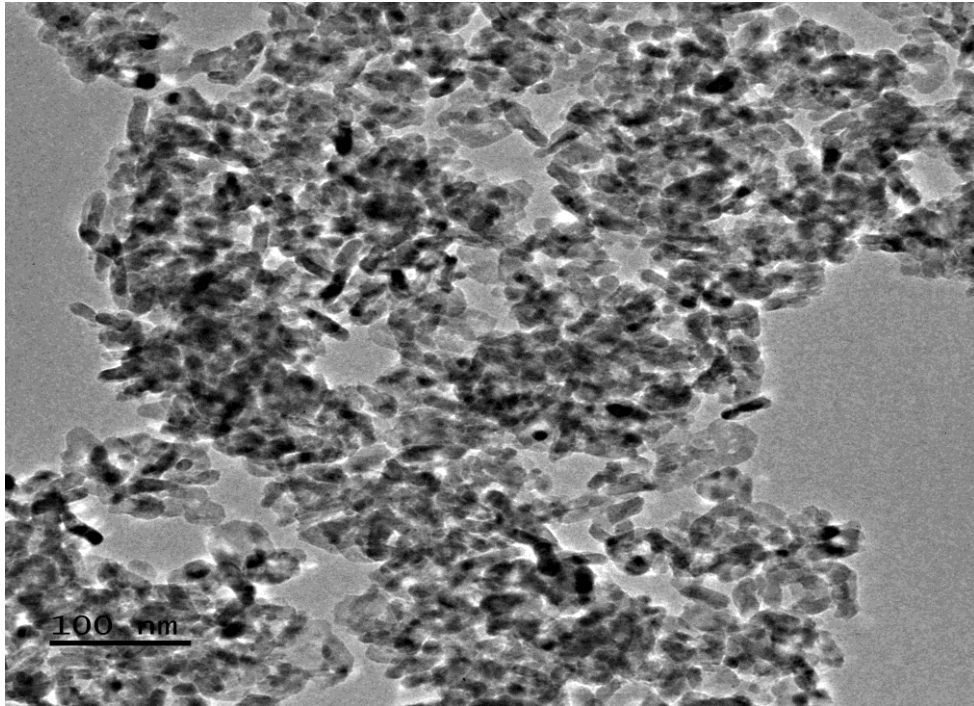


Fig. 2.6. TEM micrographs of (a & b) 2% Ag/TiO₂

(a)



(b)

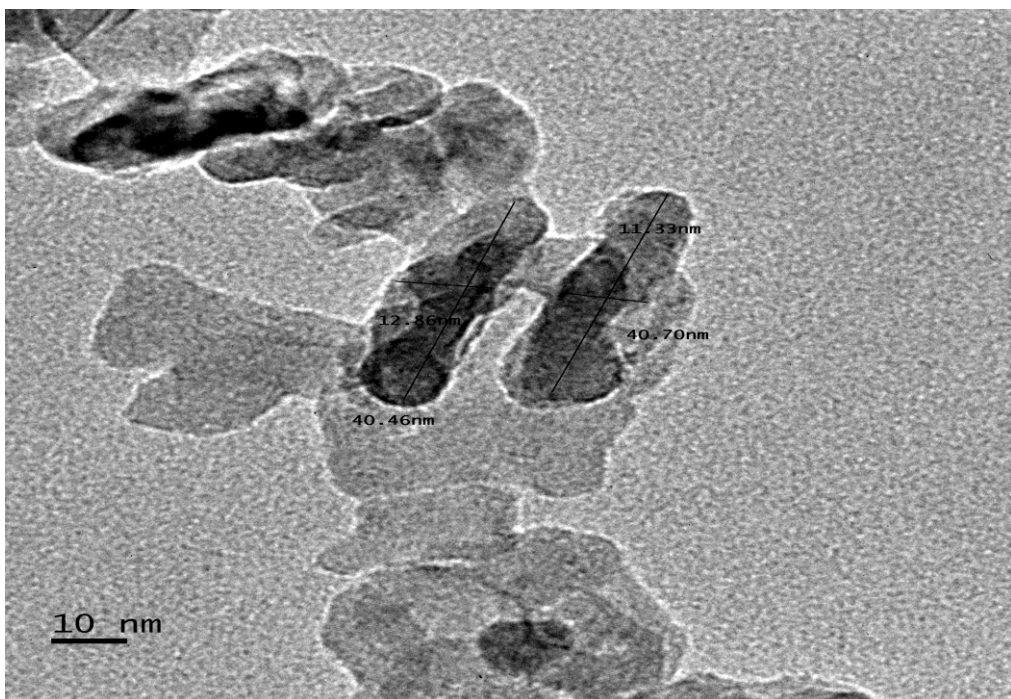
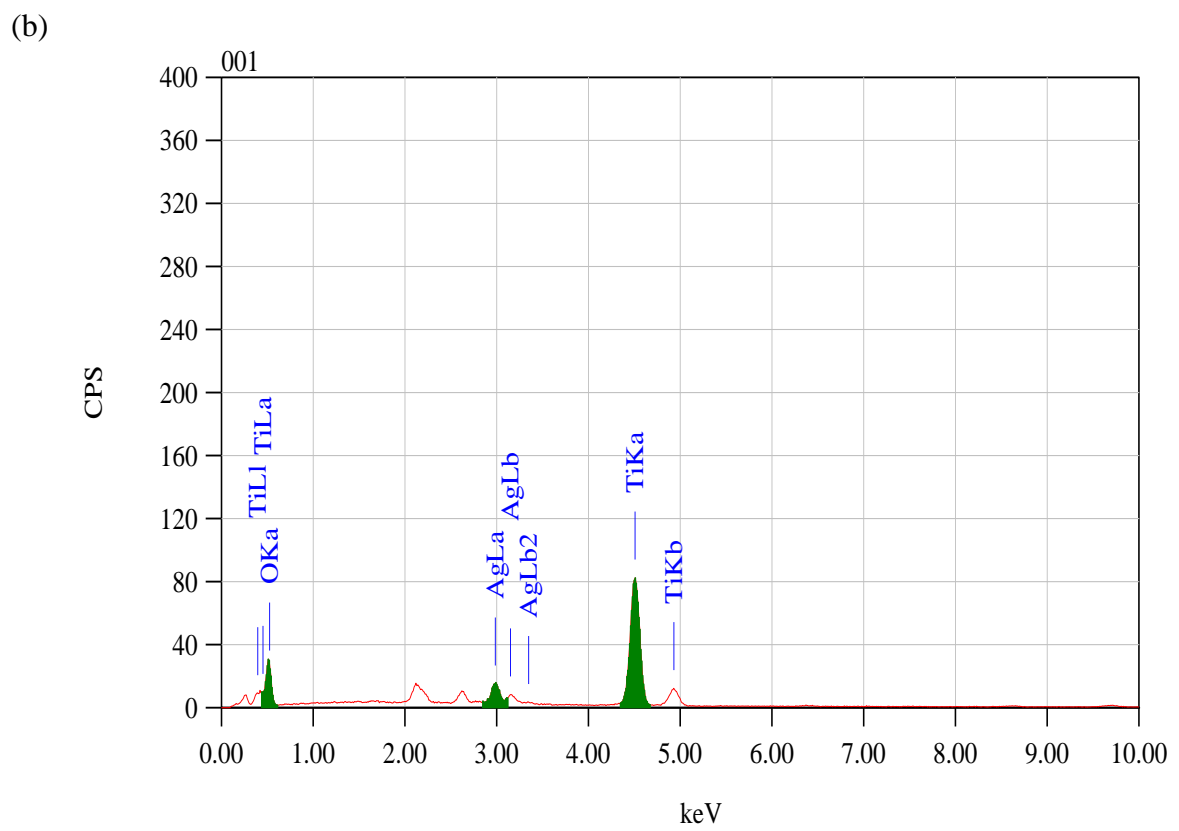
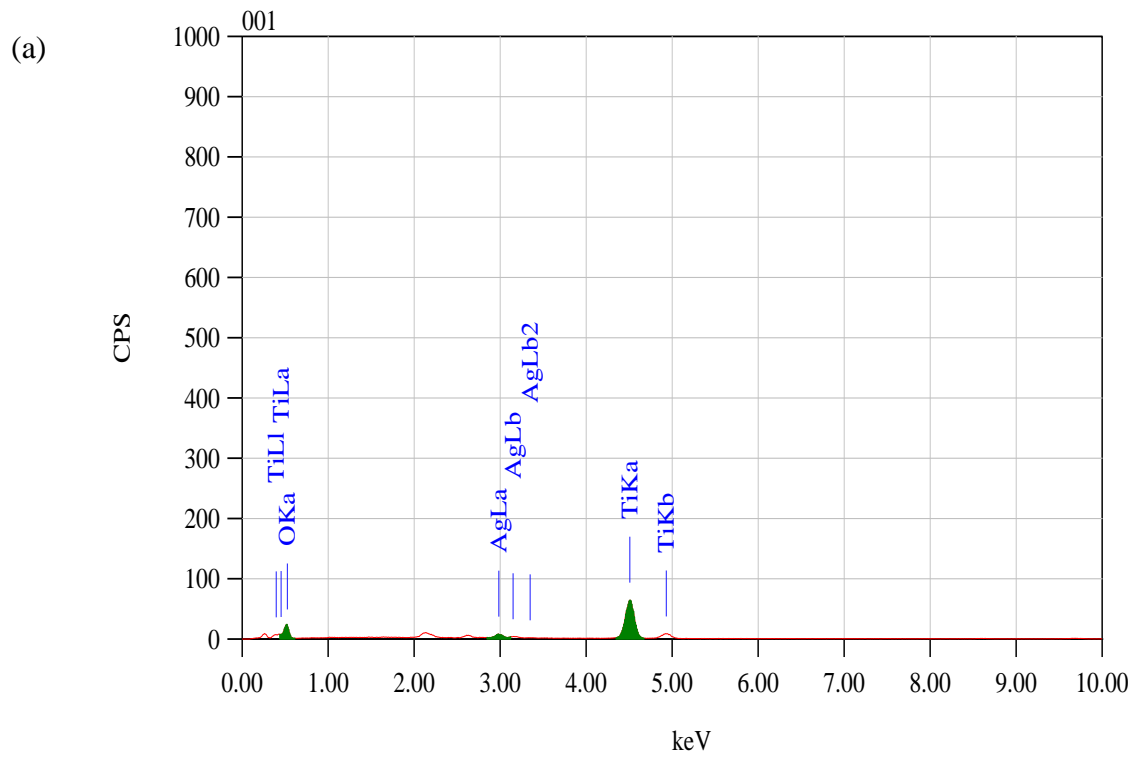


Fig. 2.7. EDX analysis of a) 1% and b) 2% Ag-TiO₂



2.3.3 Effect of photo catalyst dosage

The effect of photocatalyst dosage was investigated by varying the amount of 2% Ag-TiO₂ from 0.05 g dm⁻³ to 0.25 g dm⁻³ while maintaining [LMF] and pH 4 constant. Initially, the photocatalytic degradation rate increased up to 0.10 g dm⁻³, after this limiting value the rate of reaction almost remained constant (Table 2.2 and Fig. 2.8.). This can be explained on the basis of turbidity formation with increase in the photocatalyst dosage. As the amount of photocatalyst increases in the initial state, the exposed surface area of the photocatalyst also increases but after this limiting value (0.10 g dm⁻³) any increase in the amount of photocatalyst increases the turbidity of the solution and thus blocks UV irradiation reaching the photocatalyst, which reduces the degradation rate [14].

2.3.4 Effect of [LMF]

The effect of variation of LMF concentration was studied by taking different [LMF] from 8.00 x 10⁻⁵ to 28.00 x 10⁻⁵ mol dm⁻³ and keeping other conditions constant. It was observed that increase in the [LMF], increased the rate of photocatalytic degradation, reached maximum value at [LMF] = 20.00 x 10⁻⁵ mol dm⁻³ further increase in concentration resulted in decrease in the rate of photocatalytic degradation as shown in Table 2.3 and Fig. 2.9. It can be explained on the basis of screening effect of the drug. As [LMF] increased, more number of LMF molecules is excited and consequently available for degradation; hence the rate of degradation increases. But at concentration above 20 x 10⁻⁵ mol dm⁻³ the LMF acts as a filter for the incident light and decreases the rate of photocatalytic degradation [15].

2.3.5 Effect of pH

The pH normally influences the adsorption capacity of the adsorbent in aqueous medium by altering the surface properties of adsorbent. The effect of pH on the rate of photo degradation of LMF was studied by varying the pH from 4.0-8.0, while keeping other conditions constant. The rate of photocatalytic degradation of LMF was slightly higher in the pH range 4.0-5.0 and slightly lower in the pH range 7.0-8.0 as shown in Table 2.4 and Fig. 2.10. This behaviour may be explained on the basis that an increase in the rate of photocatalytic degradation may be due to the increased availability of OH⁻ ions at acidic pH value. OH⁻ ions will generate more hydroxyl radicals (•OH) by combining with holes, which are considered responsible for the photocatalytic degradation. The adsorption on Ag-TiO₂ primarily depends on its surface properties and surface reactivity largely related to surface hydroxyl groups. It is evident from the Table 2.5.

Table 2.2. Effect of different amount of 2% Ag-TiO₂ photocatalyst on degradation of LMF at 25 °C, [LMF] = 20 x10⁻⁵ mol dm⁻³, at pH = 4, light intensity = 4 mW/cm².

Photocatalyst	Amount of photocatalyst (g dm ⁻³)	k _{obs} x 10 ³ (min ⁻¹)
2% Ag-TiO ₂	0.05	8.00
	0.10	12.90
	0.15	10.00
	0.20	9.50
	0.25	8.80

Fig. 2.8. Effect of different amounts of photocatlyst [LMF] = $20.00 \times 10^{-5} \text{ mol dm}^{-3}$, at pH = 4.0, light intensity = 4 mW/cm^2 .

(Conditions are stated in Table 2.2 (p.54))

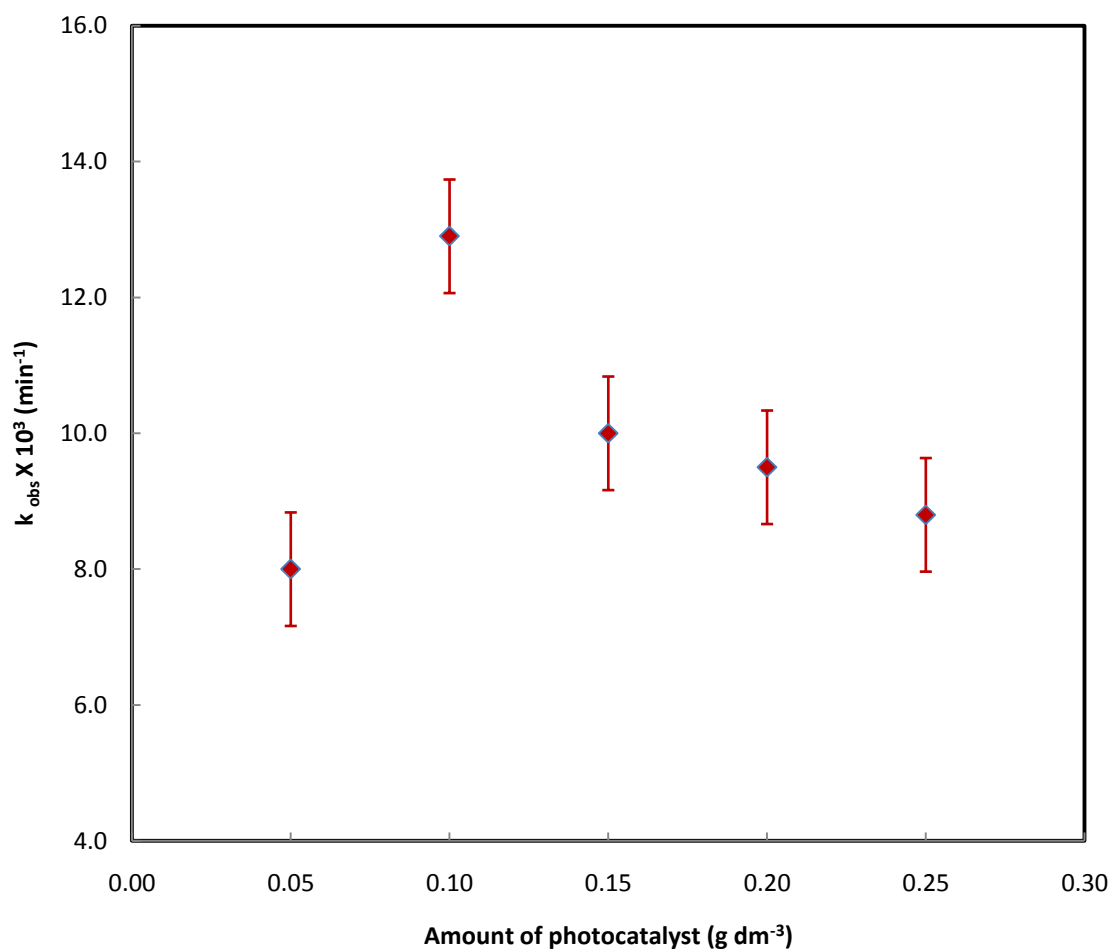


Table 2.3. Effect of [LMF] on photocatalytic rate constants with 2% Ag-TiO₂ at 25 °C, [Ag-TiO₂] = 0.10 g dm⁻³, at pH = 4.0, light intensity = 4 mW/cm².

Photocatalyst	[LMF] x 10 ⁵ (mol dm ⁻³)	k _{obs} x 10 ³ (min ⁻¹)
2% Ag-TiO ₂	8.00	06.17
	12.00	08.17
	16.00	10.21
	20.00	12.84
	24.00	09.80
	28.00	08.71

Fig. 2.9. Effect of [LMF] on photocatalytic rate constants with 2% Ag-TiO₂ at 25 °C, [Ag-TiO₂] = 0.10 g dm⁻³, at pH = 4.0, light intensity = 4 mW/cm².

(Conditions are stated in Table 2.3 (p.56))

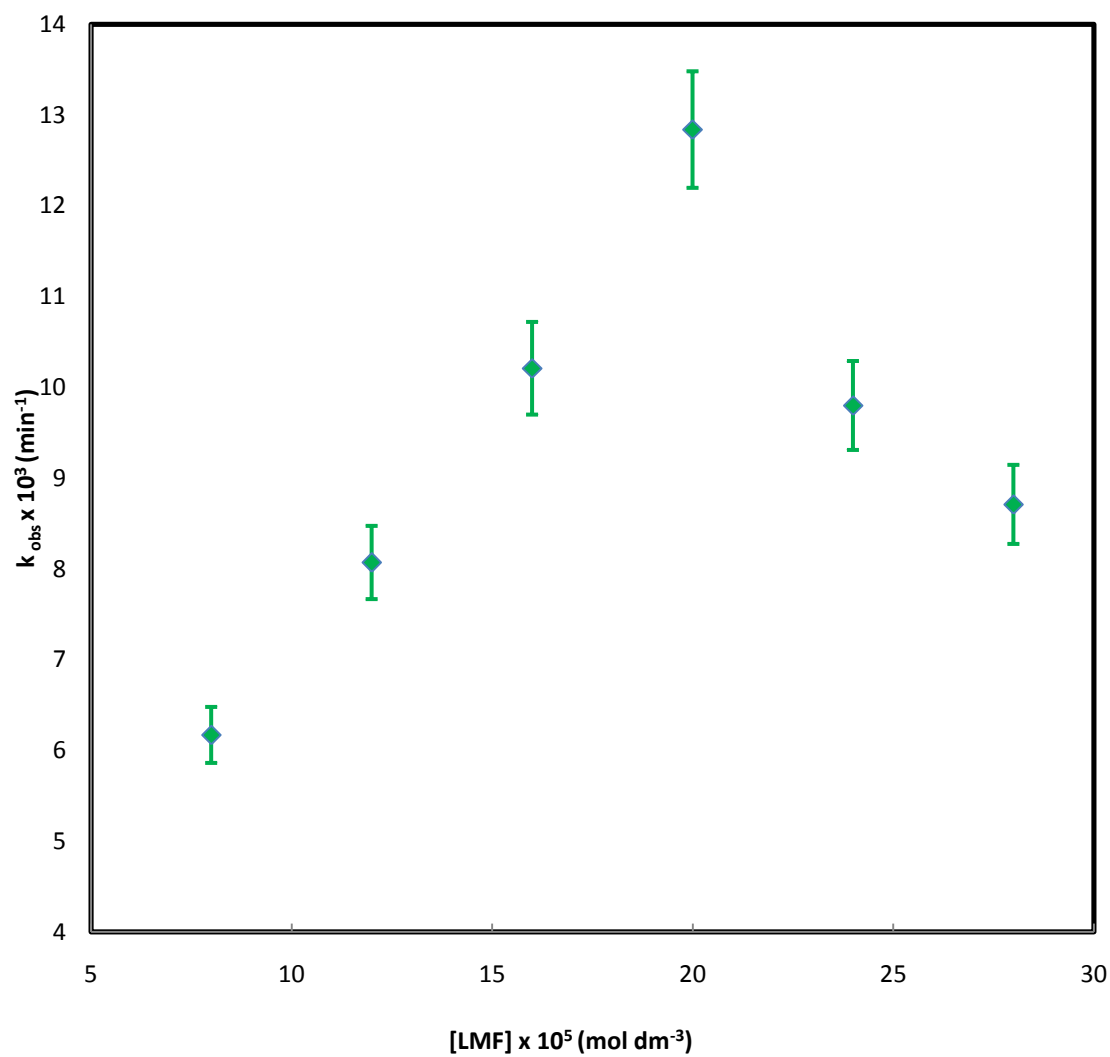
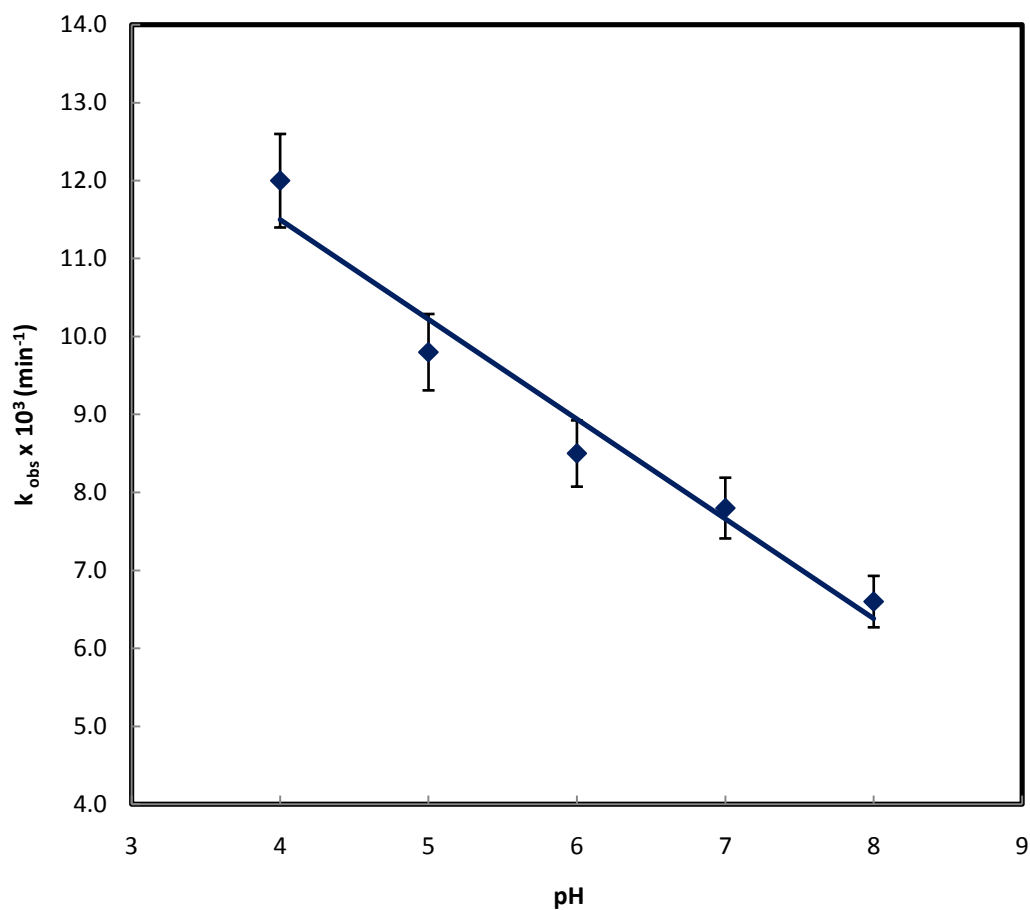


Table 2.4. Effect of pH on the rate constant of photocatalytic degradation of LMF with 2% Ag-TiO₂ at 25 °C, [Ag-TiO₂] = 0.10 g dm⁻³, [LMF] = 20.00 x 10⁻⁵ mol dm⁻³, light intensity = 4 mW/cm².

Photocatalyst	pH	k _{obs} x 10 ³ (min ⁻¹)
2% Ag-TiO ₂	4.0	12.00
	5.0	9.80
	6.0	8.50
	7.0	7.80
	8.0	6.60

**Fig. 2.10. Effect of pH on the rate constant of photocatalytic degradation of LMF with 2% Ag-TiO₂ at 25 °C, [Ag-TiO₂] = 0.10 g dm⁻³, [LMF] = 20.00 x 10⁻⁵ mol dm⁻³.
light intensity = 4 mW/cm².**

(Conditions are stated in Table 2.4 (p.58))



**Table 2.5. Adsorption capacities at different pH, [LMF] = 20.00×10^{-5} mol dm⁻³,
(2%) Ag-TiO₂ = 0.10 g dm⁻³. (Langmuir isotherm)**

Sl. No	pH	Adsorption Capacity (Langmuir Isotherm) (mol g ⁻¹)
1	4.0	0.00110
2	5.0	0.00091
3	6.0	0.00085
4	7.0	0.00072
5	8.0	0.00062

The adsorption capacity decreases with increase in the pH from 4.0 to 8.0. The LMF contains >NH and carboxyl functional groups in its molecular structure. This enables LMF to react with the H⁺ and OH⁻ in solution to form three different LMF species viz., LMFH⁺ (cation), LMF^o (neutral) and LMF⁻ (anion). The pK_a values of LMF were computed by using Chem. axon calculator and they were found to be pK_{a1} (5.64) and pK_{a2} (8.70) [16]. The proportion of LMF in different forms can be calculated from the pK_a values shown in Fig. 2.11. LMF forms about 98% LMFH⁺ at pH 4.0 by combining with H⁺ ions from the solution, which favours the LMF adsorption on the negatively charged surface of Ag-TiO₂ photocatalyst. The proportion of LMFH⁺ decreases to 81% at pH 5.0 reduces to 30% at pH 6 and further reduces to 4% (negligible) at pH 7.0. LMF neutral species dominates in the pH range 6.0 – 8.0. With the proportional decrease in the concentration of LMFH⁺ and proportional increase in the concentration of LMF neutral, the adsorption capacity of LMF on Ag-TiO₂ decreases. The adsorption of LMFH⁺ is due to the combination of cation with negatively charged surface of Ag-TiO₂, whereas the adsorption of LMF neutral is due to weak Van der Waals forces of attraction. This observation is in line with the earlier report [17].

2.3.6 Effect of light intensity.

It was observed (Table 2.6 and Fig. 2.12.) that, an increase in light intensity increased the rate of photocatalytic degradation. This can be explained on the basis of generation of more number of electron hole pair. Increase in UV light intensity excites higher number of Ag-TiO₂ nanoparticles there by generating higher number of electron hole pairs. The holes decompose the LMF molecules adsorbed on the surface of Ag-TiO₂ particles and oxidize it to water resulting in their efficient degradation [18]. This effect of UV light intensity was investigated by altering the length of UV lamp from the surface of reaction mixture.

2.3.7 Mechanism of photocatalytic degradation

On the basis of the experimental data the following tentative mechanism may be given for photocatalytic degradation of LMF.

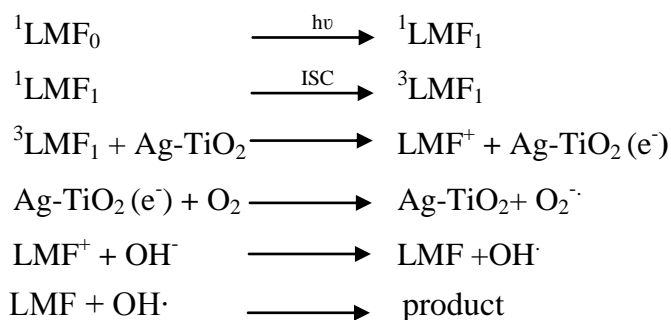


Fig. 2.11. Speciation of LMF at different pH

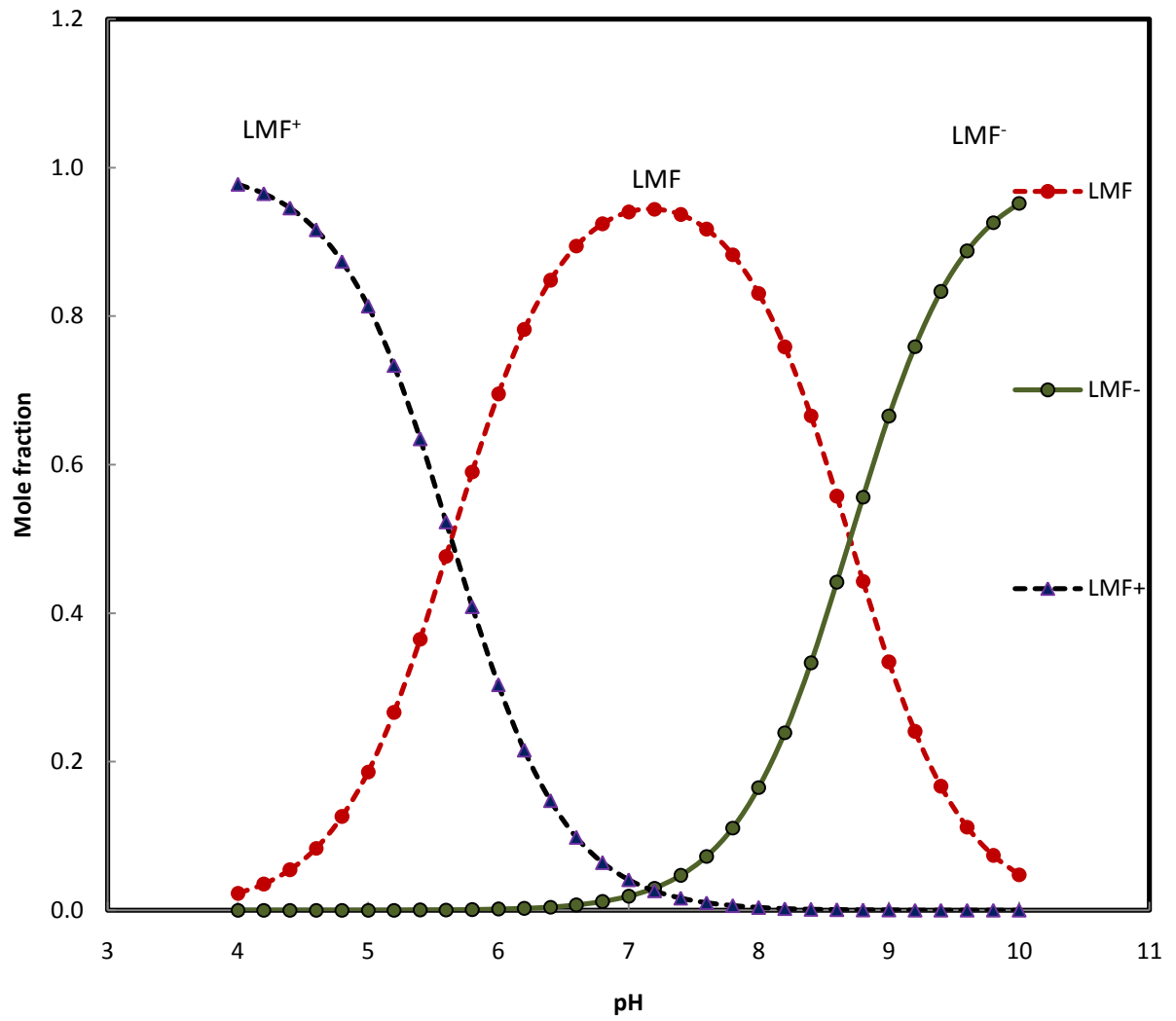
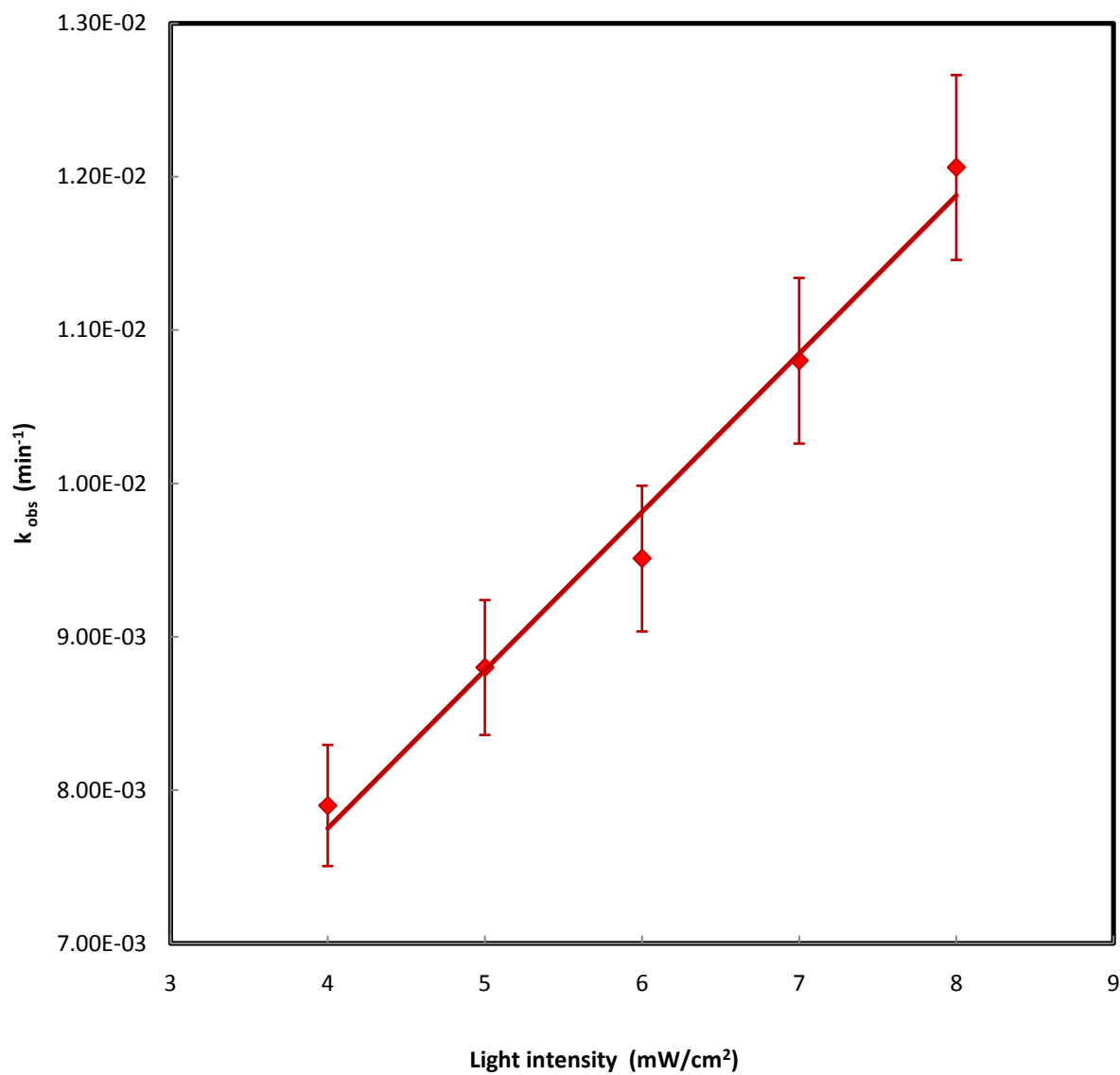


Table 2.6. LMF degradation under different UV intensities LMF with 2% Ag-TiO₂ at 25 °C, [Ag-TiO₂] = 0.10 g dm⁻³, [LMF] = 20.00 x 10⁻⁵ mol dm⁻³, at pH=4.

Photocatalyst	Light intensity (mW/cm ²)	k _{obs} x 10 ³ (min ⁻¹)
2% Ag-TiO ₂	4	7.90
	5	8.80
	6	9.51
	7	10.80
	8	12.10

Fig. 2.12. LMF degradation under different UV intensities LMF with 2% Ag-TiO₂ at 25 °C, [Ag-TiO₂] = 0.10 g dm⁻³, [LMF] = 20.00 x 10⁻⁵ mol dm⁻³, at pH=4.0. Light intensity = 4 mW/cm².

(Conditions are stated in Table 2.6 (p.63))



When the LMF solution is exposed to UV light, in the presence of Ag-TiO₂, initially LMF molecules are excited to first singlet state (¹LMF₁). Then these excited molecules are moved to the triplet state through inter system crossing (ISC). The triplet drug (³LMF₁) may provide its electron to the photocatalyst and become positively charged. The dissolved oxygen of the solution will pull an electron from the conduction band of the photocatalyst, thus generating the photocatalyst. The positively charged molecules of the drug (LMF) will immediately reacts with ⁻OH ions to form OH[•] radicals, which will convert the drug molecules in to products.

In undoped TiO₂, molecular oxygen is the only one electron trapping entity, whereas in Ag-TiO₂, two other electron trapping entities are set up, viz., Ag⁺ ions and Ag⁰. Since the Fermi level of TiO₂ is higher, hence electrons will move from TiO₂ nanoparticles to the metallic silver nanoparticles resulting in a space charge between Ag and TiO₂. The electric field finally force the electrons to the interfacial space of the TiO₂ nanoparticles. Here, silver particles act as electron traps [19]. This leads to an increase in the charge separation efficiency and slows down electron-hole recombination. Silver metal on the catalyst surface improves the quantum yields by increasing the removal and the transfer of electrons from catalyst to molecular oxygen [20]. Therefore, molecular oxygen reacts with photo generated electrons to form superoxide an ion radical, which were subsequently enhance the oxidation of LMF.

2.4 Conclusion

1% and 2% Ag-TiO₂ nanoparticles were synthesized by LI method. The obtained results revealed that Ag-TiO₂ (17.00 to 13.07 nm) particles have a good potential to be used as a photocatalyst in the degradation of LMF in acidic environment (pH 4.0). The XRD patterns of synthesized catalysts indicate anatase crystal structure. The EDX analysis and TEM topograph shows that the existence of Ag-TiO₂. Under optimum conditions, over 95% photocatalytic degradation of LMF was achieved in 100 min using 2% Ag-TiO₂ photocatalyst.

References

1. T. Kudo, Y. Nakamura, and A. Ruike, "The design of highly active rectangular column structured titanium oxide photocatalysts and their application in purification systems", *J. Catal. Today*. Vol.122, 2003, pp. 14-19.
2. G. Zayani, L. Bousselmi, F. Mhenni, and A. Ghrabi, "Solar photocatalytic degradation of commercial textile azo dyes: Performance of pilot plant scale thin film fixed-bed reactor", *J. Desalin*. Vol. 246, 2009, pp. 344-352.
3. U.I. Gaya, and A.H. Abdullah, "Heterogeneous photocatalytic degradation of organic contaminants over titanium dioxide", *J. Photochem. Photobiol. C*. Vol.19, 2008, pp.1-12.
4. C. Guillard, J. Disdier, J.M.Herrmann, C. Lehaut, T. Chopin, S. Malato, and J. Blanco, "Comparison of various titania samples of industrial origin in the solar photocatalytic detoxification of water containing 4-chlorophenol", *J. Catal.Today*. Vol. 54, 1999, pp. 217-228.
5. N. Bhullar, D. Sud, and P. Bansal, "Studies on photodegradation of malachite green using TiO_2/ZnO photocatalyst", *Desalin. Water Treat.* Vol.12 (1-3), 2009, pp. 108-113.
6. A. Jodat, and A. Jodat, "Photocatalytic degradation of chloramphenicol and tartrazine using Ag/TiO_2 nanoparticles", *Desalin. Water Treat.* Vol.52, 2014, pp. 2668-2677.
7. A. Verma, I. Chhikara, and D. Dixit, "Photocatalytic treatment of pharmaceutical industry wastewater over TiO_2 using immersion well reactor: synergistic effect coupling with ultrasound", *Desalin. Water Treat.* Vol.52, 2014, pp. 6591-6597.
8. B. Halling-Sorensen, S.N. Nielsen, P.F. Lanzky, F. Ingerslev, H.C. HoltenLutzof and S.E. Jorgensen, "Occurrence, fate and effects of pharmaceutical substances in the environment-a review", *Chemosphere*. Vol.36, 1998, pp. 357-393.
9. M.A. Behnajady, N. Modirshahla, M. Shokri and B. Rad, "Enhancement of photocatalytic activity of TiO_2 nano particles by silver doping: Photodeposition versus liquid impregnation method", *GLOBAL NEST J.* Vol.10 (1), 2008, pp.1-7.
10. H. Ilyas, I. A. Qazi, W. Asgar, M. A. Awan, and Z. Khan, "Photocatalytic degradation of nitro and chlorophenols using doped and undoped titanium dioxide nanoparticles", *J Nanomater* , Vol.2011, 2011, pp.1-8.
11. S. Ozkan, M.W. Kumthekar and G. Karakas, "Characterization and temperature-programmed studies over Pd/TiO_2 catalysts for NO reduction with methane". *Catal. Today*. Vol.40 (1), 1998, pp. 3-14.

12. D. Guin, S.V. Manorama, and J.N.L. Latha, S. Singh, "Photoreduction of Silver on Bare and Colloidal TiO₂ Nanoparticles/ Nanotubes: Synthesis, Characterization, and Tested for Antibacterial Outcome", *J. Phys. Chem. C*. Vol.111, 2007, pp. 13393 – 13397.
13. K. Wetchakun and S. Phanichphant, "Effect of Ru on photocatalytic activity of TiO₂ nanoparticles", *J. Micro. Soc. of Thailand*. Vol.22, 2008, pp. 11-14.
14. J. Sun, L. Qiao, S. Sun and G.Wang, "Photocatalytic degradation of Orange G on nitrogen doped TiO₂ catalysts under visible light and sunlight irradiation", *J. Hazard. Mater.* Vol. 155, 2008, pp. 312-319.
15. C.C. Wang, C.K. Lee, M.D. Iyu, and L.C. Juang, "Photocatalytic degradation of C.I.Basic Violet using TiO₂ catalysts supported by Y. Zeolite an investigation of the effects of operational parameters", *Dyes and Pigments*. Vol. 76, 2008, pp. 312-319.
16. Marvin 5.10.1, 2012, ChemAxon (<http://www.chemaxon.com>).
17. I.T. Horvath, "Heterogeneous Photocatalytic degradation of organic contaminants over titanium dioxide: A review of fundamentals, progress and problems", *J. Encycl. Catal.* Vol.5, 2003, pp. 577-599.
18. Z. Guo, R. Ma and G. Li, "Photocatalytic property of colloidal TiO₂ nanoparticles prepared by sparking process," *J. Chem. Eng.* Vol. 119, 2006, pp.55-59.
19. C. He, Y. Yu, X. Hu and A. Larbot, "Influence of silver doping on the photocatalytic activity of titania films", *Appl. Surface Sci.* Vol.200, 2002, pp.239-247.
20. H. Gerischer and A. Heller, "Photocatalytic oxidation of organic molecules at TiO₂ particles by sunlight in aerated water", *J. Electrochem. Soc.* Vol.139, 1992, pp. 113-118.

Chapter 3

Ru-TiO₂ semiconducting nanoparticles for the photocatalytic degradation of bromothymol blue

3.1 Introduction

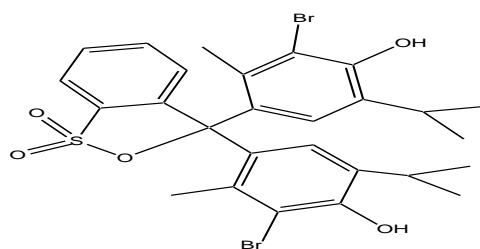
A wide variety of organic contaminants has been detected in the aquatic environment which are discharged through municipal waste-water, industrial effluents, commercial operations, runoff from agricultural lands, chemical spills etc [1]. Till now, the conventional and biological methods have not been able to get rid of these persistent organic contaminants from the environment [2].

Dye effluent released from textile and dye industries are to be considered due to its impact on flora and fauna and increasing concern over the carcinogenicity and toxicity [3-5]. This fact compels elimination of dyes in the effluent treatment plants [6].

The general importance of Titanium dioxide (TiO₂) discussed in chapter 1 (p.12-13) and Advanced oxidation processes (AOPs) discussed in chapter 2 (p.34).

These doped cat ions reduce the band gap and red shift threshold towards the absorption of visible range [7]. Ruthenium might act as a suitable element for doping of TiO₂, because of its closeness in atomic radius with TiO₂ (Ru - 0.056, Ti - 0.060 nm) [8].

The model compound used for study is bromothymol blue (BTB). BTB is a textile dye derivative, which is harmful in case of skin and eye contact (irritant). Photo-catalytic degradation of BTB by TiO₂ has been investigated earlier by Haque et al [9]. From the application point of view, kinetics of degradation of textile dye derivatives by doped nanostructure is essential. Therefore, in the present work, we have carried out a comprehensive investigation on the photo-catalytic degradation of BTB by prepared Ru-TiO₂ nanoparticles by studying the effects of pH of the reaction, substrate concentration, catalyst dosage, percentage of doping of photo-catalyst and intensity of UV- light.



Chemical Structure of Bromothymol blue (BTB)

3.2 Experimental

3.2.1 Reagents and chemicals

A bromothymol blue (BTB) (Sigma-Aldrich) stock solution was prepared by dissolving appropriate amount of sample in double distilled water. The TiO₂ (anatase) (SRL) and RuCl₃ · 3H₂O (SRL) samples were directly used to prepare Ru doped TiO₂ without any further purification. The degradation investigations were carried out with the use of all reagent grade chemicals.

The instruments used were already discussed in chapter-2 and p.no. (36-40)

3.2.2 Photocatalyst preparation

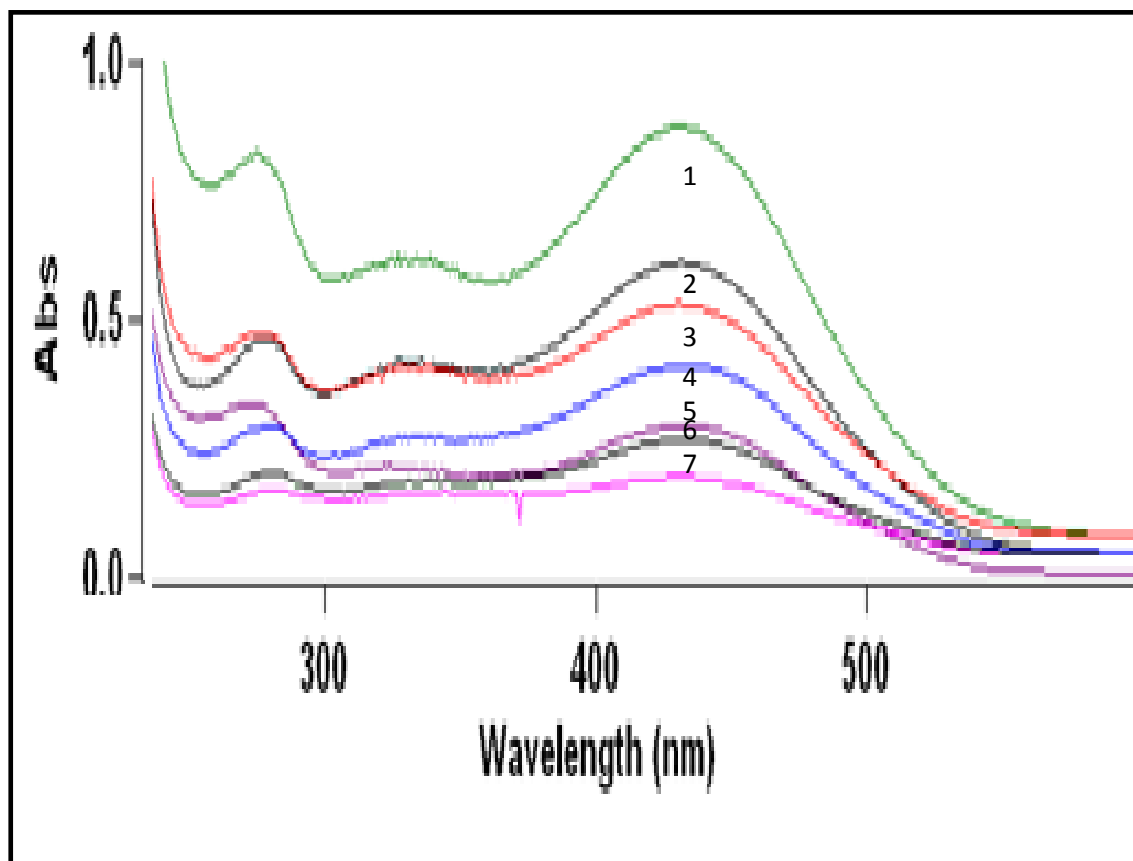
Ruthenium (Ru) doped anatase TiO₂ nanoparticles were prepared by liquid impregnation method. For ruthenium doping, 0.2%, 0.4% and 0.8% (mole ratio) of RuCl₃ · 3H₂O was dissolved in 100 ml of 0.2 M HCl solution. Further, 1.0 g of Anatase nanoparticles TiO₂ was added. The resultant slurry were thoroughly stirred continuously for 3 hours and allowed to settle at room temperature for 24 hrs. Afterward, that the water was removed from slurry by placing in electric oven at 80 °C for further 24 hrs. After the removal of water the particles were crushed then it is calcined at 400 °C in a furnace for 3 hrs, since the Anatase to Rutile phase transformation takes place above 400 °C [10-11].

3.2.3 The Photocatalysis Process

To investigate the photo-catalytic degradation, a known concentration of BTB solution and the buffer was taken in a Pyrex beaker, and then a dosage of 100 mg dm⁻³ Ru-TiO₂ nanoparticles was added. Before illumination, the suspensions were stirred at a dark place for 1 hr to attain adsorption and desorption equilibrium established between the BTB and photo-catalyst. Then, the beaker was placed in a photo-catalytic chamber under 8 W UV-lamp (Phillips) with a wavelength peak at 254 nm with continuous stirring for adsorption–desorption equilibrium and then exposed to UV light. At the interval of every 15 minutes, the solution was taken out and centrifuged at 5000 rpm for 10 min. The decrease in the concentration of BTB was monitored at 429 nm ($\epsilon = 10860 \text{ dm}^3 \text{ mol}^{-1} \text{ cm}^{-1}$) using UV-visible spectrophotometer (Varian CARY 50 Bio UV-Vis Spectrophotometer) and the degree of mineralization was studied as shown in Fig. 3.1.

Fig. 3.1. UV–visible spectral changes during the degradation of BTB at $25 \pm 0.2^\circ\text{C}$, $[\text{BTB}] = 5.00 \times 10^{-5} \text{ mol dm}^{-3}$, $\text{pH} = 4.0$, $0.8 \text{ \% Ru-TiO}_2 = 100 \text{ mg dm}^{-3}$ and light intensity = 4 mW/cm^2 .

Time (1) 00.00 min (2) 15.00 min (3) 30.00 min (4) 45.00 min
 (5) 60.00 min (6) 75.00 min (7) 90.00 min



3.3 Results and discussion

3.3.1 Effect of Ruthenium doping

Effect of ruthenium doping on anatase TiO₂ was studied by changing the percentage of ruthenium from 0.2 to 0.8% (mole ratio) an increase in the content of ruthenium leads to decrease in the particle size and increase in the photo-catalytic activity [12] as shown in Fig. 3.2. Smaller particle size increases surface area and higher content ruthenium may also favour separating charge carriers efficiently, inhibiting the recombination of electron-hole pairs, and thus increase the photo-catalytic activity [13]. The rates of photo-catalytic degradation of BTB treatment with UV/0.8% Ru-TiO₂; was more efficient than other four treatments namely UV, UV/TiO₂, UV/0.2% Ru-TiO₂, UV/0.4% Ru-TiO₂. The % degradation efficiency of BTB was studied under same conditions with UV, UV/TiO₂, UV/0.2% Ru-TiO₂, UV/0.4% Ru-TiO₂, UV/0.8% Ru-TiO₂ and percentage adsorption in dark was also determined. The percentage degradation efficiency of BTB was found to be 48%, 60%, 75%, 82% and 95% with UV, UV/TiO₂, UV/0.2% Ru-TiO₂, UV/0.4% Ru-TiO₂ and UV/0.8% Ru-TiO₂ respectively with in 100 minute as shown in Fig. 3.3. The % degradation efficiency of UV/0.8% Ru-TiO₂ is about 35% higher than UV/TiO₂ report by Haque et al under our experimental conditions with [Photocatalyst] = 100 mg dm⁻³, [BTB] = 5.00 x 10⁻⁵ mol dm⁻³ at pH 4.0 and light intensity 4 mW cm⁻². hence, further studies were carried out with 2% Ag-TiO₂.

3.3.2 Characterization of TiO₂ and Ru-TiO₂

3.3.2.1 X-ray Diffraction Studies (XRD)

XRD pattern of pure TiO₂ and Ru-TiO₂ was studied by using XRD using Cu K_α emission over a scan range of 2θ (10° - 90°). XRD patterns of pure and 0.2, 0.4 and 0.8% Ru-TiO₂ were shown in (Fig. 3.4). Several well defined diffraction reflections were appeared in the pattern 25.2, 38.0, 48.2, 53.9, 55.0, 62.5, 70.2, 70.8, and 78.5, 82.9, which corresponds to the XRD pattern of all the ten peaks of anatase TiO₂ with lattice planes of (101), (004), (200), (105), (211), (204), (116), (220), and (215), (224), respectively. The absence of metal peaks is due to the ultrafine dispersion of TiO₂ nanoparticles and or due to very low metal concentration. The mean particle dimensions of prepared nanoparticles were determined from a full width half maximum of A (101) peak of anatase TiO₂ by applying Scherrer equation (1) [14].

$$D = \frac{k\lambda}{\beta \cos \theta} \quad (1)$$

Where k is a constantly called shape factor is equal to 0.94, λ is the X-ray wavelength is equal 0.154 nm, β, is the full width at half maximum and θ is the half diffraction angle.

Fig. 3.2 Rate constants for the photo-catalytic degradation of BTB by various treatments at $25 \pm 0.2^\circ\text{C}$, $[\text{BTB}] = 5.00 \times 10^{-5} \text{ mol dm}^{-3}$, $\text{pH} = 4.0$, $0.8 \text{ \% Ru-TiO}_2 = 100 \text{ mg dm}^{-3}$ and light intensity = 4 mW/cm^2 .

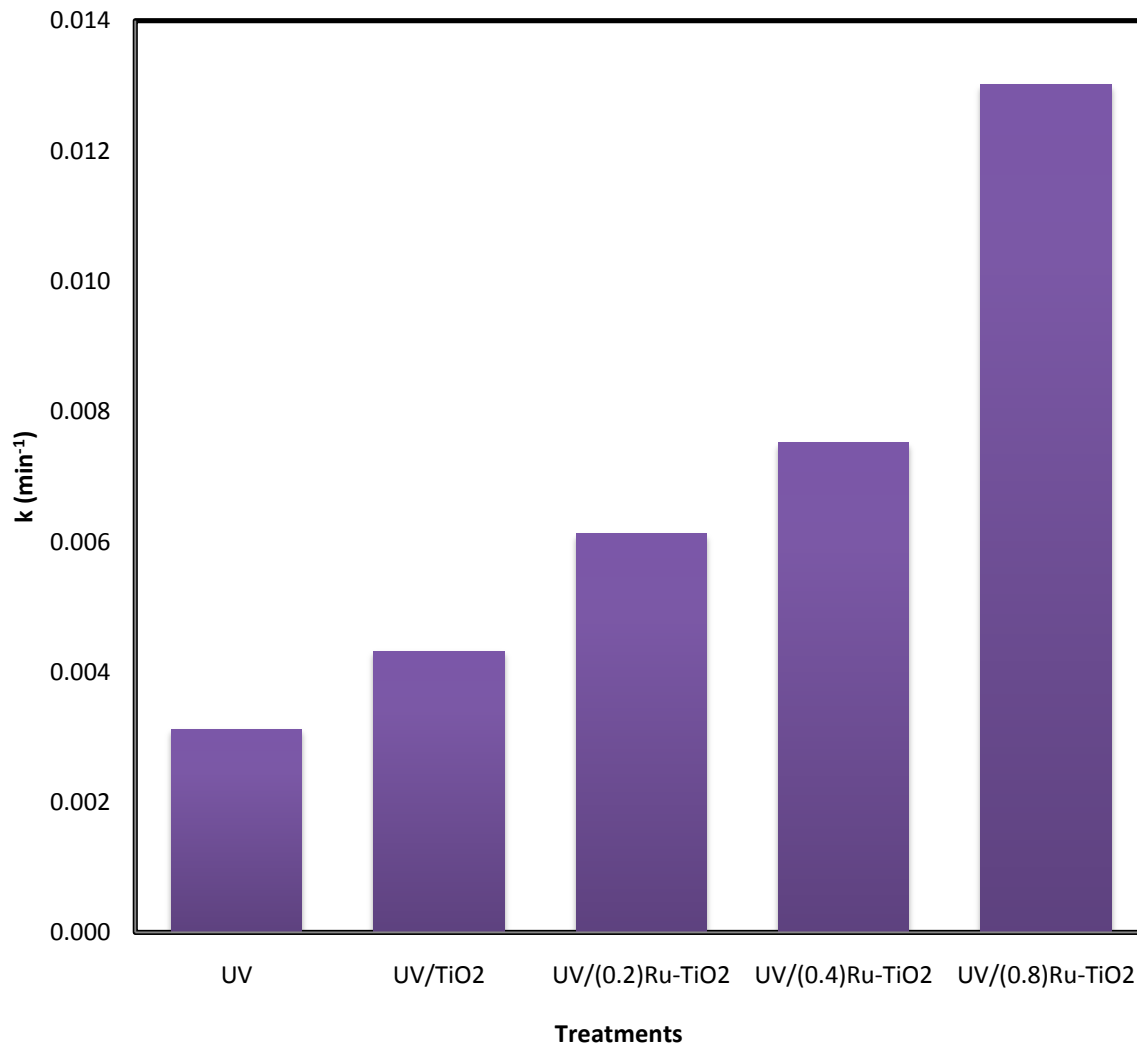


Fig. 3.3. % degradation efficiencies of various treatment methods with time at $25 \pm 0.2^\circ\text{C}$, $[\text{BTB}] = 5.0 \times 10^{-5} \text{ mol dm}^{-3}$, $\text{pH} = 4.0$, $0.8\% \text{ Ru-TiO}_2 = 100 \text{ mg dm}^{-3}$ and light intensity = 4 mW/cm^2 .

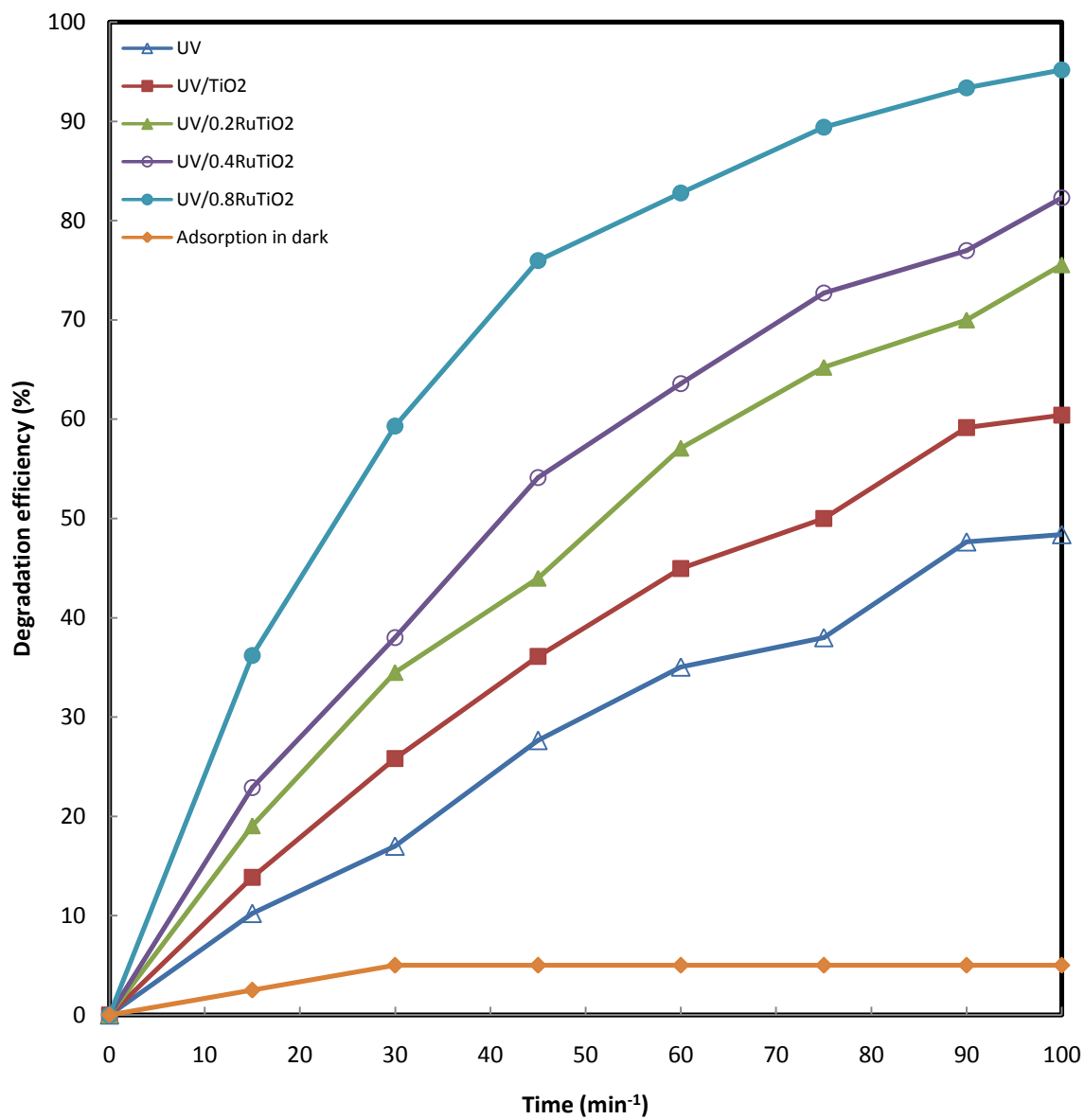
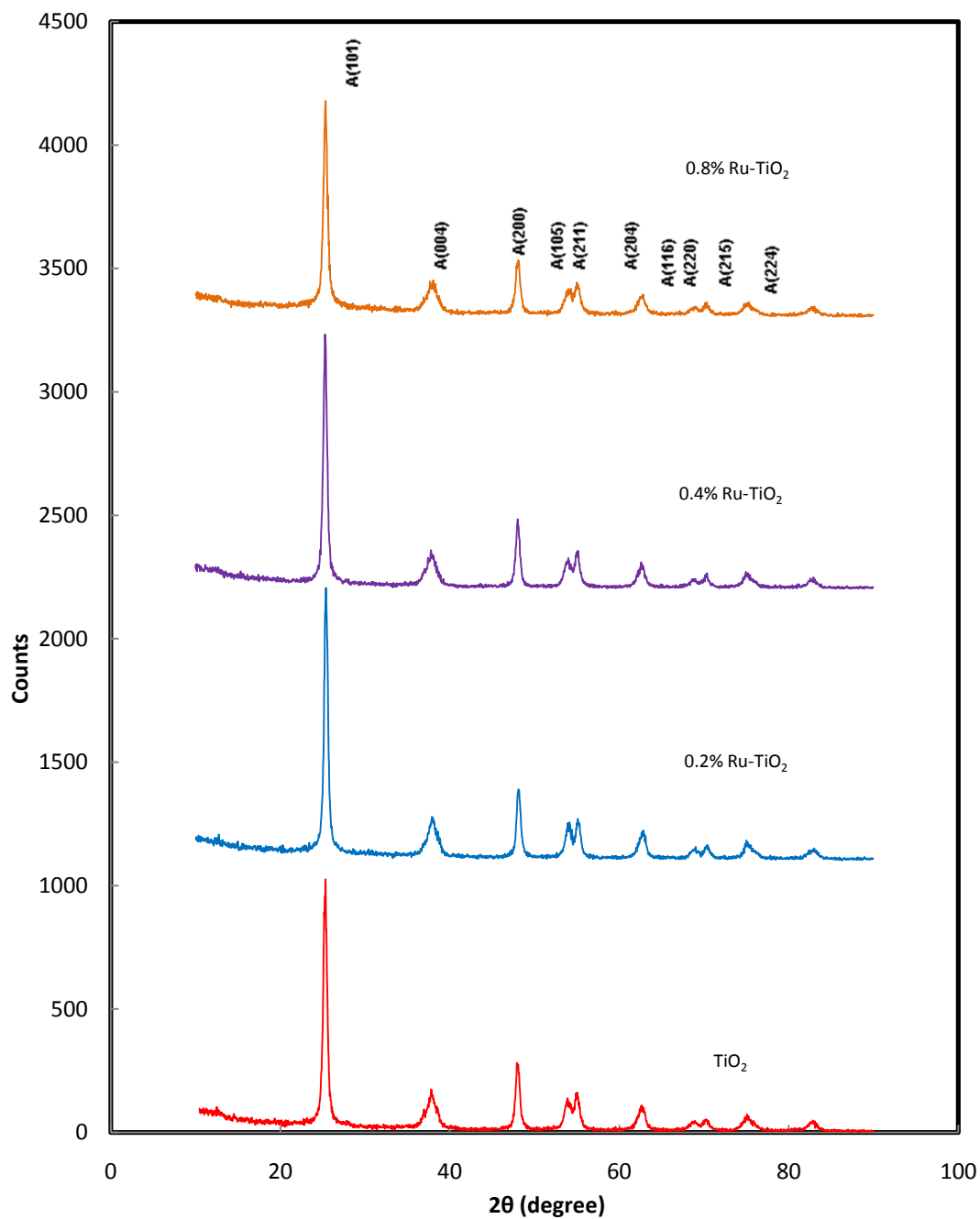


Fig. 3.4. X-ray diffraction patterns of a) Undoped TiO₂ b) 0.2% Ru- TiO₂ c) 0.4% Ru- TiO₂ d) 0.8% Ru- TiO₂



The average particle size of TiO₂, 0.2% Ru-TiO₂, 0.4% Ru-TiO₂, 0.8% Ru-TiO₂ are given in (Table 3.1) were found to be 17.00, 16.67, 15.70 and 14.40 nm respectively.

3.3.2.2 Scanning Electron Microscope (SEM)

The SEM images of undoped and Ru-doped TiO₂ nanoparticles obtained at the high magnification 15000x using JEOL JSM-6360 are presented in (Fig. 3.5 a and Fig. 3.5 b). Thin films of the sample were prepared on a carbon coated copper grid by just dropping a very small amount of the sample on the grid, extra solution was removed using a blotting paper and then the film on the SEM grid were allowed to dry by putting it under a mercury lamp for 5 min. which reveal that synthesized nanoparticles possess a porous and spongy network of unequal shapes resulting in the high surface area. SEM images show that ruthenium is not equally coated on the surface of TiO₂; this is in agreement with the earlier literature [15].

3.3.2.3 Transmission Electron Microscope (TEM)

A typical TEM image of Ru-TiO₂ powders synthesized by Liquid Impregnation method is presented in Fig. 3.6 a and Fig. 3.6 b, which reveals that the synthesized Ru-TiO₂ nanoparticles is well crystallized uniformly dispersed aggregates having the spherical rod in shape without defects. The average particle size of the nanoparticles was found to be 15.00-20.00 nm. These results are in good agreement with that of calculated particle size by Scherrer equation. The selected area electron diffraction pattern (SAED) is shown in inset of Fig. 6b. The D values of diffractions were obtained from the rings which can be assigned [101], [004], [200], and [211] (Table 3.2) and these values are in agreement with the D values obtained from XRD. In SAED, the small spots making up rings, each spot arising from Bragg reflection from an individual crystallite indicates our sample is poly nano crystalline in nature. In poly-nano-crystalline samples, if more than one crystal contributes to the selected area diffraction pattern, it can be difficult or impossible to analyze. SAED is similar to XRD but unique in that areas as small as several hundred nanometers in size can be examined, whereas XRD typically samples areas several centimetres in size due to that we could observe small difference in the D values of SAED and XRD [16-17].

3.3.2.4 Energy Dispersive X-ray Spectroscopy (EDX)

The EDX pattern of Ru-TiO₂ (Fig. 3.7.) was obtained using the JEOL JED-2300 equipment. The EDX shows the existence of 3 different X-ray peaks linked to O K α , Ru K α and Ti K α [18]. The peaks from the spectrum reveal the presence of Ti, O and Ru at 4.508, 0.525 and 2.558 keV respectively. The atomic % of Ti, O and Ru is 36.40, 62.79 and 0.81 respectively. This composition of Ti, O and trace amount of Ru revealed that the

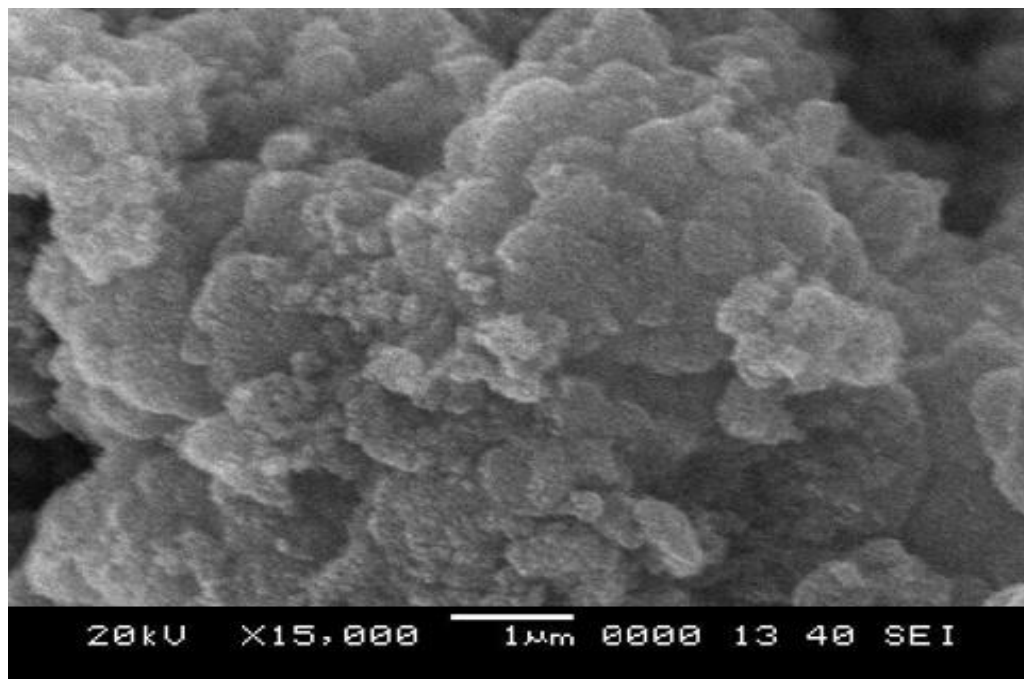
Table 3.1. Particle size of un-doped and Ru doped TiO₂ nanoparticles

Sr. No	Particles	Particle Size *
1	Un doped TiO ₂	17.00
2	0.2% Ru-TiO ₂	16.67
3	0.4% Ru-TiO ₂	15.70
4	0.8% Ru-TiO ₂	14.40

* Computed from XRD-data applying Scherrer equation

Fig. 3.5. SEM micrographs of a) Undoped TiO₂ b) 0.8% Ru-TiO₂ nanoparticles

(a)



(b)

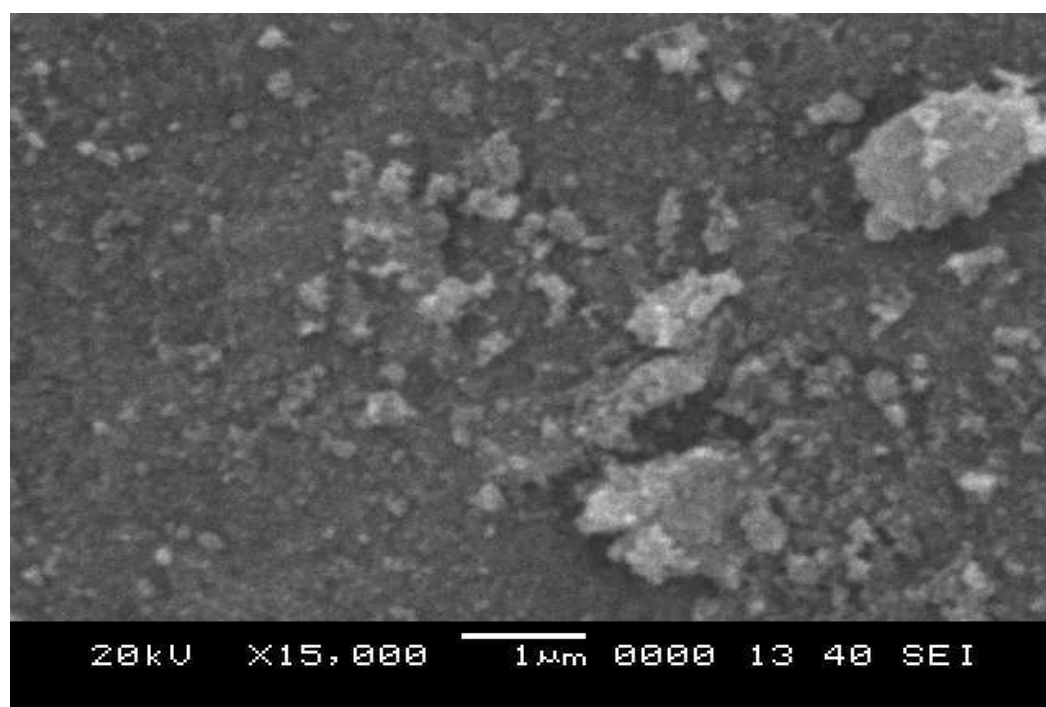
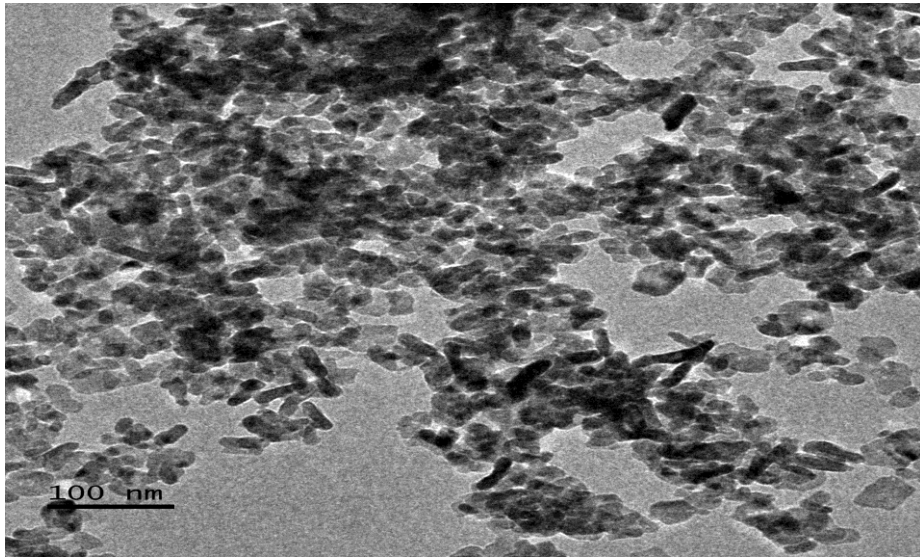


Fig. 3.6. TEM micrographs a&b of 0.8% Ru/TiO₂

(a)



(b)

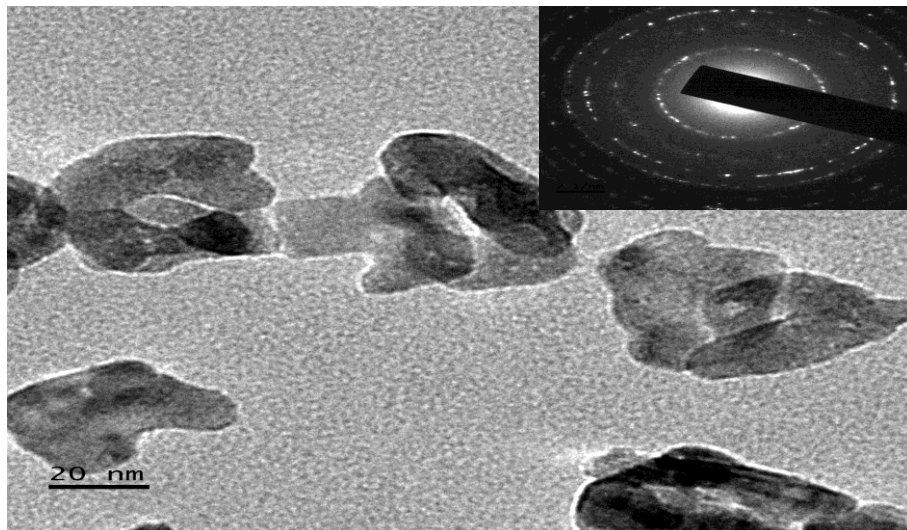
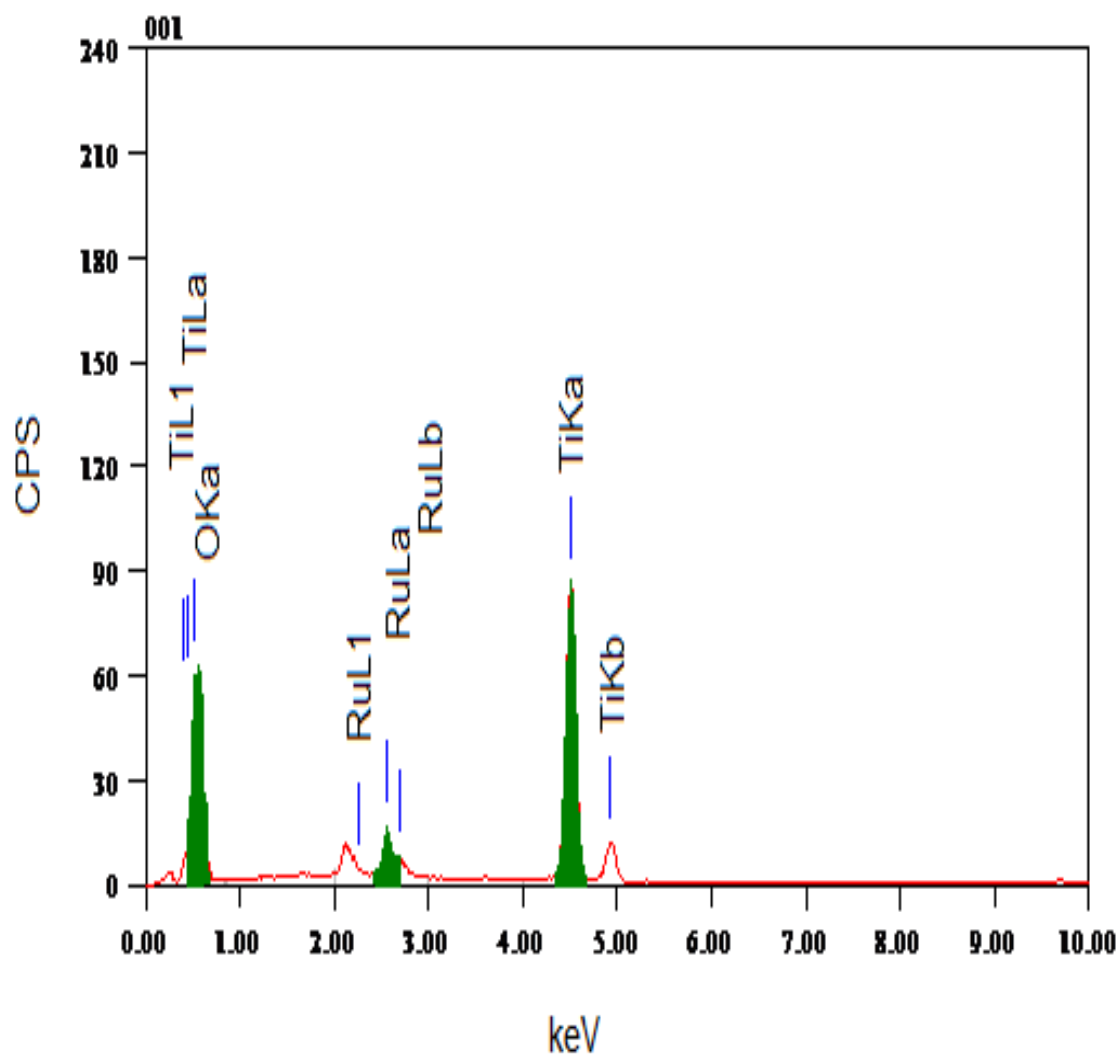


Table 3.2. Comparison of D values from XRD and Selected area electron diffraction data

2R [1/nm]	R [1/nm]	SAED D [nm]	XRD D [nm]	Difference SAED and XRD	D [Å]	h k l	2-theta
5.92	2.96	0.3378	0.3496	0.0118	3.38	101	25.45
8.87	4.43	0.2254	0.2352	0.0098	2.25	004	38.22
10.60	5.30	0.1886	0.1882	0.0004	1.89	200	48.28
12.60	6.30	0.1587	0.1667	0.0080	1.59	201	55.00

Fig. 3.7. EDX analysis of 0.8% Ru/TiO₂



Formation of non-stoichiometric TiO₂ with oxygen vacancy, which leads to better photo-catalytic activity [19].

3.3.2.5 Fourier Transform Infrared (FTIR) Spectra Analysis

The FT-IR spectra of pure TiO₂ and Ru-TiO₂ nanoparticles were shown in Fig. 3.8. The FT-IR spectra of TiO₂ and Ru-TiO₂ show a broad band between 3500 cm⁻¹ to 3000 cm⁻¹, which is a characteristic band of associated hydroxyl groups. The other peaks at 1635 cm⁻¹ correspond to the stretching vibration of a hydroxyl group and representing the water as moisture [20]. The peak observed between 750 and 500 cm⁻¹ indicates the Ti-O stretching bands. Calcination of TiO₂ and Ru-TiO₂ sample at 600 °C leaves a strong band between 800 and 450 cm⁻¹, which can be attributed to the formed of TiO₂ nanoparticles [21].

3.3.2.6 Band Gap Measurement

The bandgap measurements of nanoparticles were made from the diffuse reflectance spectra collected using a Perkin Elmer Lambda 950 UV/Vis/NIR spectrophotometer with a 150 mm integrating sphere attachment. Diffuse reflectance measurements were made between 800 – 200 nm using BaSO₄ as a reflectance standard. The optical band gaps (E_g) of the nanoparticles were determined from the Tauc plot of the Kubelka-Munk function obtained from the diffuse reflectance spectra. The Kubelka-Munk function is given by the equation $F(R) = (1-R)^2/2R$, where R is the diffuse reflectance of the sample. Extrapolation of the linear portion of the modified Kubelka-Munk function, $[F(R)hv]^{1/2}$ vs the photon energy (hv) curve on the zero ordinate gives the E_g (Fig. 3.9).

The band gap of 0.2, 0.4 and 0.8% Ru-TiO₂ was found to be 3.10, 3.04 and 2.96 eV respectively. However, in the literature it is reported that the pure anatase TiO₂ nanoparticles shows the band gap 3.2 eV. This red shift is due to the localized energy level introduced by the Ru in the forbidden energy range of TiO₂ [22]. From the reduction in the band-gap value indicates that Ruthenium is effectively doped in TiO₂ lattice [17].

3.3.2.7 Surface Area Measurement

Photo-catalytic activity of Ru-doped TiO₂ also depends on the surface area of the particles. Hence, it would be interesting to determine the surface area of Ru-doped TiO₂ nanoparticles. The specific surface area of the nanoparticles was measured by the BET nitrogen gas adsorption method using Smart Instruments Surface Area Analyser (Smart Sorb 92/93). Our studies indicate that synthesized nanoparticles showed a surface area of 85.23 m² g⁻¹, 88.79 m² g⁻¹, 92.91 m² g⁻¹ and 94.28 m² g⁻¹ for pure TiO₂, 0.2% -Ru-TiO₂, 0.4% -Ru-TiO₂ and 0.8%- Ru-TiO₂ nanoparticles respectively.

Fig. 3.8. FT-IR spectra of (a) Pure TiO₂ (b) 0.2 % Ru-TiO₂ (c) 0.4% Ru-TiO₂ (d) 0.8% Ru-TiO₂ nanoparticles

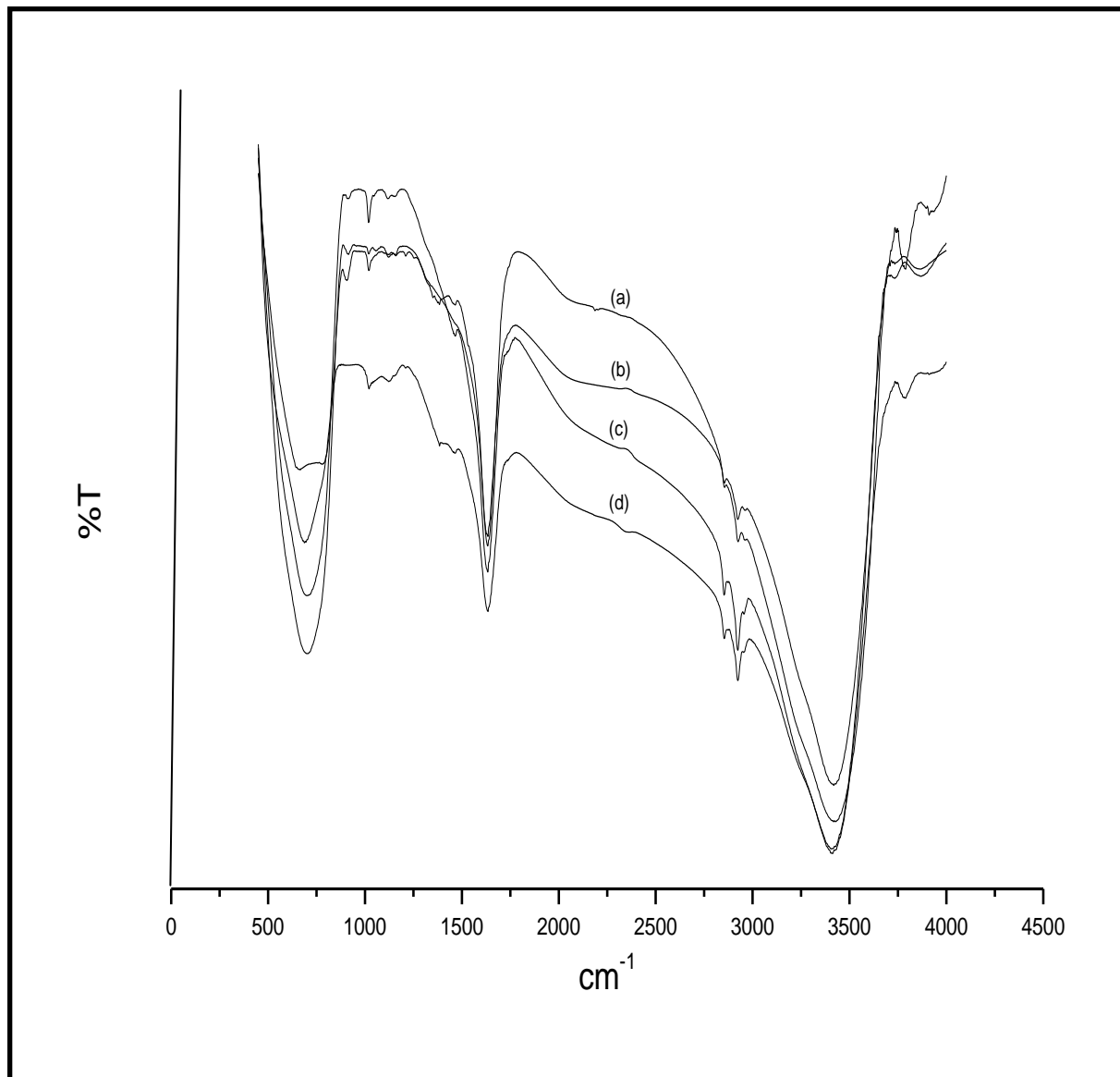
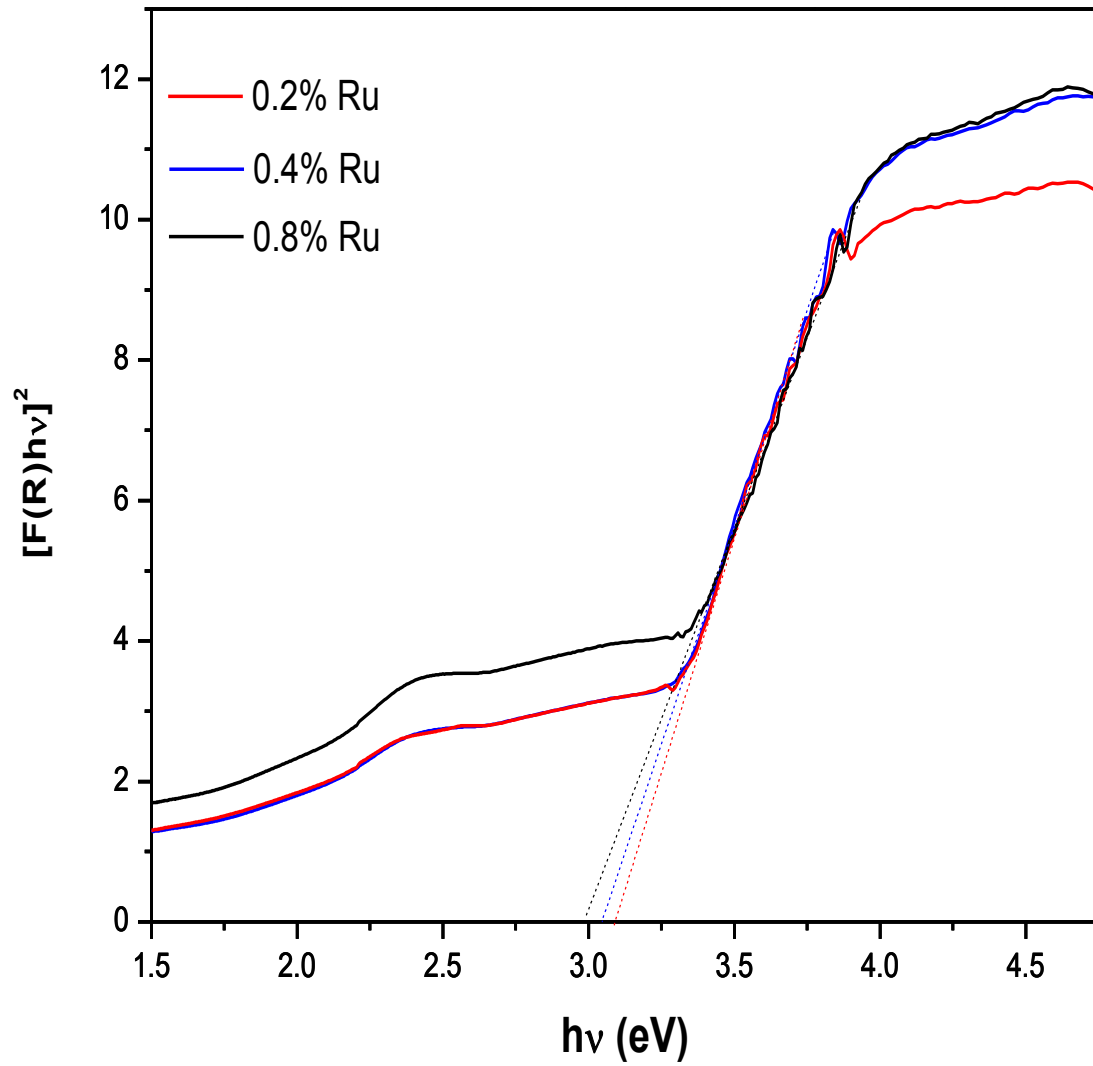


Fig. 3.9. Plot of $[F(R)h\nu]^{1/2}$ vs the photon energy ($h\nu$)



The decrease in particle size can be explained on the basis of Nae-Lih Wu's theory [23]. According to Nae-Lih Wu's theory, the motion of the crystallites is restricted due to the interaction on the boundaries between TiO₂ and Ru [24-26], which results in the reduction of particle size of TiO₂. Hence, the specific surface area increases with decrease in particle size. The very high surface area of 0.8% Ru-TiO₂ nanoparticles is responsible for the enhanced photo-catalytic degradation of BTB.

3.3.3 Effect of Photocatalyst Dosage

The effect variation in the photo-catalyst dosage on the degradation kinetics of BTB was examined using a various concentration of 0.8% Ru-TiO₂ varying from 0 mg dm⁻³ to 250 mg dm⁻³ and keeping other parameters constant. The rate constant, k_{obs} , was found to increase with an increase in the dosage of a catalyst as shown in Table 3.3 and Fig. 3.10. This can be attributed to the fact that, as the dosage of Ru-TiO₂ increases, the exposed surface area of the photo-catalyst also increases. The results in line with the earlier reports [27-28].

3.3.4 Effect of [BTB]

The rate of photo-catalytic degradation of bromothymol blue at pH 4 was examined by varying concentrations of BTB from 2.00×10^{-5} mol dm⁻³ to 20.00×10^{-5} mol dm⁻³. Initially, the rate constant, k_{obs} , was found to increase with the increase in substrate concentration from 2.00×10^{-5} mol dm⁻³ to 12.00×10^{-5} mol dm⁻³. A further increase in BTB concentration above 12.00×10^{-5} mol dm⁻³ resulted in a decrease in the rate constant (Table 3.4 and Fig. 3.11). It can be explained on the basis of screening effect of the dye. As [BTB] increased, more number of BTB molecules is excited and consequently available for degradation; hence the rate of degradation increases. But at concentration above 12.00×10^{-5} mol dm⁻³ the dye acts as a filter for the incident light and decreases the rate of photo-catalytic degradation [9].

3.3.5 Adsorption Study

The adsorption experiment was carried by varying the BTB concentration from 2.00×10^{-5} to 20.00×10^{-5} mol dm⁻³. The appropriate amount of BTB solution was taken in 100 ml beaker and 10 mg of Ru-TiO₂ nanoparticles was added. The pH value of the each set was adjusted to 4.0, 5.0, 6.0, 7.0 and 8.0 respectively. The solution was sealed and stirred at 25°C for overnight in the absence of UV light. The solution was centrifuged and the BTB concentration of the supernatant was measured by UV spectrophotometer. The adsorption amount (Capacity) was calculated using the following equation (Table 3.5).

$$S = \frac{(C_0 - C)V}{m}$$

Table 3.3. Effect of different amount of 0.8%Ru-TiO₂ photocatalyst on the degradation of BTB at [BTB] = 5.00 x 10⁻⁵ mol dm⁻³, at pH=4.0, light intensity = 4 mW/cm².

Photo-catalyst	Amount of photocatalyst (g dm ⁻³)	k _{obs} x 10 ³ (min ⁻¹)
0.8% Ru-TiO ₂	0.05	8.10
	0.10	13.00
	0.15	15.80
	0.20	17.10
	0.25	21.00

Fig. 3.10. Effect of different amount of 0.8% Ru-TiO₂ photocatalyst on the degradation of BTB at [BTB] = 5.00 x 10⁻⁵ mol dm⁻³, at pH=4.0, light intensity = 4 mW/cm².

(Conditions are stated in Table 3.3 (p.85))

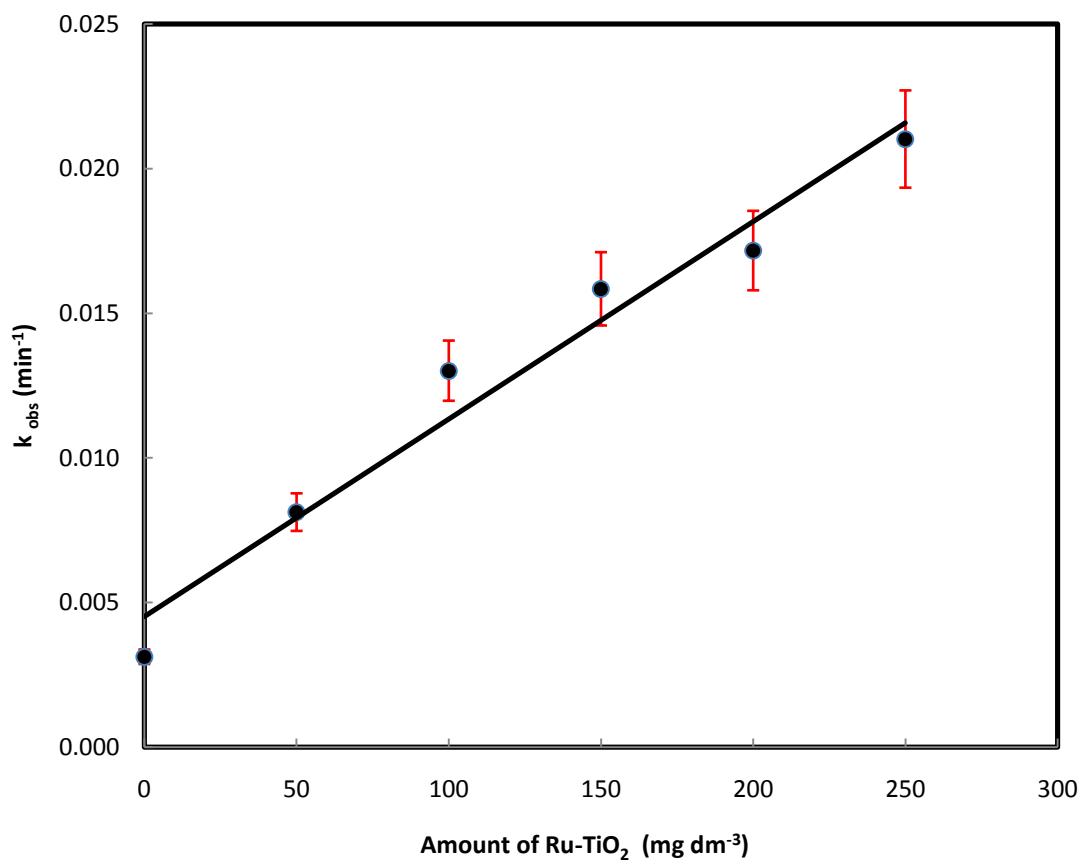
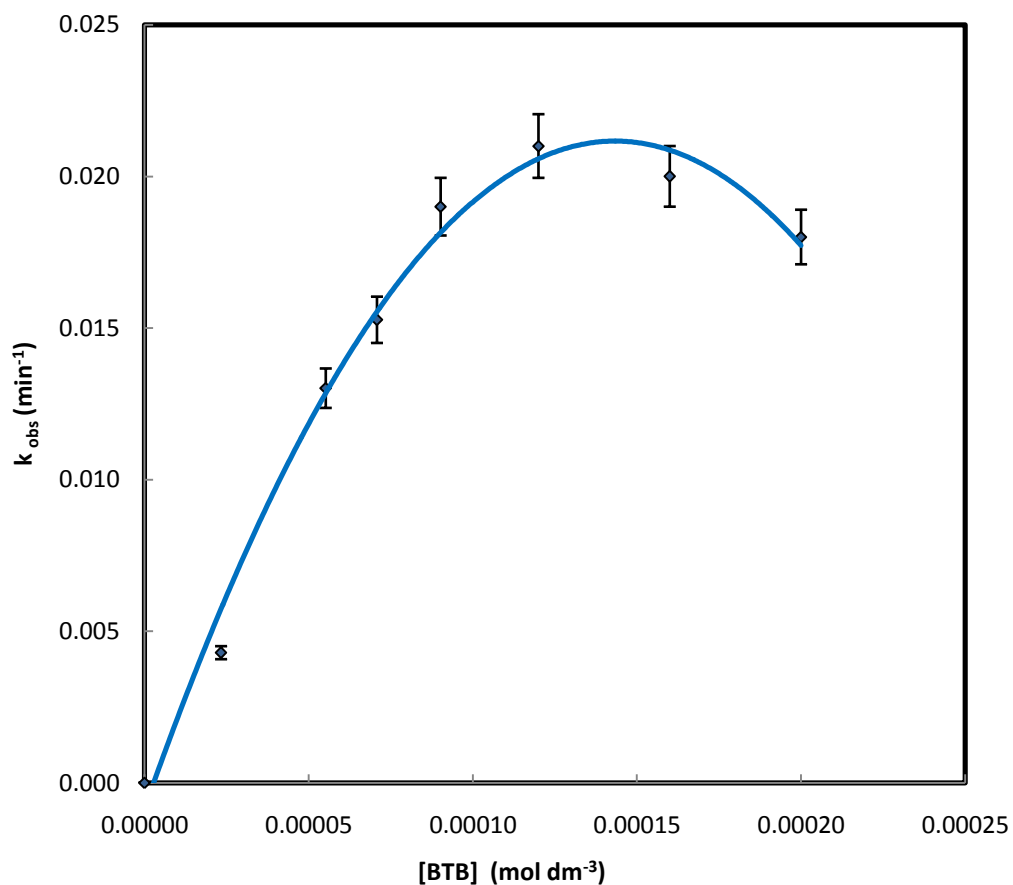


Table 3.4. Effect of [BTB] on photo-catalytic rate constant with 0.8% Ru-TiO₂ at 25 °C [Ru-TiO₂] = 100 mg dm⁻³ at pH = 4.0, light intensity = 4 mW/cm².

Photocatalyst	[BTB] x 10 ⁵ (mol dm ⁻³)	k _{obs} x 10 ³ (min ⁻¹)
0.8% Ru-TiO ₂	2.33	4.29
	5.52	13.00
	7.08	15.20
	9.02	19.00
	12.00	21.00
	16.00	20.00
	20.00	18.00

Fig. 3.11. Effect of [BTB] on photo-catalytic rate constant with 0.8% Ru-TiO₂ at 25 °C [Ru-TiO₂] = 100 mg dm⁻³ at pH = 4.0, light intensity = 4 mW/cm².

(Conditions are stated in Table 3.4 (p.87))



**Table 3.5. Adsorption capacities at different pH, [BTB] = 5×10^{-5} mol dm⁻³, (0.8%)
Ru-TiO₂ = 100 mg dm⁻³. (Langmuir isotherm)**

Sl. No	pH	Adsorption Capacity (Langmuir Isotherm) (mol g ⁻¹)
1	4.0	0.00091
2	5.0	0.00083
3	6.0	0.00074
4	7.0	0.00060
5	8.0	0.00060

Where S basically represents efficiency of adsorption (mol g^{-1}), C_0 is the initial concentration of BTB, C is the BTB is the equilibrium concentration (mol dm^{-3}), V is the volume (dm^3) of the solution, and m is the mass of added Ru-TiO₂ (g).

The adsorption of the BTB on the surface of Ru-TiO₂ photo-catalyst was studied by continuous stirring the aqueous solution of BTB in the dark for 24 h in a flask containing varying amounts of Ru-TiO₂. The analysis of BTB concentration after centrifugation shows no observable loss of the dye. Hence, adsorption has no significant effect on the degradation rate.

3.3.6 Effect of pH

pH is an key parameter in photo-catalytic reactions, it gives information pertaining to the morphological properties of the photo-catalyst and adsorption performance of contaminants. Effect of pH on the degradation of BTB in water medium of Ru-TiO₂ was examined between pH 4.0 to 8.0 under UV-light. Whilst maintaining other reaction conditions constant. The photo-catalytic degradation of BTB was higher in the pH range 4.0-6.0 and slightly lower in the pH range 7.0-8.0 as shown in Table 3.6 and Fig. 3.12. This performance possibly elucidated on the bases that increase in the rate of photo-catalytic degradation was due to the surface activity of photo-catalyst. The adsorption at pH 4.0 to 6.0 is favoured by attractive electrostatic forces existing between BTB anion and as Ru-TiOH₂⁺,

Where Ru-TiOH₂⁺ is a major active species in this pH range. Where as in basic medium, i.e. pH 7.0 to 8.0 Ru-TiO⁻ is a major active species, Hence electrostatic repulsion between two negatively charged species, Ru-TiO⁻ and BTB anion disfavours photo-catalytic degradation [29,30]. The adsorption capacity decreases with increase in the pH from 4.0 to 8.0. The BTB react with the H⁺ and OH⁻ in solution to form two different BTB species viz., BTB^o (neutral) and BTB⁻ (anion). The proportion of BTB in different forms can be calculated from the pK_a (7.1) [31] as shown in Fig. 3.13. BTB neutral species dominates in the pH range 4.0 – 7.0 and are adsorbed at a higher degree than highly ionised species. Whereas BTB⁻ dominates in the pH range above 7.0 and are less adsorbed due to electrostatic repulsion forces. Whereas above pH 7.0 the adsorption of BTB neutral is due to weak van der Waals forces of attraction. This observation is in line with the earlier report [32].

Table 3.6. Effect of pH on the rate constant of photo catalytic degradation of BTB with 0.8% Ru-TiO₂ at 25 °C, [Ru-TiO₂] = 100 mg dm⁻³ [BTB] = 5 x 10⁻⁵ mol dm⁻³, light intensity = 4 mW/cm².

Photocatalyst	pH	$k_{\text{obs}} \times 10^3$ (min ⁻¹)
0.8% Ru-TiO ₂	4.0	13.00
	5.0	16.30
	6.0	19.00
	7.0	9.20
	8.0	6.00

Fig. 3.12. Effect of pH on the rate constant of photo-catalytic degradation of BTB with 0.8% Ru-TiO₂ at 25 °C, [Ru-TiO₂] = 100 mg dm⁻³ [BTB] = 5.00 x 10⁻⁵ mol dm⁻³, light intensity = 4 mW/cm².

(Conditions are stated in Table 3.6 (p.91))

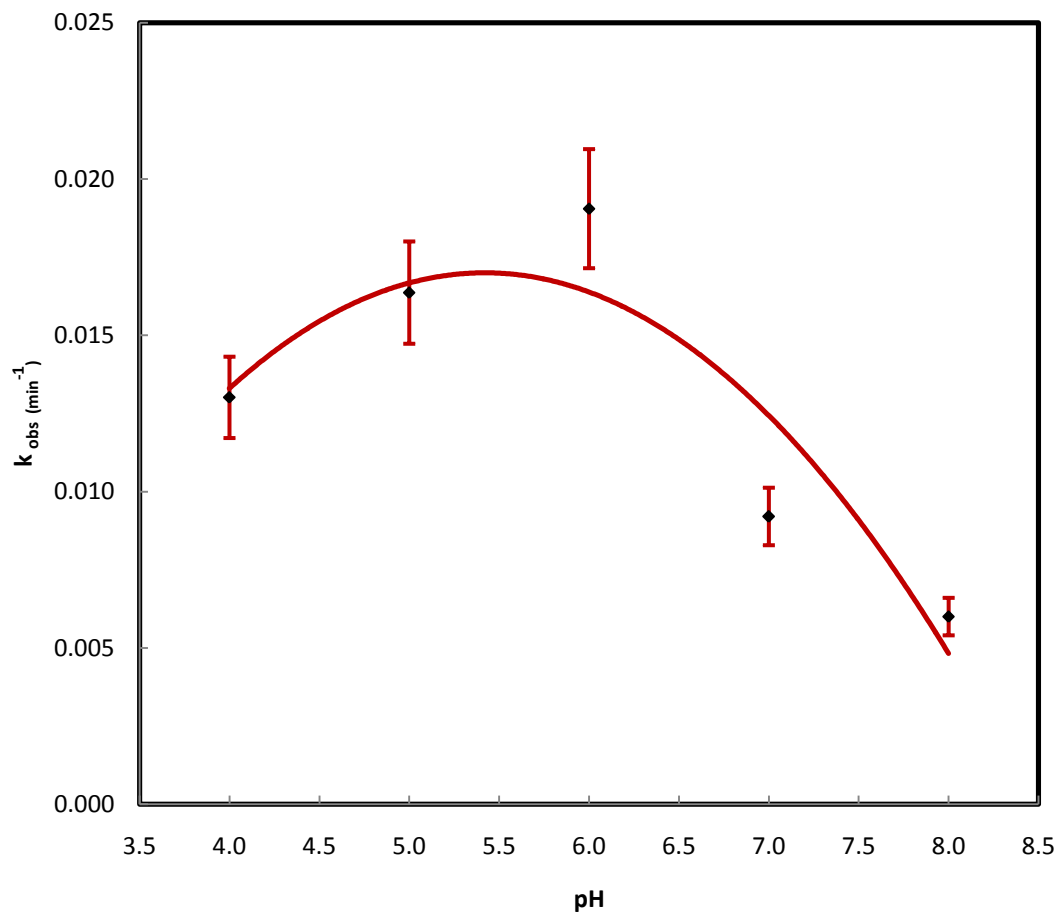
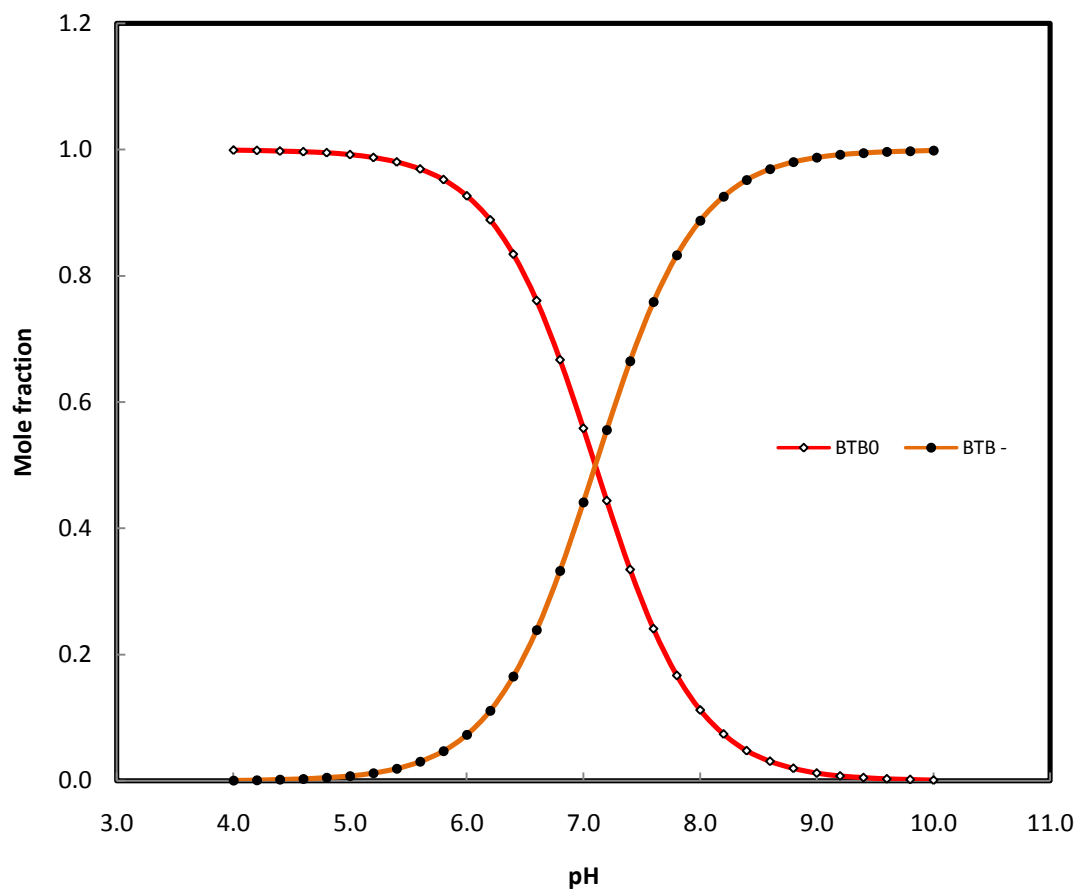


Fig. 3.13. Speciation of BTB at different pH

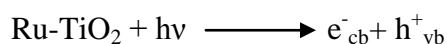


3.3.7 Effect of UV Lamp Distance

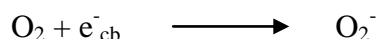
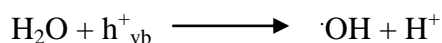
The variation of UV light intensity on the rate constant of photo-catalytic degradation of BTB was studied by altering the distance of UV lamp from the reaction mixture as shown in Table 3.7 and Fig. 3.14. It is observed that the rate constant increased with enhance in the light intensity. This can be attributed due to the fact that as the intensity of light increases, the number of photons reaching the surface of photo-catalyst (Ru-TiO₂) also increases, consequently, increasing the number of electron-hole pairs. The holes decompose the BTB molecules adsorbed on the surface of Ru-TiO₂ particles and oxidize it to water resulting in their efficient degradation.

3.3.8 The Mechanism of Photo-catalytic Degradation of BTB with Ru-TiO₂

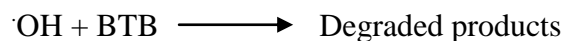
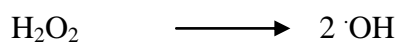
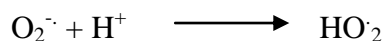
When UV light was allowed fall on the photo-catalyst, electrons in the valence band were to the conduction band. Consiquently, an e⁻_{cb}- h⁺_{vb} is generated [33].



Here e⁻_{cb} represents electrons in the conduction band and h⁺_{vb} represents the holes in the valence band. The positive hole of the valence band reacts with a water molecule to produce hydroxide free radicals, where as the oxygen accepts the trapped electrons from Ru metal to generate O₂⁻ as shown in Fig. 3.15 [34].



The above reaction eliminates the possibility of e⁻_{cb}- h⁺_{vb} recombination. The ·OH and O₂⁻ generated then attack the BTB to yield degradation products.



The above photocatalytic reactions occur only in the presence of dissolved oxygen and water molecules. In absence of water molecules, the high concentration of ·OH radicals may not be possible. This may hinder the photo-catalytic degradation of organic moieties.

Table 3.7. BTB degradation under different UV intensities BTB with 0.8% Ru-TiO₂ at 25 °C, [Ru-TiO₂] = 100 mg dm⁻³, [BTB] = 5 x 10⁻⁵ mol dm⁻³, at pH=4.

Photocatalyst	Light intensity (mW/cm ²)	k _{obs} x 10 ³ (min ⁻¹)
0.8% Ru-TiO ₂	4.0	13.00
	5.0	15.00
	6.0	18.00
	7.0	21.00
	8.0	25.00

Fig. 3.14. BTB degradation under different UV intensities BTB with 0.8% Ru-TiO₂ at 25 °C, [Ru-TiO₂] = 100 mg dm⁻³, [BTB] = 5.00 x 10⁻⁵ mol dm⁻³, at pH=4.0.

(Conditions are stated in Table 3.7 (p.95))

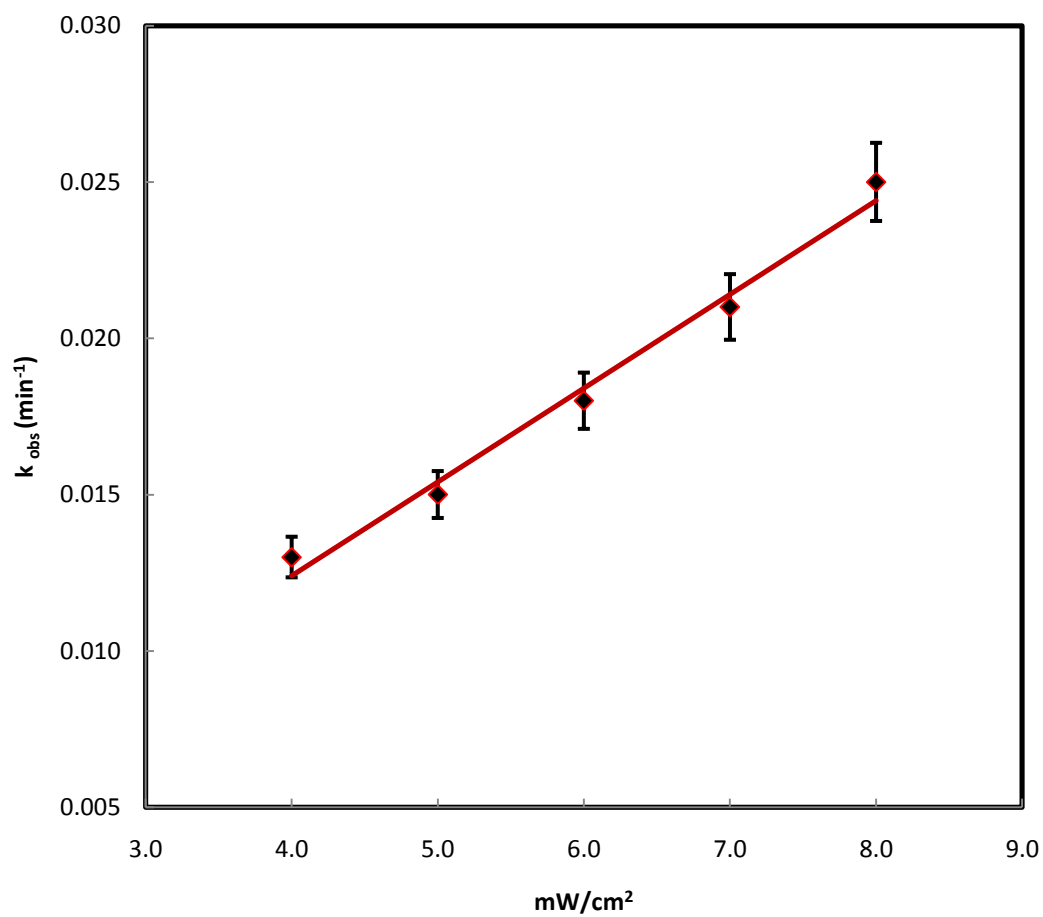
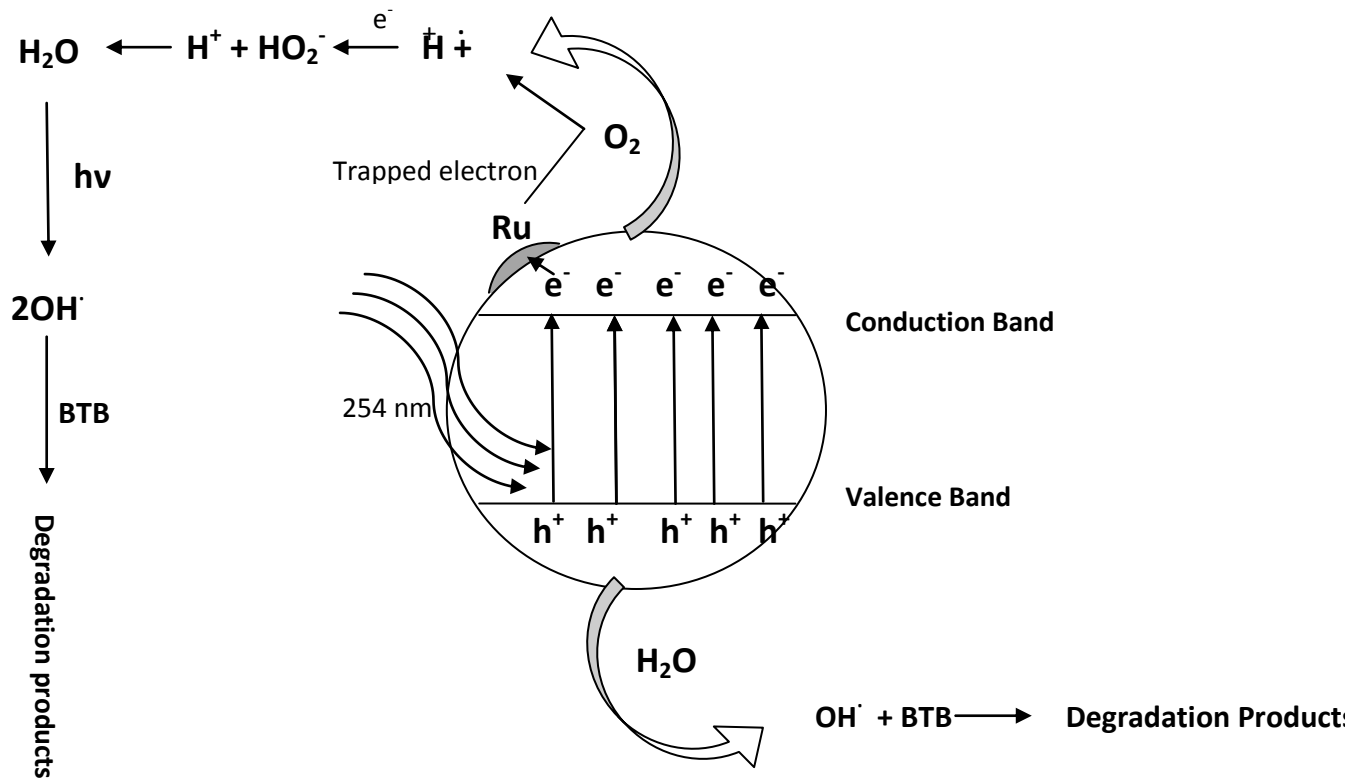


Fig. 3.15. Mechanism of photo-catalytic degradation of BTB with Ru-TiO₂



3.4 Conclusion

Liquid impregnation method was used to synthesize Ru-TiO₂ nanoparticles. The particle size of TiO₂ decreases with increasing percentage of ruthenium doping. 0.8% Ru-TiO₂ nanoparticles exhibited a better potential compared to UV and UV/TiO₂ techniques for the effective photo-catalytic degradation of bromothymol blue in acidic medium (pH 4.0 to pH 6.0). Photo-catalytic degradation of bromothymol blue could be achieved in 1 hour with 100 mg dm⁻³ dosage of 0.8% Ru-TiO₂.

References

1. S. Akbar Hosseini and P. Moalemzade, "CuFe₂-xLuxO₄ nanoparticles: synthesis through a green approach and its photocatalyst application", *J. Mater. Sci.: Mater. Electron.* Vol. 27, 2016, pp. 8802-8806.
2. O.E. Ligrini and A. Oliveros, A.M. Braun, "Photochemical processes for water treatment", *Chem. Rev.* Vol. 93, 1993, pp. 671-698.
3. N.S. Arul, D. Mangalaraj, P.C. Chen, N. Ponpandian, P. Meena and Y. Masuda, "Enhanced photocatalytic activity of cobalt-doped CeO₂ nanorods", *J. Sol-Gel. Sci. Technol.* Vol. 64, 2012, pp. 515-523.
4. S.K. Kansal, P. Kundu, S. Sood, R. Lamba, A. Umar and S.K. Mehta, "Photocatalytic degradation of the antibiotic levofloxacin using highly crystalline TiO₂ nanoparticles", *New J. Chem.* Vol. 38, 2014, pp. 3220 -3226.
5. D. Chen, Z. Jiang, J. Geng, Q. Wang and D. Yang, "Carbon and Nitrogen Co-doped TiO₂ with Enhanced Visible-Light Photocatalytic Activity", *Ind. Eng. Chem. Res.* Vol. 46, 2007, pp. 2741-2746.
6. Q. Sun and Y.M. Xu, "Evaluating intrinsic photocatalytic activities of anatase and rutile TiO₂ for organic degradation in water", *J. Phys. Chem. C* Vol. 114, 2010, pp. 18911-18918.
7. S.G. Ansari, Fatima Tuz-Zehra, H. Fouad, Azza S. Hassenein and Z.A. Ansari, "Effect of flower extracts on the photoconversion efficiency of dye sensitized solar cells fabricated with Sn-doped TiO₂", *J. Mater. Sci.: Mater. Electron.* Vol. 26, 2015, pp. 5170-5174.
8. S.I. Shah, W. Li, C.P. Huang, O. Jung and C. Ni, "Proceedings of the National Academy of Sciences of the United States of America PNAS", Vol. 99, 2002, pp. 6482-6486.
9. M.M. Haque and M. Muneer, "TiO₂-mediated photocatalytic degradation of a textile dye derivative, bromothymol blue, in aqueous suspensions", *Dyes Pigments.* Vol. 75, 2007, pp. 443-448.
10. J. Choi, H. Park and M.R. Hoffmann, "Effects of Single Metal-Ion Doping on the Visible-Light Photoreactivity of TiO₂", *J. Phys. Chem. C.* Vol. 114 (2), 2009, pp. 783-792.
11. K. Wetchakun, N. Wetchakun and S. Phanichphant, "Enhancement of the Photocatalytic Performance of Ru-Doped TiO₂ Nanoparticles", *Adv. Mater. Res.* Vol. 55-57, 2008, pp. 853-856.
12. V. Marinova, S.H. Lin, K.Y. Hsu, M.L. Hsieh, M.M. Gospodinov and V. Sainov,

- “Optical and holographic properties of $\text{Bi}_4\text{Ge}_3\text{O}_{12}$ crystals doped with ruthenium”, *J. Mater. Sci.: Mater. Electron.* Vol. 14, 2003, pp. 857-858.
13. S. Ozkan, M.W. Kumthekar and G. Karakas, “Characterization and temperature-programmed studies over Pd/TiO₂ catalysts for NO reduction with methane”, *Catal. Today.* Vol. 40, 1998, pp. 3-14.
 14. T. An, H. Yang, W. Song, G. Li, H. Luo and W.J. Cooper, “Mechanistic considerations for the advanced oxidation treatment of fluoroquinolone pharmaceutical compounds using TiO₂ heterogeneous catalysis”, *J. Phys. Chem. A.* Vol. 114 (7), 2010, pp. 2569-2575.
 15. M. Kalamuei, M. Kamazani, M. Niasari, S. M. Mashkani, “A simple sonochemical approach for synthesis of selenium nanostructures and investigation of its light harvesting application”, *Ultrason. Sonochem.* Vol. 23, 2015, pp. 246-256.
 16. M.S. Lee, S.S. Hong and M. Mohseni, “Synthesis of photocatalytic nanosized TiO₂-Ag particles with sol-gel method using reduction agent”, *J. Mol. Catal. A.* Vol. 242 (1-2), 2005, pp. 135-140.
 17. A.N. Kadam, R.S. Dhabbe, M.R. Kokate, Y.B. Gaikwad and K.M. Garadkar, “Preparation of N doped TiO₂ via microwave-assisted method and its photocatalytic activity for degradation of Malathion”, *Spectrochim. Acta A: Mol. Biomol. Spectrosc.* Vol. 133, 2014, pp. 669-676.
 18. S. Ullah, E.P. Ferreira-Neto, A.A. Pasa. C.C.J. Alcantara, J.J.S. Acuna, S.A. Bilmes, M.L. Martinez Ricci, R. Landers, T.Z. Fermino and U.P. Rodrigues-Filho, “Enhanced photocatalytic properties of core@shell SiO₂@TiO₂ nanoparticles” *Appl. Catal. B: Env.* Vol. 179, 2015, pp. 333-343.
 19. D. Williams and C. Carter, *Transmission electron microscopy: A Textbook for Material Science.* Newyork, USA: Springer. p. 35 (2009)
 20. M.M. Ba-Abbad, A.H. Kadhum , A.B. Mohamad , M.S. Takriff and K. Sopian, “Synthesis and Catalytic Activity of TiO₂ Nanoparticles for Photochemical oxidation of Concentrated Chlorophenols under Direct Solar Radiation”, *Int. J. Electrochem. Sc.* Vol. 7, 2012, pp. 4871-4888.
 21. M.A. Hema, Yelil Arasi, P. Tamilselvi and R. Anbarasan, “Titania Nanoparticles Synthesized by Sol-Gel Technique”, *Chem. Sci. Trans.* Vol. 2(1), 2013, pp. 239-245.
 22. L. Liu, S. Chen, W. Sun and J. Xin, “Enhancing the visible light absorption via combinational doping of TiO₂ with nitrogen (N) and chromium (Cr) ”, *J. Mol. Struct.* Vol. 1001, 2011, pp. 23-28.
 23. C. Xu, J. Tamaki, N. Miura and N. Yamazoe, “Grain size effects on gas sensitivity

- of porous SnO₂-based elements”, *Sens. Actuators B: Chem.* Vol. 3, 1991, pp. 147-155.
24. B.K. Min and S.D. Choi, “Undoped and 0.1 wt % Ca-doped Pt- catalyzed SnO₂ sensors for CH₄ detection” *Sens. Actuators B: Chem.*, Vol. 108, 2005, pp. 119-124.
25. G. Neri, A. Bonavita, G. Micali, N. Donato, F.A. Deorsola, P. Mossino, I. Amato and B. de Benedetti, “Ethanol sensors based on Pt-doped tin oxide nanopowders synthesised by gel-combustion.Sens”, *Actuat. B.* Vol. 117, 2006, pp. 196-204.
26. N.L. Wu, S.Y. Wang and I.A. Rusakova, “Inhibition of crystallite growth in the sol-gel synthesis of nanocrystalline metal oxides. *Science* Vol. 285, 1999, pp. 1375-1377.
27. M.M. Haque and M. Muneer, “Heterogeneous photocatalysed degradation of a herbicide derivative, isoproturon in aqueous suspension of titanium dioxide”, *J. Environ. Manag.* Vol. 69, 2003, pp. 169-176.
28. M. Muneer, M. Qamar and M. Saquib, “Semiconductor-mediated photocatalytic degradation of an azo dye, chrysoidine Y in aqueous suspensions”, *Desalination.* Vol. 171, 2004, pp. 185-193.
29. H. Chun, W. Yizhong and T. Hongxiao. “Destruction of phenol aqueous solution by photocatalysis or direct photolysis”, *Chemosphere* Vol. 41, 2000, pp. 1205-1209.
30. C. Hu, Y. Tang, J.C. Yu and P.K. Wong, “Photocatalytic degradation of cationic blue X-GRL adsorbed on TiO₂/SiO₂ photocatalyst”, *Appl. Catal. B: Env.* Vol. 40, 2003, pp. 131-140.
31. E. Klotz, R. Doyle, E. Gross and B. Mattson. “The Equilibrium Constant for Bromothymol Blue: A General Chemistry Laboratory Experiment Using Spectroscopy”, *J. Chem. Edu.* Vol. 88, 2011, pp. 637–639.
32. A. Verma, M. Sheoran and A.P. Toor, “Titanium dioxide mediated photocatalytic degradation of malathion in aqueous phase”, *Indian J. Chem. Technol.* Vol. 20, 2013, pp. 46-51.
33. I.K. Konstantinou and T.A. Albanis, “TiO₂-Assisted Photocatalytic Degradation of Azo Dyes in Aqueous Solution: Kinetic and Mechanistic Investigations”, *Appl. Catal. B: Env.* Vol. 49, 2004, pp. 1-14.
34. N.M. Mahmoodi, M. Arami, N.Y. Limaee and N.S. Tabrizi, “Kinetics of heterogeneous photocatalytic degradation of reactive dyes in an immobilized TiO₂ photocatalytic reactor”, *J. Colloid. Interface Sci.* Vol. 295, 2006, pp. 159-164.

Chapter 4

Ba-ZnO nanoparticles for photocatalytic degradation of chloramphenicol

4.1 Introduction

The total amount of water present on earth is about $1.4 \times 10^9 \text{ km}^3$, from which only $1.3 \times 10^7 \text{ km}^3$ corresponds to drinking water [1]. The ground water and surface water contaminated by the industrial waste water, irrigation runoff, chemical spills, commercial operations that contain many non-biodegradable substrates that are harmful to the humankind and also significant threat for flora and fauna of the environment [2-6]. So far, it is difficult to treat these organic contaminants by usual conventional and biological treatment techniques [7].

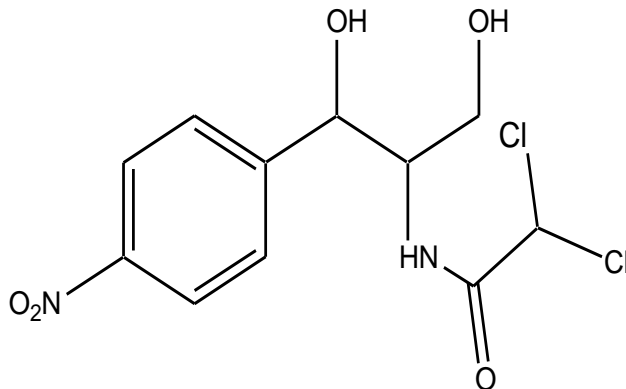
The general importance of Advanced oxidation processes (AOPs) discussed in chapter 2 (p.34).

The ZnO nanoparticles have been extensively applied in the field of photocatalytic mineralization [8]. ZnO is believed to be a good substitute to TiO_2 (3.2 eV), due to their broad energy gap (3.3 eV), low cost, greater efficiency, stability with a high excitation binding energy and ecofriendly. The above characteristics make the material very attractive and potentially useful for a wide range of applications. Its photodegradation mechanism similar to that of Titanium dioxide. In recent years, ZnO or doped-ZnO nanoparticles are synthesized by various methods [8].

Decorating ZnO with impurity/dopant (transition metal ions) improves the optical, electrical, magnetic properties by changing its electronic structure and showing other enhancement in the different application like photoreaction and photocatalytic activity. These transition metal ions not only serve as trapping sites, but also reduce charge re-combination and facilitate interfacial electron transfer process that in turn enhances the surface reactivity. Doping also induces the widening of wavelength from UV to the visible-range [9-10].

Now-a-days, antibiotics and public care products are largely discharged into the water bodies without proper treatment. This causes a threat to the ecosystem and human health. Chloramphenicol (CLP) belongs to tetracycline family of antibiotics and commonly known

as Chloromycetin [11]. CLP is believed to be proto-typical wide range spectrum antibacterial agent [12], hence, it can be used to cure an variety of microscopic organisms causing illness [13]. These antibiotics enter the public waste water streams due to incomplete metabolism of antibiotics dosage in the human body [14].



Chemical Structure of Chloramphenicol (CLP)

4.2 Experimental

4.2.1 Chemicals and methods

Analar grade CLP was procured from Sigma-Aldrich, Bangalore. It was used as received without additional purification. A suitable quantity of sample was dissolved in deionized water to prepare stock solution of CLP. The $Zn(NO_3)_2 \cdot 4H_2O$, NaOH and $Ba(NO_3)_2$ procured from HIMEDIA. The acetate, phosphate, and borate buffers were prepared to maintain pH during reaction condition, all reagents and chemicals were used are analytical grade.

The instruments used were already discussed in chapter-2 and p.no. (36-40)

4.2.2 Photocatalyst preparation

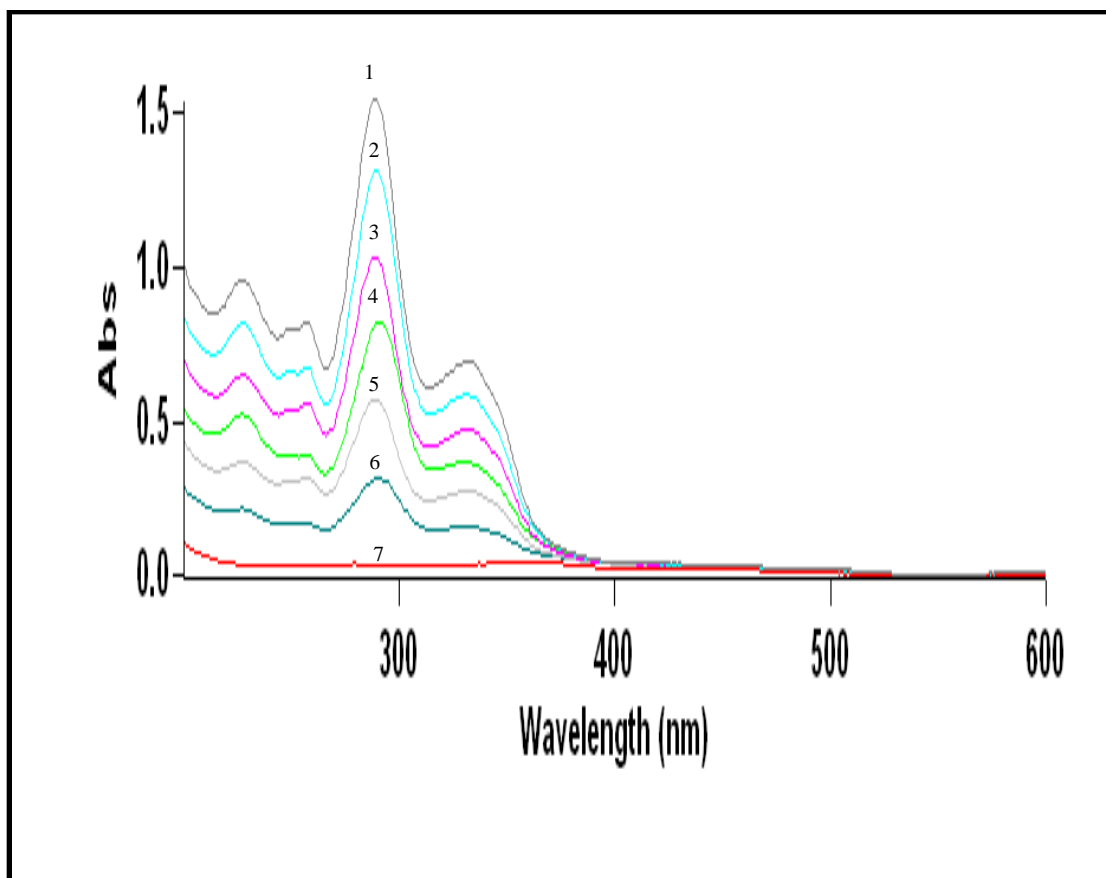
For synthesizing undoped and copper doped ZnO nanoparticles, known quantity of zinc nitrate salt was dissolved in deionized water to prepare 0.1M zinc nitrate solution and 10 mg dm⁻³ of sodium dodecyl sulphate (surfactant) was added to control particle size, and serves as a capping agent during preparation of zinc nitrate solution [15]. 0.1M NaOH solution was added to Zn(NO₃)₂ solution. NaOH was added drop wise for 3 hrs with constant stirring at the rate 1000 RPM. The nanoparticles were formed and settle for overnight. The suspension was decanted carefully, the residual was washed and filtered several time with distilled water then washed with ethanol to remove other contaminants. The nanoparticles were dried in an oven at 120 °C for 3 hrs then powder is grounded in a mortar then calcined at 500 °C for about 1 hr in a muffle furnace (with a heating rate about 10 °C per minute). During the drying process, complete transformation of zinc hydroxide to Zinc oxide takes place. The same procedure was followed to synthesize 5% Ba doped ZnO nanoparticles the only difference was the addition of 0.1M barium nitrate solution in zinc nitrate solution. The barium concentration was 5 (% mole ratio). The barium when doped with ZnO nanoparticles it enters in to the interstitial position of ZnO lattice. Similar literatures were earlier reported [16, 17].

4.2.3 The Photocatalysis Process

To study the photocatalytic degradation of CLP, a required quantity of CLP and buffer mixture was kept in a pyrex beaker. A dose of 0.10 g dm⁻³ of 5% Ba-ZnO nano particles was added. Before illumination, the suspensions were stirred for 60 min in dark place to reach adsorption and desorption equilibrium between CLP and photocatalyst. Then, it was transferred in to the photoreactor and then kept under 8 W UV lamps (Philips) with a wavelength peak at 254 nm and of 4mW/cm² intensity with continuous magnetic stirring. After every 10 minutes interval the solution was taken out and centrifuged at 5000 rpm for 5 min. The decrease in the concentration of CLP was monitored at 278 nm ($\epsilon = 27471 \text{ dm}^3 \text{ mol}^{-1} \text{ cm}^{-1}$) using visible spectrophotometer (a CARY 50 Bio UV-Visible Spectrophotometer) and the degree of mineralization was studied as shown in Fig. 4.1.

Fig. 4.1. UV–Visible spectral changes during the degradation of Chloramphenicol at 25 °C, [CLP] = 3.00×10^{-5} mol dm⁻³, pH = 5.0, 5% Ba-ZnO = 0.10 g dm⁻³ and light intensity 4 mW/cm².

Time (1) 00.00 min (2) 15.00 min (3) 30.00 min (4) 45.00 min
(5) 60.00 min (6) 75.00 min (7) 90.00 min



4.3 Results and discussion

4.3.1 Comparison of different photocatalysts

The degree of mineralization of CLP with UV, UV- ZnO, and UV- 5% Ba-ZnO was reported. It is seen that the mineralization efficiency of CLP with UV- 5% Ba-ZnO was most efficient than UV and UV-ZnO as shown in Fig. 4.2.

Influence of barium doping on ZnO was investigated by using 5% (mole ratio) of barium, higher content of barium may facilitate efficiently separating charge carrier and hindered the recombination of $e^- - h^+$ pairs and this increases the photocatalytic efficiency. The photodegradation rate was maximum with 5% Ba-ZnO compared with UV and UV-ZnO. Hence, further studies were carried out with 5% Ba-ZnO.

The % degradation activity of CLP was performed under identical conditions with UV, UV-ZnO, and UV- 5% Ba-ZnO and % adsorption in dark was also determined. The % mineralization of CLP in 100 minutes was given in Fig. 4.3.

4.3.2 Characterization of ZnO and 5% Ba-ZnO

4.3.2.1 X-ray Diffraction Studies (XRD)

To study the crystal-size and phase purity of prepared laboratory photocatalysts, the samples were identified using XRD. XRD spectra of 5% Ba-ZnO, are shown in Fig. 4.4. The intense sharp peak indicates that the synthesized nanoparticles were crystalline in nature. The appearance of (100) (002) (101) (102) (110) (103) (200) and (112) diffraction peaks at different lattices at angle 2θ ($20-90^\circ$) indicate hexagonal wurzite structure.

The sharp peak of 101 indicates that the enlargement of nano crystal has taken-up along the easy route of crystallization of zinc oxide [18]. The XRD peaks confirmed no significant impurity present in the prepared samples.

The broadening of the wurzite main intense peak (101) was used, to determine the crystallite size of prepared nanoparticles, using Scherrer equation (1), it was estimated that the average grain size of 5% Ba-ZnO samples is about 35.20 nm (± 3).

$$D = \frac{0.94 \lambda}{\beta \cos \theta} \quad (1)$$

Where “D = average crystalline diameter, λ = wavelength in angstrom, β = is the line width at half–maximum and θ = Bragg’s angle”.

Fig. 4.2. Rate constants for the Photocatalytic degradation of CLP by various treatments at 25 °C, [CLP] = 3.00×10^{-5} mol dm⁻³, pH = 5.0, 5% Ba-ZnO = 0.10 g dm⁻³ and light intensity = 4 mW/cm².

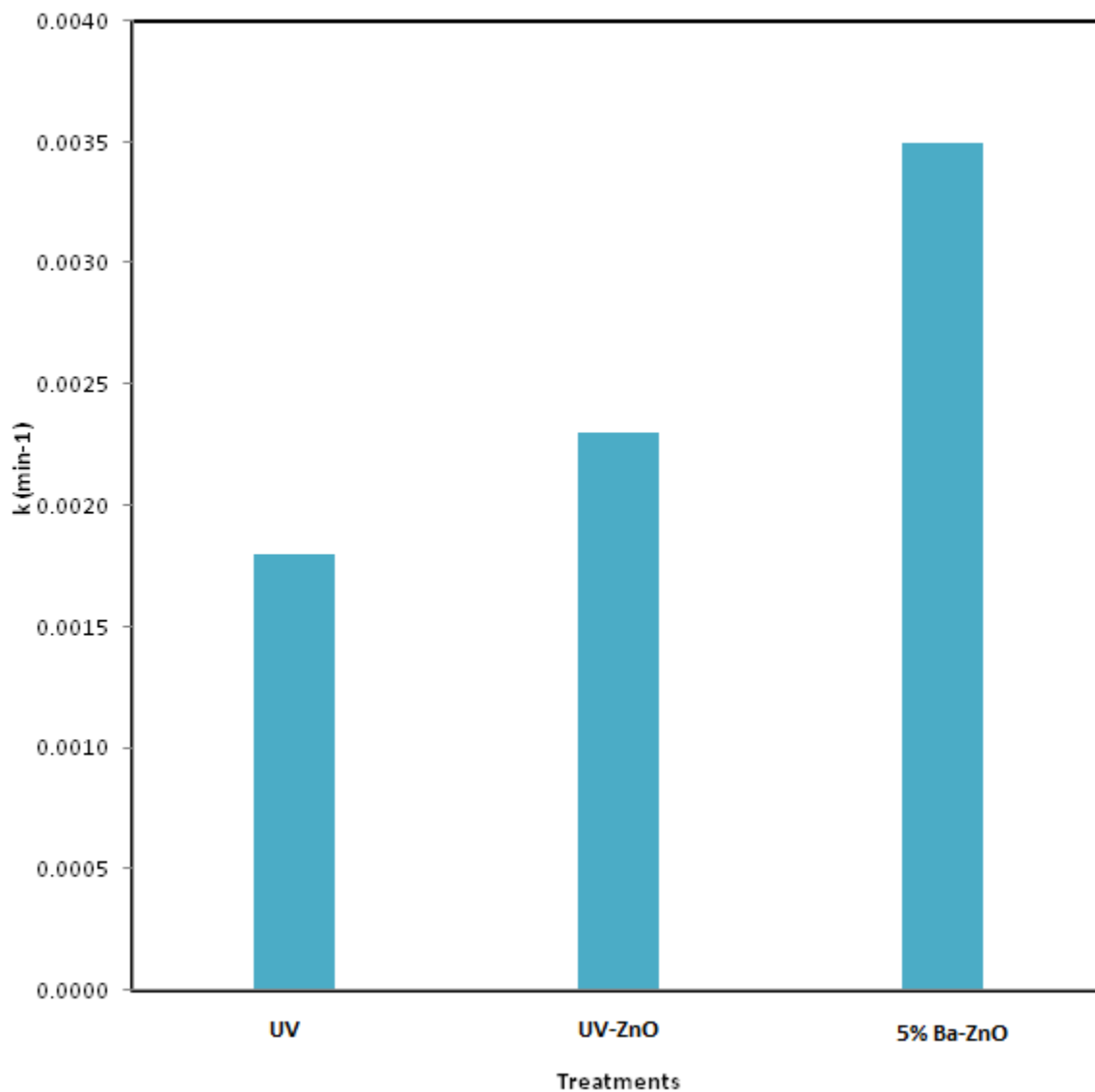


Fig. 4.3. % degradation efficiencies of various treatment methods with time at 25 °C.
5% Ba-ZnO = 0.10 g dm⁻³, [CLP] = 3.00 x 10⁻⁵ mol dm⁻³, at pH = 5.0 and light intensity = 4 mW/cm².

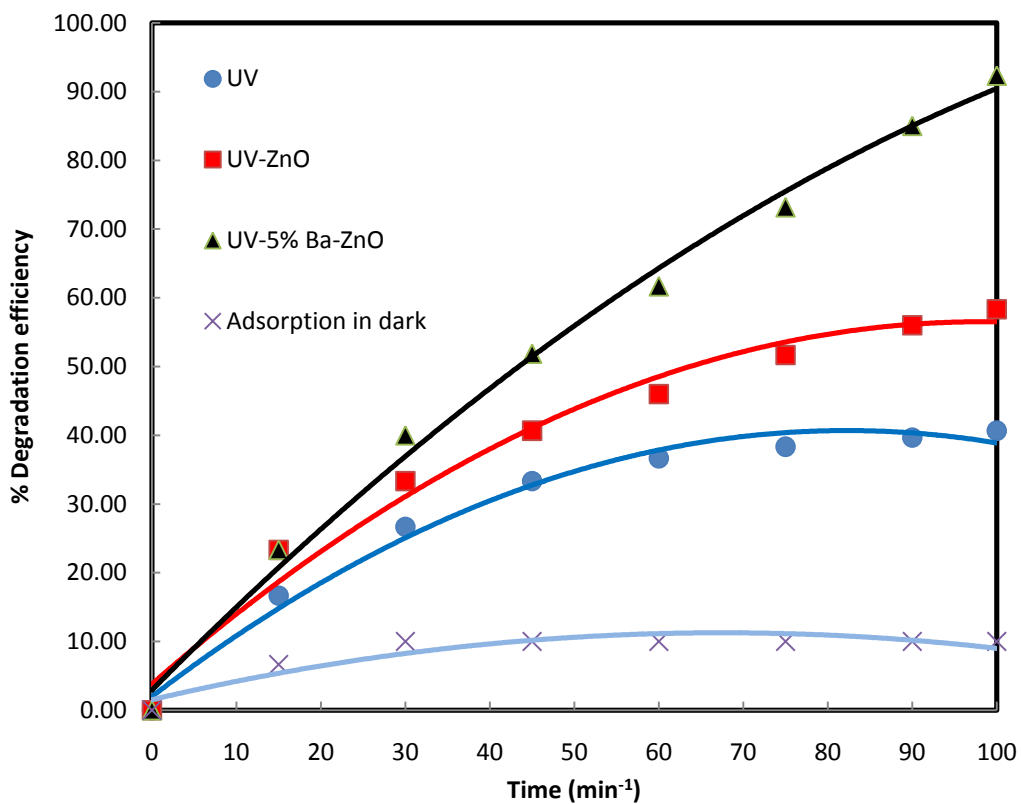
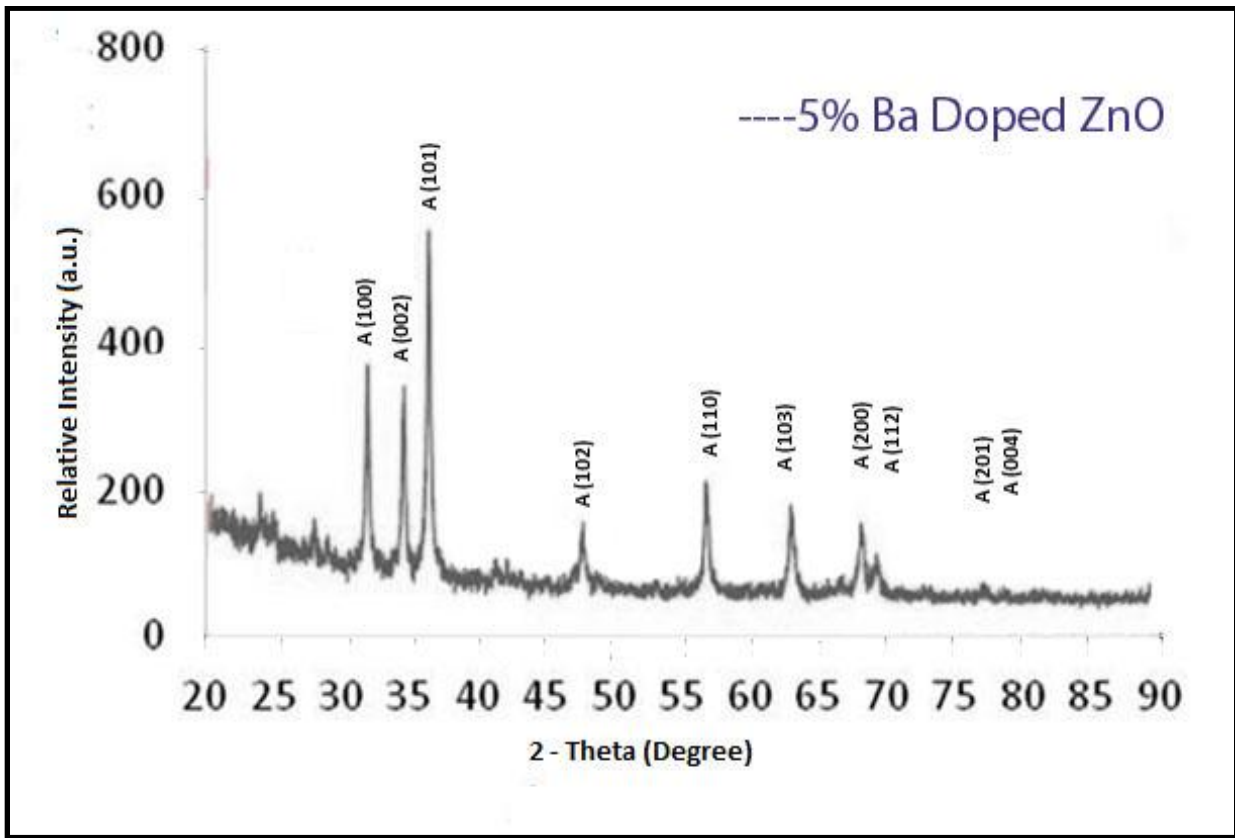


Fig. 4.4. XRD patterns of 5% Ba-ZnO



4.3.2.2 Scanning Electron Microscope (SEM)

The SEM analysis of ZnO and 5% Ba-ZnO was done to study the surface morphology (Fig. 4.5 a and Fig. 4.5 b). It shows that 5% Ba-ZnO nanoparticles are irregular shape and size. This irregular shape the surface area of the nanoparticles is very high [18].

4.3.2.3 Transmission Electron Microscope (TEM)

TEM images shows that Ba doped ZnO nanoparticles were agglomerated with non-uniformly distributed having barrel shaped crystalline structures as shown in Fig. 4.6 a and Fig. 4.6 b. Diffusion of small black spots observed were assumed as Ba atoms on ZnO nanoparticles with approximately 15.00 - 20.00 and 25.00 - 30.00 nm in width and length dimension respectively. It is confirmed that the synthesized nanoparticles crystal dimension is nearer to that of data extracted from XRD results for ZnO nanoparticles.

4.3.2.4 Energy Dispersive X-ray Spectroscopy (EDX)

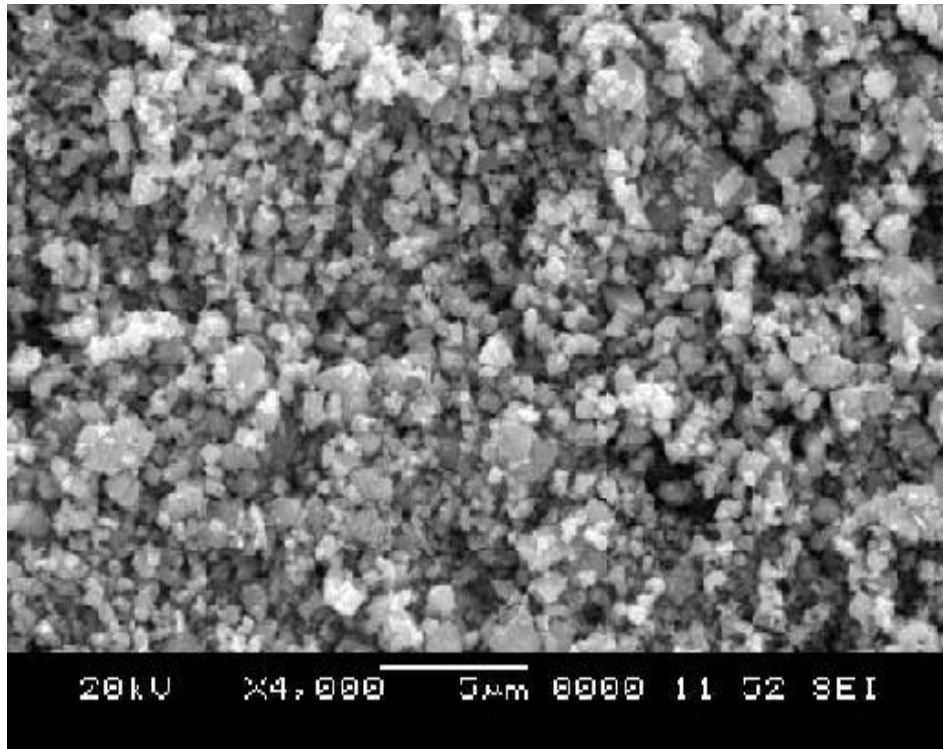
In order to study elemental composition of prepared nanoparticles EDX - analysis was done which shown in Fig. 4.7 a and Fig. 4.7 b (ZnO and 5% Ba-ZnO). The EDX spectrum reveals that existence of Zn, O and Ba at 8.630, 0.525 and 4.464 keV correspondingly. The % composition of Zn, O and Ba is 71.26, 23.95 and 4.78 respectively, It is evident from elemental composition that 4.78% barium is present in 5 (mol %) Ba-ZnO nanoparticles.

4.3.3 Effect of Photocatalyst Dosage

The rate of photocatalytic degradation of CLP was studied using different amount of a 5% Ba-ZnO photocatalyst ranging from 0.025 g dm⁻³ to 0.250 g dm⁻³ whilst [CLP] and pH=5.0 were kept constant. The rate of photo-degradation increases with increase in the quantity of photocatalyst up to limiting value 0.10 g dm⁻³, beyond 0.10 g dm⁻³ the rate of photo-degradation decreases (Table 4.1 and Fig. 4.8). This behavior might be due to increase in amount of photocatalyst increases the exposed surface area of photocatalyst which in turn increases the active centers on photocatalyst. Consequently, which produces more number of ·OH radicals eventually these radicals involve in reaction to increase the rate of photocatalytic reaction. But after limiting value (0.10 g dm⁻³) increase in amount of photocatalyst increases the turbidity of the CLP suspension, thus it prevents UV-light to reach the photocatalyst. Hence, the rate of photo-degradation decreases [19].

Fig. 4.5. Sem micrographs of a) ZnO, and b) 5% Ba - ZnO.

a)



b)

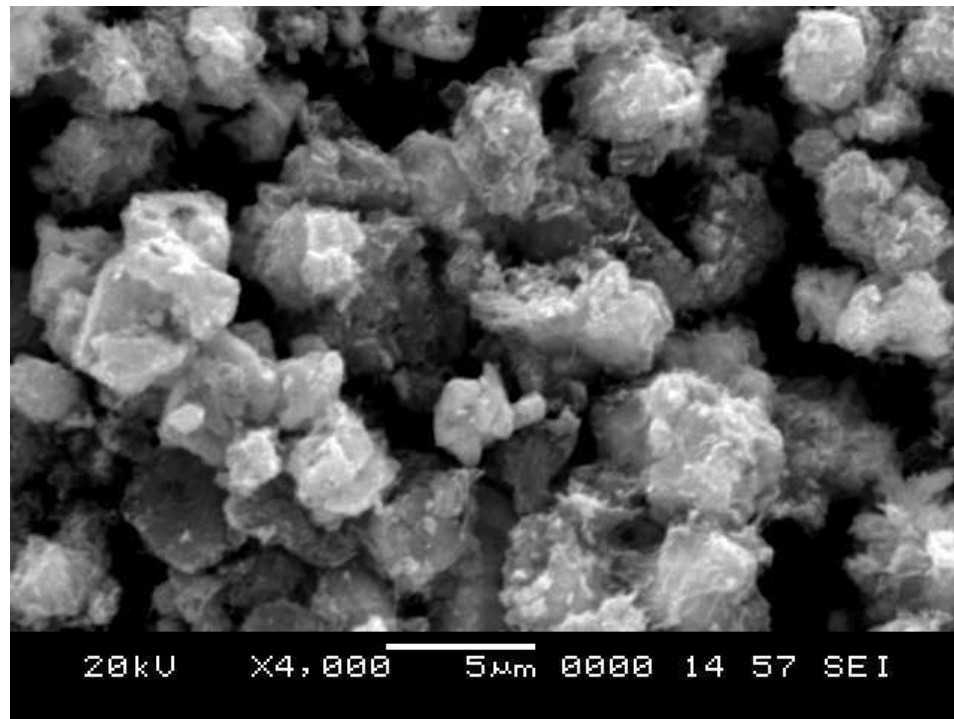
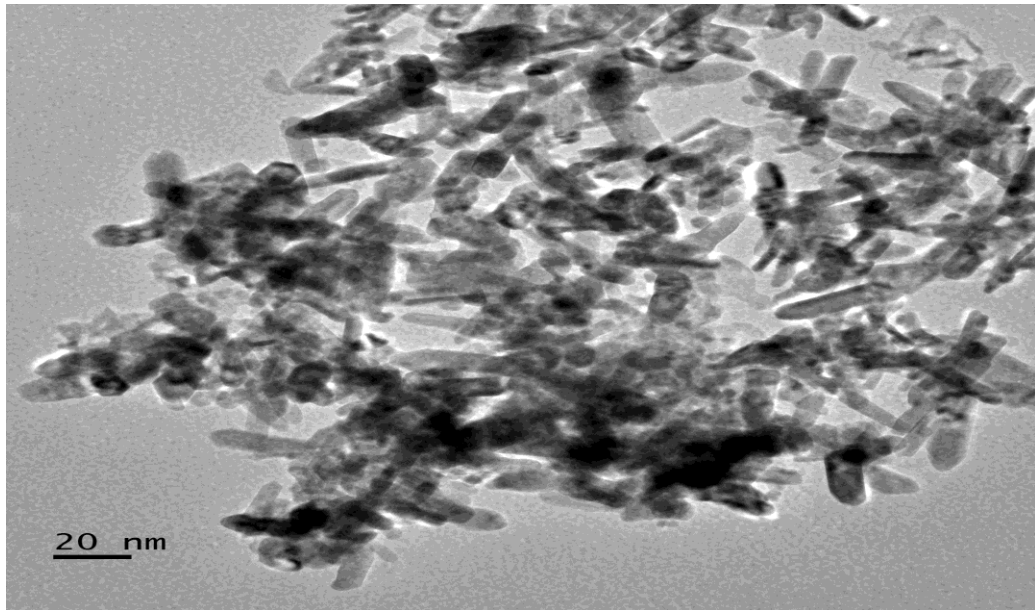


Fig. 4.6. TEM micrographs of (a&b) 5% Ba – ZnO

a)



b)

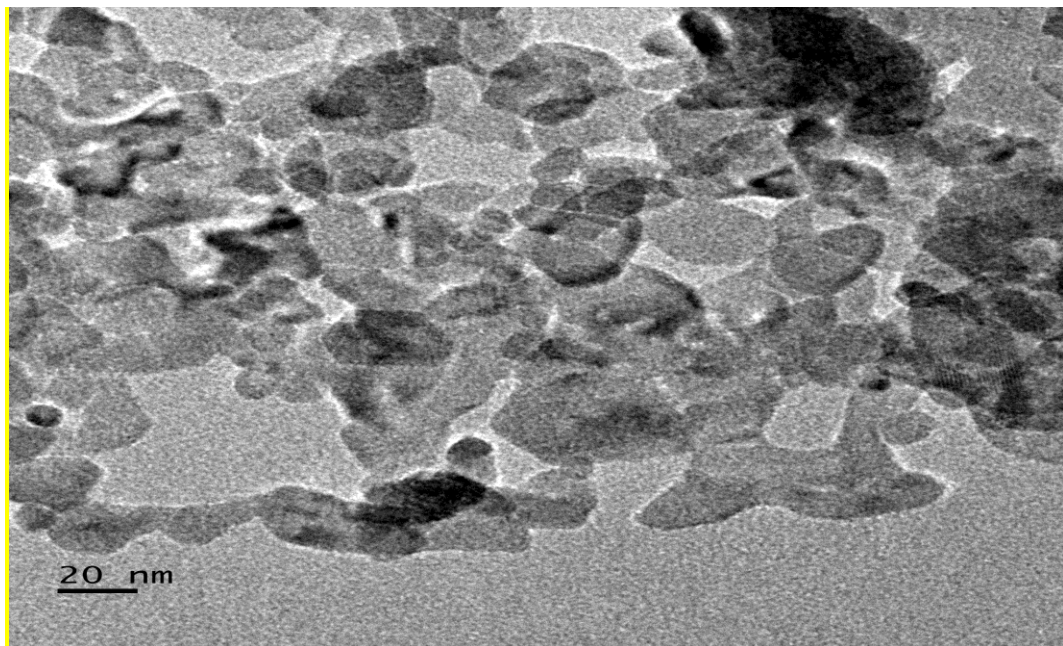


Fig. 4.7. EDX analysis of a) Pure ZnO b) 5% Ba-ZnO

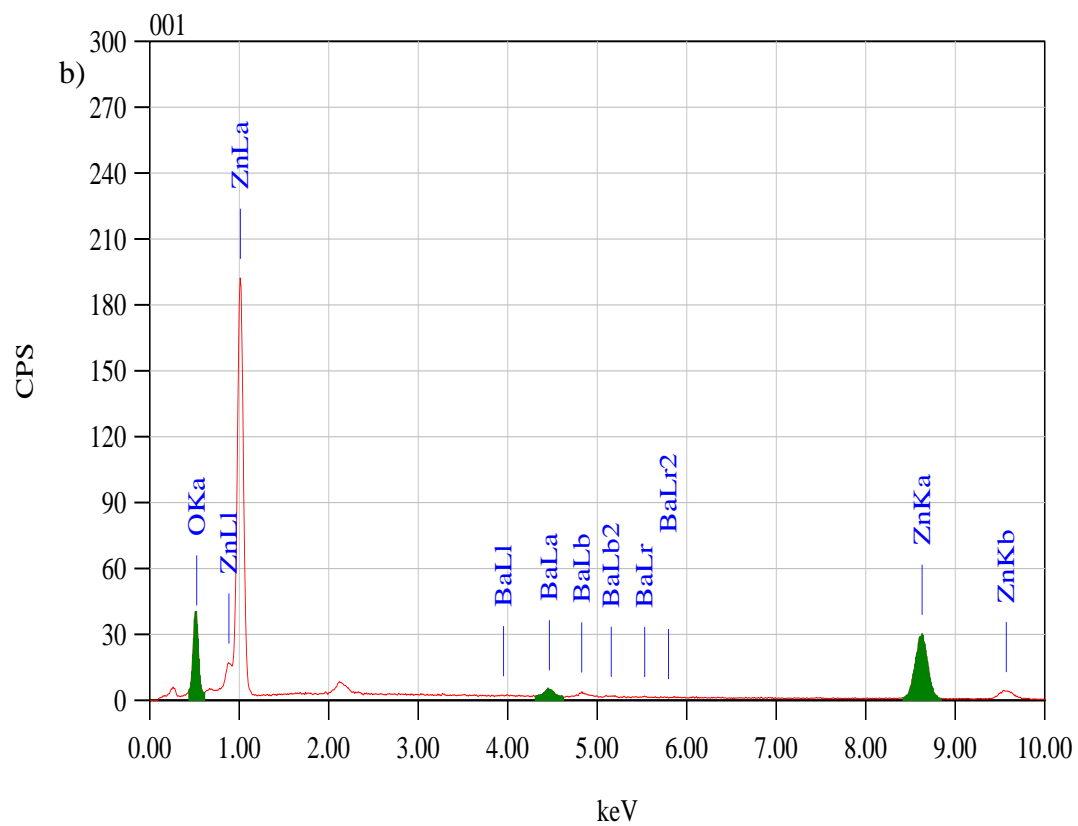
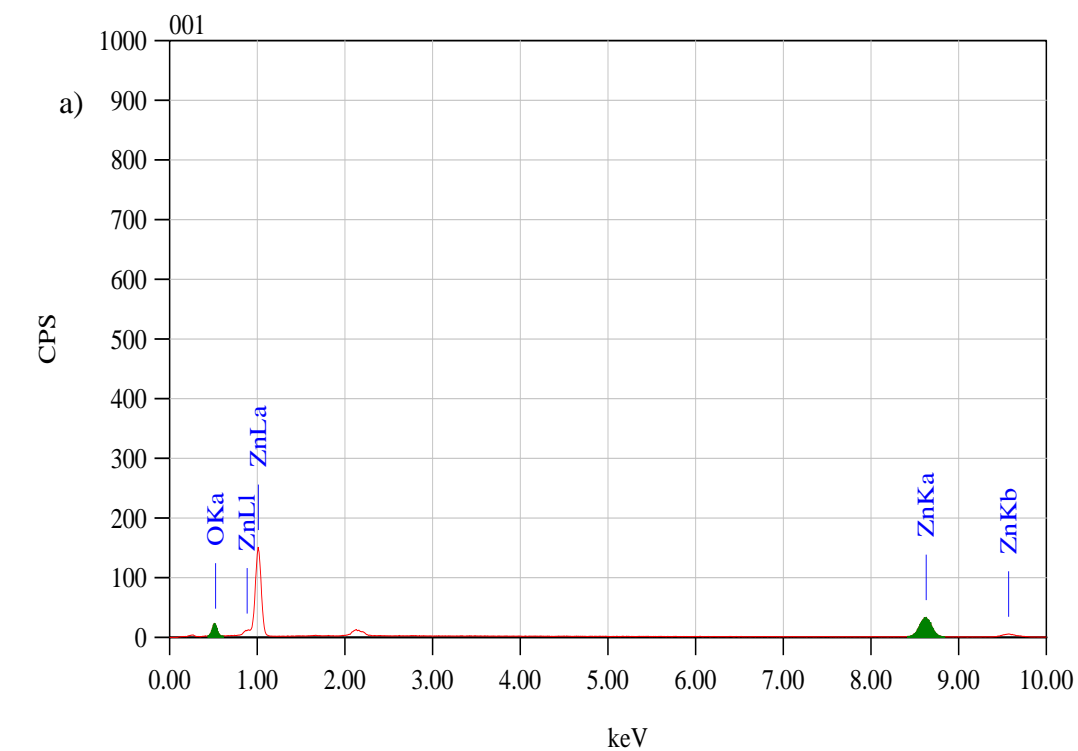
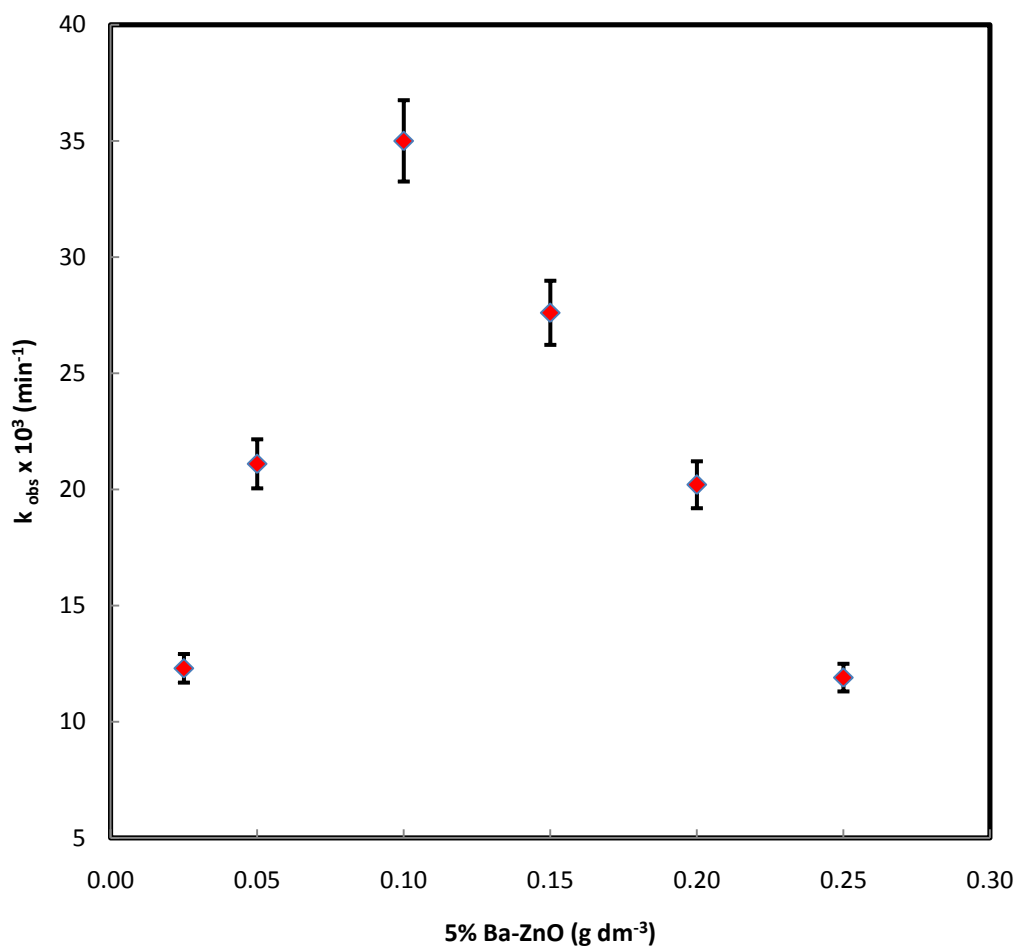


Table 4.1. Effect of different amounts of 5% Ba-ZnO photocatalyst on the degradation of CLP at [CLP] = 3.00×10^{-5} mol dm⁻³, at pH=5.0, light intensity = 4 mW/cm²

Photocatalyst	Amount of 5% Ba-ZnO(g dm ⁻³)	k _{obs} × 10 ³ (min ⁻¹)
5% Ba-ZnO	0.025	12.30
	0.050	21.10
	0.100	35.00
	0.150	27.60
	0.200	20.20
	0.250	11.90

Fig. 4.8. Effect of different amounts of 5% Ba-ZnO photocatalyst on the degradation of CLP at $[CLP] = 3.00 \times 10^{-5} \text{ mol dm}^{-3}$, at pH=5.0, light intensity = 4 mW/cm^2

(Conditions are stated in Table 4.1 (p.114))



4.3.4 Effect of [CLP]

The rate of photocatalytic degradation of CLP was studied by taking different [CLP] from 5.00×10^{-6} to 5.00×10^{-5} mol dm⁻³ by keeping other reaction conditions constant. It has been experimentally investigated that initially increase in the [CLP], the rate of photocatalytic degradation increases till [CLP] = 3.00×10^{-5} mol dm⁻³. Further increase in [CLP], decreases the rate of photocatalytic degradation as shown in Table 4.2 and Fig. 4.9. This was due to, as the [CLP] increases, plenty of drug molecules are adsorbed on the active centers of the photocatalyst surface, hence effective degradation takes place. But after limiting value (3.00×10^{-5} mol dm⁻³) the CLP itself acts as a filter for the light. Hence, the photons can't reach the photocatalyst surface and thus, the rate of photocatalytic degradation decreases [20-22].

4.3.5 Effect of pH

The pH normally influences the adsorption capacity of the adsorbent in aqueous medium by altering the surface properties of adsorbent. The effect of pH on the rate of photo degradation of CLP was studied by varying the pH from 5.0 - 9.0, while keeping other reaction conditions constant. The rate of photo-catalytic degradation of CLP ($Pk_a=5.5$) was higher in the pH range 5.0 - 6.0 and lower in the pH range 7.0 - 9.0 as shown in Table 4.3 and Fig. 4.10. This increase in the rate of photocatalytic degradation may be due to the fact that in acidic medium the photocatalytic surface is positively charged (PZC=6) and it adsorbs more partial negatively charged CLP ions hence, effective collision between CLP and Ba-ZnO photocatalyst takes place so rate of degradation is maximum at pH 5.0 -6.0.

On the contrary in alkaline medium the OH⁻ ions accumulate on the surface of photocatalyst making it negatively charged and CLP is also negatively charged in alkaline medium. Hence, the electrostatic repulsion between CLP ion and photocatalyst takes place leading to decrease rate of photodegradation at pH 7.0 to 9.0. This observation is in line with the earlier report [23].

**Table 4.2. Effect of [CLP] on photocatalytic rate constants with 5% Ba-ZnO at 25 °C,
 [Ba-ZnO] = 0.10 g dm⁻³, at pH=5.0, light intensity = 4mW/cm²**

Photocatalyst	[CLP] x 10 ⁵ mol dm ⁻³	k _{obs} x 10 ³ (min ⁻¹)
5% Ba-ZnO	0.50	07.70
	1.00	18.10
	2.00	27.40
	3.00	34.70
	5.00	30.00

Fig. 4.9. Effect of [CLP] on photocatalytic rate constants with 5% Ba-ZnO at 25 °C,

[Ba-ZnO] = 0.10 g dm⁻³, at pH=5.0, light intensity = 4mW/cm²

(Conditions are stated in Table 4.2 (p.117))

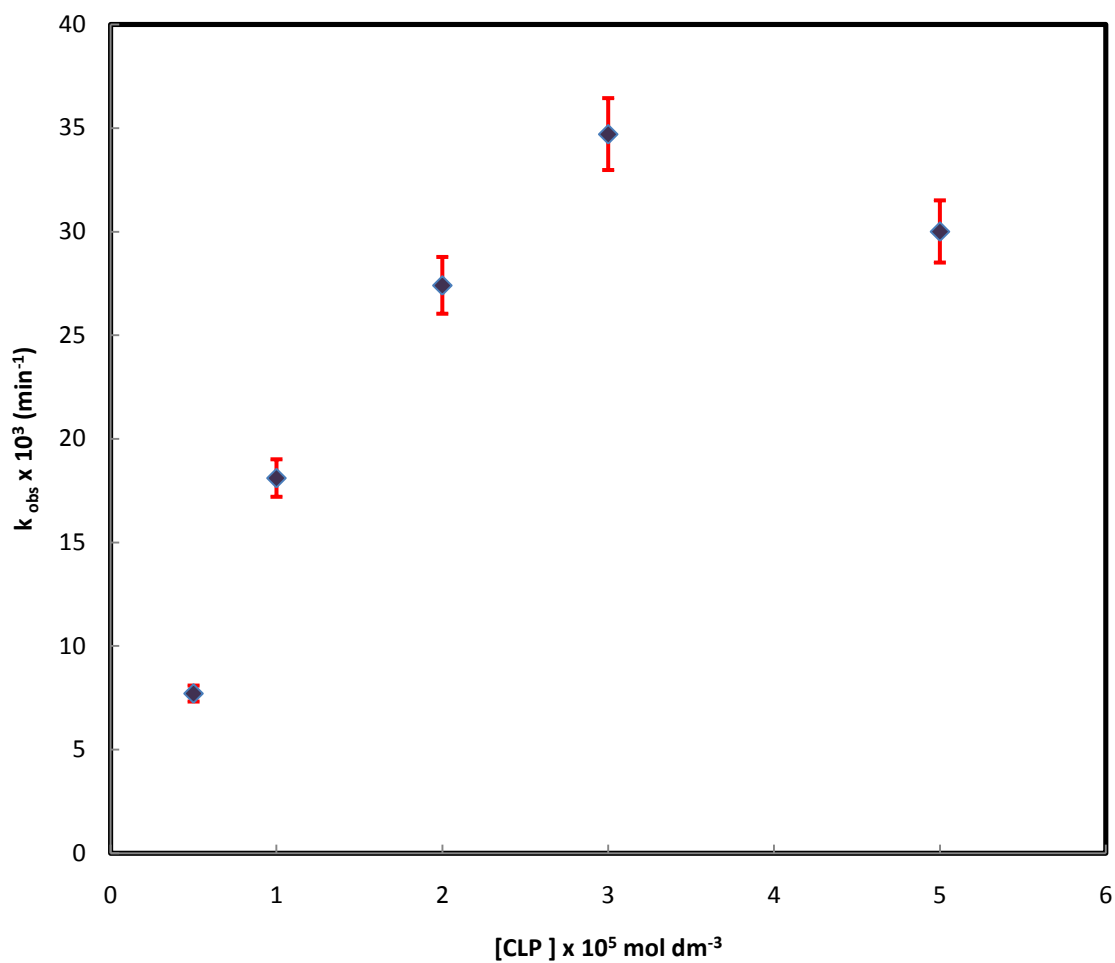
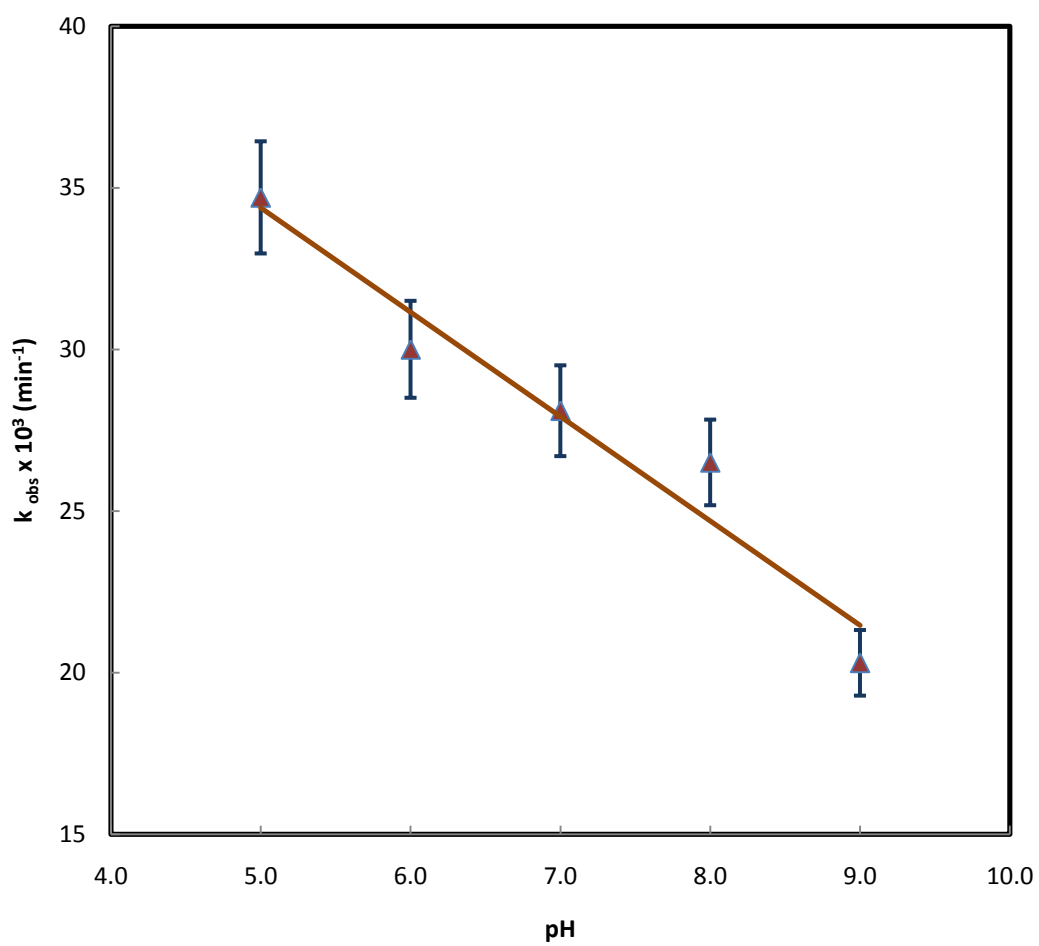


Table 4.3. Effect of pH on the rate constant of photocatalytic degradation of CLP with 5% Ba-ZnO at 25 °C, [Ba-ZnO] = 0.10 g dm⁻³, [CLP] = 3.00 x 10⁻⁵ mol dm⁻³, light intensity = 4mW/cm²

Photocatalyst	pH	$k_{obs} \times 10^3$ (min ⁻¹)
5% Ba-ZnO	5.0	34.70
	6.0	30.00
	7.0	28.10
	8.0	26.50
	9.0	20.30

Fig. 4.10. Effect of pH on the rate constant of photocatalytic degradation of CLP with 5% Ba-ZnO at 25 °C, [Ba-ZnO] = 0.10 g dm⁻³, [CLP] = 3.00 x 10⁻⁵ mol dm⁻³, light intensity = 4mW/cm²

(Conditions are stated in Table 4.3 (p.119))



4.3.6 Effect of UV Lamp Distance

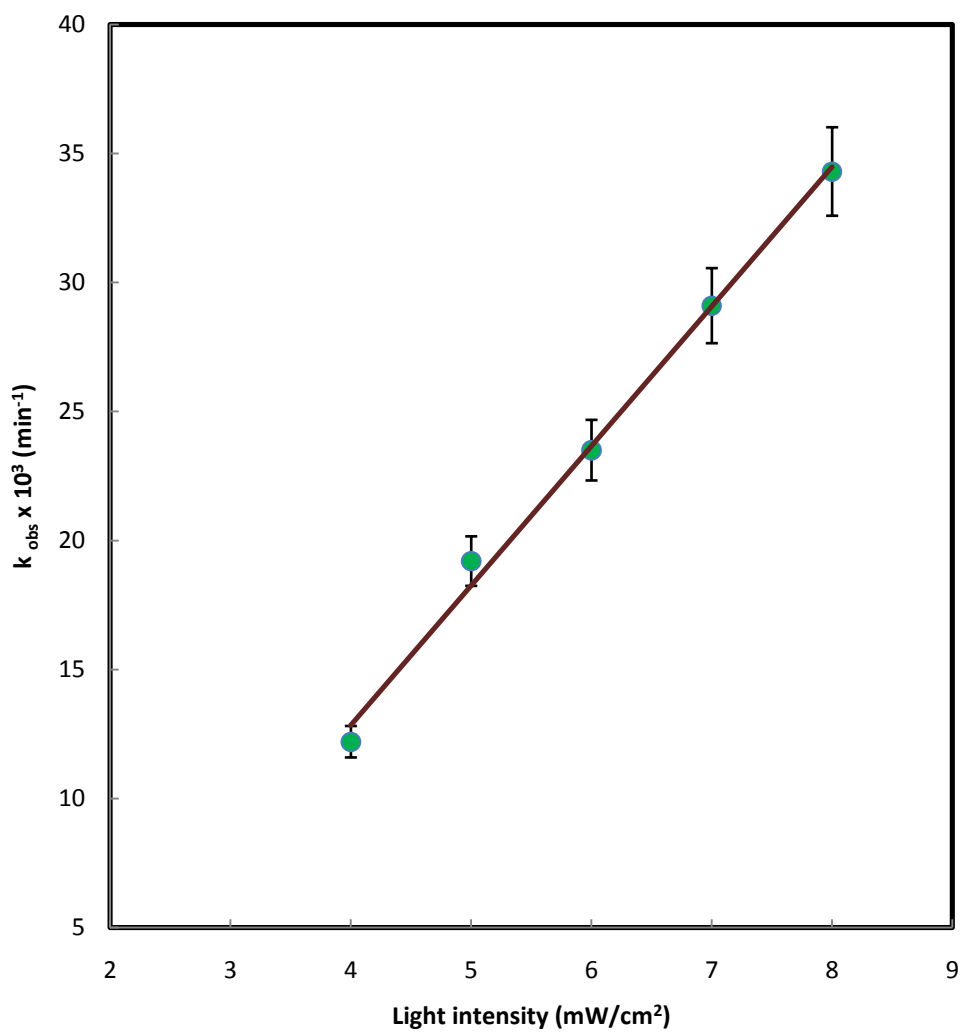
To study the rate of photocatalytic degradation of CLP at different UV light intensity the distance of UV lamp is varied from the surface of the mixture. It is observed that an increase in UV intensity of light increases the rate of photocatalytic degradation of CLP, as depicted in Table 4.4. and Fig. 4.11. This is due to the fact that, as the light intensity increases, the amount of Ba doped ZnO nanoparticles excitation also increases, hence, more $e^- - h^+$ pairs are generated consequently the h^+ degrade the CLP moiety adsorbed on the photocatalyst surface and oxidize to carbon dioxide and water. This results in the effective demineralization.

Table 4.4. CLP degradation under different UV intensities CLP with 5% Ba-ZnO at 25 °C, [Ba-ZnO] = 0.10 g dm⁻³, [CLP] = 3.00 x 10⁻⁵ mol dm⁻³, at pH = 5.0.

Photocatalyst	Light Intensity (mW/cm ²)	k _{obs} x 10 ³ (min ⁻¹)
5% Ba-ZnO	4	12.20
	5	19.20
	6	23.50
	7	29.10
	8	34.30

Fig. 4.11. CLP degradation under different UV intensities CLP with 5% Ba-ZnO at 25 °C, [Ba-ZnO] = 0.10 g dm⁻³, [CLP] = 3.00 x 10⁻⁵ mol dm⁻³, at pH = 5.0.

(Conditions are stated in Table 4.4 (p.122))



4.3.7 Proposed Reaction Mechanism

The reaction mixture containing CLP and buffer was kept in beaker. A dosage of 0.1g dm^{-3} 5% Ba-ZnO nanoparticles were added. Then, Post-illumination the suspensions were agitated at the black for 1 hr to accomplish adsorption-desorption equilibrium b/n the CLP and photocatalyst. Then, it was kept into the photo-reactor having 8 W UV lamps (Philips) with a wavelength peak at 254 nm and of 4 mW/cm^2 intensity with continuous magnetic stirring. Then the reaction blend was set aside for one day and the products of CLP were analyzed by Agilent quadru-pole 6130 series HPLC system. For HPLC examination 0.1% formic acid, acetonitrile be used as a solvent with a run rate $1.2\text{ cm}^3\text{ min}^{-1}$. This was continued using Column-Atlantis C18 ($50 \times 4.6\text{mm} \times 5\mu\text{m}$) dual model as shown in Fig 4.12. a and 4.12. b. Chloramphenicol MS fragmentation indicates no degradation of the molecule under this experimental conditions. In conclusion, only one major product is obtained at ($m/z = 150$). The observed product reveals that only one plausible pathway for the degradation of chloramphenicol oxidation. The proposed mechanism shows in Scheme 4.1.

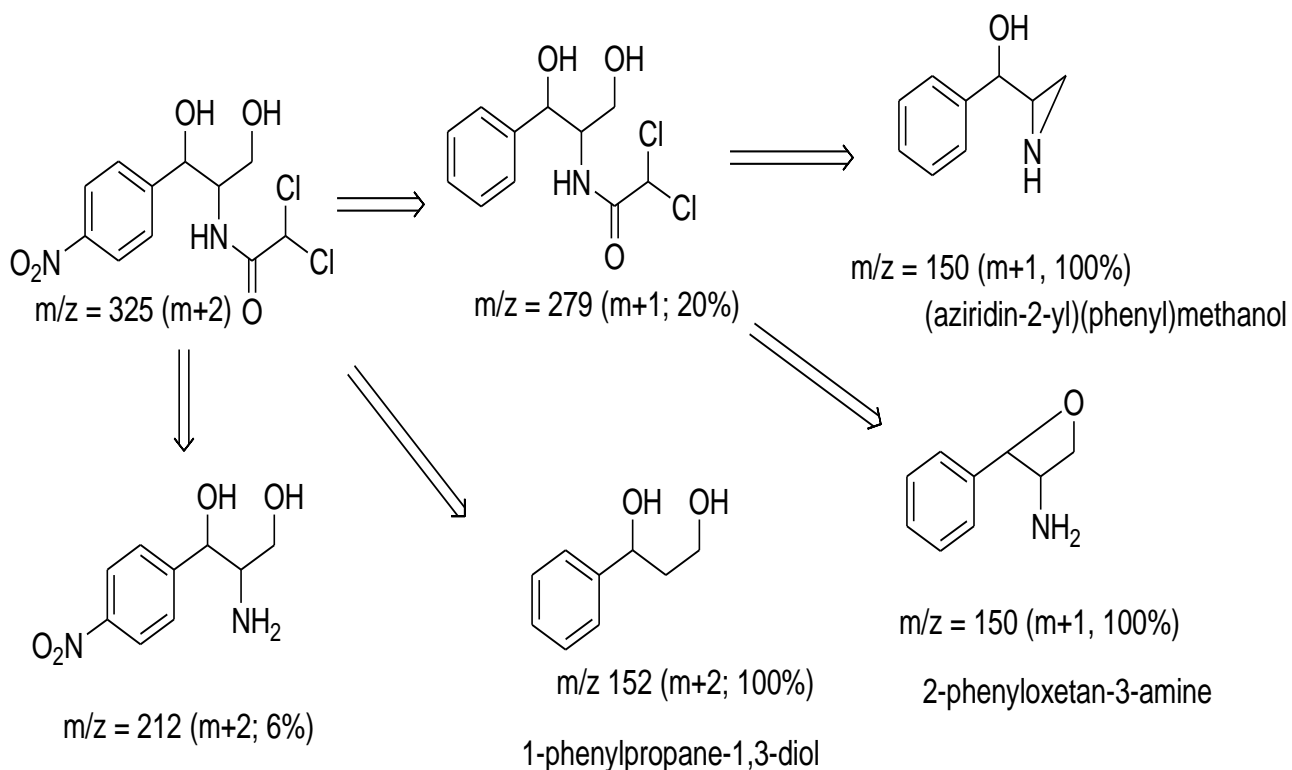
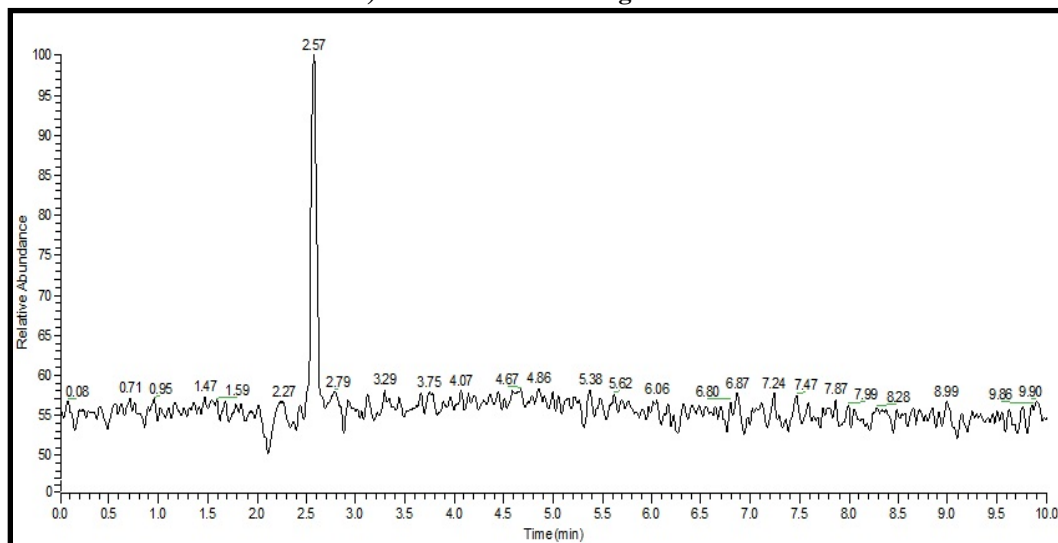
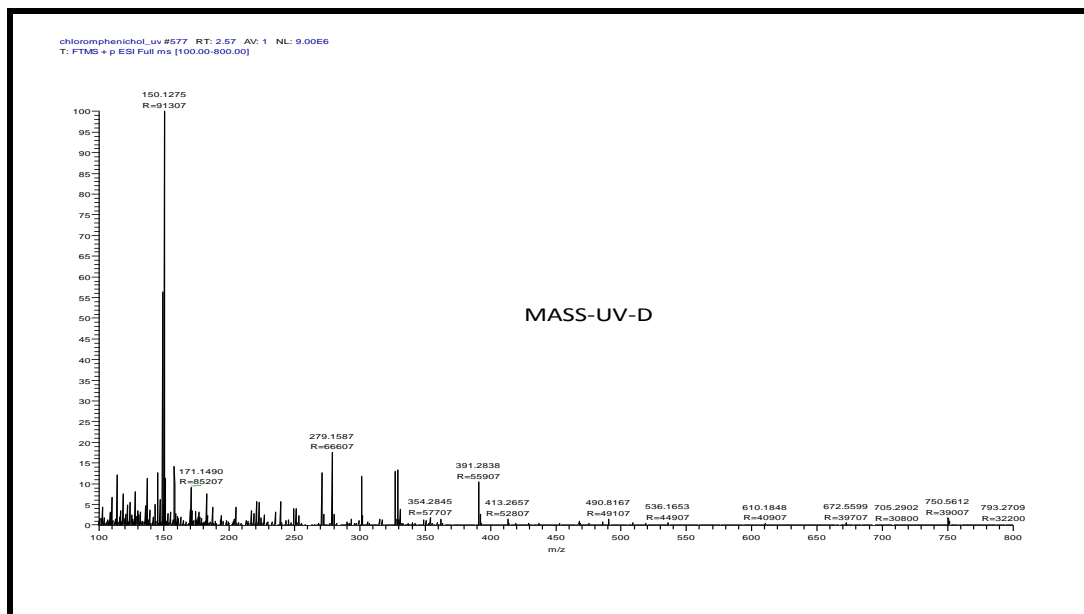


Fig. 4.12. LC/MS spectra of CLP oxidation products

a) Total ion chromatogram



b) Mass spectrum of reaction product m/z 150



4.4 Conclusion

Pure and Ba doped ZnO nanoparticles were synthesised by chemical precipitation method. The average particle size of 5% Ba-ZnO (24.50 to 35.00 nm) exhibited excellent achievable photocatalytic mineralization of CLP in the acidic condition (pH 5.0). The XRD patterns shows prepared nanoparticles were wurzite structure. The EDX and TEM topography shows that the existence of Ba in ZnO. Under optimum conditions, over 92% photocatalytic degradation of CLP was achieved in 100 min using 5% Ba-ZnO photocatalyst.

References

1. World Resources Institute 1994-95, N.Y.O., 1994.
2. O. Ligrini, E. Oliveros and A.M. Braun, "Photochemical processes for water treatment", *Chem. Rev.* Vol. 93, 1993, pp. 671-698.
3. C.E. Searle, American Chemical Society, Washington, DC. *Am. Chem. Soc. Monograph.* Vol. 173, 1976, pp. 491-625.
4. C.T. Helmes, C.C. Sigman, Z.A. Fund, M.K. Thompson, M.K. Voeltz and M.M.A. Makie, "A study of azo and nitro dyes for the selection of candidates for carcinogen bioassay", *J. Environ. Sci. Health A.* Vol. 19, 1984, pp. 197-231.
5. M. Boeninger "Carcinogenicity and metabolism of azo dyes especially those derived from benzidine DHHS (NIOSH)". Vol. 5, 1980, pp. 80-119.
6. J.J. Roxon, A.J. Ryan, and S.E. Wright, "Reduction of water-soluble azo dyes by intestinal bacteria", *Food. Cosmet. Toxicol.* Vol. 5, 1967, pp. 367-369.
7. H. Zollinger, "Colour Chemistry: Synthesis, properties and applications of organic dyes and pigments", New York, VCH Publishers, New York. 1987, pp. 92-102.
8. Y. Dong, S. Zhan and P. Wang, "A Facile Synthesis of Ag Modified ZnO Nanocrystals with enhanced Photo-catalytic activity, *Journal of Wuhan University of Technology-Mater*", *Sci. Ed.*, Vol. 27, 2012, pp. 615-620.
9. D.F. Zhang, "Photocatalytic oxidation of organic dyes with nanostructured zinc dioxide modified with silver metals", *Russ. J. Phys. Chem. A.* Vol. 85 (8), 2011, pp. 1416-1422.
10. D.F. Zhang, and F.B. Zeng, "Characterization, activity and mechanisms of a visible light driven photocatalyst: Manganese and iron co-modified TiO₂ nanoparticles", *Russ. J. Phys. Chem. A.* Vol. 85 (10), 2011, pp. 1825-1831.
11. I. Justicia, P. Ordejón, G. Canto, J.L. Mozos, J. Fraxedas, G.A. Battiston, R. Gerbasi, and A. Figueras, "Designed Self-Doped Titanium Oxide Thin Films for Efficient Visible-Light Photocatalysis", *Adv. Mater.* Vol. 14, 2002, pp. 1399 -1402.
12. British Pharmacopoeia on CD-Rom" The Stationery Office on behalf of the Medicines and Healthcare products Regulatory Agency (MHRA). London. 5th., ed., 2007.
13. British Pharmacopoeia on CD-Rom, The Stationery Office on behalf of the Medicines and Healthcare products Regulatory Agency (MHRA). London. 5th., ed., (2007)
14. The American Society of Health-System Pharmacists. Retrieved Aug 1, 2015.

15. J. Zhang, D. Fu, Y. Xu, and C. Liu, "Optimisation of parameters on photocatalytic degradation of chloramphenicol using TiO₂ photocatalyst by response surface methodology", *J. Environ. Sci.* Vol. 22 (8), 2010, pp. 1281–1289.
16. C.H. Kuo, T.F. Chiang, L.J. Chen, and M.H. Huang, "Synthesis of Highly Faceted Pentagonal and Hexagonal-Shaped Gold Nanoparticles with Controlled Sizes by Sodium Dodecyl Sulfate", *Langmuir*, Vol. 20, 2004, pp. 7820-7824.
17. W. Water, T. Fang, L. Ji, T. Meen and Y. Yan, "Surface Morphology and Liquid Sensor Sensitivity of Barium-Doped ZnO Thin Film", *J. Sci. Innov.* Vol. 1, No. 1, 2011, pp. 25-32.
18. M. Kalamuei, M. Kamazani, M. Niasari, S. M. Mashkani, "A simple sonochemical approach for synthesis of selenium nanostructures and investigation of its light harvesting application", *Ultrason. Sonochem.* Vol. 23, 2015, pp. 246-256.
19. F. Gallino, C.D. Valentin, G. Pacchioni, M. Chiesa and E. Giamello, "Nitrogen impurity states in polycrystalline ZnO. A combined EPR and theoretical study", *J. Mater. Chem.*, Vol. 20, 2010, pp. 689-697.
20. H. Lin, S. Liao, and S. Hung, "The dc thermal plasma synthesis of ZnO nanoparticles for visible-light photocatalyst", *J. Photochem. Photo boil. A: Chem.* Vol. 174, 2005, pp. 82-87.
21. J. Sun, L. Qiao, S. Sun, and G. Wang. "Photocatalytic degradation of Orange G on nitrogen-doped TiO₂ catalysts under visible light and sunlight irradiation", *J. of hazard. Materi.* Vol. 155, 2008, pp. 312-319.
22. C.C.Wang, C.K. Lee, M.D. Lyu, and L.C. Juang, "Photocatalytic degradation of C.I. basic violet 10 using TiO₂ catalysts supported by Y zeolite: an investigation of the effects of operational parameters", *Dyes Pigment* Vol. 76, 2008, pp. 817–824.
23. I.T. Horvath, *Encyclopedia of Catalysis*, Wiley, New York, 2003.
24. N. Modirshahla, A. Hassani, M.A. Behnajady, and R. Rahbarfam, "Effect of operational parameters on decolorization of Acid Yellow 23 from wastewater by UV irradiation using ZnO and ZnO/SnO₂ photocatalysts", *Desalination* Vol. 271, 2011, pp. 187–192.
25. N. Daneshvar, M. Rabbani, N. Modirshahla, and M.A. Behnajady, "Kinetic modeling of photocatalytic degradation of acid red 27 in UV/TiO₂ process", *J. Photochem. Photobiol. A.* Vol. 168, 2004, pp. 39–45.

Chapter 5

Cu-ZnO nanoparticles for photocatalytic degradation of methyl orange

5.1 Introduction

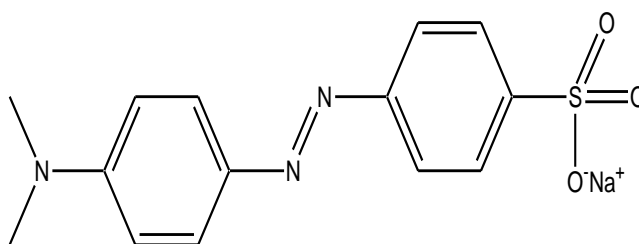
Air and Water contamination are the two major problems affecting the natural surroundings due to waste pollutants generated by households and industries. Detoxification and cleansing of water and air has become the main centre of today's scientific study. The major origin of air and ground-water contamination is the industrial recalcitrant (present in minute quantity), extreme disposal of pesticides, domestic waste landfills and fertilizers (agrochemicals). These non-degradable organic contaminants are not efficiently treated by biological treatment methods or conventional treatment methods [1].

Textile industries generate huge amount of colour recalcitrant which are hazardous and non-bio-degradable. These colouring matter generate several ecological problems by discharging poisonous and destroying materials into the water system [2]. Heterogeneous photocatalysis believed to have considerable potential for appliances relating the eradication of untreated recalcitrant's. In this method, when photocatalyst particles are exposed by suitably energetic illumination ($< 388 \text{ nm}$) $e^- - h^+$ pairs are generated. This $e^- - h^+$ pair move to the surface of photocatalyst and reacts with adsorbed dye molecules to form CO_2 and H_2O [3-4]. However the major disadvantage of the heterogeneous photo-catalysis is quick re-combination of the $e^- - h^+$ pair. To avoid recombination of $e^- - h^+$ pair the metal oxides are doped with d-block elements such as Ru, Pt, Ag, Cu etc., which decrease the band gap as well as enhance the charge separation of photocatalyst [5].

The general importance of Advanced oxidation processes (AOPs) discussed in chapter 2 (p.34), and Zinc Oxide (ZnO) photocatalyst discussed in chapter 4 (p.102).

In this paper we report, photocatalytic degradation of reactive synthetic dye methyl orange (M.O.) using 2% Cu doped ZnO photocatalyst synthesized by inexpensive simple precipitation method. Synthesized nano-crystals were analysed by analytical techniques viz. X-ray diffraction (XRD), Scanning electron microscope (SEM), and Energy dispersive X-ray spectroscopy (EDX). The photo-degradation efficiency, kinetics

as well as rate constants related to the catalyst concentration, pH, substrate variation, and intensity variation on 2% Cu-ZnO were investigated.



Chemical Structure of Methyl Orange (M.O)

5.2 Experimental

5.2.1 Materials and methods

The reagent grade Methyl orange (M.O.) is procured from Sigma-Aldrich (Bangalore) and is directly used without any further treatment. A known concentration of M.O. stock solution is prepared during experiment. $\text{Zn}(\text{NO}_3)_2 \cdot 6\text{H}_2\text{O}$, NaOH and $\text{Cu}(\text{NO}_3)_2$ procured from HIMEDIA. To maintain pH of the medium acetate, phosphate, and borate buffer solutions were prepared. All reagents used were of analytical grade.

The instruments used were already discussed chapter-2 and p.no. (36-40)

5.2.2 Photocatalyst preparation

For synthesizing un-doped and copper doped ZnO, known quantity of zinc nitrate salt was added to deionized water to prepare 0.1M zinc nitrate solution. Similarly, 0.1 M NaOH solutions are prepared separately. NaOH was added drop-drop with steady stirring thoroughly to zinc nitrate solution for 3 hrs. The resultant mixture was allowed to settle for overnight and suspension was then decanted carefully, the residual suspension was filtered and cleaned number of times with deionized water then followed with ethanol. The white residue was dehydrated in oven at 120 °C for 3 hrs. Then powder is crushed in a mortar then ignited at 500 °C for about 1 hr by maintaining temperature gradient of about 10° C per minute within a furnace. During the drying process, complete transformation of $\text{Zn}(\text{OH})_2$ in to ZnO takes place. The same procedure was followed for the synthesis of 1%, and 2% Cu - ZnO nanosized particles, while, the copper concentration was maintained at 1% and 2% (mole ratio). Copper when doped with ZnO nanoparticles it enters into the interstitial position of ZnO lattice. Similar literature was also reported earlier study [6].

5.2.3 The Photocatalysis Process

To observe the photocatalytic degradation of M.O., a known quantity of M.O and buffer solution was kept in a Pyrex beaker. Doses of 0.10 g dm^{-3} of 2% Cu-ZnO nanoparticles were added. Before illumination the suspensions were allowed for 1 hr in dark to reach equilibrium adsorption and desorption between M.O and photocatalyst. Then, it was transferred in to the photoreactor and then kept under 8 W UV lamps (Philips) with a wavelength peak at 254 nm and of 4mW/cm^2 intensity with continuous magnetic stirring. After every 10 minutes the solution was taken out and centrifuged at 5000 rpm for 5 min. The decrease in the concentration of CLP was monitored at 464 nm ($\epsilon = 29933 \text{ dm}^3 \text{ mol}^{-1} \text{ cm}^{-1}$) using UV-visible spectrophotometer (a CARY 50 Bio UV-Visible Spectrophotometer) and the degree of degradation was studied as shown in Fig. 5.1.

5.3 Results and discussion

5.3.1 Comparison of different photocatalysts.

The degree of photocatalytic efficiency of M.O with UV, UV-ZnO, UV- 1% Cu-ZnO and UV- 2% Cu-ZnO was reported. It was seen that the degradation efficiency of M.O with UV- 2% Cu-ZnO was more potential than UV, UV-ZnO and UV- 1% Cu-ZnO as shown in Fig. 5.2.

Influence of copper doping on ZnO was examined by using 2% (mole ratio) of copper, higher content of copper may favours separating charge-carriers effectively and hindered the re-combination of $e^- - h^+$ pairs. Hence, enhances the photocatalytic activity. The photo degradation rate was maximum with 2% Cu-ZnO compared with UV and UV-ZnO, and UV-1% Cu-ZnO hence, further studies were carried out with UV-2% Cu-ZnO.

The % degradation efficacy of M.O was examined under similar environment by UV, UV-ZnO, UV-1% Cu-ZnO and UV-2% Cu-ZnO and % adsorption in dark was also investigated. The % degradation activity of M.O was found to be 40%, 50%, 63%, and 90% with UV, UV-ZnO, UV-1% Cu-ZnO and UV-2% Cu-ZnO respectively within 100 minutes as shown in as shown in Fig. 5.3.

Fig. 5.1. UV–visible spectral changes during the degradation of Methyl Orange at 25 ± 0.2°C, [M.O] = 2.00 x 10⁻⁵ mol dm⁻³, pH = 4.0, 2% Cu-ZnO = 0.10 g dm⁻³, light intensity 4 mW/ cm²

Time (1) 00.00 min (2) 15.00 min (3) 30.00 min (4) 45.00 min
(5) 60.00 min (6) 75.00 min (7) 90.00 min

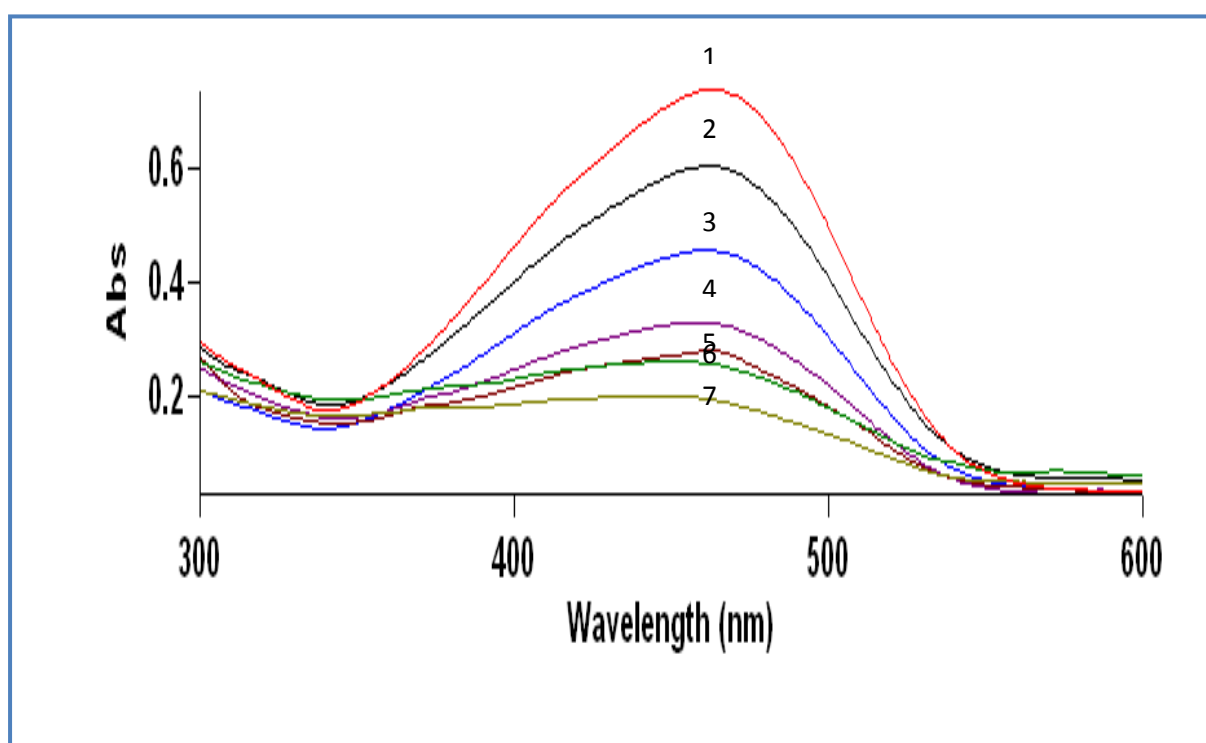


Fig. 5.2. Rate constants for the Photocatalytic degradation of M.O. by various treatments at 25 °C, [M.O] = 2.00×10^{-5} mol dm⁻³, pH = 4.0, 2% Cu-ZnO = 0.10 g dm⁻³, light intensity 4 mW/ cm²

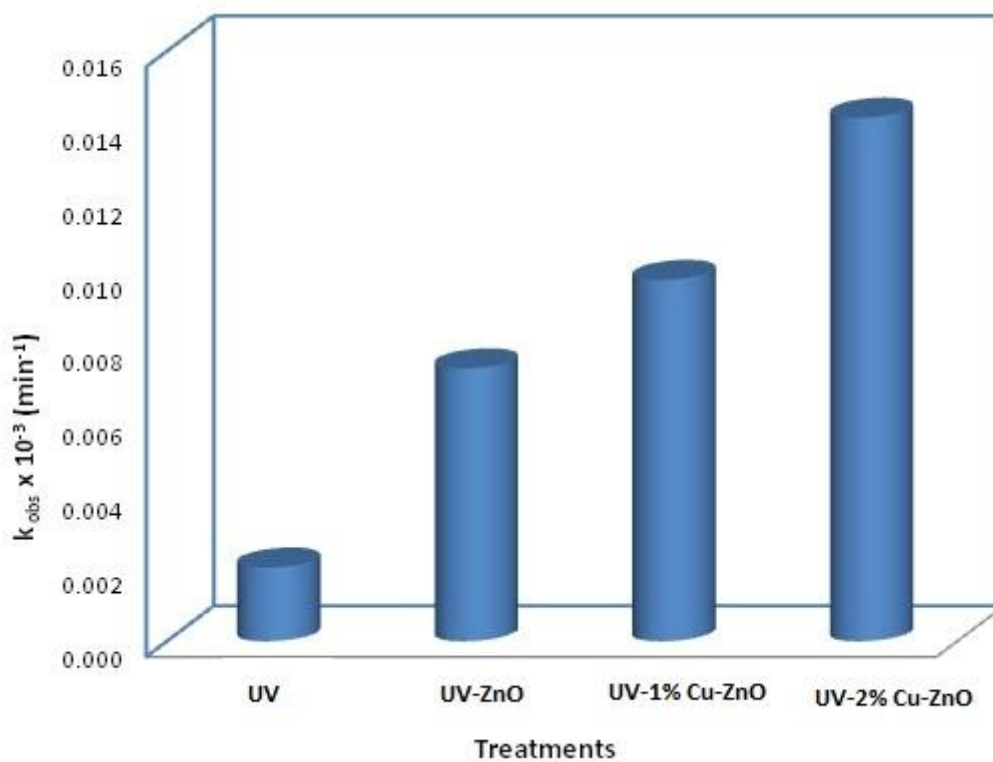
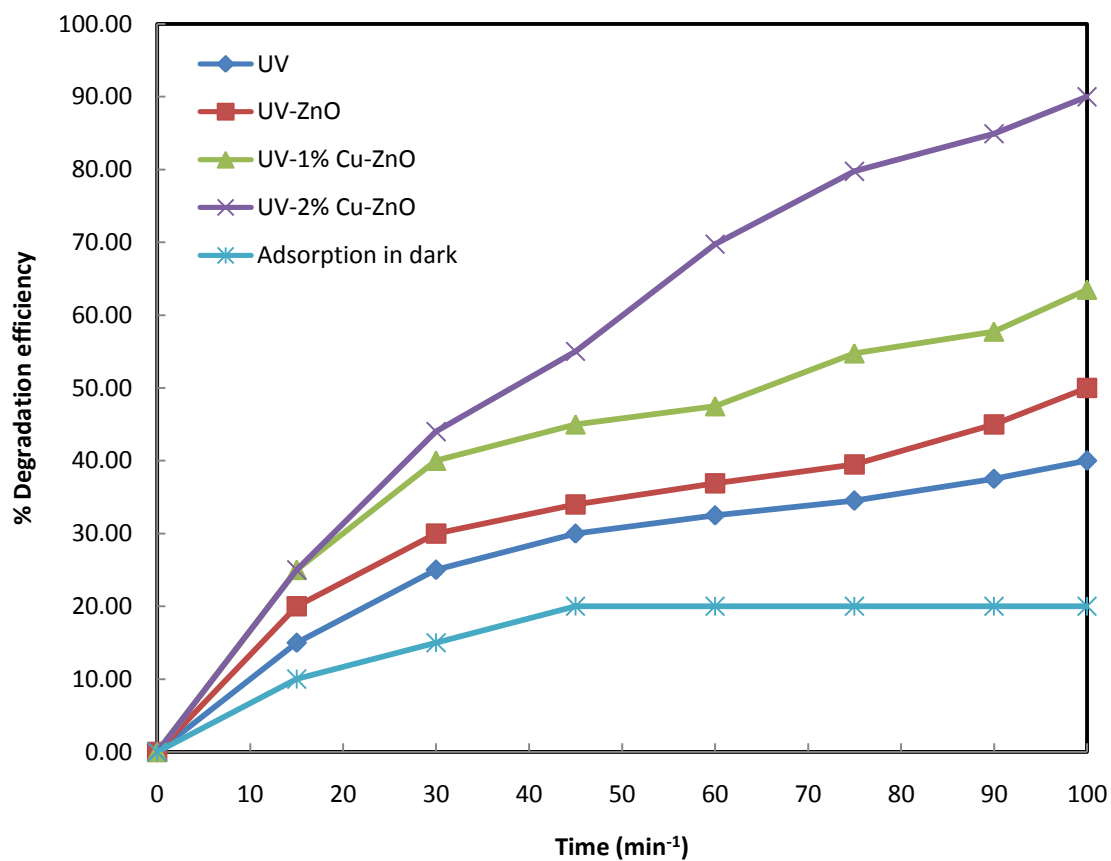


Fig. 5.3. % degradation efficiencies of various treatment methods with time at 25 °C.
[Photocatalyst] = 0.10 g dm⁻³, [M.O] = 2.00 x 10⁻⁵ mol dm⁻³ at pH 4.0 and light intensity 4 mW/cm².



5.3.2 Characterization of ZnO and Cu-ZnO

5.3.2.1 X-ray Diffraction Studies (XRD)

XRD spectra of un-doped and copper doped zinc oxide ($\text{Zn}_{1-x}\text{Cu}_x\text{O}$, where $x=0.00-0.02$) nanoparticles at 600°C temperature as shown in Fig. 5.4. The intense sharp peak confirmed that the synthesized samples were crystalline in nature with hexagonal - wurtzite structure. It can be confirmed by the appearance of [100] [002] [101] [102] [110] [103] [200] and [112] diffraction peaks from different lattices at angles 2θ ($10-90^\circ$). The intense peak of [101] indicates that the expansion of nano-crystal has taken place along the easy route of crystallisation of zinc oxide [7]. No additional peaks were observed which implies that the wurzite-structure is not disrupted by Cu-doped ZnO. This indicates that prepared zinc oxide nanoparticles were hexagonal wurzite structure.

The mean particle sizes of synthesized nano-particles were computed by Debye Scherrer equation (1) taking full width half-maxima of A (101) intense line.

$$D = k\lambda/\beta\cos\theta \quad (1)$$

Where “k = dimension less shape factor (0.94), Cu ($K\alpha$) = wavelength radiation of X-ray (0.154 nm). β = full width at half max. θ = 1/2 diffraction angle”. The particle size of ZnO, 1% Cu-ZnO, and 2% Cu-ZnO was found to be 18.76, 38.45 and 41.12 nm respectively.

5.3.2.2 Scanning Electron Microscope (SEM)

To study the topography of prepared samples, the SEM analysis of pure ZnO, 1% and 2% Cu-ZnO nanoparticles are carried out at similar magnifications (15000). This image confirms the arrangement of Cu-ZnO nanoparticles. These images show that the non-uniform distribution of nearly egg-shaped arrangement in clusters to form a pointer as shown in Fig. 5.5 a, Fig. 5.5 b, Fig. 5.5 c.

5.3.2.3 Transmission Electron Microscope (TEM)

TEM images show the heterogeneously dispersed aggregates of Cu-ZnO nanoparticles having oval in shape crystalline structures which can be clearly observed in (Fig. 5.6). Tiny dark dots seen in TEM were recognized as Cu particles dispersed on ZnO nanoparticles with a particle size of approximately 10.00-15.00nm in breadth and 40.00-45.00nm in length. The crystallite size of the synthesized nanoparticles observed in TEM image was close to the values obtained from XRD.

Fig. 5.4. XRD patterns of (a) Undoped ZnO, (b) 1% Cu-ZnO (c) 2% Cu-ZnO

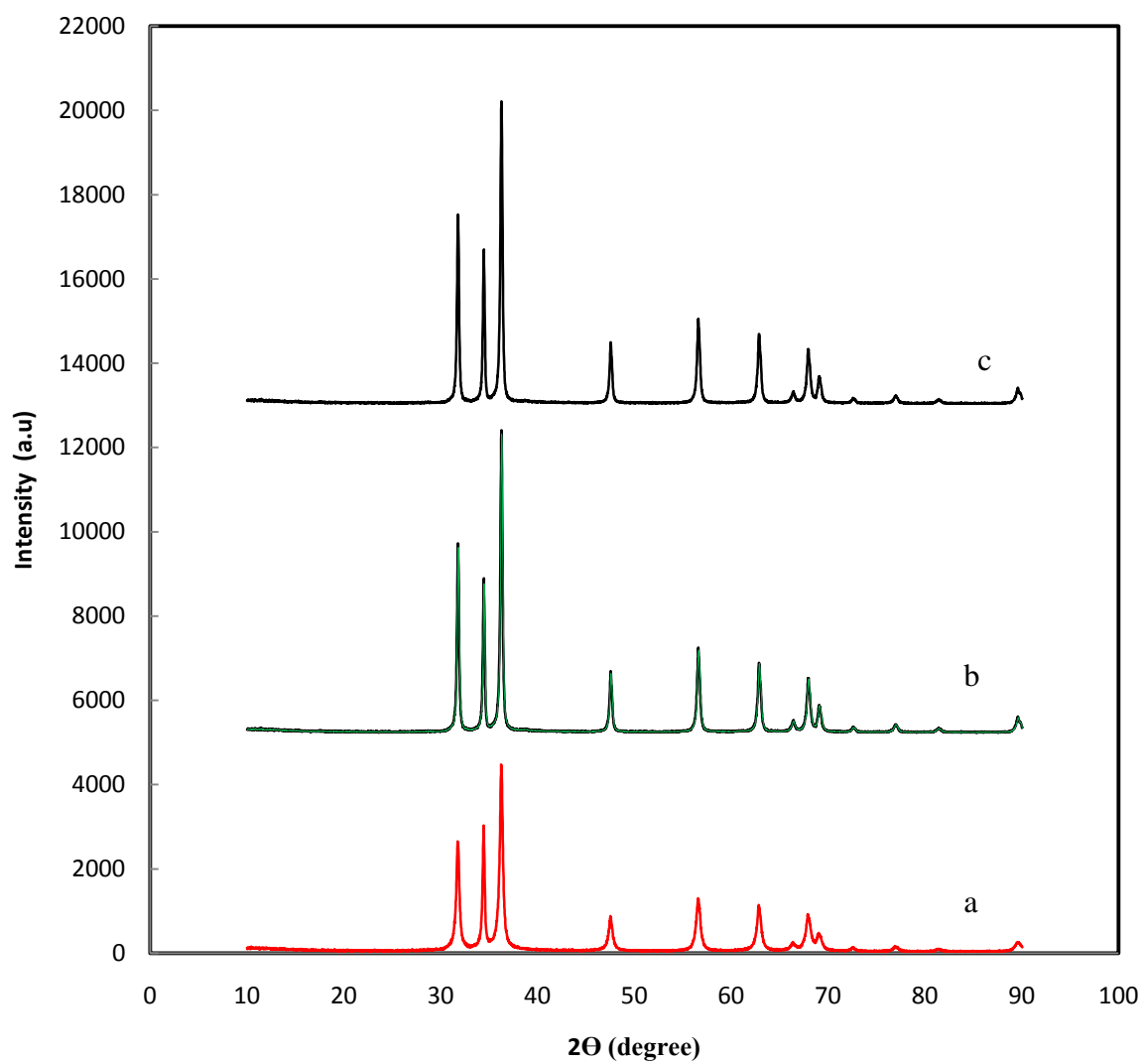
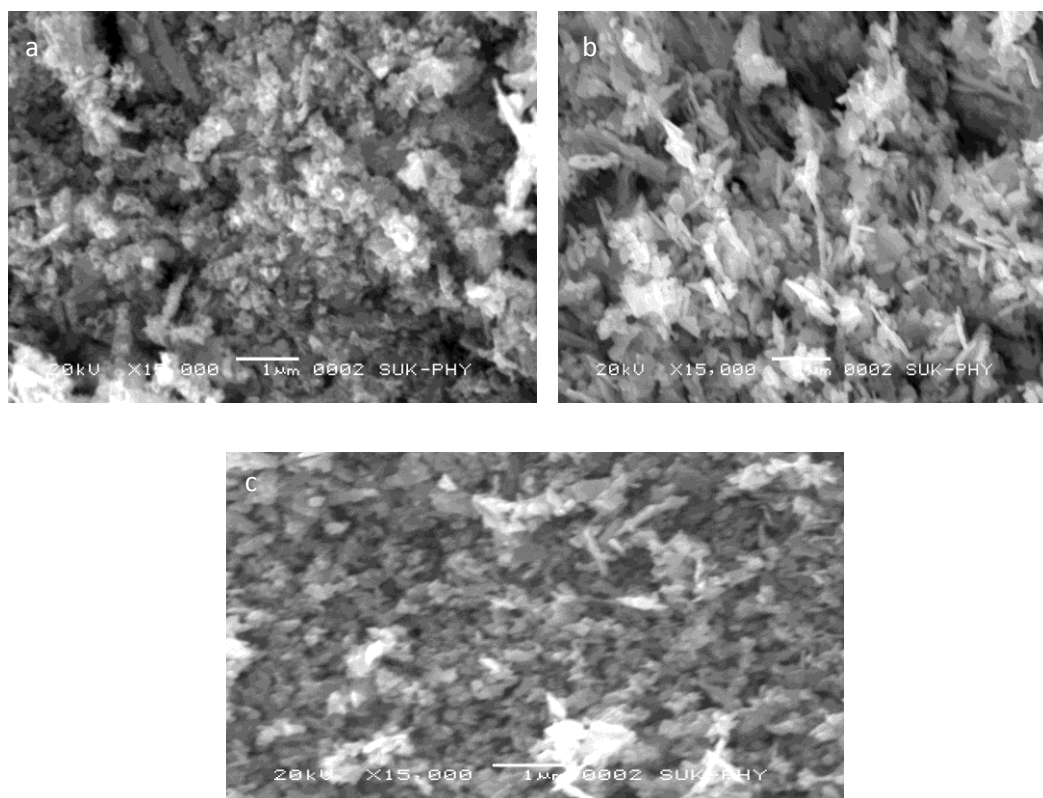
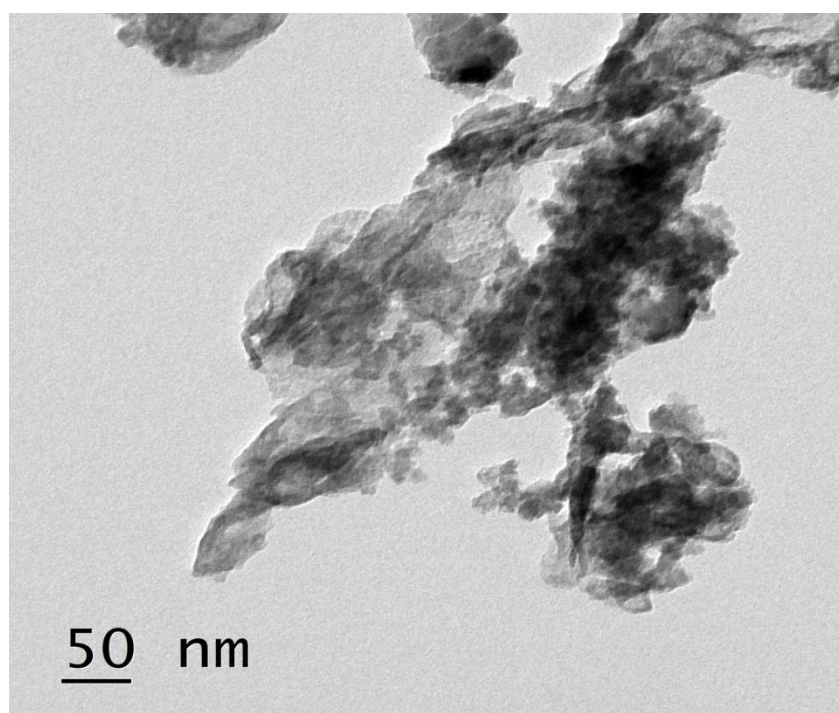


Fig. 5.5. SEM Images of (a) Undoped ZnO, (b) 1% and (c) 2% Cu-ZnO



5.6. TEM micrographs of 2% Cu/ZnO



5.3.2.4 Energy Dispersive X-ray Spectroscopy (EDX)

To study the composition of prepared nanoparticles of 1% and 2 % Cu-ZnO, EDX analysis was done. Spectra shows that the existence of only 3-distinct X-ray spectral lines which are related with O K α , Cu K α , and Zn K α . The atomic % of 1% Cu-ZnO, Zn = 30.17, O = 68.76 and Cu = 1.07 and for 2% Cu-ZnO, Zn = 26.71, O = 71.32 and Cu = 1.97 respectively. The spectral peaks suggest that presence of Zn, O, and Cu in the prepared nano crystals indicating no other impurity in prepared samples by the simple precipitation method as shown in Fig. 5.7 a and Fig. 5.7 b.

5.3.3 Effect of Photocatalyst Dosage

The rate of photocatalytic degradation was studied taking various amounts of 2% Cu-ZnO from 0.025 g dm⁻³ to 0.250 g dm⁻³ and keeping other parameters constant. It is observed that initially, when amount of photocatalyst increased, the rate of photo-degradation increases as shown in Table 5.1 and Fig. 5.8 But, when the amount of photocatalyst exceeds the optimum amount (0.10 g dm⁻³) the photo-degradation efficiency decreases. This behaviour may be due to increase in the amount of active centres on photocatalyst. In-turn the rate of radical formation increases. Hence, photocatalytic rate of reaction increases initially. Whereas, at higher amount of photocatalyst above 0.10 g dm⁻³, led to increase in the turbidity of the M.O. solution, as a result the light can't reach the photocatalyst surface due to masking effect. Hence, decrease in the rate of photo-degradation was observed [8].

5.3.4 Effect of [M.O.]

Rate of photocatalytic degradation of M.O. was studied by altering the [M.O.] from 0.50 x 10⁻⁵ to 5.00 x 10⁻⁵ mol dm⁻³ and keeping other parameters constant. The degradation rate of M.O. was initially increases with increase in the [M.O.]. After 2.00 x 10⁻⁵ mol dm⁻³ limiting value, increase in [M.O.] leads to decrease in the rate constant (Table 5.2 and Fig. 5.9). It is due to fact that the more number of active centres on the semiconductor photocatalyst existing initially for reaction which is incredibly vital for the degradation of M.O., but as the M.O concentration increased above 2.00 x 10⁻⁵ mol dm⁻³ the suspension became more turbid and covers the photocatalyst surface. Hence, the light entering the solution decreased there by only less number of photons strikes the surface of photocatalyst leading to limited formation of OH \cdot and O₂ \cdot^- radicals. Even at higher [M.O.] the path length was further condensed and the photo-degradation was insignificant [9].

Fig. 5.7. EDX of (a) 1% and (b) 2% Cu-ZnO

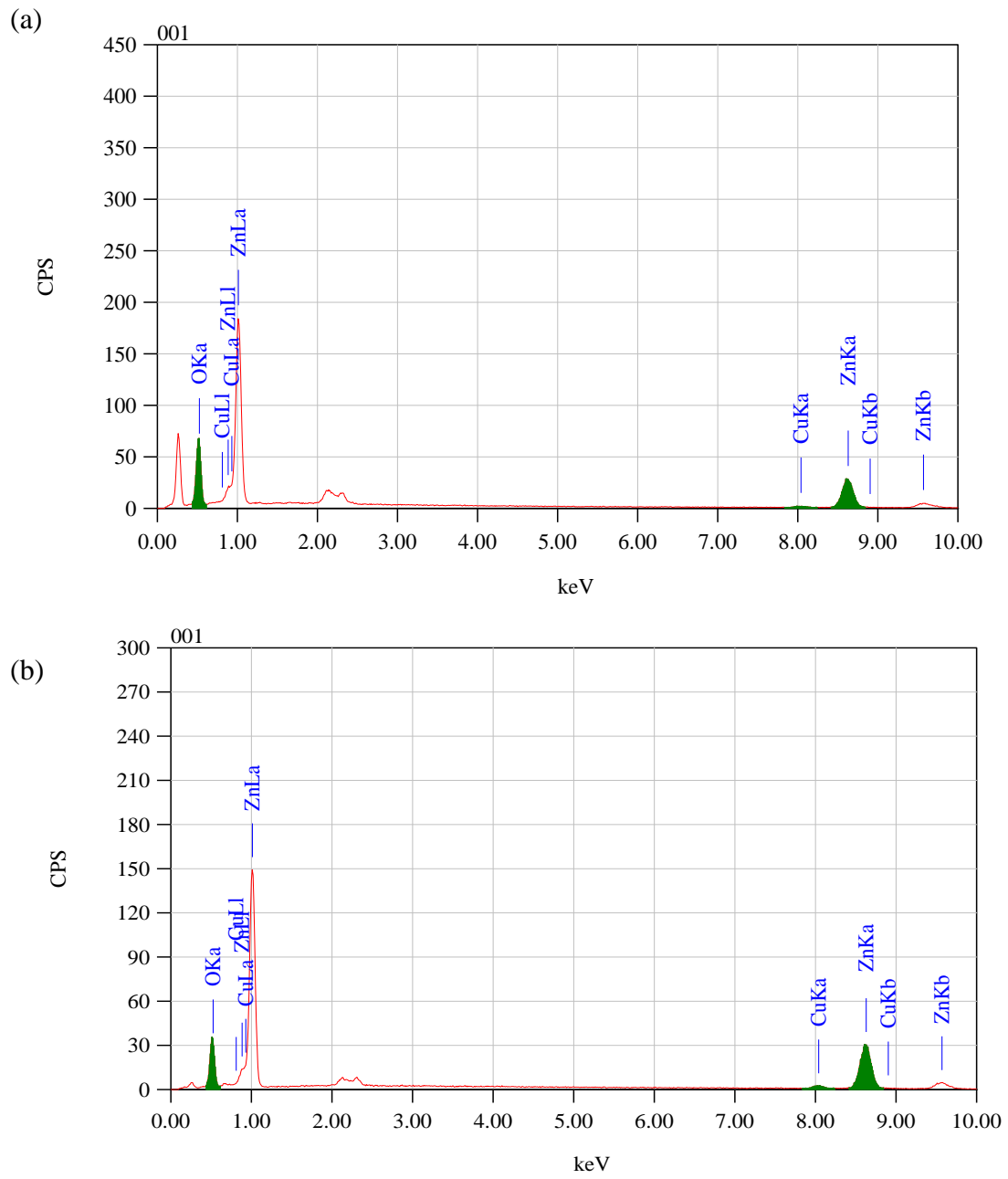


Table 5.1. Effect of different amounts of 2% Cu-ZnO photocatalyst on the degradation of M.O. at [M.O.] = $3.00 \times 10^{-5} \text{ mol dm}^{-3}$, at pH=4.0, light intensity = 4mW/cm^2

Photocatalyst	Amount of Photocatalyst (g dm^{-3})	$k_{\text{obs}} \times 10^3 (\text{min}^{-1})$
2% Cu-ZnO	0.025	9.00
	0.050	11.00
	0.100	15.40
	0.150	10.20
	0.200	8.50
	0.250	07.6

Fig. 5.8. Effect of different amounts of 2% Cu-ZnO photocatalyst on the degradation of M.O. at $[M.O.] = 3.00 \times 10^{-5} \text{ mol dm}^{-3}$, at pH=4.0, light intensity = 4mW/cm^2

(Conditions are stated in Table 5.1 (p.140))

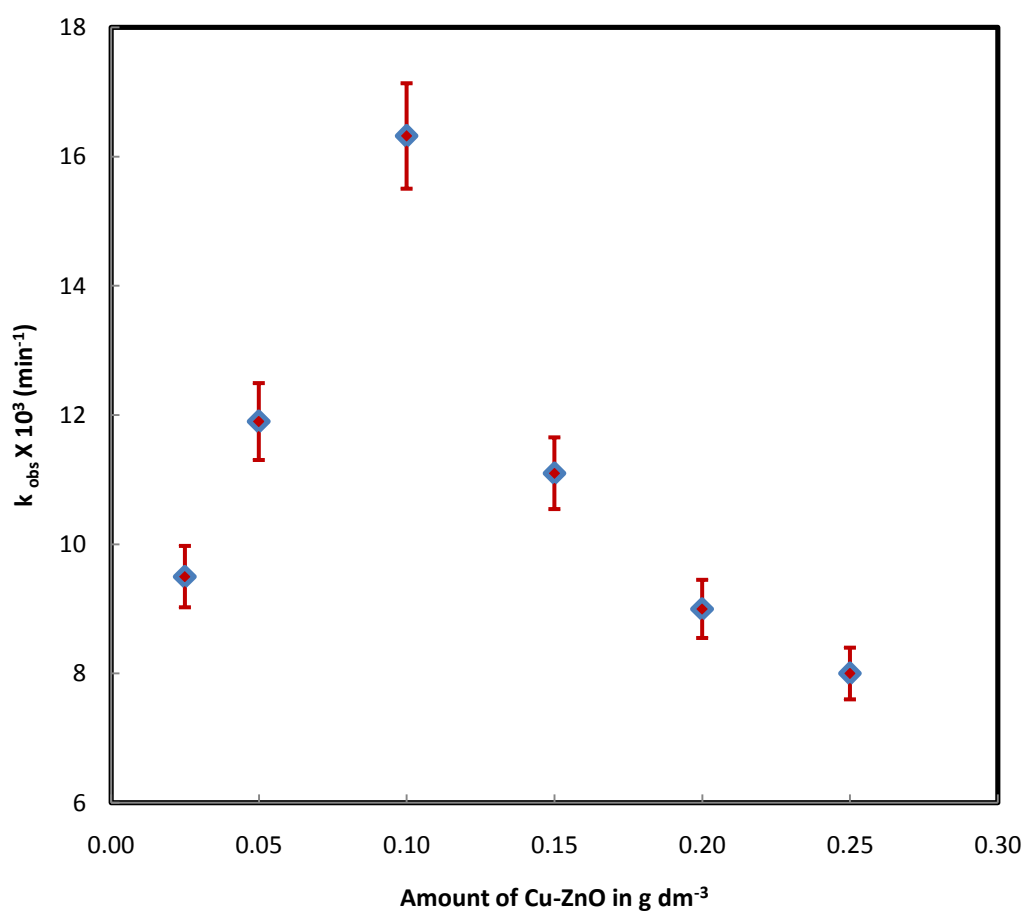
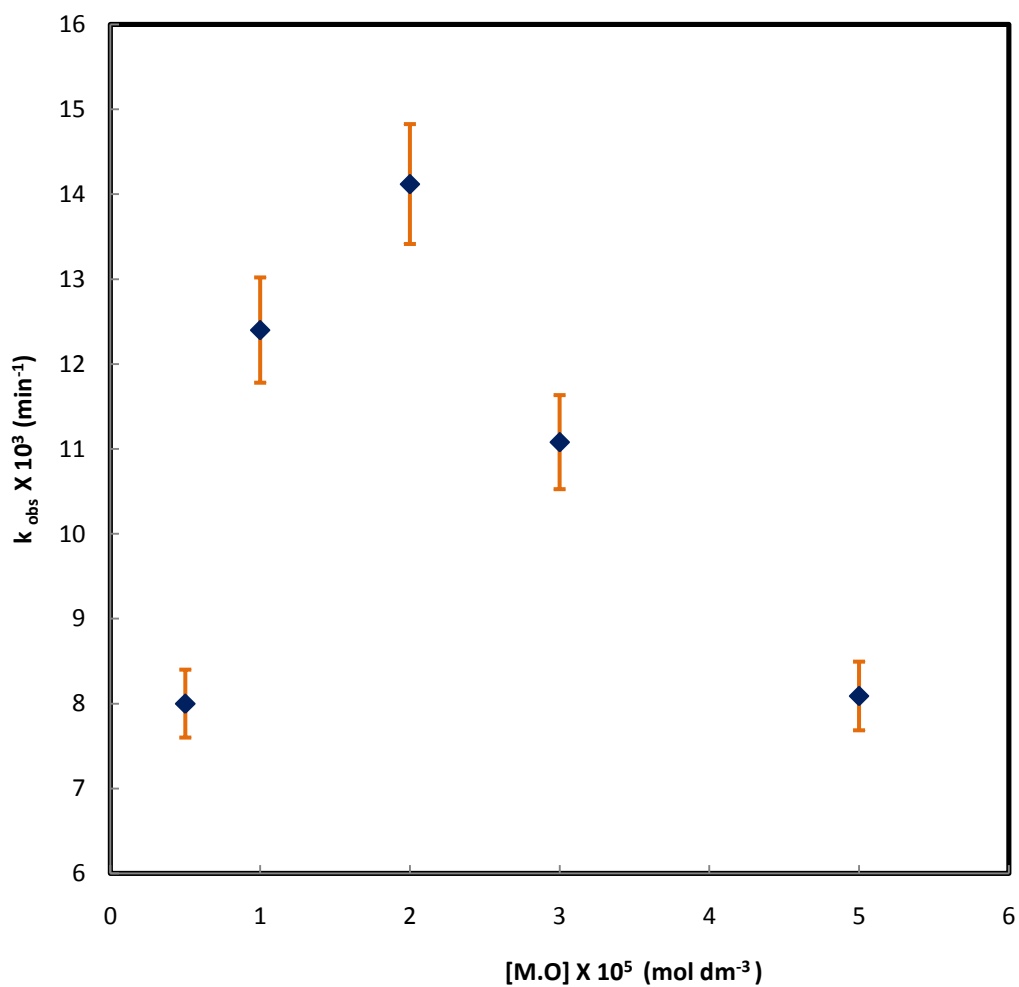


Table 5.2. Effect of of [M.O.] on photocatalytic rate constants with 2% Cu-ZnO at 25 °C, [Cu-ZnO] = 0.10 g dm⁻³, at pH=4.0, light intensity = 4mW/cm²

Photocatalyst	[M.O] x 10 ⁵ (mol dm ⁻³)	k _{obs} x 10 ³ (min ⁻¹)
2% Cu-ZnO	0.5	8.00
	1.0	12.40
	2.0	14.12
	3.0	11.08
	5.0	8.09

Fig. 5.9. Effect of of [M.O.] on photocatalytic rate constants with 2% Cu-ZnO at 25 °C, [2% Cu-ZnO] = 0.10 g dm⁻³, at pH=4.0, light intensity = 4mW/cm²

(Conditions are stated in Table 5.2 (p.142))



5.3.5 Effect of pH

The degree of photocatalytic reaction rate was examined by altering the pH from 4.0 to 9.0, and keeping other reaction conditions constant. Initially, it was observed that with increase in pH of the solution the rate of reaction also increases. Further, increase in pH, (pH > 6.0) the rate of photocatalytic degradation starts decreasing as shown in Table 5.3 and Fig. 5.10. This behaviour may be explained on the basis of charge properties of adsorbent and adsorbate. The Pka value of M.O is 3.8 [9]. In acidic medium below pH 6.0 the surface of a photocatalyst acts as a positive surface where as dye molecule act as a negative ion, hence strong electrostatic force of attraction leads to strong adsorption and consequent degradation takes place hence the rate of photocatalytic degradation increases. Whereas above pH 6.0 the photocatalyst surface acts as a negative surface and dye molecule also acts as negatively charged. Hence, the electrostatic repulsion between two negatively charged species takes place. Thus, the rate of degradation of M.O decreases at higher pH value [10].

5.3.6 Effect of UV Lamp Distance

Effect of intensity of light on the degradation of rate constant of M.O. was observed by differing UV lamp distance from the target. It is observed that an increase in UV intensity of light increases the rate of photocatalytic degradation of M.O as depicted in Table 5.4 and Fig. 5.11. This is due the fact that, as UV- light-intensity increases the amount of photons hitting per unit area of the photocatalyst (2% Cu-ZnO) also increases. Subsequently, plenty of $e^- - h^+$ pairs are generated, consequently the h^+ mineralize the M.O. molecules adsorbed on the photocatalyst surface and oxidise to carbon dioxide and water. This results in effective degradation of MO [11].

5.3.7 Efficacy of reusable catalyst

The 2% Cu-ZnO nano-crystals used in the photocatalytic degradation was taken out and centrifuged at 2000 RPM, then it is washed a number of times with deionised water and followed by ethanol, then evaporated moisture in a hot oven (30-40 °C) then taken out the white solid crushed in a mortar. Then, photocatalyst was used for next succeeding photocatalytic treatment, the marginal change after repetitive use of photo-degradation efficiency was observed [12-13].

Table 5.3. Effect of pH on the rate constant of photo catalytic degradation of M.O. with 2% Cu-ZnO at 25 °C, [Cu-ZnO] = 0.10 g dm⁻³, [M.O.] = 3.00 x 10⁻⁵ mol dm⁻³, light intensity = 4mW/cm²

Photocatalyst	pH	k _{obs} x 10 ³ (min ⁻¹)
2% Cu-ZnO	4.0	12.84
	5.0	9.80
	6.0	8.51
	7.0	7.80
	8.0	6.60

Fig. 5.10. Effect of pH on the rate constant of photo catalytic degradation of M.O. with 2% Cu-ZnO at 25 °C, [Cu-ZnO] = 0.10 g dm⁻³, [M.O.] = 3.00 x 10⁻⁵ mol dm⁻³, light intensity = 4mW/cm²

(Conditions are stated in Table 5.3 (p.145))

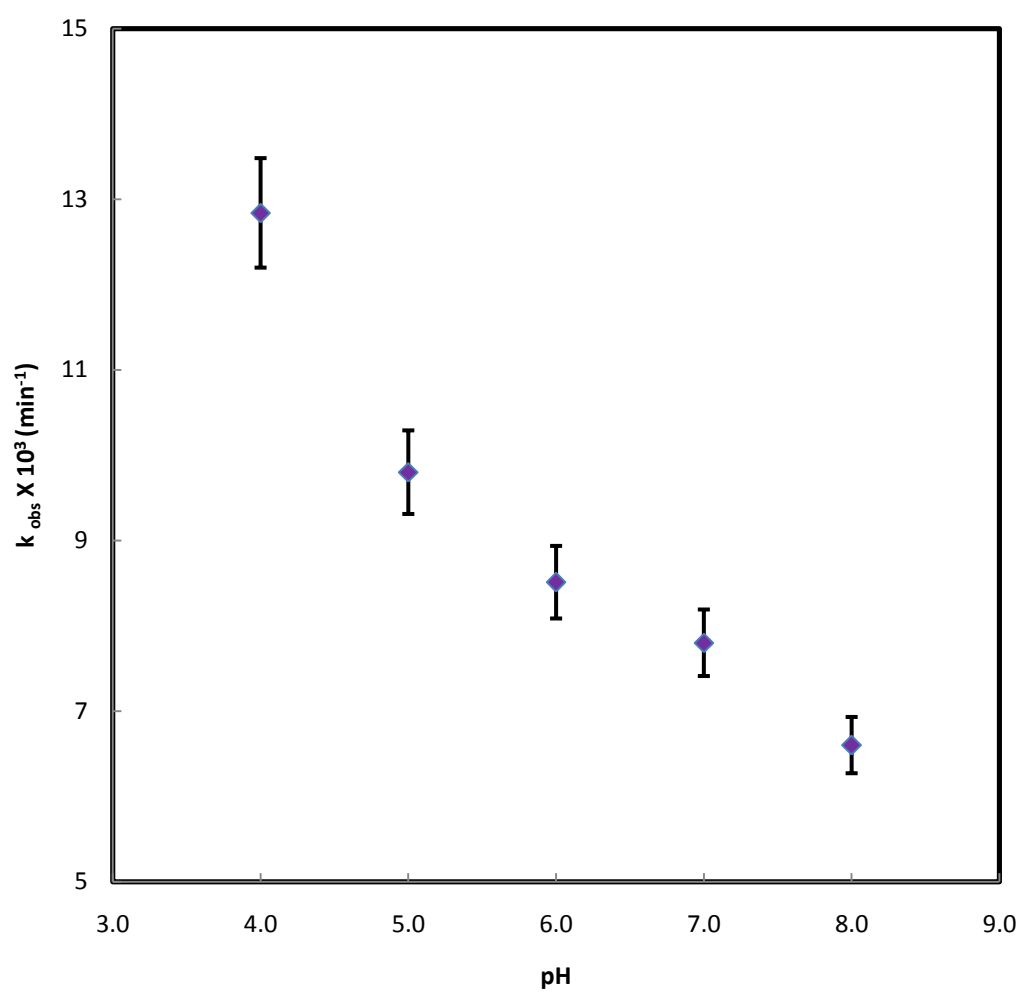
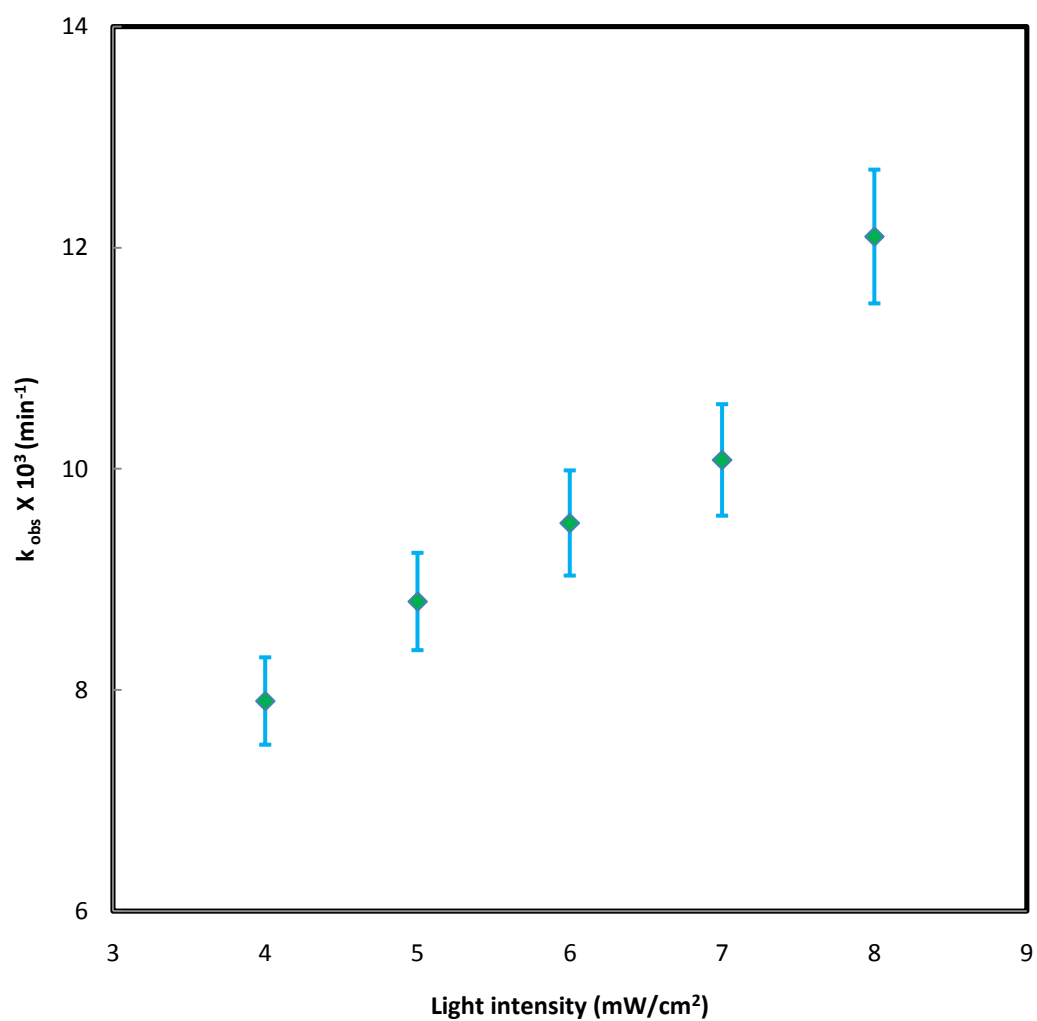


Table 5.4. M.O. degradation under different UV intensities M.O. with 2% Cu-ZnO at 25 °C, [Cu-ZnO] = 0.1 g dm⁻³, [M.O.] = 3 x 10⁻⁵ mol dm⁻³, at pH = 4.

Photocatalyst	Light intensity (mW/cm ²)	k _{obs} x 10 ³ (min ⁻¹)
2% Cu-ZnO	4	7.90
	5	8.80
	6	9.51
	7	10.08
	8	12.10

Fig. 5.11. M.O. degradation under different UV intensities M.O. with 2% Cu-ZnO at 25 °C, [Cu-ZnO] = 0.10 g dm⁻³, [M.O.] = 3.00 x 10⁻⁵ mol dm⁻³, at pH = 4.0.

(Conditions are stated in Table 5.4 (p.147))



5.4 Conclusion

Chemical precipitation method was used to prepare pure and Cu-ZnO nanoparticles. The XRD patterns and SEM topography shows that prepared nanoparticles were wurzite structure. The EDAX analysis shows that presence of Cu in ZnO. The average particle size of 2% Cu-ZnO (20.0 to 35.0 nm) exhibited excellent achievable photocatalytic degradation of M.O. in the acidic condition (pH 4.0). It was found that 2% Cu-ZnO shows the highest potential for degradation of methyl orange compare to ZnO and 1% Cu-ZnO.

References

1. S. Malatoa, P. Fernández-Ibáñez, M.I. Maldonado, J. Blanco, and W. Gernjakb, “Decontamination and disinfection of water by solar photocatalysis: Recent overview and trends”, *Catal. Today*. Vol. 147, 2007 pp. 1-59.
2. S. K. Kansal, M. Singh and D. Sud, “Studies on photo degradation of two commercial dyes in aqueous phase using different photocatalysts”, *J. Hazard. Mater.* Vol. 141, 2007, pp. 581-590.
3. M. Hoffman, S. Martin, W. Choi and D. Bahnemann, “Environmental Applications of Semiconductor Photocatalysis”, *Chem. Rev.* Vol. 95, 1995, pp. 69-96.
4. D. Beydoun, R. Amal, G. Low and S. McEvoy, “Role of nanoparticles in photocatalysis”, *J. Nano. Res.* Vol. 1, 1999, pp. 439-458.
5. Y. Dong, S. Zhan and P. Wang, “A Facile Synthesis of Ag Modified ZnO Nanocrystals with enhanced Photocatalytic activity, *Journal of Wuhan University of Technology-Mater*”, *Sci. Ed.*, Vol. 27, 2012, pp. 615-620.
6. R. Chauhan, Ashavani Kumar and R. P. Chaudhary, “Photocatalytic studies of silver doped ZnO nanoparticles synthesized by chemical precipitation method”, *J. sol-gel Sci. Technol.* Vol. 63, 2012, pp. 546-553.
7. H. Lin, S. Liao and S. Hung, “The dc thermal plasma synthesis of ZnO nanoparticles for visible-light photocatalyst”, *J. Photochem. Photo boil. A: Chem.*, Vol. 174, 2005, pp. 82-87.
8. S.R. Shirsath, D.V. Pinjari, P.R. Gogate, S.H. Sonawane, and A.B. Pandit, “Ultrasound assisted synthesis of doped TiO₂ nanoparticles: characterization and comparison of effectiveness for photocatalytic oxidation of dyestuff effluent”, *Ultrason. Sonochem.*, Vol. 20, 2013, pp. 277-286.
9. H.R. Pouretdal, H. Eskandari, M.H. Keshavarza and A. Semnani, “Photodegradation of organic dyes using nanoparticles of cadmium sulfide doped with manganese, nickel and copper as nanophotocatalyst”, *Acta Chimica Slovenica*. Vol. 56, 2009, pp. 353-361.
10. M.B. Moghaddam and A.H. Yangjeh, “Effect of operational parameters on photodegradation of methylene blue on ZnS nanoparticles prepared in presence of an ionic liquid as a highly efficient photocatalyst”, *J. Iran. Chem. Soc.*, Vol. 8, 2011, pp. 169-175.

11. N.J. Peill and M.R. Hoffmann, "Mathematical model of a photocatalytic fiber-optic cable reactor for heterogeneous photocatalysis", *Env. Sci. Technol.*, Vol. 32, 1998, pp. 398-404.
12. P. Fernández-Ibañez, J. Blanco, S. Malato and F. J. delos-Nieves. "Application of the colloidal stability of TiO₂ particles for recovery and reuse in solar photocatalysis", *Water Res.*, Vol. 37, 2003, pp. 3180-3188.
13. P. Sivakumar, G.K.G. Kumar, S. Renganathan, "Synthesis and characterization of ZnS-Ag nanoballs and its application in photocatalytic dye degradation under visible light", *J. nanostructure chem.*, Vol. 4, 2014, pp. 1-9.

Chapter 6

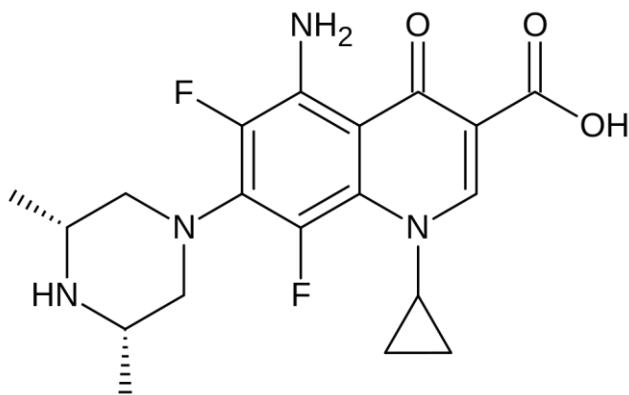
Ag-TiO₂ nanoparticles for photocatalytic degradation of sparfloxacin

6.1 Introduction

Contamination of ground water and surface water due to industrial organic contaminant creates several threats to flora and fauna in the ecosystem [1]. The existence of such contaminants in the ecosystem increases the environmental pollution. Degradation of such pollutants becomes the necessary to minimize the pollution. Use of semiconductor photocatalysts activated by UV-light or visible light has attracted attention as they potentially degrade the organic contaminants in water [2-5]. The important characteristic of photocatalytic reaction is it can work at ambient conditions, without producing any side products [6].

The general importance of Titanium dioxide (TiO₂) discussed in chapter 1 (p.12-13) and Advanced oxidation processes (AOPs) discussed in chapter 2 (p.34).

Sparfloxacin (SPF) belonging to fluoroquinolone homologous series. It is potent antibiotic widely used for the treatment of bacterial infections such as corneal ulcer in case of eye infection. It is active towards broad range of Gram positive and Gram negative microorganisms like *Streptococcus pneumoniae*, *Staphylococcus aureus*.



Chemical Structure of Sparfloxacin (SPF)

In the present work, to enhance the photocatalytic activity of TiO₂. Liquid Impregnation (L.I.) method was used to synthesize Ag-TiO₂ nanoparticles. These nanoparticles characterized by the analytic techniques such as X-Ray Diffraction (XRD), Scanning Electron Microscope (SEM), Energy Dispersive X-ray Spectroscopy (EDX) and Transmission Electron Microscopy (TEM). Photocatalytic efficiency of these prepared nanoparticles was studied on SPF in water environment examining different conditions such as initial substrate concentration, pH, catalyst loading and intensity of UV light.

6.2 Experimental

6.2.1 Chemicals and methods

Analar grade Sparfloxacin (SPF) procured from Dr. Reddy's laboratory. It is used as received without additional purification. A suitable quantity of sample is dissolved in deionized water to prepare stock solution of SPF. The TiO₂ (Anatase) procured from Sisco Research Pvt. Ltd. Mumbai. AgNO₃ was procured from HIMEDIA. Acetate, phosphate, and borate buffers were prepared to maintain pH during reaction condition, all reagents and chemicals were used were analytical grade.

The instruments used were already discussed in chapter-2 and p. no. (36-40)

6.2.2 Synthesis of photocatalyst

Liquid Impregnation Method (LI)

Ag-TiO₂ (anatase) nanoparticles were prepared by LI method. Slurry of TiO₂ was prepared by adding 500 mg TiO₂ in 100 ml double distilled water. The silver nitrate solution of 1% and 2 % (molar ratio) was added to the slurry. The resulting slurry was thoroughly mixed by vigorous stirring and allowed to settle at room temperature over night. The liquid so obtained was dried in an oven at 100 °C for 12 hrs to get rid of any remaining moisture. The nanoparticles resulting from this step was calcined at 500 °C for 3 hrs in a muffle furnace to get silver doped TiO₂ nanoparticles [7-8].

6.2.3 The Photocatalysis Process

To examine the photocatalytic degradation, a known concentration of SPF solution and buffer was taken in a Pyrex beaker. Doses of 100 mg dm⁻³ of 2% Ag-TiO₂ nanoparticles were added. Then, it was transferred in to the photoreactor and then kept under 8 W UV lamps (Philips) with a wavelength peak at 254 nm and of 4mW/cm² intensity with continuous stirring. After every 15 minutes interval the solution was taken out and centrifuged at 5000

rpm for 5 min. The degradation of centrifuged solution was measured at 290 nm ($\epsilon = 21913 \text{ dm}^3 \text{ mol}^{-1} \text{ cm}^{-1}$) using UV visible spectrophotometer (a CARY 50 Bio UV-Vis Spectrophotometer (Varian BV, The Netherlands)) and the degree of mineralization was studied as shown in Fig. 6.1.

6.3 Results and discussion

6.3.1 Effect of silver doping

Effect of silver doping on anatase TiO_2 was studied by changing the percentage of silver from 1% to 2% (mole ratio) an increase in the content of silver leads to decrease in the particle size and increase in the photocatalytic activity as shown in Fig. 6.2. Smaller particle size increases surface area and higher content silver may also favor separating charge carriers efficiently, inhibiting the recombination of electron - hole pairs, and thus increasing the photocatalytic activity [9]. The rates of photocatalytic degradation of SPF by prepared photocatalysts were compared and it was observed that the degradation effect of SPF treatment with UV/ 2% Ag- TiO_2 was more efficient than other three treatments namely UV, UV/ TiO_2 and UV/1% Ag- TiO_2 . The % degradation efficiency of SPF was studied under same conditions with UV, UV/ TiO_2 , UV/1% Ag- TiO_2 and UV/2% Ag- TiO_2 and % adsorption in dark was also determined. The % degradation efficiency of SPF was found to be 43%, 58%, 75% and 90% with UV, UV/ TiO_2 , UV/1% Ag- TiO_2 and UV/2% Ag- TiO_2 respectively within 100 minute as shown in as shown in Fig. 6.3. The photo degradation rate was highest with 2% Ag- TiO_2 hence, further studies were carried out with 2% Ag- TiO_2 .

Fig. 6.1. UV–Visible spectral changes during the degradation of SPF at 25 °C, [SPF] = $0.875 \times 10^{-5} \text{ mol dm}^{-3}$, pH = 5.0, 2% Ag-TiO₂ = 0.20 g dm^{-3} and light intensity 4 mW/cm².

Time (1) 0.00 min (2) 15.00 min (3) 30.00 min (4) 45.00 min
(5) 60.00 min (6) 75.00 min (7) 90.00 min

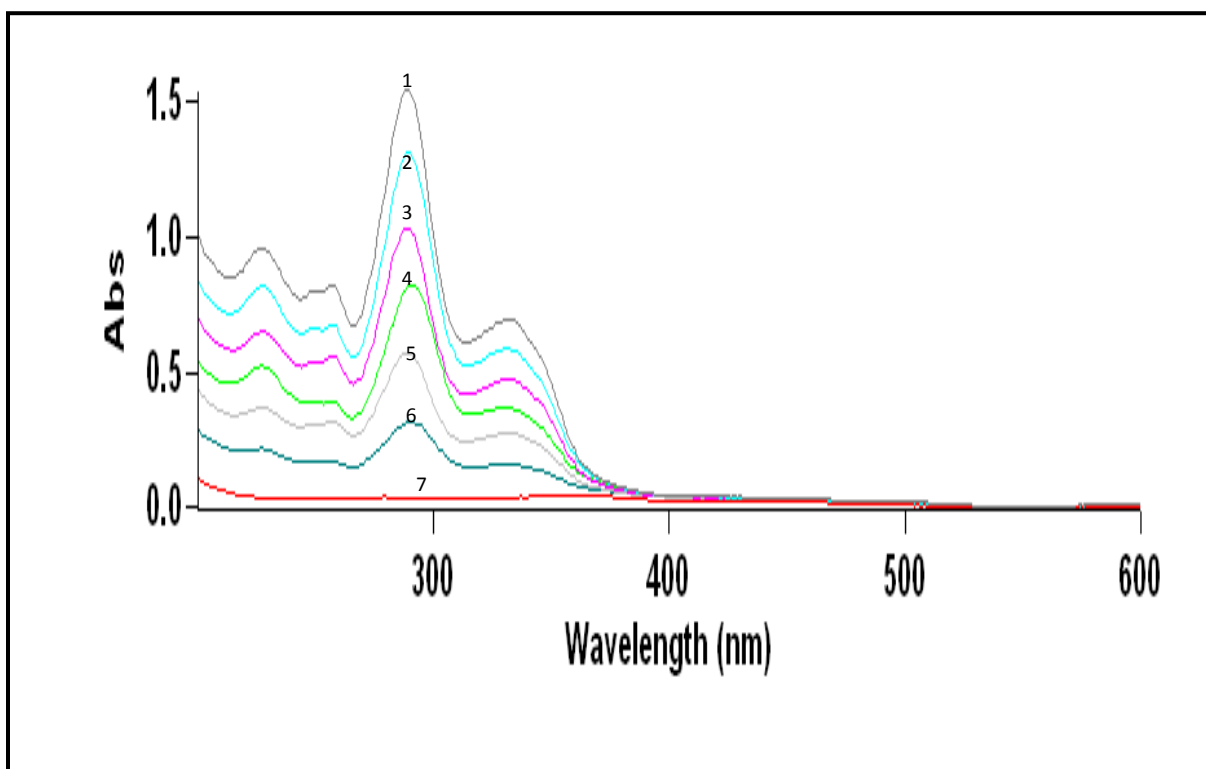


Fig. 6.2. % degradation efficiencies of various treatment methods with time at 25 °C, [SPF] = $0.875 \times 10^{-5} \text{ mol dm}^{-3}$, pH = 5.0, 2% Ag-TiO₂ = 0.20 g dm^{-3} and light intensity 4 mW/cm².

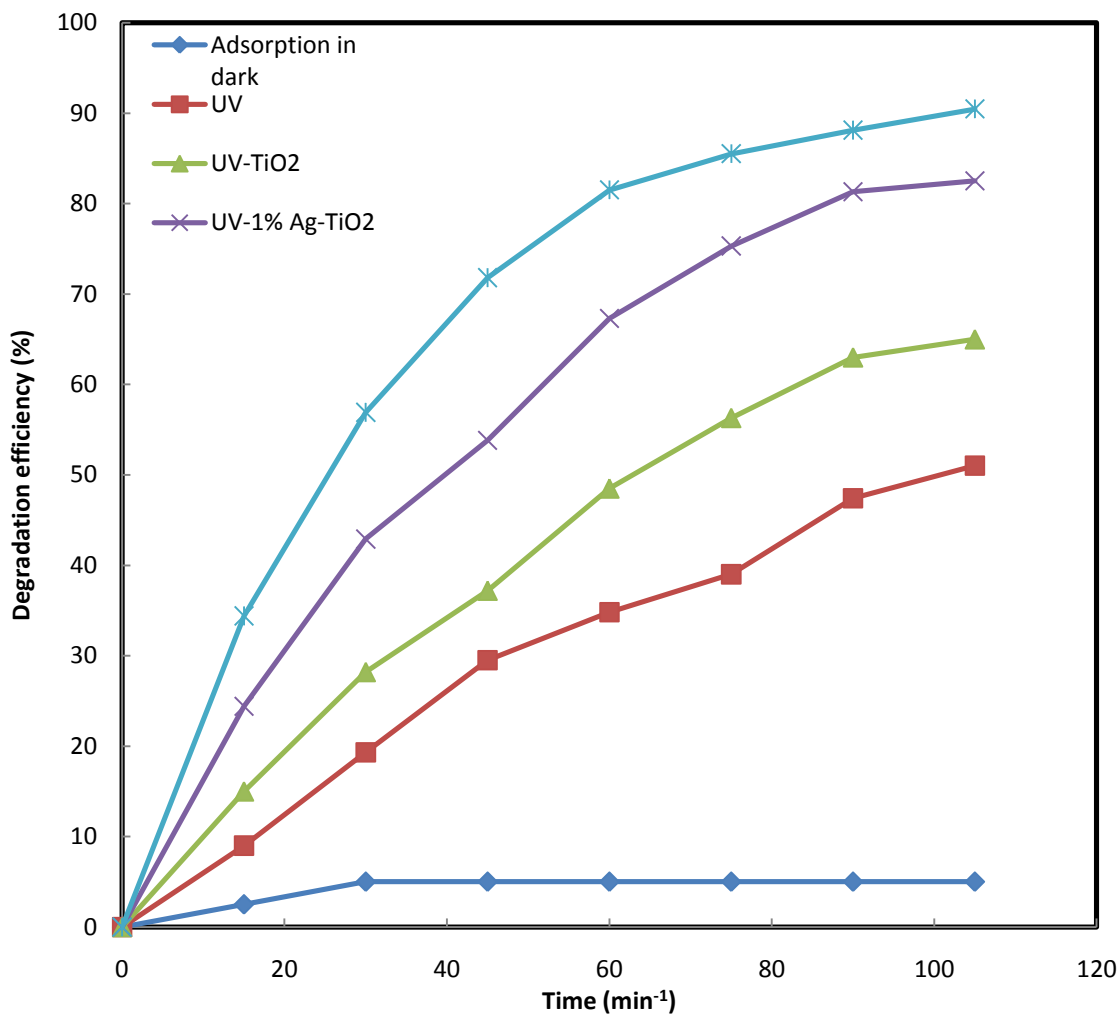
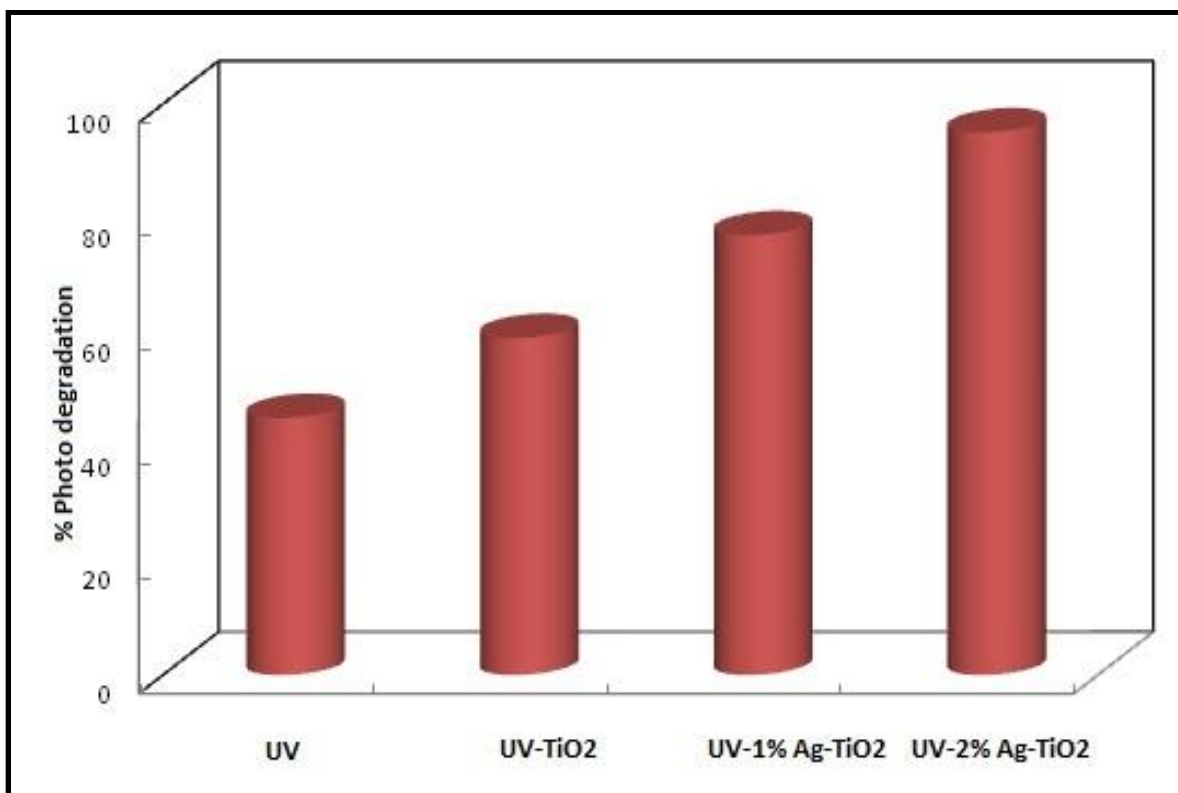


Fig. 6.3. Rate constants for the Photocatalytic degradation of SPF by various treatments at 25 °C, [SPF] = 0.875×10^{-5} mol dm⁻³, pH = 5.0, 2% Ag-TiO₂ = 0.20 g dm⁻³ and light intensity 4 mW/cm².



6.3.2 Characterization TiO₂ and Ag-TiO₂

6.3.2.1 X-ray Diffraction Studies (XRD)

Identification of crystal phase of prepared nanoparticles was done using X-ray diffractometer (Fig. 6.4). The 2θ values indicate that the major phase of all the synthesized nanoparticles is anatase. Scherrer equation was applied to anatase main peak to calculate the average crystallite size of synthesized nanoparticles as shown in Table 6.1. The crystallite size of TiO₂ is of 17.00 nm while the crystallite size of 1% Ag-TiO₂ is 14.17 nm, 2% Ag-TiO₂ 13.07. Our results are in agreement with earlier work [10], where 15.00 nm to 37.00 nm of Ag-TiO₂ nanoparticles sizes were reported.

6.3.2.2 Scanning Electron Microscope (SEM)

The Synthesized nanoparticles morphology, size and shape were analyzed using SEM (Fig. 6.5 (a) and Fig. 6.5 (b)). The resulting SEM images indicate that the Ag nanoparticles distributed unevenly TiO₂ to form non-uniform aggregates, which results in a high surface area. Our results were in line with previous work [11].

6.3.2.3 Transmission Electron Microscope (TEM)

Figures. 6.6 (a) and 6.6 (b) shows the TEM images of synthesized nanoparticles, which indicates that the Ag doped TiO₂ nanoparticles were cylindrical in structure and heterogeneously dispersed formed agglomeration. The small dark spots observed on TiO₂ surface is presumed as Ag particles. Where the particle size of prepared nanoparticles were about 10.00 - 15.00 nm in breadth and 40.00 - 45.00 nm in length. The resulting crystal size of the prepared nanoparticles in line with XRD results.

6.3.2.4 Energy Dispersive X-ray Spectroscopy (EDX)

The elemental analyses of prepared nanoparticles were analyzed using EDX, which depicted in Fig. 6.7 (a) and Fig. 6.7 (b). It shows that the only three peaks, it is presumed to be due to Ti and O with little amount of Ag that increases with increase number of loading. Ag L peak was found but peak of Ag K cannot be detected because low electron accelerating voltage was applied [12]. The peaks from the spectra indicates that the presence of Ti, O and Ag at 4.508, 0.525 and 2.983 keV respectively. The atomic % of Ti, O and Ag is 77.51, 20.49 and 2.00 respectively. This composition of Ti, O and trace amount of Ag, which leads to better photocatalytic activity.

Fig. 6.4. XRD patterns of a) Undoped TiO₂, b) 1% Ag - TiO₂ and c) 2% Ag - TiO₂

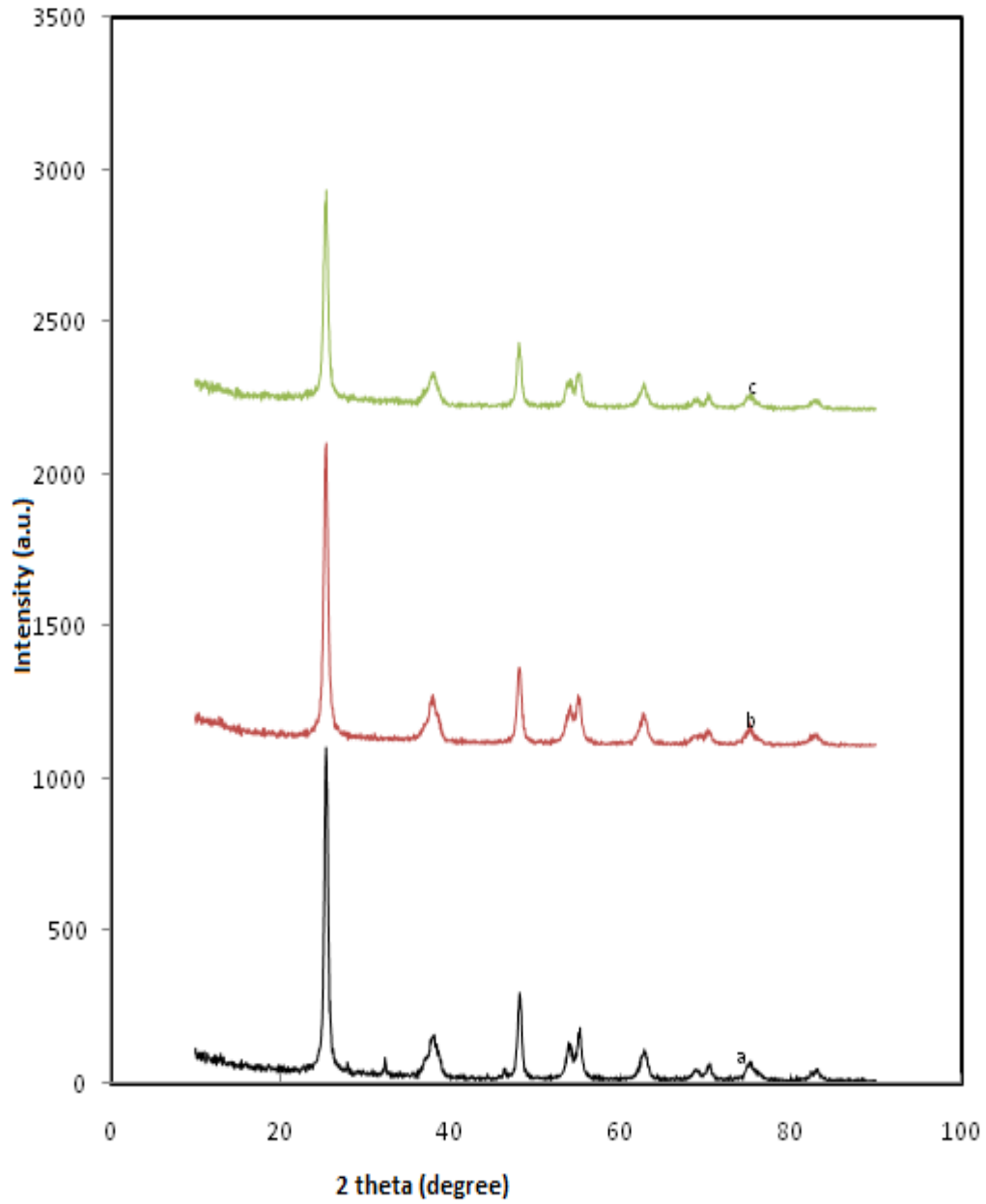
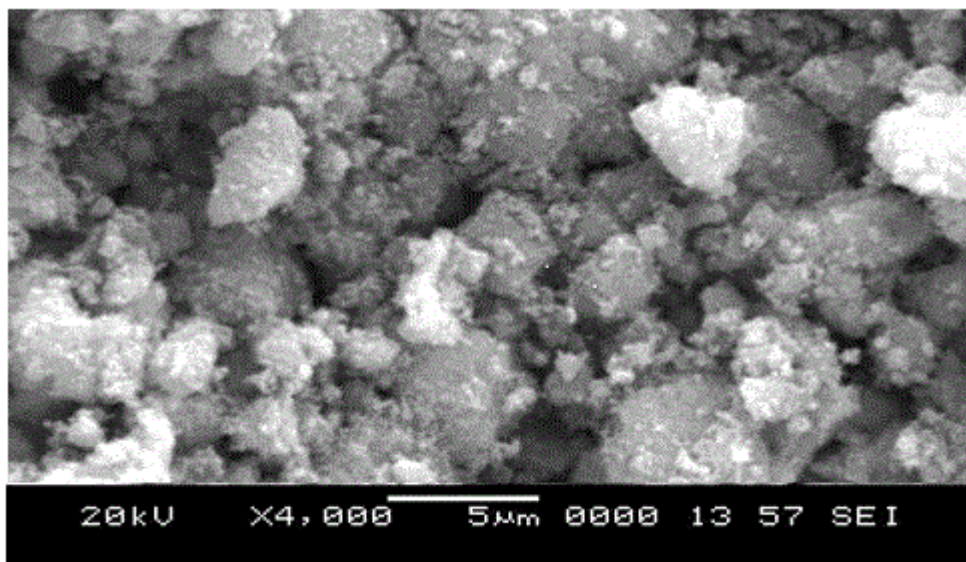


Table 6.1. Crystal size of undoped and Ag doped TiO₂ nanoparticles from Scherrer equation

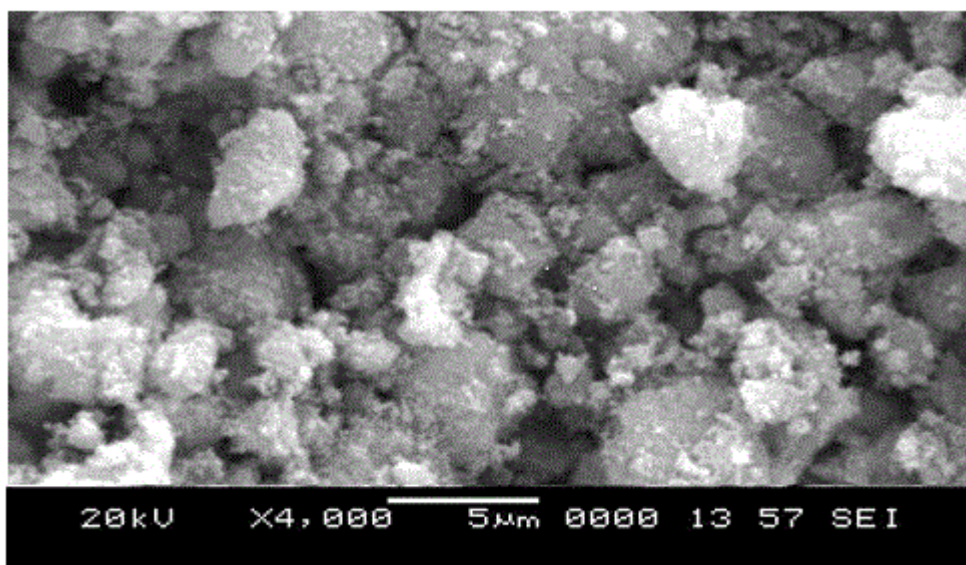
Sr. No	Particles	Particle size (nm)
1	Un doped TiO ₂	17.00
2	1% Ag-TiO ₂	14.17
3	2% Ag-TiO ₂	13.07

**Fig. 6.5. SEM micrographs of a) Undoped TiO₂, b) 1% Ag - TiO₂ and
c) 2% Ag - TiO₂**

a)



b)



c)

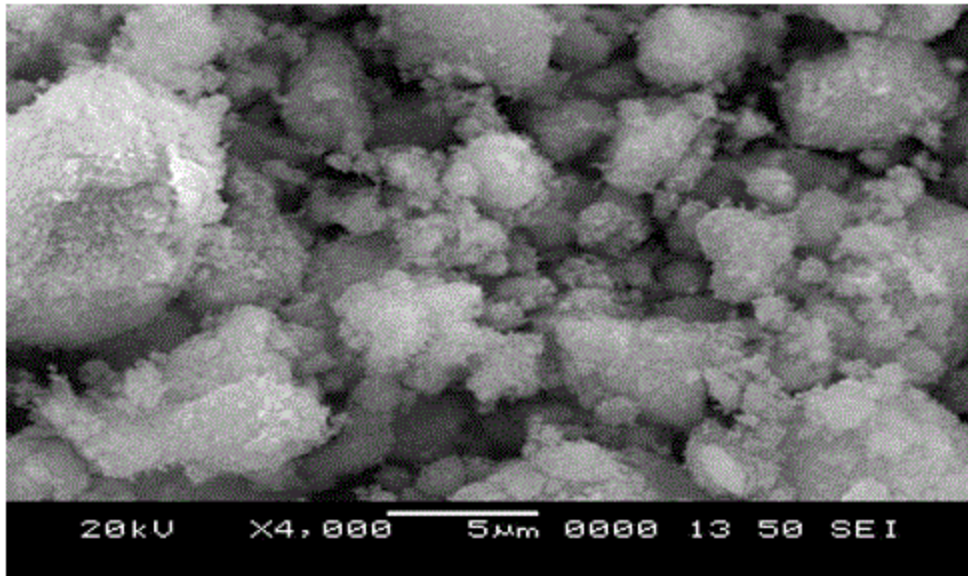
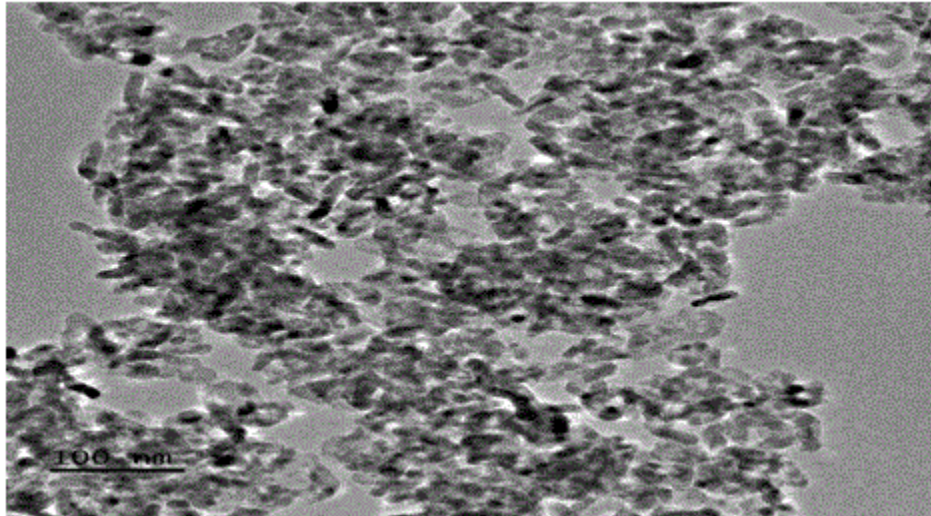


Fig. 6.6. TEM micrographs of (a & b) 2% Ag/TiO₂

a)



b)

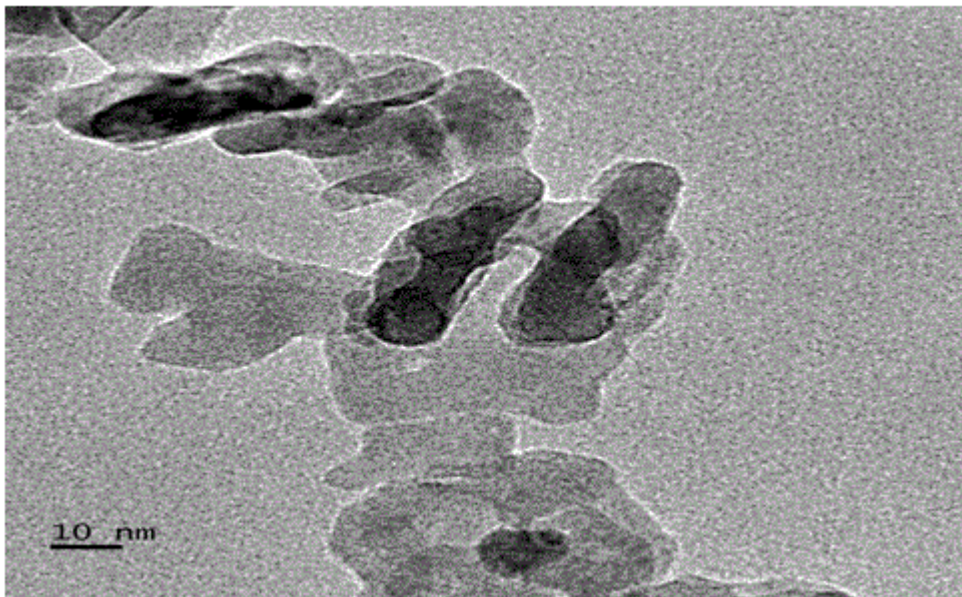
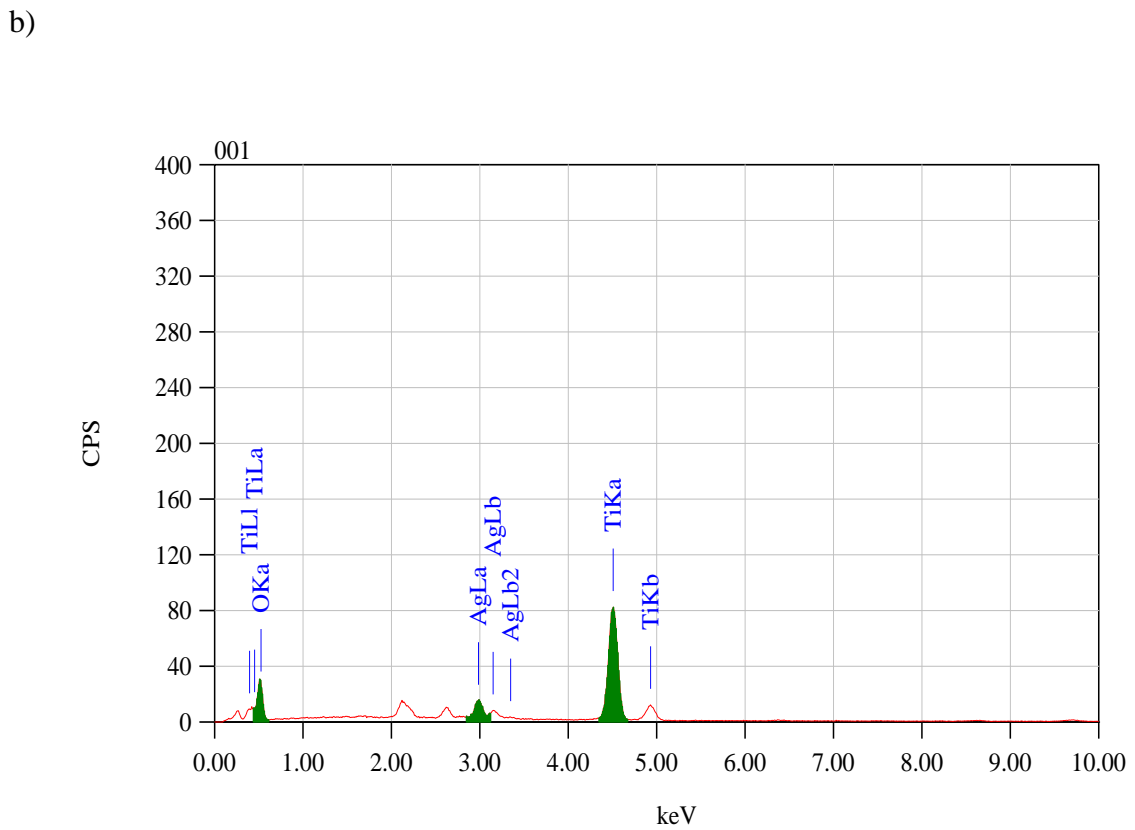
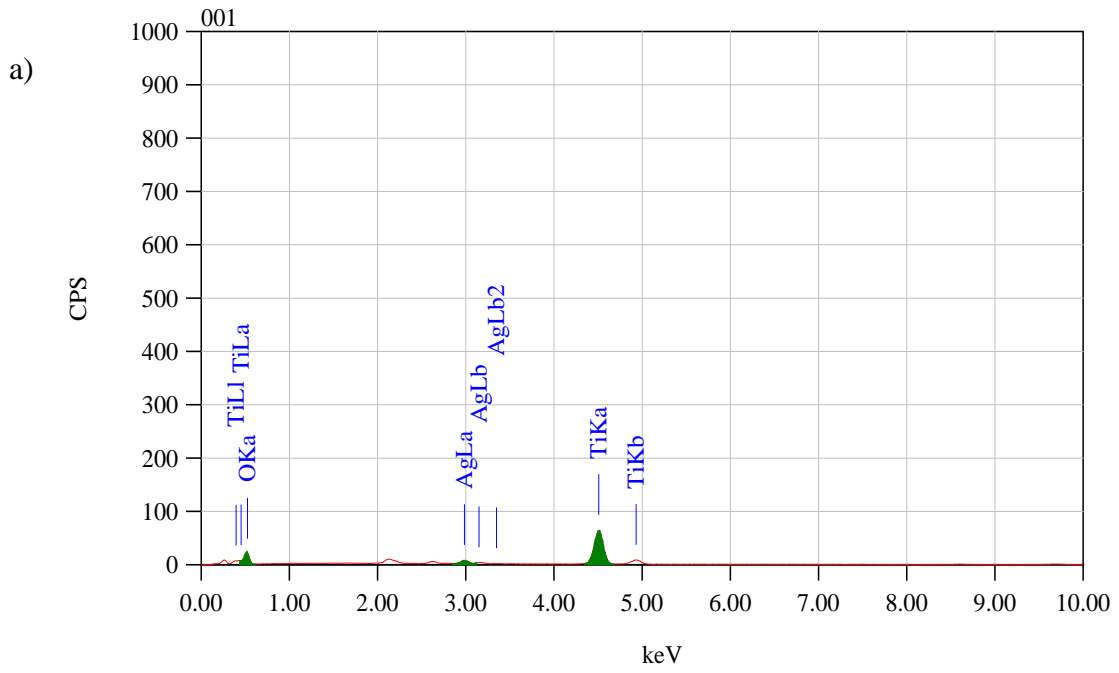


Fig. 6.7. EDX analysis of a) 1% and b) 2% Ag-TiO₂



6.3.3 Effect of Photocatalyst Dosage

To examine the influence of amount of catalyst, disparate quantity of catalyst is used from 0.05 g dm^{-3} to 0.50 g dm^{-3} while keeping [SPF] and $\text{pH} = 4.0$ constant. It has been observed that initially the rate of photo degradation increases up to 0.25 g dm^{-3} , beyond 0.25 g dm^{-3} the rate of reaction almost constant (Table 6.2 and Fig. 6.8). This may be due to the fact that as the amount of semiconductor was increased in the initial state, the exposed surface area of the semiconductor photocatalyst also increases but after this limiting value (0.25 g dm^{-3}) any increase in the amount of semiconductor photocatalyst increases the turbidity of the solution and thus masks photocatalyst from UV irradiation for the reaction to proceed, and therefore degradation starts decreasing [13].

6.3.4 Effect of [SPF]

The influence of variation of SPF concentration was studied by taking different concentration of SPF from 0.350×10^{-5} to $3.500 \times 10^{-5} \text{ mol dm}^{-3}$ by keeping other condition constant. It has been observed that initially increase in the concentration of SPF the rate of photo-catalytic degradation increases, reaching maximum value $[\text{SPF}] = 0.875 \times 10^{-5} \text{ mol dm}^{-3}$ further increase in concentration resulted in decrease in the rate of photo-catalytic degradation as shown in Table 6.3 and Fig. 6.10. It may be due to the fact that, as the concentration of the drug increased, more number of drug molecules are available for degradation hence the rate of degradation increases. But at concentration above $0.875 \times 10^{-5} \text{ mol dm}^{-3}$ the drug acts as a filter for the incident light, thus decreasing in the rate of photocatalytic degradation [14].

6.3.5 Effect of pH

The pH normally influences the adsorption capacity of the adsorbent in aqueous medium by altering the surface properties of adsorbent. The effect of pH on the rate of photo degradation of SPF was studied by varying the pH from 5.0 - 9.0, while keeping other reaction conditions constant. The rate of photo-catalytic degradation of SPF was higher in the pH 5.0 and lower in the pH range 6.0 - 9.0 as shown in Table 6.4 and Fig. 6.11. This increase in the rate of photocatalytic degradation may be due to the fact that in acidic medium the photocatalytic surface is positively charged and it adsorbs more negatively charged ions hence, effective collision between drug and catalyst takes place so rate of degradation is maximum at pH 5.0.

Table 6.2. Effect of different amount of 2% Ag-TiO₂ photocatalyst on the degradation of SPF at 25 °C, [SPF] = 0.875 x10⁻⁵ mol dm⁻³, at pH = 5.0, light intensity = 4 mW/ cm².

Photocatalyst	Amount of photocatalyst (g dm ⁻³)	k _{obs} (min ⁻¹)
2% Ag-TiO ₂	0.05	0.01238
	0.10	0.01568
	0.15	0.02194
	0.25	0.03145
	0.35	0.02449
	0.50	0.02390

Fig. 6.8. Effect of different amount of 2% Ag-TiO₂ photocatalyst on the degradation of SPF at 25 °C, [SPF] = 0.875 x10⁻⁵ mol dm⁻³, at pH = 5.0, light intensity = 4 mW/ cm².

(Conditions are stated in Table 6.2 (p.166))

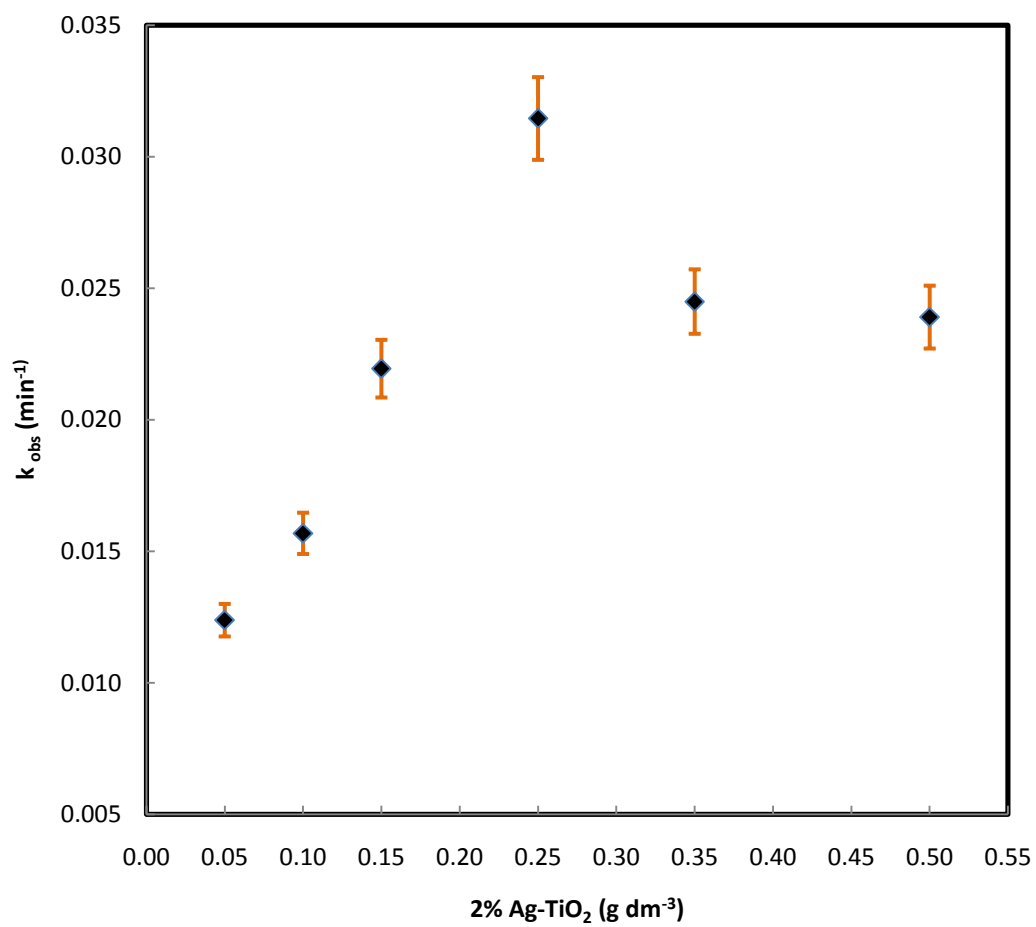


Table 6.3. Effect of [SPF] on photocatalytic rate constants with with 2% Ag-TiO₂ at 25 °C, [Ag-TiO₂] = 0.20 g dm⁻³, at pH=4.0, light intensity = 4 mW/ cm².

Photocatalyst	[SFC] x 10 ⁵ (mol dm ⁻³)	k _{obs} (min ⁻¹)
2% Ag-TiO ₂	0.350	0.0083
	0.525	0.0110
	0.875	0.0310
	1.400	0.0106
	2.500	0.0105
	3.500	0.0095

Fig. 6.9. Effect of [SPF] on photocatalytic rate constants with 2% Ag-TiO₂ at 25 °C, [Ag-TiO₂] = 0.20 g dm⁻³, at pH=4.0, light intensity = 4 mW/ cm².

(Conditions are stated in Table 6.3 (p.168))

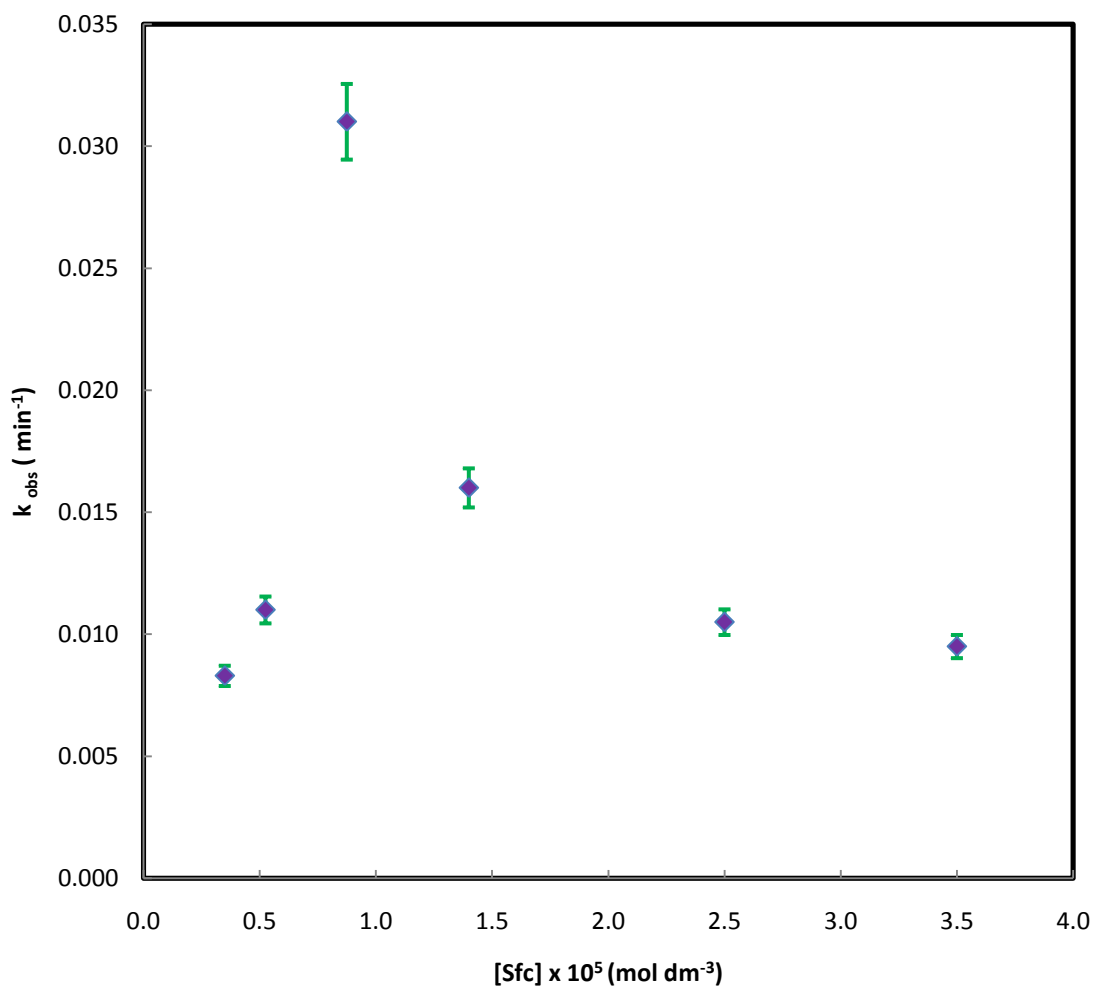
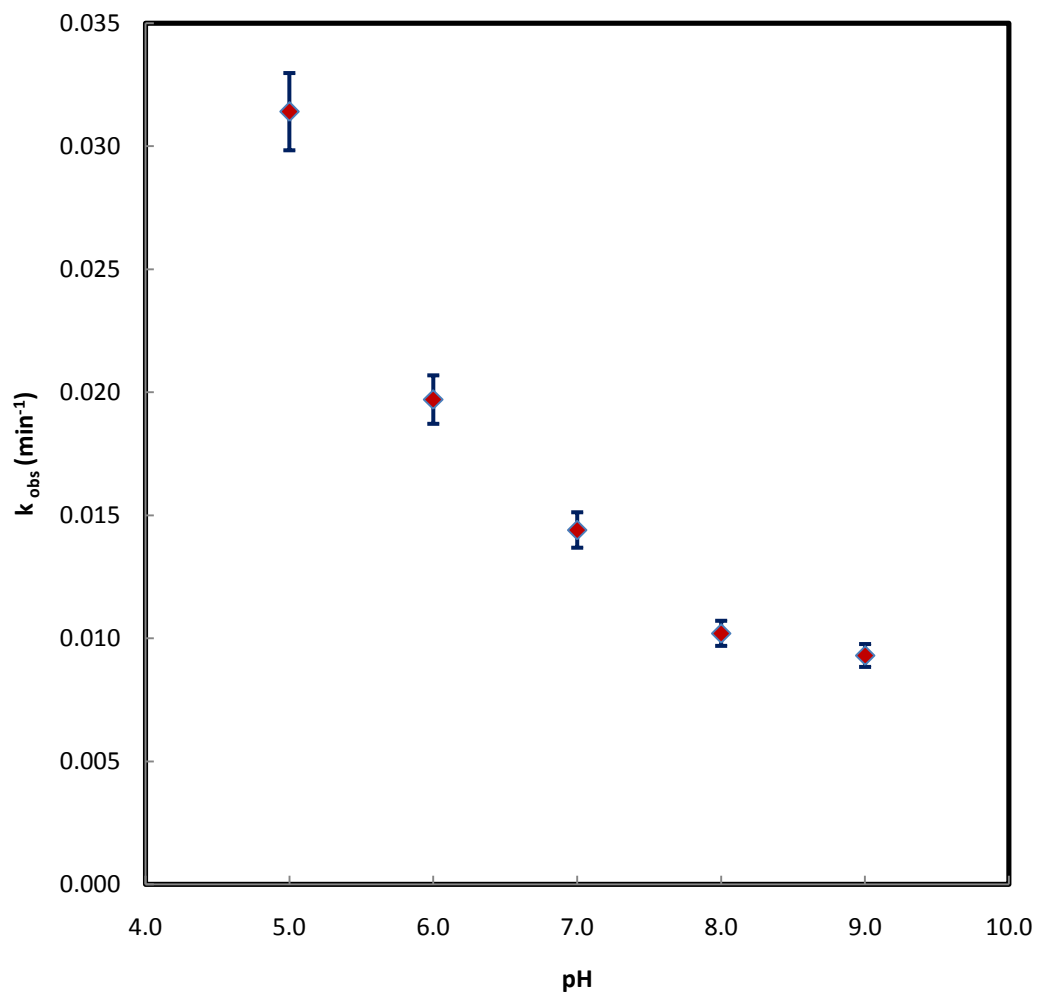


Table 6.4. Effect of pH on the rate constant of photocatalytic degradation of SPF with 2% Ag-TiO₂ at 25 °C, [Ag-TiO₂] = 0.20 g dm⁻³, [SPF] = 0.875 x 10⁻⁵ mol dm⁻³, light intensity = 4 mW/cm².

Photocatalyst	pH	k _{obs} (min ⁻¹)
2% Ag-TiO ₂	5.0	0.0314
	6.0	0.0197
	7.0	0.0144
	8.0	0.0102
	9.0	0.0093

Fig. 6.10. Effect of pH on the rate constant of photocatalytic degradation of SPF with 2% Ag-TiO₂ at 25 °C, [Ag-TiO₂] = 0.20 g dm⁻³, [SPF] = 0.875 x 10⁻⁵ mol dm⁻³, light intensity = 4 mW/cm².

(Conditions are stated in Table 6.4 (p.170))



On the contrary in alkaline medium the OH^- ions accumulate on the surface of photocatalyst making it negatively charged and SPF is also negatively charged in alkaline medium. Hence, the repulsion between SPF ion and photocatalyst takes place leading to decrease rate of photodegradation at pH 6.0 to 9.0. This observation is in line with the earlier report [15].

6.3.6 Effect of UV lamp distance

Effect of UV light intensity on the degradation of SPF was studied by varying the distance of UV lamp from the target. The results are reported in Table 6.5 and Fig. 6.12. It is observed, that, an increase in light intensity increased the rate of photocatalytic degradation. This is due to the fact that increase in UV light intensity excites higher number of Ag-TiO₂ nanoparticles there by generating higher number of electron hole pairs. The holes decompose the SPF molecules adsorbed on the surface of Ag-TiO₂ particles and oxidize it to water resulting in their efficient degradation [16].

6.4 Conclusion

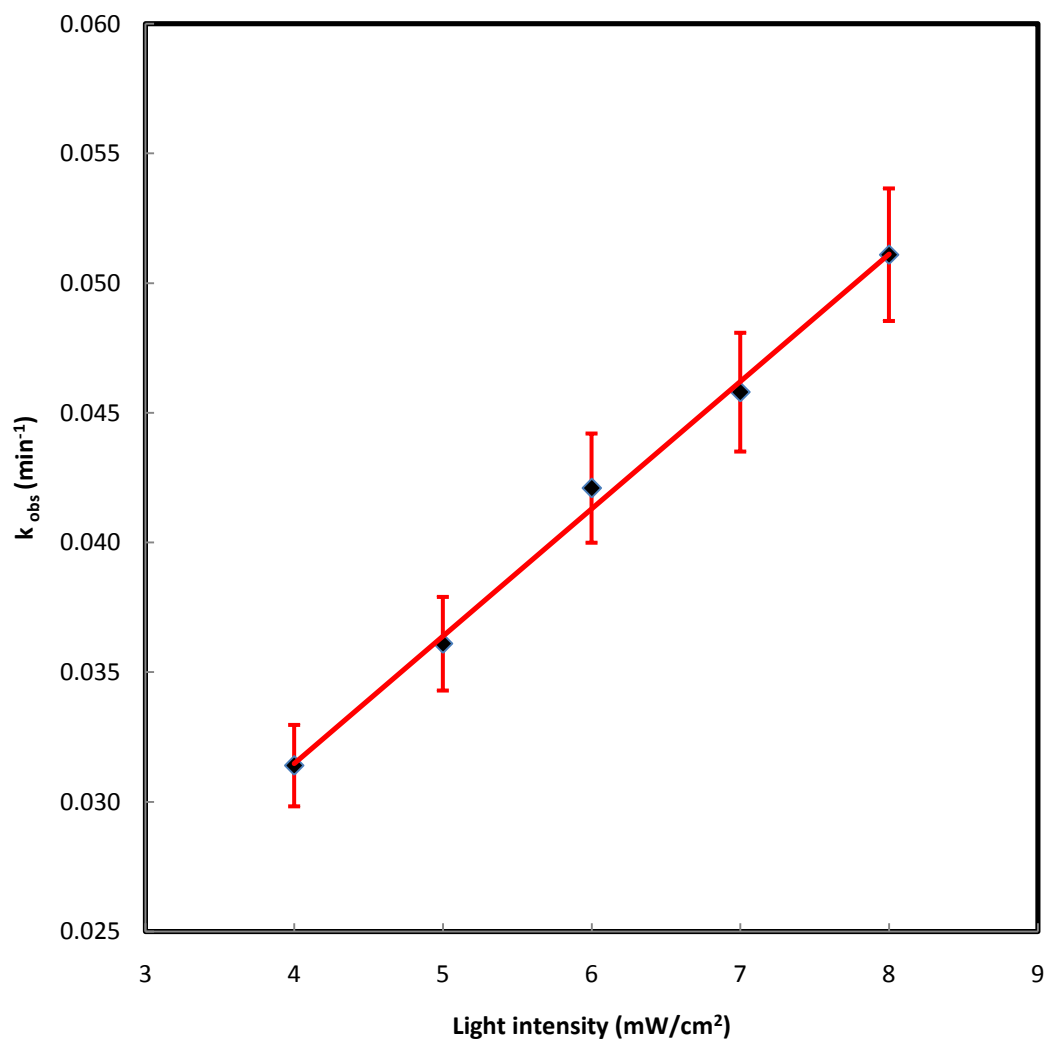
LI method was used to prepare 1% and 2% Ag-TiO₂ nanoparticles. The resulting Ag-TiO₂ (17.00 to 13.07 nm) nanoparticles having better potential towards the mineralization of SPF in acidic medium (pH 4.0). The XRD analysis shows that the prepared Ag doped TiO₂ nanoparticles were anatase in crystal phase. TEM and EDX analysis shows that the presence of Ag in TiO₂. Under optimal conditions, over 90% photocatalytic degradation of SPF was achieved in 100 min using 2% Ag-TiO₂ photocatalyst.

Table 6.5. SPF degradation under different UV intensities SPF with 2% Ag-TiO₂ at 25 °C, [Ag-TiO₂] = 0.20 g dm⁻³, [SPF] = 0.875 x 10⁻⁵ mol dm⁻³, at pH=5.0.

Photocatalyst	Light intensity (mW/cm ²)	k _{obs} (min ⁻¹)
2% Ag-TiO ₂	4	0.0314
	5	0.0361
	6	0.0421
	7	0.0458
	8	0.0511

Fig. 6.11. SPF degradation under different UV intensities SPF with 2% Ag-TiO₂ at 25 °C, [Ag-TiO₂] = 0.20 g dm⁻³, [SPF] = 0.875 x 10⁻⁵ mol dm⁻³, at pH=5.0, light intensity = 4 mW/cm².

(Conditions are stated in Table 6.5 (p.173))



References

1. R.W. Matthews, "Photooxidative degradation of coloured organics in water using supported catalysts TiO₂ on sand", *Water Res.* Vol. 25, 1991, pp. 1169-1176.
2. A. Sharma, P. Rao, R.P. Mathur and S.C. Ameta, "Photocatalytic reactions of xylidine ponceau on semiconducting zinc oxide powder", *J. Photochem. Photobiol. A: Chem.* Vol. 86 1995, pp. 197-200.
3. S. Sakthivel, B. Neppolian, M. V. Shankar, B. Arabindoo, M. Palanichamy and V. Murugesan, "Solar photocatalytic degradation of azo dye: comparison of photocatalytic efficiency of ZnO and TiO₂ Sol", *Energy Mater. Sol. Cells* Vol. 77 2003, pp. 65-82.
4. A.L. Linsebigler, G.Q. Lu and J. T. Yates, "Photocatalysis on TiO₂ surfaces: principles, mechanisms, and selected results", *Chem. Rev.* Vol. 95 1995, pp. 735-758.
5. T. L. Thompson and J. T. Yates, "Surface science studies of the photoactivation of TiO₂ new photochemical processes", *Chem. Rev.* Vol. 106, 2006, 4428-4453.
6. S. K. Pardeshi and A. B. Patil, "Effect of morphology and crystallite size on solar photocatalytic activity of zinc oxide synthesized by solution free mechanochemical method", *J. Mol. Catal. A: Chem.* Vol. 308, 2009, pp. 32-40.
7. M.A. Behnajady, N. Modirshahla, M. Shokri and B. Rad, "Enhancement of photocatalytic activity of TiO₂ nano particles by silver doping: Photodeposition versus liquid impregnation methods", *Global NEST Journal.* Vol. 10 (1), 2008, pp. 1-7.
8. H. Ilyas, I.A. Qazi, W. Asgar, M.A. Awan and Z. Khan, "Photocatalytic degradation nitro and chloro phenols using doped and undoped titanium dioxide nanoparticles", *J. of nanomateri.* Vol. 2011, 2011, pp. 1-8.
9. S. Ozkan, M.W. Kumthekar and G. Karakas, "Characterization and temperature-programmed studies over Pd/TiO₂ catalysts for NO reduction with methane", *Catal. Today.* Vol. 40 (1), 1998, pp. 3-14.
10. T. Kudo, Y. Nakamura and A. Ruike, "The design of highly active rectangular column structured titanium oxide photocatalysts and their application in purification systems", *J. Catal. Today.* Vol. 122, 2003, 14-19.
11. A. Jodat and A. Jodat, "Photocatalytic degradation of chloramphenicol and tartrazine using Ag/TiO₂ nanoparticles", *Desalin. Water Treat.* Vol. 52, 2014, pp. 2668-2677.

12. K. Wetchakun and S. Phanichphant, "Effect of Ru on photocatalytic activity of TiO₂ nanoparticles", J. Micro. Soc. of Thailand. Vol. 22, 2008, pp. 11-14.
13. J. Sun, L. Qiao, S. Sun and G.Wang, "Photocatalytic degradation of Orange G on nitrogen doped TiO₂ catalysts under visible light and sunlight irradiation", J.Haz. Mater. Vol. 155, 2008, pp. 312-319.
14. C.C. Wang, C.K. Lee, M.D. Iyu and L.C. Juang, "Photocatalytic degradation of C.I. Basic Violet using TiO₂ catalysts supported by Y. Zeolite an investigation of the effects of operational parameters", Dyes and Pigments. Vol. 76, 2008, pp. 312-319.
15. I.T. Horvath, Encyclopedia of Catalysis, Wiley, New York, 2003.
16. Z. Guo, R. Ma and G. Li, "Photocatalytic property of colloidal TiO₂ nanoparticles prepared by sparking process", J. Chem. Eng. Vol. 119, 2006, pp. 55-59.

Chapter 7

Kinetics and mechanism of uncatalyzed and palladium (II)-catalyzed oxidation of lomefloxacin by permanganate in acidic medium.

7.1 Introduction

In synthetic, analytical and organic chemistry permanganate is extensively employed as an oxidizing agent (acidic, alkaline or neutral medium) [1-2]. The reaction mechanism not only dependent upon permanganate it also depends upon pH of the reaction medium [3]. Oxidation via permanganate ion gets an importance in the organic synthetic field after the invention of phase transfer catalytic reactions [4-5]. Since, from five decades permanganate widely used as disinfectants in untreated water treatment [6]. Variable oxidation states of permanganate facilitate the oxidation of the organic compounds hence it has strong oxidation behavior in the neutral, acidic and basic medium [7-8].

Pharmaceuticals are used for the treatment of diseases to maintain good health of human being [9-10]. Amongst pharmaceuticals, containing antibacterial has been considered as emerging contaminants [11]. They have the potential of adverse impact on the environment and also on human health [12-13]. The large fraction clinically prescribed a dose of fluoroquinolones goes into the local sewage water due to partial digestion in the animal body. It is the main route for the passage of such clinical drug contaminated with the regular water system. Fluoroquinolones have been distinguished in civil sewage in the range of $\mu\text{g dm}^{-3}$ to nano g dm^{-3} [14].

The general importance of antibacterial agent lomefloxacin, in particular, is discussed in chapter 1(p.5) and chapter 2 (p.34).

In most of the literatures reveal that Pd^{2+} used as a catalyst the as in the form PdCl_2 [15-18]. The reaction mechanism involving Pd^{2+} depends on the oxidant and substrate used. The Pd^{2+} usually forms an activated complex with substrate molecule before forming the final products [19-20].

An earlier study reported that the existence of micro amount of Pd²⁺ catalyst in acidic or basic medium becomes facilitates the reaction faster [21-22]. Hence, we carried out the detail study of kinetics and mechanism of oxidation of LMF with permanganate in presence of Pd²⁺ catalyst in acidic medium.

7.2 Experimental

7.2.1 Chemicals and Methods

All the chemical reagents were used during the experiment were of analar grade. The stock solution of LMF (Dr. Reddy's Laboratory) was prepared by dissolving known amount of LMF in 100 ml of deionised water. The KMnO₄ (MERCK Specialties Pvt. Ltd) solution was made and standardized by oxalic acid [23]. The PdCl₂ (SD Fine Chem.) was made in 0.20 mol dm⁻³ HCl and standardized with EDTA. NaClO₄ of 2.9 mol dm⁻³ and HClO₄ of 1.0 mol dm⁻³ stock solution were prepared to maintain the acidic medium and ionic strength of 0.5 mol dm⁻³ individually.

7.2.2 Instruments -Used

(i) For the kinetic investigation, UV-Vis Spectrophotometer (CARY 50 Bio, Varian BV, and The Netherlands) with a temperature controller and HPLC framework (Agilent 1100 arrangement, USA) were utilized.

(ii) For product identification, Agilent 6130 Series Quadrupole LC/MS. Column-Atlantis C18 (50 x 4.6mm - 5µm) double mode was utilized

(iii) For pH estimations Elico display LI 120 pH meter was utilized.

7.2.3 Kinetic procedure

The oxidation of LMF with permanganate was performed in pseudo first-order conditions, where LMF was taken in higher concentration than permanganate at 25 ± 0.2°C. The reaction mixture was started with adding permanganate to the prior thermostated solutions. The reaction proceeds through a decrease in the Abs of permanganate @ 526 nm with time Fig. 7.1. The UV-Vis variation of spectra with the oxidation of LMF by permanganate in the presence of Pd²⁺ catalyst is 25 ± 0.2°C are shown in Fig. 7.2.

Fig. 7.1. Verification of Beer's law for [permanganate] at 526 nm in 0.50 mol dm^{-3} alkali

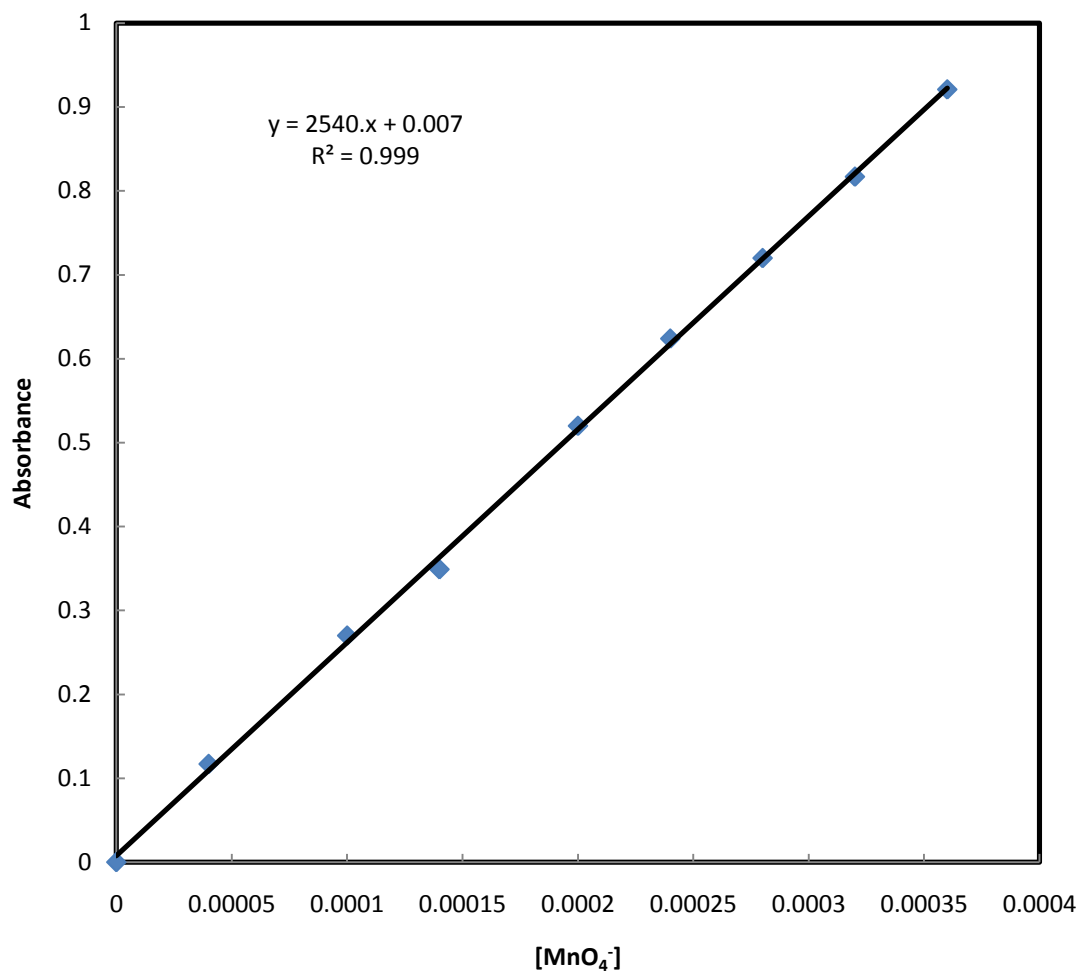
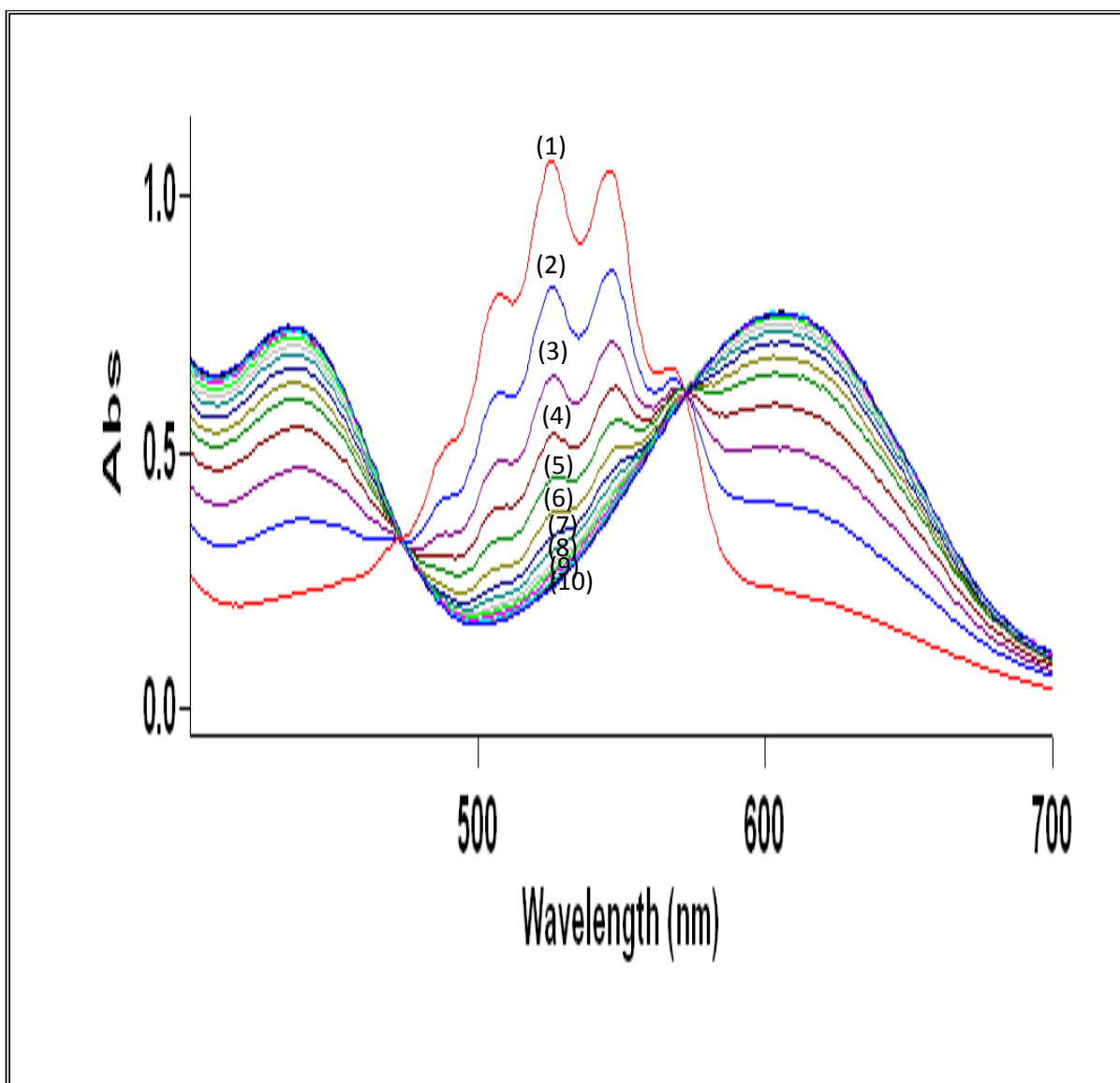


Fig. 7.2. UV-Visible spectral changes during the permanganate oxidation of lomefloxacin (LMF) at 25°C

Time (1) 0.50 min (2) 1.00 min (3) 1.50 min (4) 2.00 min (5) 2.50 min
(6) 3.00 min (7) 3.50 min (8) 4.00 min (9) 4.50 min (10) 5.00min

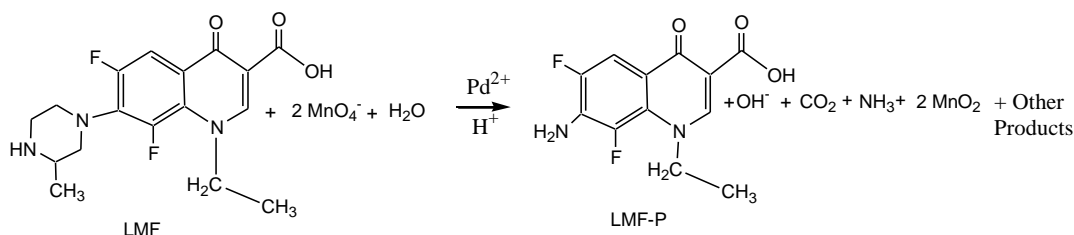


The Beer's law of permanganate was verified @ 526 nm and giving $\epsilon = 2283 \pm 20 \text{ dm}^{-3} \cdot \text{mol}^{-1} \cdot \text{cm}^{-1}$ (literature $\epsilon = 2200 \text{ dm}^{-3} \cdot \text{mol}^{-1} \cdot \text{cm}^{-1}$). It was observed that there is an insignificant effect from different species at this wavelength [14]. The graph was straight, at about 80% completion of the reaction in Pd^{2+} catalyzed reaction (Fig. 7.3. and Table 7.1). The experimentally determined rate constants k_{obs} were reproduced within $\pm 7\%$ error, Table 7.2., k_{obs} value computed by plotting graph $\log \text{Abs}$ Vs. Time. The product analysis was finished done by HPLC system (Shimadzu noticeable quality) and Thermo Scientific Q-Exactive HR-MS and Column-Thermo Scientific Hypersil Gold C18 (150 x 4.6mm-8 μm).

7.3 Results and discussion

7.3.1 Stoichiometry and Product identification method

A reaction mixture having a higher concentration of permanganate than LMF, HClO_4 of 0.10 mol dm^{-3} , and total ionic strength 0.50 mol dm^{-3} was kept for reaction for 24 hrs at $25 \pm 0.2 \text{ }^\circ\text{C}$. The unreacted permanganate concentration was estimated after the reaction. The results revealed that 2.0 M of permanganate were used by 1.0 M of LMF in the presence of Pd^{2+} catalyst, Scheme 1.



The reaction side products were determined. Ammonia tested by Nessler's test [24], UV-Spectrum confirms the presence of Mn (VI) and the presence of CO_2 by lime water test [25]. The reaction mixture containing LMF with higher [permanganate] with constant $[\text{H}^+]$ was kept in a flask. Then, the reaction mixture was stored for 1day and products of LMF were identified using HPLC (Agilent quadrupole 6130 series) and LC-MS spectra as shown in Fig. 7.4.

Fig. 7.3. First-order plots of oxidation of LMF by acidic permanganate at 25 °C
 $[LMF] = 3.00 \times 10^{-3}$ $[H^+] = 0.10 \text{ mol dm}^{-3}$; $I = 0.50 \text{ mol dm}^{-3}$; $[Pd^{+2}] = 5.00 \times 10^{-8} \text{ mol dm}^{-3}$, $[Permanganate] = x \times 10^{-4} \text{ mol dm}^{-3} =$ (A) 0.5, (B) 1.0, (C) 2.0, (D) 3.0, (E) 4.0, (F) 5.0

(Conditions are stated in Table 7.2. (p.184))

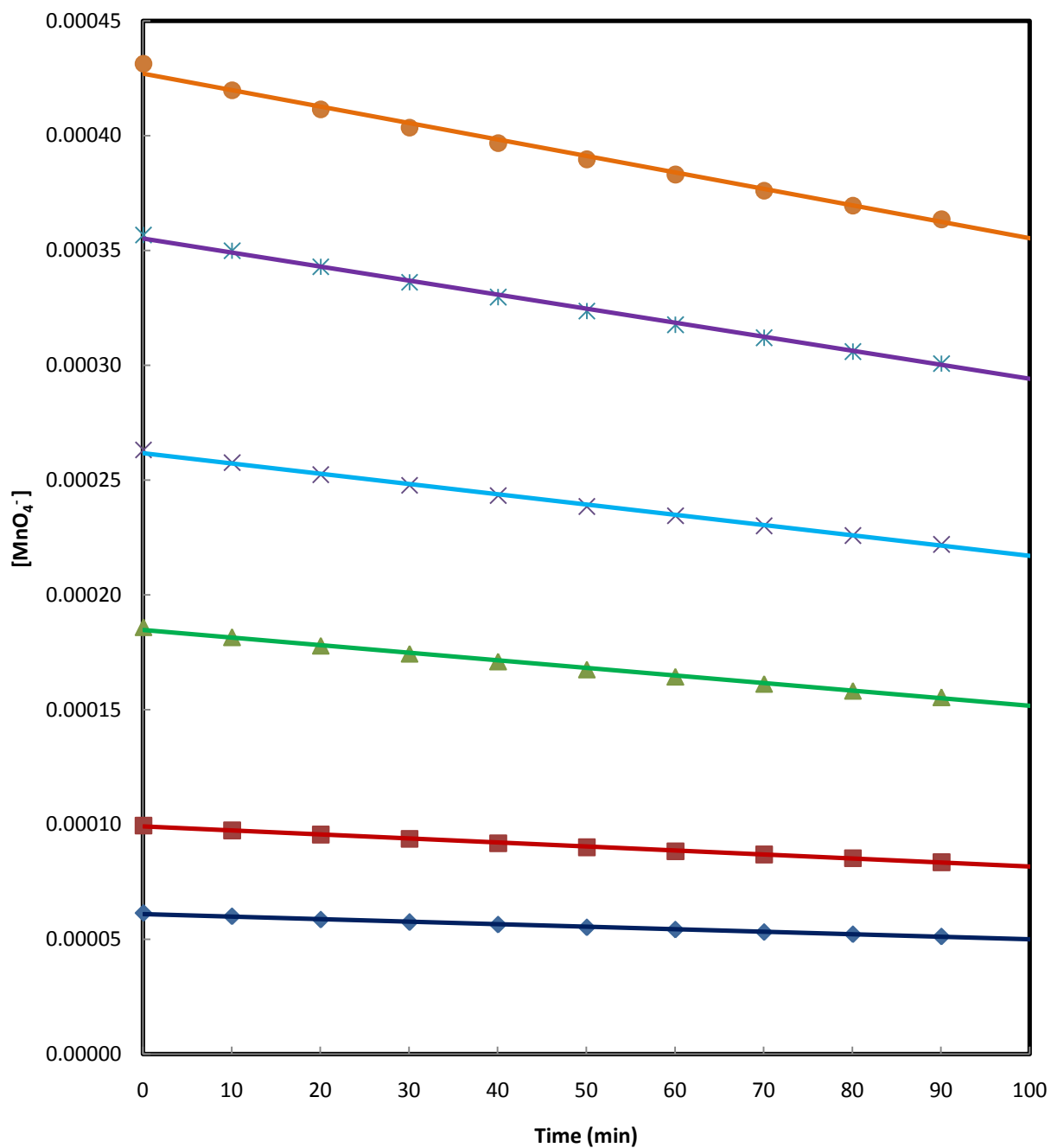


Table 7.1. Example run for the Pd (II) catalyzed oxidation of lomefloxacin by permanganate at $25 \pm 0.2^\circ\text{C}$ in acidic medium

[LMF] = $3.00 \times 10^{-3} \text{ mol dm}^{-3}$ [Permanganate] = $3.00 \times 10^{-4} \text{ mol dm}^{-3}$ [NaClO₄] = 0.4 mol dm^{-3}
 [H⁺] = $1.00 \times 10^{-3} \text{ mol dm}^{-3}$ [Pd²⁺] = $5.00 \times 10^{-8} \text{ mol dm}^{-3}$

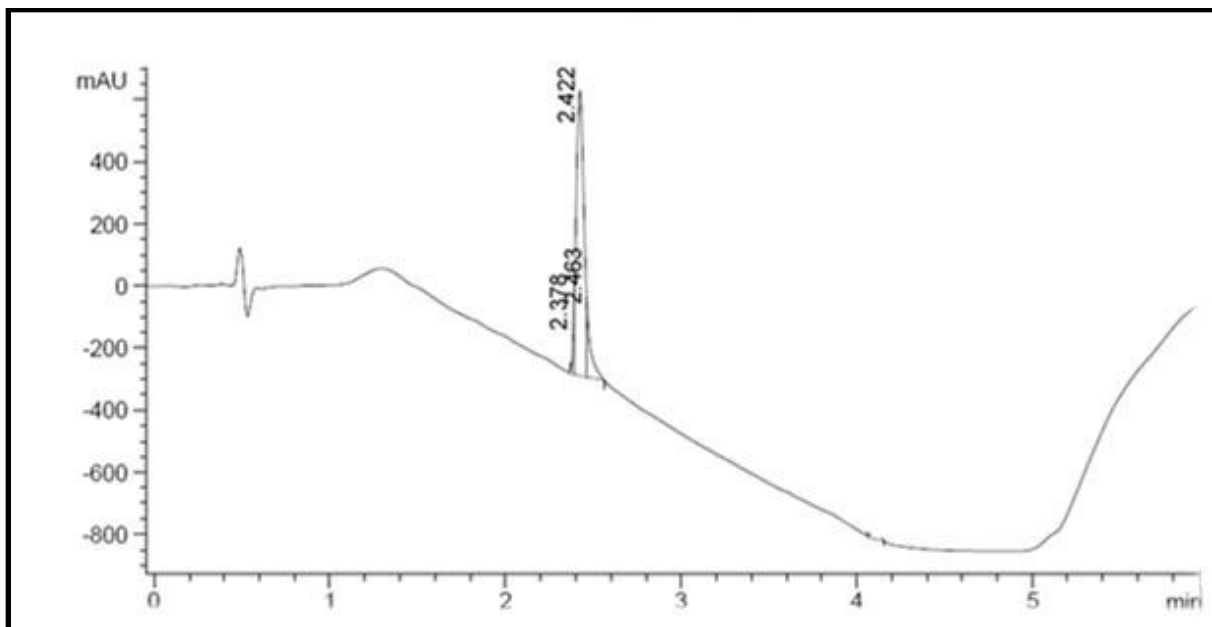
Time sec	Optical density (A) At 526 nm	[Permanganate] mol dm ⁻³
0.00	0.6227	2.73 E-04
5.00	0.4769	2.09 E-04
10.00	0.3889	1.70 E-04
15.00	0.3215	1.41 E-04
20.00	0.2662	1.17 E-04
25.00	0.2211	9.68E-05
30.00	0.1822	7.98E-05
35.00	0.1495	6.55E-05
40.00	0.1228	5.38E-05
45.00	0.0994	4.35E-05
50.00	0.0806	3.53E-05
55.00	0.0652	2.86E-05
60.00	0.0534	2.34E-05
65.00	0.0444	1.94E-05
70.00	0.0380	1.66E-05
75.00	0.0332	1.45E-05
80.00	0.0291	1.27E-05

Table 7.2. Influence of variation of [Permanganate], [LMF] and [Perchlorate] on the rate of oxidation of lomefloxacin in acidic medium. I = 0.5 mol dm⁻³ at 25 °C.

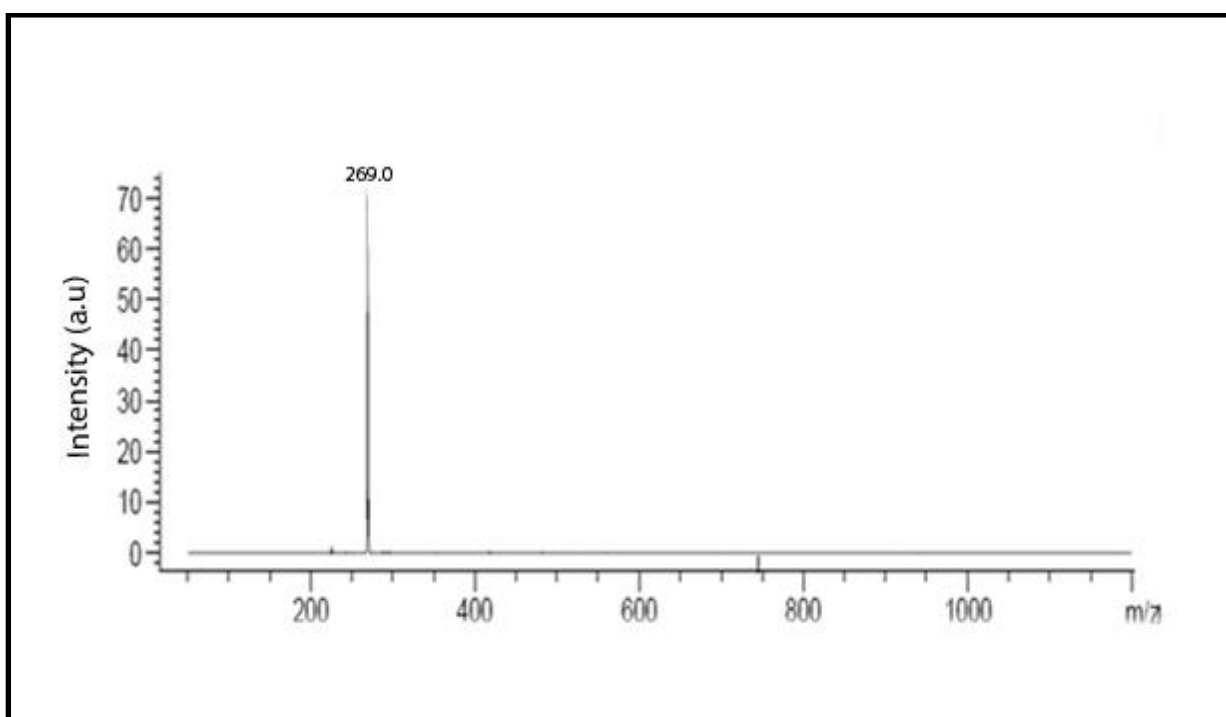
10 ⁴ [MnO ₄ ⁻] (mol dm ⁻³)	10 ³ [LMF] (mol dm ⁻³)	10 ¹ [HClO ₄] (mol dm ⁻³)	10 ¹ [NaClO ₄] (mol dm ⁻³)	10 ⁸ [Pd ²⁺] (mol dm ⁻³)	10 ³ k _U (s ⁻¹)	10 ³ k _T (s ⁻¹)	10 ³ k _C s ⁻¹
0.50	1.00	1.00	4.00	5.00	1.33	2.37	1.04
1.00	1.00	1.00	4.00	5.00	1.61	2.72	1.11
2.00	1.00	1.00	4.00	5.00	1.23	2.31	1.08
3.00	1.00	1.00	4.00	5.00	1.02	2.03	1.01
4.00	1.00	1.00	4.00	5.00	1.56	2.64	1.08
5.00	1.00	1.00	4.00	5.00	1.20	2.18	0.98
3.00	0.20	1.00	4.00	5.00	0.32	0.69	0.37
3.00	0.60	1.00	4.00	5.00	0.73	1.26	0.53
3.00	1.00	1.00	4.00	5.00	1.02	2.03	1.01
3.00	1.50	1.00	4.00	5.00	1.12	2.95	1.83
3.00	2.00	1.00	4.00	5.00	1.22	3.88	2.66
3.00	2.50	1.00	4.00	5.00	1.40	4.51	3.11
3.00	1.00	0.05	4.50	5.00	0.76	1.48	0.72
3.00	1.00	1.00	4.00	5.00	1.02	2.03	1.01
3.00	1.00	2.00	3.00	5.00	1.45	2.83	1.38
3.00	1.00	3.00	2.00	5.00	2.01	3.96	1.95
3.00	1.00	4.00	1.00	5.00	2.41	4.66	2.25
3.00	1.00	5.00	0.00	5.00	2.81	5.22	2.41

Fig. 7.4 LC/MS spectra of lomefloxacin oxidation products

(a) Total ion chromatogram (TIC)



(b) Mass spectrum of reaction product m/z 269.



7.3.2 Reaction order

During the experiment either of [permanganate]/ [LMF] / [Pd²⁺] is varied, whilst all other experimental conditions are kept constant. A graphical method was used to determine reaction order by plotting log k' _{obs} vs. log C the slope of gives the order of reaction.

7.3.3 Dependence on permanganate

To study the order of the permanganate, the [Permanganate] was varied from 5.00 x 10⁻⁵ mol dm⁻³ to 5.00 x 10⁻⁴ mol dm⁻³ with constant [LMF] = 3.00 x 10⁻³ mol dm⁻³, Pd (II) = 5.00 x 10⁻⁸ mol dm⁻³, I = 0.5 mol dm⁻³. The plot of log [Abs] v/s Time was linear as depicted in Fig. 7.3. With R² > 0.900 (un-catalyzed) and R² > 0.9516; k' _{obs} as depicted in Table 7.2. It shows the first order dependence w. r. t. Permanganate.

7.3.4 Dependence of [LMF]

To examine the rate of reaction of LMF. The [LMF] was varied from 2.00 × 10⁻⁴ mol dm⁻³ to 2.50 × 10⁻³ mol dm⁻³ with fixed [LMF], [Pd²⁺], and Ionic strength. It shows that increase in [LMF] increases the rate constant (k' _{obs}) as depicted in Table 7.2. The graph of log k' _{obs} vs. log [LMF] shows the fractional order i.e., 0.77 with R² > 0.985 for the catalyzed Pd²⁺ reaction and (0.57) (R² > 0.966) for uncatalyzed reaction, as depicted in Figures. 7.5 a, 7.5 b and 7.5 c. The order w. r. t. LMF reveals that there is complex formation between permanganate and LMF.

7.3.5 Dependence of [HClO₄]

To examine the dependence of [HClO₄] on the reaction rate, the [HClO₄] changed from 0.05 to 0.50 mol dm⁻³ by keeping other parameters constant. The k' _{obs} (rate constant) increases with increases the [HClO₄] as depicted in Table 7.2. The graph of log k' _{obs} vs. log [HClO₄] for Pd²⁺ catalyzed fractional order w. r. t. HClO₄ i.e., 0.52 (R² > 0.961) and for uncatalyzed reaction (0.53) (R² > 0.952) as depicted in Figures 7. 6 a and 7.6 b.

7.3.6 Dependence on [Pd (II)]

To examine the dependence of [Pd²⁺] catalyst on reaction rates, the catalyst concentration changed from 1.00 × 10⁻⁸ mol dm⁻³ to 1.00 × 10⁻⁷ mol dm⁻³, keeping other conditions constant. The rate constant increases with increase in [Pd²⁺]. Graph of log k' _{obs} vs. log [Pd²⁺] as depicted in Fig. 7.7. The order w. r. t. [Pd²⁺] was found to be fractional order i.e. 0.58 (R² > 0.963).

**Fig. 7.5. a) Order in [LMF] on the permanganate oxidation of lomefloxacin in aqueous acidic medium at 25 °C (Uncatalysed) [Permanganate] = $3.00 \times 10^{-4} \text{ mol dm}^{-3}$
[H⁺] = 0.10 mol dm^{-3} ; I = 0.50 mol dm^{-3} .**

(Conditions are stated in Table 7.2. (p.184))

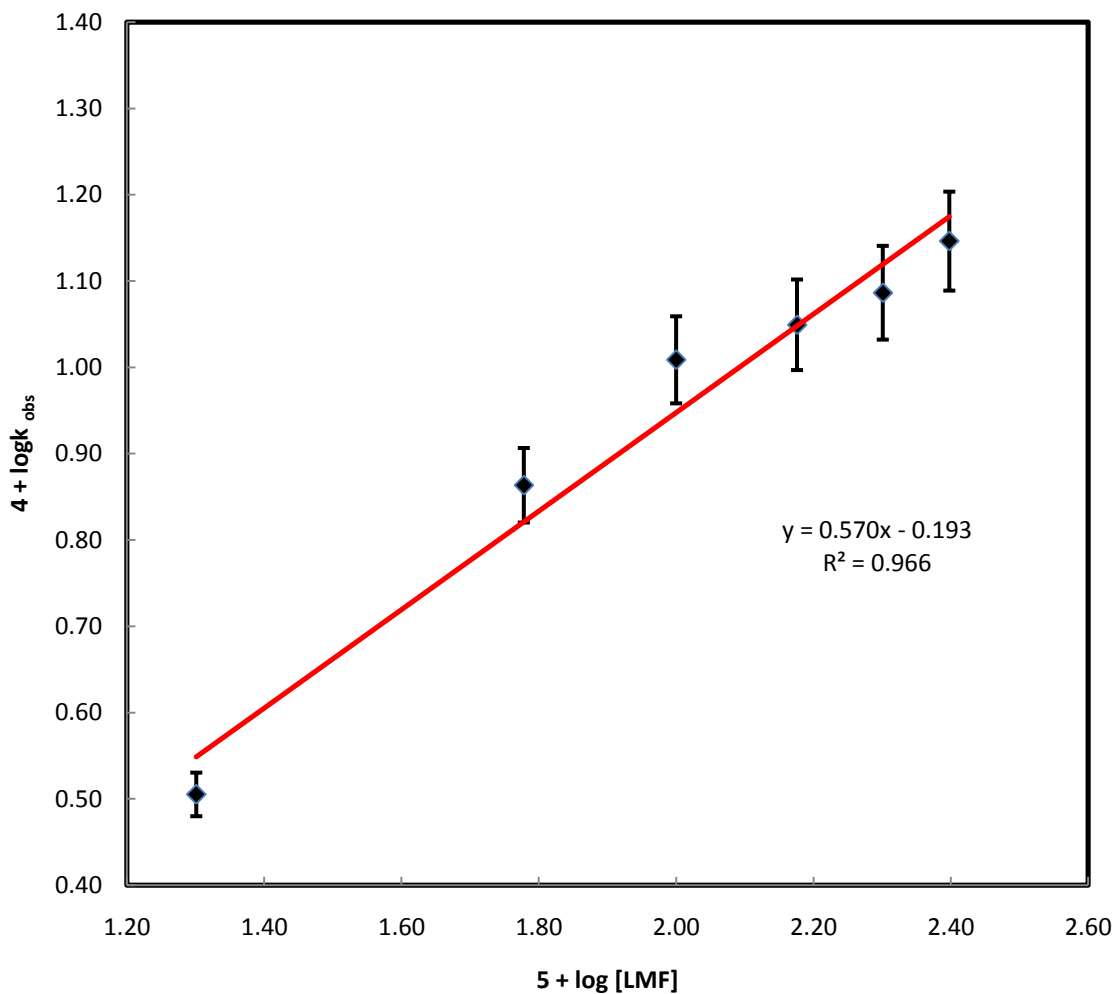


Fig. 7.5. b) Order in [LMF] on the permanganate oxidation of lomefloxacin in aqueous acidic medium at 25 °C (Pd²⁺ catalyzed). [Permanganate] = 3.00 x 10⁻⁴ mol dm⁻³ [H⁺] = 0.10 mol dm⁻³; I = 0.50 mol dm⁻³; [Pd²⁺] = 5.00 x 10⁻⁸ mol dm⁻³.

(Conditions are stated in Table 7.2. (p.184))

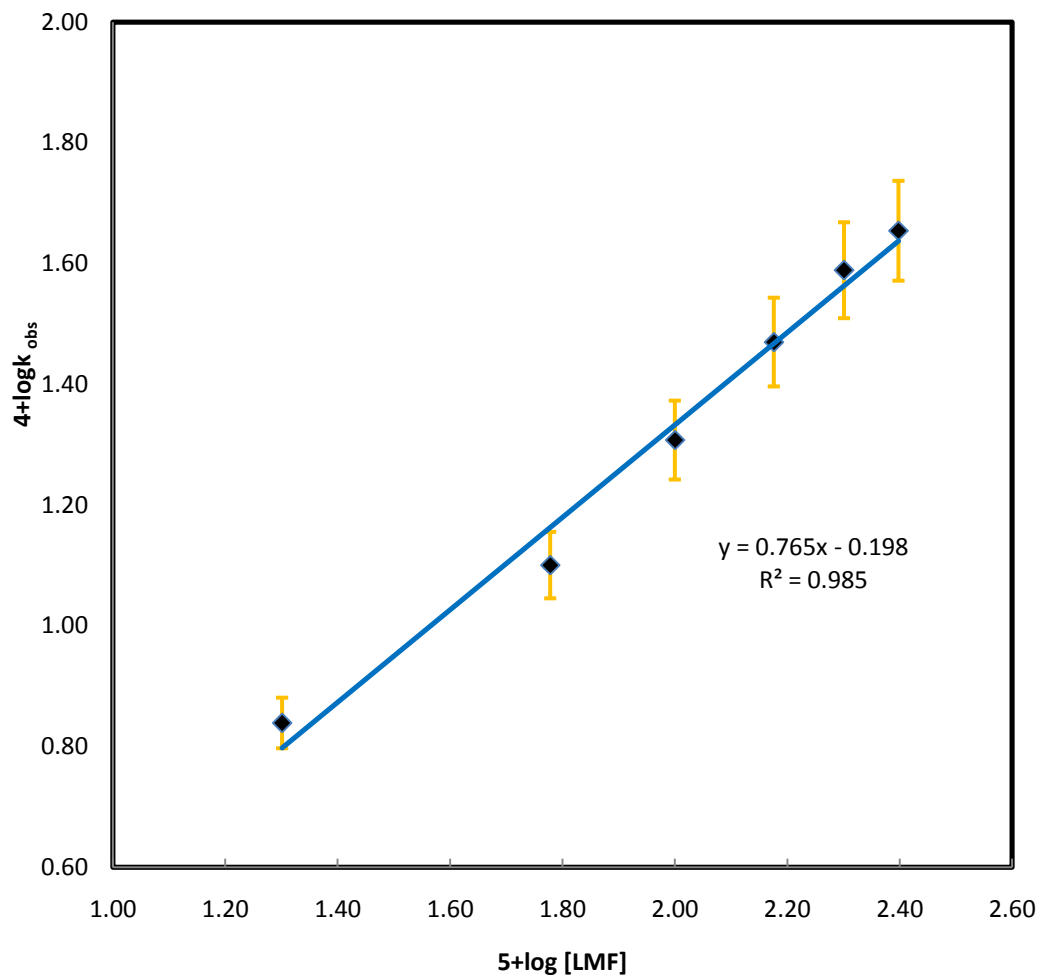


Fig. 7.5. c) The first order plots for rate constants catalyzed, uncatalysed and total reaction plot of k_{obs} Vs [LMF]

(Conditions are stated in Table 7.2. (p.184))

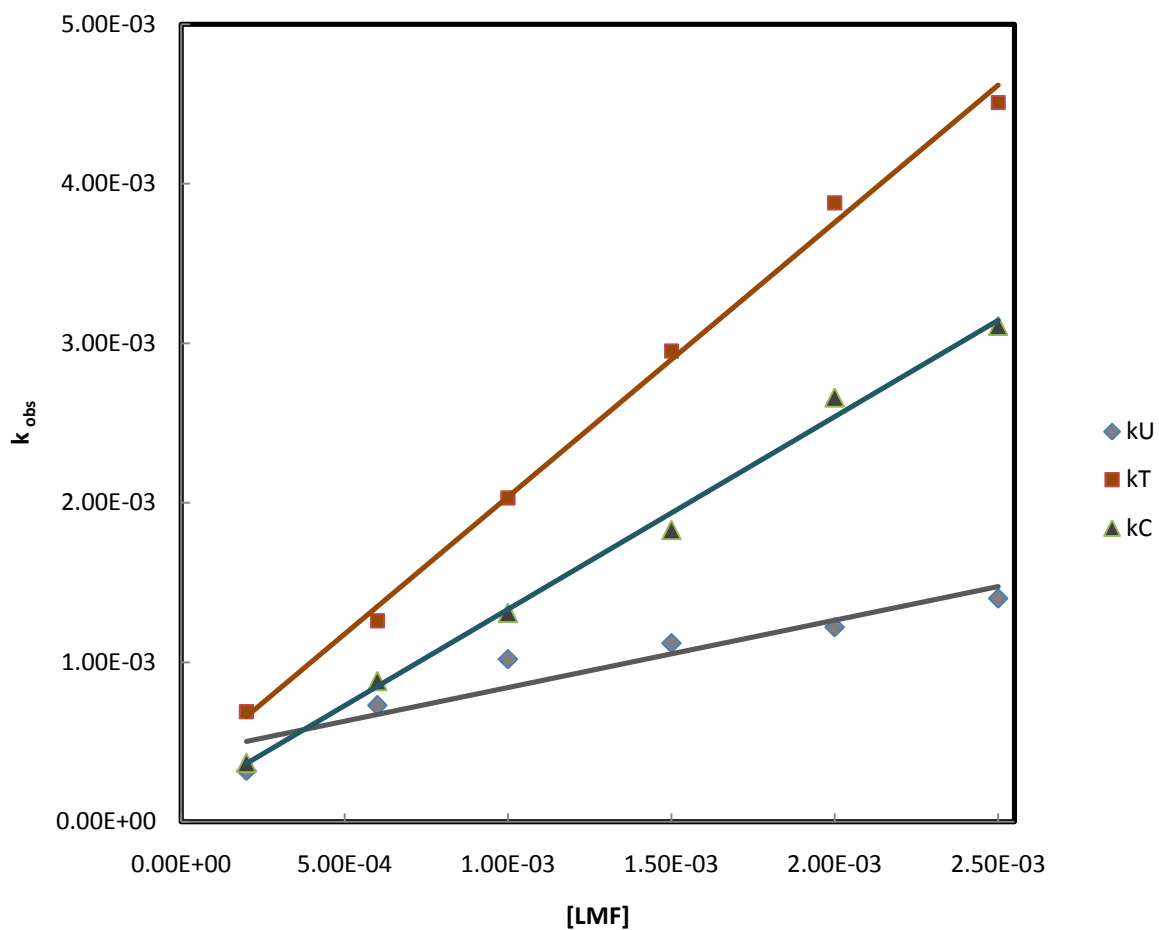


Fig. 7.6. a) Order in $[H^+]$ on the permanganate oxidation of lomefloxacin in aqueous acidic medium at 25 °C (Uncatalysed) $[LMF] = 1.00 \times 10^{-3}$; $[Permanganate] = 3.00 \times 10^{-4} \text{ mol dm}^{-3}$; $I = 0.50 \text{ mol dm}^{-3}$.

(Conditions are stated in Table 7.2. (p.184))

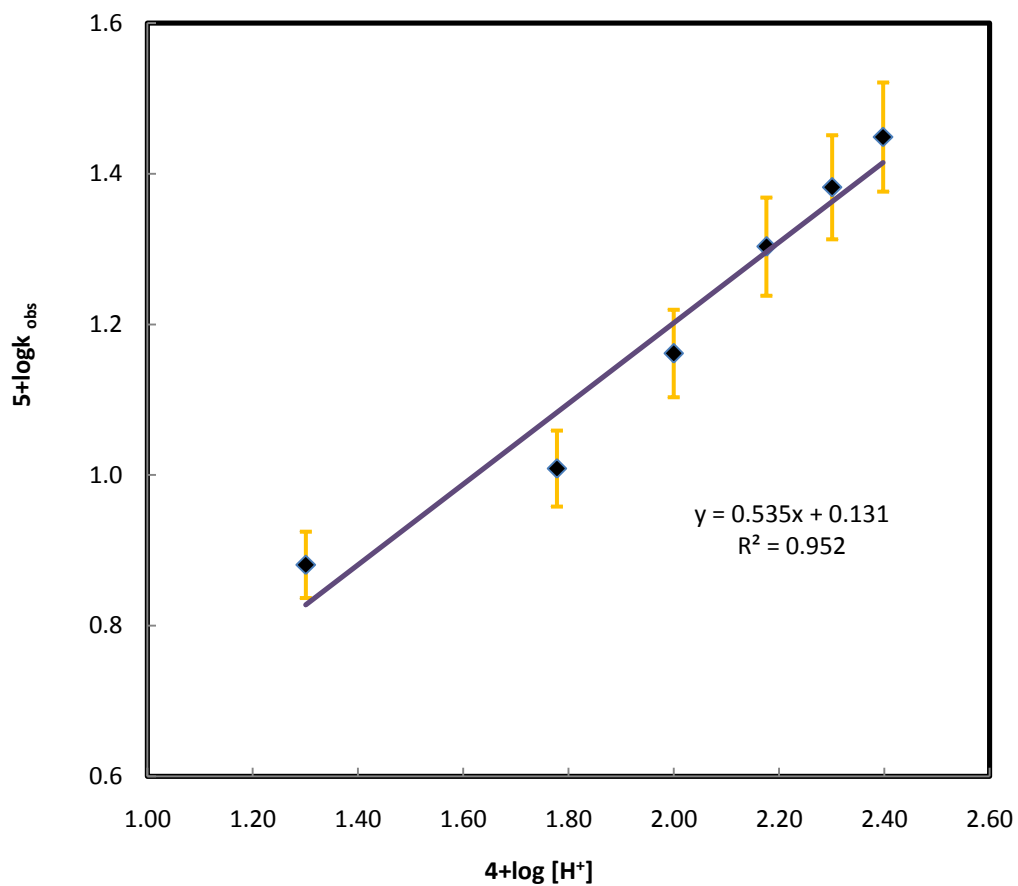


Fig. 7.6. b) Order in $[H^+]$ on the permanganate oxidation of lomefloxacin in aqueous acidic medium at 25 °C (Pd²⁺ catalyzed) $[LMF] = 1.00 \times 10^{-3}$; $[Permanganate] = 3.00 \times 10^{-4} \text{ mol dm}^{-3}$; $[pd^{+2}] = 5.00 \times 10^{-8}$; $I = 0.50 \text{ mol dm}^{-3}$.

(Conditions are stated in Table 7.2. (p.184))

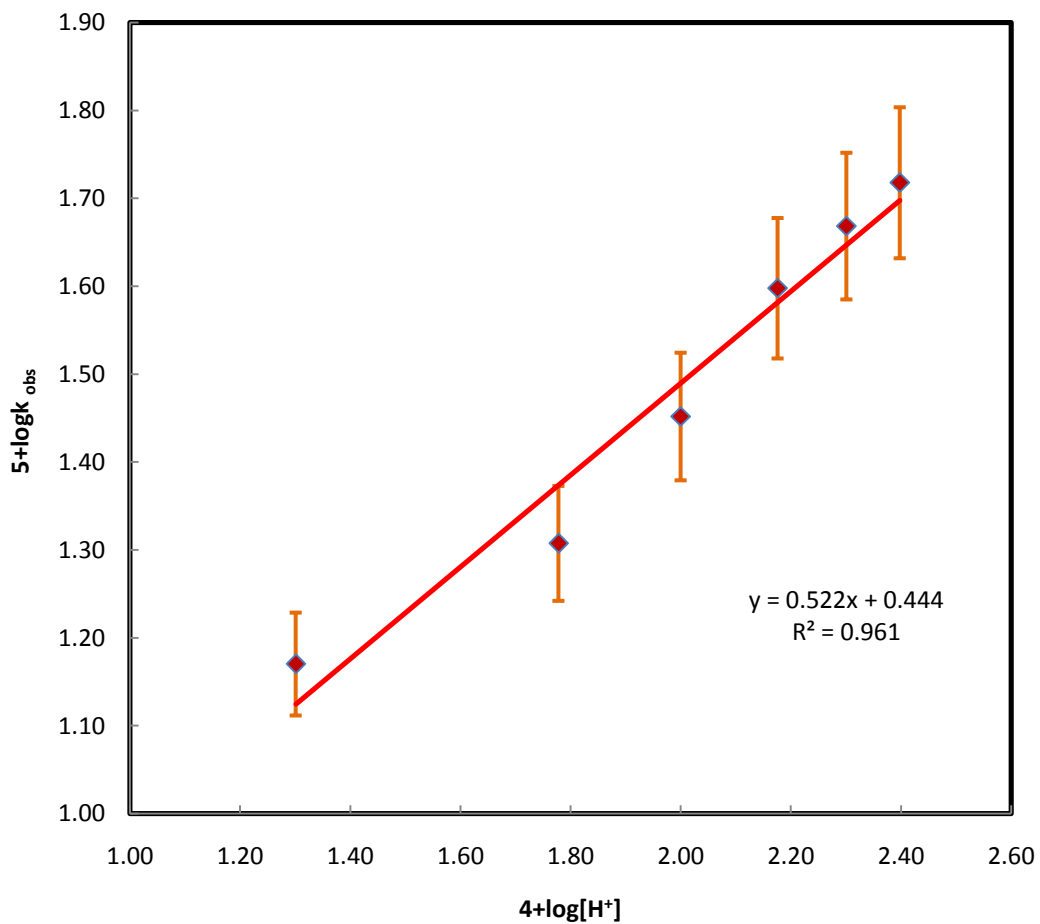
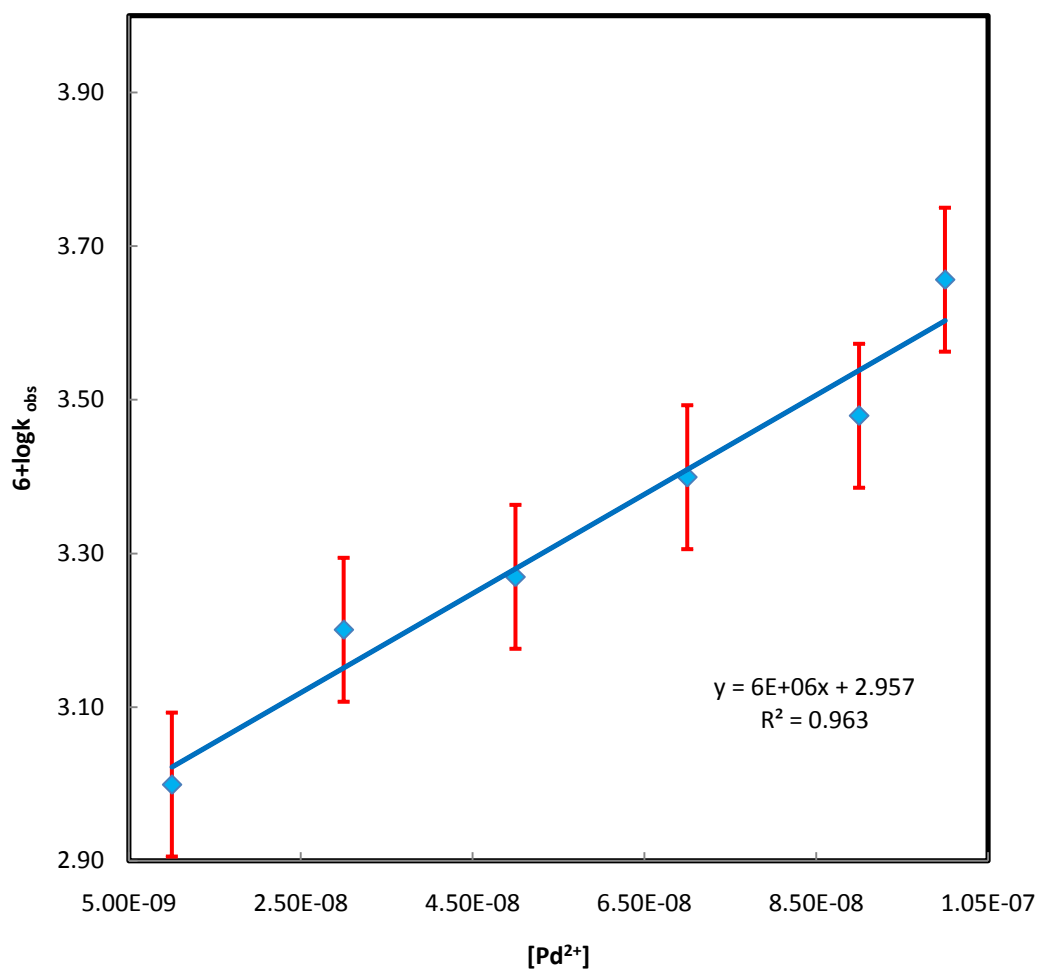


Fig. 7.7. Influence of variation of $[Pd^{2+}]$ on the rate of oxidation of lomefloxacin in acidic medium at 25 °C. [Permanganate] = 3.00×10^{-4} ; [LMF] = 1.00×10^{-3} ; $[H^+] = 0.10 \text{ mol dm}^{-3}$; $I = 0.50 \text{ mol dm}^{-3}$.

(Conditions are stated in Table 7.2. (p.184))



7.3.7 Dependence of ionic strength (I)

The rate of reaction of ionic strength was studied by changing $[\text{NaClO}_4]$ from 0.1 to 1.0 mol dm^{-3} with constant permanganate, LMF and Pd^{2+} catalyst concentration. It shows that, no effect of ionic strength on the rate of reaction. This implies the reaction taken place between two neutral species or neutral and charged species [26].

7.3.8 Dependence of relative permittivity (D)

The dependence of relative permittivity (D) was examined by altering the volume of T-butanol with H_2O in the ratio of 1:10. While other conditions are kept constant. The results reveal that insignificant influence on the reaction rate [27-28].

7.3.9 Dependence of initially added products

Permanganate-ion concentration altered from $0.50 \times 10^{-4} \text{ mol dm}^{-3}$ to $3.50 \times 10^{-4} \text{ mol dm}^{-3}$ at constant [LMF], $[\text{HClO}_4]$, $[\text{Pd}^{2+}]$ and ionic strength. The results were found that originally present permanganate ions have doesn't dependence on the k'_{obs} (rate constant). The Rate equation is given below.

$$\text{Rate} = \frac{-d[\text{MnO}_4^-]}{dt} = k[\text{MnO}_4^-]^1 [\text{LMF}]^{0.77} [\text{H}^+]^{0.53} [\text{Pd}^{2+}]^{0.58} \text{ --- (2)}$$

7.3.10 Polymerization study

The involvement of free radical in the reaction was investigated by adding acrylonitrile in an inert atmosphere for 8-hrs. Then, methanol is added to reaction mixture, there will be no development of white ppt this implies no appearance of free radicals [29].

7.3.11 Dependence of temperature

The rate of reaction of LMF was investigated at four different temperatures by altering [LMF] and fixed other conditions. It shows that the rate constants (k'_{obs}) were enhanced when temperature increase from 15°C to 45°C as appeared in Table 7.3.

By using Arrhenius equation, thermodynamic activation parameters are calculated. The activation energy (E_a) $48.66 \pm 2.0 \text{ kJ mol}^{-1}$ ($R^2 > 0.975$) un-catalyzed reaction and $39.75 \pm 2.0 \text{ kJ mol}^{-1}$ ($R^2 > 0.983$) with catalyst. The rate of reaction measured from the graph ($\log k'_{\text{obs}}$ Vs. $1/T$) as depicted in Figures 7.8 a and 7.8 b and ΔH^\ddagger , ΔS^\ddagger , ΔG^\ddagger activation parameters are given in Table 7.4.

Table 7.4. a) Effect of temperature b) Activation parameters for the uncatalyzed and Pd (II) catalyzed oxidation of LMF by permanganate in aqueous acidic medium

(a) Effect of temperature

Temperature (Kelvin)	$10^3 k_U s^{-1}$	$10^3 k_C s^{-1}$
288	0.84	1.61
298	1.23	3.44
308	2.92	5.10
318	5.35	8.01

(b) Activation parameters

Activation parameters	Values (Uncatalyzed)	Values Pd(II) catalyzed
E_a (kJ mol ⁻¹)	48.66 ± 2.00	39.75 ± 2.00
ΔH^\ddagger (kJ mol ⁻¹)	45.82 ± 2.00	37.23 ± 2.00
ΔS^\ddagger (JK ⁻¹ mol ⁻¹)	-145.06 ± 1.00	-168.14 ± 1.00
ΔG^\ddagger (kJ mol ⁻¹)	88.18 ± 1.00	86.25 ± 1.00

Fig. 7.8. a) Influence of variation of Temperature on the rate of oxidation of lomefloxacin in acidic medium (Uncatalyzed). [Permanganate]= $3.00 \times 10^{-4} \text{ mol dm}^{-3}$; $[\text{H}^+] = 0.10 \text{ mol dm}^{-3}$; $\text{I} = 0.50 \text{ mol dm}^{-3}$.

(Conditions are stated in Table 7.4. (p.194))

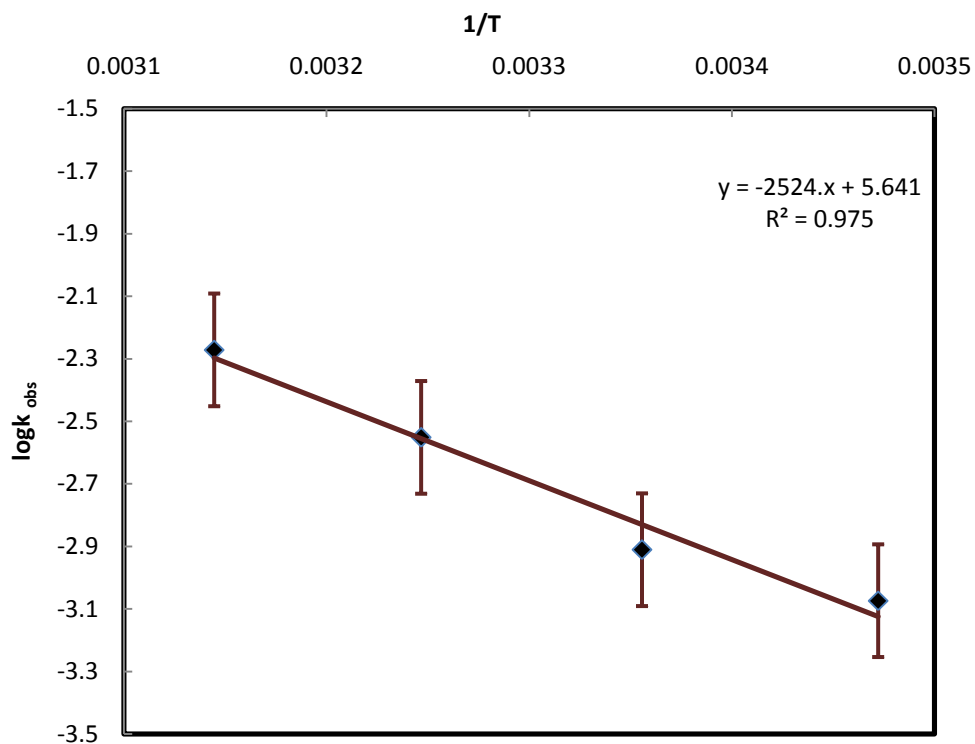
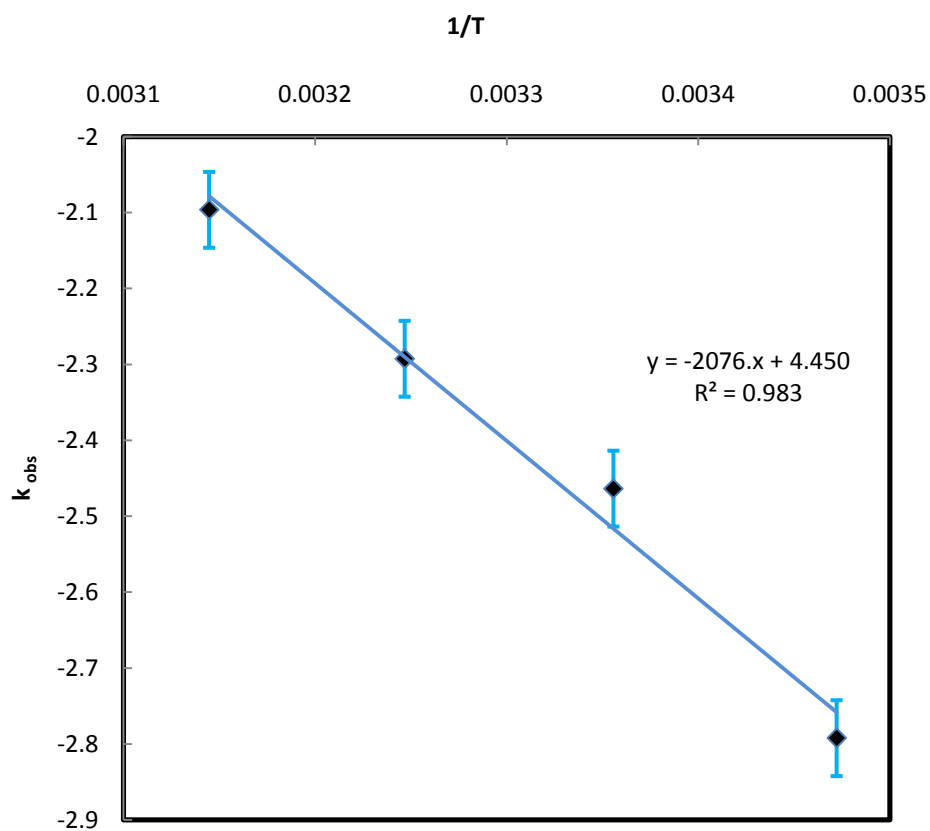


Fig. 7.8 b) Influence of variation of Temperature on the rate of oxidation of lomefloxacin in acidic medium (Pd²⁺ catalyzed). [Permanganate]= 3.00 x 10⁻⁴; [H⁺] = 0.10 mol dm⁻³; I = 0.50 mol dm⁻³; [pd²⁺] = 5.00 x 10⁻⁸ mol dm⁻³.

(Conditions are stated in Table 7.4. (p.194))



7.3.12 Catalytic activity

Moelwyn–Hughes stated that [13] in both the uncatalyzed and catalyzed reaction progresses parallel. Hence,

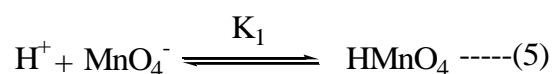
$$k_t = k_u + K_c [\text{Pd}^{2+}]^x \text{ --- (3)}$$

Where k_t , k_u , catalyzed and uncatalyzed rate constants. K_c , and x Michaels constant and order of the reaction relating to Pd^{2+} . Present investigation, x value < unity (0.58). Afterward, the results of K_c can be computed using the equation. The average value of K_c for the reaction was found to be 20 ± 2.0 .

$$K_c = \frac{[k_t - k_u]}{[\text{Pd(II)}]^x} = \frac{k_c}{[\text{Pd(II)}]^{0.58}} \quad \text{Where } k_t - k_u = k_c \text{ --- (4)}$$

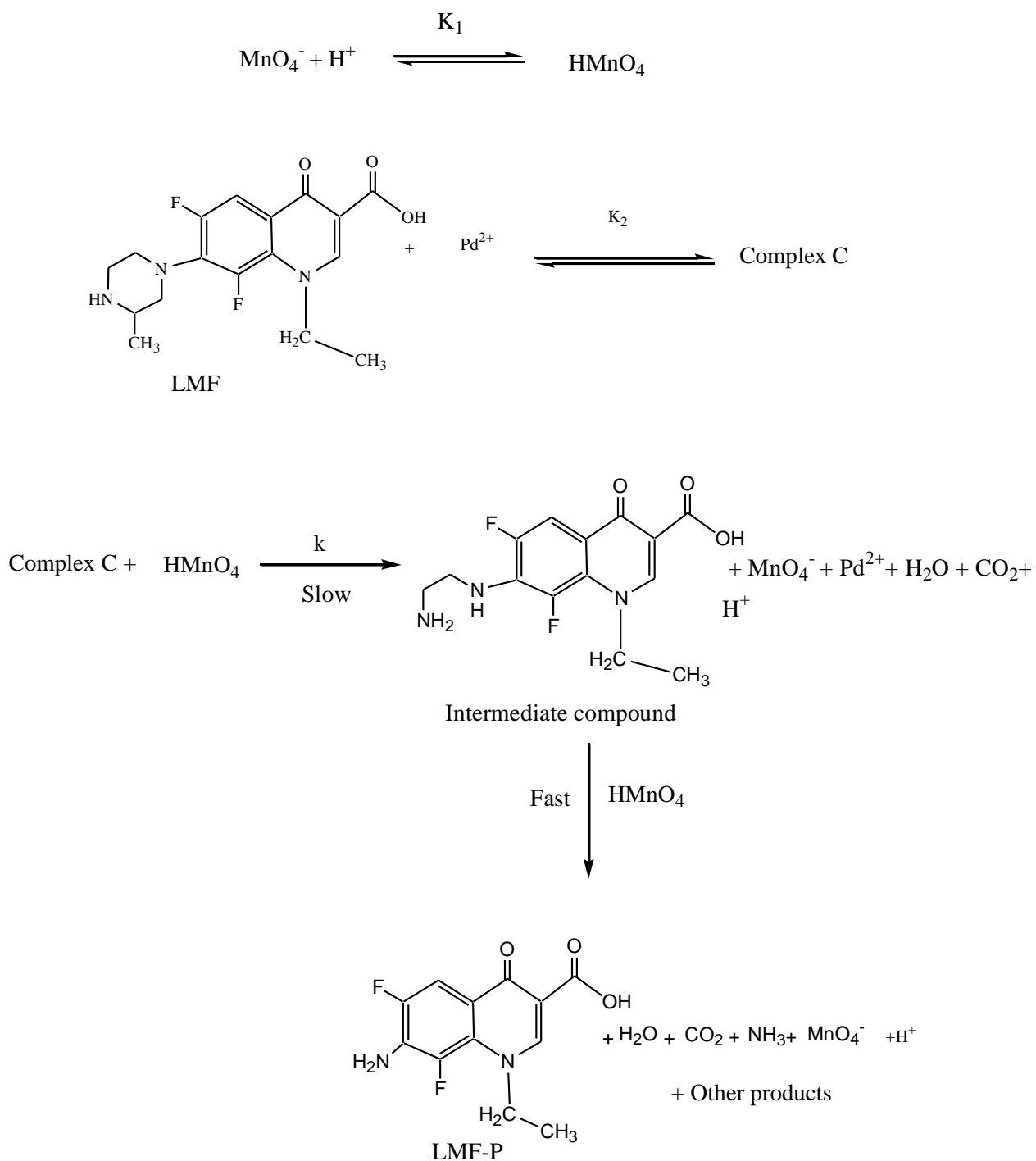
7.3.13 Proposed reaction pathway

The reactivity of permanganate species depends on the order of $[\text{H}^+]$ in the reaction media, the permanganate ions will form permanganic acid and the order w. r. t. $[\text{H}^+] < 1$. It is a most powerful oxidant than permanganate ion. At a very low pH when the rate of reaction attains limiting value then the protonation is almost complete, specifying that only the protonated form i.e. permanganic acid is active in the reaction mixture. The following equation shows the acid-permanganate equilibrium.



The significance of the equilibrium constant for protonation of permanganate, i.e. K_1 reported as $3.05 \times 10^2 \text{ dm}^3 \text{ mol}^{-1}$ at 25°C . The result of K_1 is also in concurrence with pKa result of HMnO_4 , as reported earlier [30,31]. In fast step, the intermediate product of the LMF decomposes to give the major product LMF-P and other by-products, Scheme 2.

Scheme 2 Proposed mechanism for Pd²⁺ catalyzed the oxidation of lomefloxacin by acidic Permanganate



The UV-Visible spectra of LMF (2.00×10^{-3} mol dm⁻³) and Pd²⁺ (1.00×10^{-8} mol dm⁻³) mixture reveal that hypsochromic shift (i.e., 287 - 283 nm) of 4 nm variation, which gives the spectroscopic confirmation for the complex formation. The complex formed between LMF

and catalyst depicted by Michaelis-Menten plot. Which also elucidate the order with respect to [LMF], < 1. The formation of a complex in line with previous work [32].

LC/MS spectrum was used to analyze the major reaction product (LMF-P). LMF containing piperazine moiety where the amino group is substituted. Hence the loss of 99 daltons in the mass of LMF and due to amino group substitution increases the mass of 16 daltons. Therefore, the resultant mass difference between LMF (M.W. =351) and LMF-P (M.W. =268). The oxidation LMF by MnO₂ in the presence TiO₂ photocatalysis was reported with same oxidation product [33-34]. The oxidation mechanism of LMF by heptavalent manganese in acidic media is given Scheme 2, the proposed that there is the complete exclusion of piperazine moiety by -NH₂ from LMF and ammonia transforms into ammonium ion (NH₄⁺ ions) by the oxidation. This result was formerly reported with ciprofloxacin and norfloxacin [17,35].

As stated in schemes 1 and 5:

$$\begin{aligned} \text{Rate} &= \frac{-d[\text{MnO}_4^-]}{dt} = k[\text{Complex C}][\text{HMnO}_4] \\ &= k K_1 K_2 [\text{LMF}_f] [\text{Pd}^{2+}]_f [\text{MnO}_4^-] [\text{H}^+] \quad \text{--- (1)} \end{aligned}$$

The Total concentration of [MnO₄⁻]_T is given by,

$$\begin{aligned} [\text{MnO}_4^-]_T &= [\text{MnO}_4^-]_f + [\text{HMnO}_4] + [\text{Complex C}] \\ &= [\text{MnO}_4^-]_f + K_1 [\text{H}^+] [\text{MnO}_4^-]_f + K_1 K_2 [\text{LMF}] [\text{H}^+] [\text{MnO}_4^-]_f \\ &= [\text{MnO}_4^-]_f \{1 + K_1 [\text{H}^+] + K_1 K_2 [\text{LMF}] [\text{H}^+]\} \end{aligned}$$

T and f refer to the total and free concentrations

$$[\text{MnO}_4^-]_f = \frac{[\text{MnO}_4^-]_T}{1 + K_1 [\text{H}^+] + K_1 K_2 [\text{H}^+] [\text{LMF}]} \quad \text{--- (2)}$$

Similarly,

$$\begin{aligned} [\text{H}^+]_T &= [\text{H}^+]_f + [\text{HMnO}_4] \\ &= [\text{H}^+]_f + K_1 [\text{H}^+] [\text{MnO}_4^-] \end{aligned}$$

In view of lower concentration of [H⁺] in the second term can be neglected. Therefore,

$$[\text{H}^+]_T = [\text{H}^+]_f \quad \text{--- (3)}$$

Similarly,

$$[\text{LMF}]_T = [\text{LMF}]_f \quad \text{--- (4)}$$

Now,

$$[\text{Pd}^{2+}]_T = [\text{Pd}^{2+}]_f + [\text{Complex C}]$$

$$\begin{aligned}
&= [\text{Pd}^{2+}]_f + K_2[\text{LMF}][\text{Pd}^{2+}]_f \\
&= [\text{Pd}^{2+}]_f \{1 + K_2[\text{LMF}]\} \\
[\text{Pd}^{2+}]_f &= \frac{[\text{Pd}^{2+}]_T}{1 + K_2[\text{LMF}]}
\end{aligned}$$

Since the value of second term in the denominator is less than unity, it can be neglected.

Hence, the second term $K_2[\text{LMF}]$ can be neglected

Substituting the values of $[\text{MnO}_4^-]_f, [\text{LMF}]_f, [\text{H}^+]_f$ and $[\text{Pd}^{2+}]_f$ into Equation 1 and omitting the subscripts, we get,

$$[\text{Pd}^{2+}]_f = [\text{Pd}^{2+}]_T \quad \text{----(5)}$$

$$\text{Rate} = \frac{-d[\text{MnO}_4^-]}{dt} = \frac{k K_1 K_2 [\text{MnO}_4^-] [\text{LMF}] [\text{H}^+] [\text{Pd}^{2+}]}{1 + K_1 [\text{H}^+] + K_1 K_2 [\text{H}^+] [\text{LMF}]} \quad \text{-----(6)}$$

$$\frac{\text{Rate}}{[\text{MnO}_4^-]} = k_C = k_T - k_U = \frac{k K_1 K_2 [\text{MnO}_4^-] [\text{LMF}] [\text{H}^+] [\text{Pd}^{2+}]}{1 + K_1 [\text{H}^+] + K_1 K_2 [\text{H}^+] [\text{LMF}]} \quad \text{-----(7)}$$

The rate law eqn.(7) can be rearranged into the following form

$$\frac{[\text{Pd}^{2+}]}{k_C} = \frac{1}{k K_1 K_2 [\text{LMF}] [\text{H}^+]} + \frac{1}{k K_2 [\text{LMF}]} + \frac{1}{k} \quad \text{-----(8)}$$

To compute the activation energy, Arrhenius equation was employed. The plot ($\log k_1$ Vs $1/T$) was a straight line. From the help of a graph, we calculated E_a , ΔS , ΔG and ΔH (values are shown in Table 7.4). The E_a is $39.75 \pm 2.00 \text{ kJ mol}^{-1}$ for oxidation in the presence of Pd^{2+} and $48.66 \pm 2.00 \text{ kJ mol}^{-1}$ for un-catalyzed, ΔS is $-168.14 \pm 1.00 \text{ J K}^{-1} \text{ mol}^{-1}$ for Pd^{2+} catalyzed oxidation and $-145.06 \pm 1.00 \text{ J K}^{-1} \text{ mol}^{-1}$ for un-catalyzed, ΔG is $86.25 \pm 1.00 \text{ kJ mol}^{-1}$ for Pd^{2+} catalyzed oxidation and $88.18 \pm 1.00 \text{ kJ mol}^{-1}$ for un-catalyzed and ΔH is $37.23 \pm 2.00 \text{ kJ mol}^{-1}$ for Pd^{2+} catalyzed oxidation and $45.82 \pm 2.00 \text{ kJ mol}^{-1}$ for un-catalyzed.

The above estimations of ΔS demonstrate that higher -ve value shows that the development of stable activated complex, while ΔG and ΔH value is + ve, indicating move state is very solvated than the reactants states. The activation parameter demonstrates that Pd^{2+} forms the activated complex mere easily with catalyst [19-20]. The calculated activation parameter for both the reactions (catalyzed and un-catalysed) reveals the impact of catalytic action in the reaction. In presence of Pd^{2+} the direction of reaction alters by decreasing the activation energy. The existence of a catalyst provides a sufficient energy to reactants pass through the intermediate state and gives products [21].

7.4 Conclusion

The HMnO_4 is most important reactive active species of permanganate. The oxidation of permanganate with LMF in an acidic medium was studied by spectrophotometric method. The role of hydrogen ion in the reaction is very important. The mechanism was illustrated with the reliable experimental investigation. The oxidation of LMF by Pd^{2+} catalyst with permanganate is employed. Experimentally determined k for the reaction suggests Pd^{2+} catalyzed reactions are about ten times greater than uncatalyzed reaction. It is evident that the role of the medium was a vital role for reaction. In acidic medium, the rate of reaction of oxidation of LMF by permanganate is a slow reaction, but in presence of Pd^{2+} catalyst, the rate of reaction is fast. The overall reaction order agreeable with the product. Based on observed results the reaction mechanism is proposed.

References

1. S. Caron, R.W. Dugger, S.G. Ruggeri, J.A. Ragan, D.H. Brown Ripin, "Large-scale oxidations in the pharmaceutical industry", *Chem. Rev.* Vol. 106, 2006, pp. 2943-2989.
2. A. Shaabani, F. Tavasoli-Rad, D.G. Lee, "Potassium Permanganate Oxidation of Compounds", *Synth. Commun.* Vol. 35, 2005, pp. 571-580.
3. D.G. Lee, E.J. Lee, K.C. Brown, *Phase Transfer Catalysis, New Chemistry, Catalysis and Applications*, ACS Symposium Series, American Chemical Society, Washington, DC., Vol. 326, 1987, pp. 82-95.
4. A.J. Fatiadi, *The Classical Permanganate Ion: Still a Novel Oxidant in Organic Chemistry*, *Synth.* Vol. 106, 1987, pp. 85-127.
5. S.M. Desai, N.N. Halligudi, S.K. Mavalangi, S.T. Nandibewoor, "Oxidation of (+)-(R)-Pantothenic Acid by Aqueous Alkaline Potassium Permanganate: A Kinetic and Mechanistic Approach", *Z. Phys. Chem.* Vol. 216, 2002, pp. 803-814.
6. K.A. Thabaj, S.D. Kulkarni, S.A. Chimatadar, S.T. Nandibewoor, "Oxidative transformation of ciprofloxacin by alkaline permanganate- A kinetic and mechanistic study", *Polyhedron.* Vol. 26, 2007, pp. 4877-4885.
7. D.C. Bilehal, R.M. Kulkarni, S.T. Nandibewoor, "Comparative study of the chromium (III) catalyzed oxidation of l-leucine and l-isoleucine by alkaline permanganate: A kinetic and mechanistic approach", *J. Mol. Cat.* Vol. 232, 2005, pp. 21 -28.
8. R.M. Kulkarni, D.C. Bilehal, S.T. Nandibewoor, "Deamination and decarboxylation in the chromium(III)-catalysed oxidation of L-valine by alkaline permanganate and analysis of chromium(III) in microscopic amounts by a kinetic method", *Tran. Met. Chem.* Vol. 28, 2003, pp. 199-208.
9. M.L. Johnson, L. Berger, L. Phillips, R. Speare, "Fungicidal effects of chemical disinfectants, UV light, desiccation and heat on the amphibian chytrid *Batrachochytrium dendrobatidis*", *Diseases aqua. Organ.* Vol. 57, 2003, pp. 255-260.
10. H. Yuan, X. Zhou, Y.L. Zhang, "Degradation of Acid Pharmaceuticals in the UV/H₂O₂ Process: Effects of Humic Acid and Inorganic Salts", *Clean- Soil Air Water.* Vol. 41, 2013, pp. 43-50.
11. M.L. Johnson, L. Berger, L. Phillips, R. Speare, "Fungicidal effects of chemical disinfectants, UV light, desiccation and heat on the amphibian chytrid, *Batrachochytrium dendrobatidis*", *Diseases aqua. Organ.* Vol. 57, 2003, pp. 255-260.

12. H. Yuan, X. Zhou, Y.L. Zhang, "Degradation of Acid Pharmaceuticals in the UV/H₂O₂ Process: Effects of Humic Acid and Inorganic Salts", *Clean- Soil Air Water*. Vol. 41, 2013, pp. 43-50.
13. M.S. Gudaganatti, M.S. Hanagadakar, R.M. Kulkarni, R.S. Malladi, R.K. Nagarale, "Transformation of levofloxacin during water chlorination process: kinetics and pathways", *Prog. React. Kinet. Mech.* Vol. 37, 2012, pp. 366–382.
14. B. Halling-Sorensen, S.N. Nielsen, P.F. Lanzky, F. Ingerslev, H.C. HoltenLutzof, S.E. Jorgensen, "Occurrence, fate and effects of pharmaceutical substances in the environment-a review", *Chemosphere*. Vol. 36, 1998, pp. 357-393.
15. K.A. Thabaj, S.A. Chimatadar, S.T. Nandibewoor, "Mechanistic study of oxidation of palladium (II) by cerium (IV) in aqueous acid", *Transition Met. Chem.* Vol. 31, 2006, pp. 186-193.
16. S.A. Chimatadar, S.B. Koujalagi, S.T. Nandibewoor, "Kinetics and mechanism of palladium (II) catalyzed chromium (VI) oxidation of mercury (I) in aqueous sulphuric acid", *Transition. Met. Chem.* Vol. 26, 2001, pp. 662-667.
17. A.K. Singh, R. Negi, B. Jain, Y. Katre, S.P. Singh, V.K. Sharma, "Pd(II) Catalyzed degradation of paracetamol by Chloramine-T in Acidic and Alkaline Media", *I.E.C. Res.* Vol. 50, 2011, pp. 8407-8419.
18. G.P. Tikhonova, S. Bovkovets, *Russ. J. Inorg. Chem.*, 23, 1687 ,(1978); S.M. Tuwar, S.T. Nandibewoor, *Indian J Chem.* Vol. 29A, 1990, 235-239.
19. S. Ashish, S.P. Singh, A.K. Singh, B. Singh, "Mechanistic study of palladium (II) catalyzed oxidation of crotonic acid by periodates in aqueous perchloric acid medium", *J. Mol. Catal. A.* Vol. 266, 2007, pp. 226–232.
20. M.K. Ghosh, S.K. Rajput, "Kinetics and Mechanism of Palladium (II) Catalyzed Oxidation of D-(+) Galactose by Cerium(IV) in Aqueous Acidic Medium, *American Chemical Science* in presence of chlorocomplex of Pd(II) as homogenous catalyst: A kinetic and mechanistic study", *Open Catal. J.* Vol. 2, 2009, pp. 12–20.
21. M.K. Ghosh, S.K. Rajput, "Kinetics and Mechanism of Palladium (II) Catalyzed Oxidation of D-(+) Galactose by Cerium(IV) in Aqueous Acidic Medium", *American Chemical Science Journal.* Vol. 4(3), 2014, pp. 384-400.

22. V.C. Seregar, C.V. Hiremath, S.T. Nandibewoor, "Palladium(II) catalysed oxidation of L-proline by heptavalent manganese in aqueous alkaline medium: a free radical intervention and decarboxylation", *Transition. Met. Chem.*, Vol. 31, 2006, pp. 541–548.
23. G.H. Jeffery, J. Bassett, J. Mendham, R.C. Denny, *Vogel's Textbook of Quantitative Chemical Analysis*, 5th ed., ELBS, Longman, Essex, UK, 1996, pp. 370-377.
24. F. Feigl, *Spot Tests in Organic Analysis*, 6th Ed., Elsevier, New York, NY, (1960), pp.195.
25. A.K. Das, M. Das, "Kinetics and mechanism of ruthenium (III) catalyzed oxidation of formic acid by cerium (IV) in aqueous sulfuric acid media", *J. Chem. Soc. Dalton Trans.* Vol. 4, 1994, pp. 589-593.
26. K.J. Laidler, *Chemical Kinetics*, vol. 183, 3rd Ed., Pearson Education, Delhi, 2004, p.198-199.
27. A.K. Kini, S.A. Farokhi, S.T. Nandibewoor, "A comparative study of ruthenium(III) catalysed oxidation of L-leucine and L-isoleucine by alkaline permanganate", *A kinetic and mechanistic approach Trans. Metal. Chem.*, Vol. 27, 2002, pp. 532–540.
28. E.S. Amis, "Solvent Effects on Reaction Rates and Mechanisms, Academic Press, New York, NY. 1966.
29. S. Bhattacharya, P. Benerjee, "Kinetic Studies on the Electron Transfer between Azide and Nickel (IV) Oxime Imine Complexes in Aqueous Solution", *Bull. Chem. Soc.* Vol. 69 1996, pp. 3475-3482.
30. G.A. Hiremath, P.L. Timmanagoudar, S.T. Nandibewoor, "Kinetics and oxidation of thallium (I) by permanganate in aqueous hydrochloric acid medium using the stopped-flow technique", *Trans Metal Chem*, Vol. 21 1996, pp. 560-572.
31. N. Bailey, A. Carrington, K.A.K. Lotto, M.C.R. Syammon, *J Chem Soc.* 1960, 290
32. M.D. Meti, K.S. Byadagi, S.T. Nandibewoor, S.A. Chimatadar, "Mechanistic studies of un-catalyzed and ruthenium(III)-catalyzed oxidation of the antibiotic drug chloramphenicol by hexacyanoferrate(III) in aqueous alkaline medium: a comparative kinetic study", *Monatsh Chem.*, Vol. 145, 2014, 1561–1573.
33. H. Zhang, C.H. Huang, "Oxidative Transformation of Fluoroquinolone Antibacterial Agents and Structurally Related Amines by Manganese Oxide", *Environ. Sci. Technol.* Vol. 39, 2005, pp. 4474-4483.

34. A. Taicheng, Y. Hai, S. Weihua, L. Guiying, L. Haiying, W.J. Cooper, "Mechanistic Considerations for the Advanced Oxidation Treatment of Fluoroquinolone Pharmaceutical Compounds using TiO₂ Heterogeneous Catalysis", *J. Phys. Chem. A.*, Vol. 114 2010, pp. 2569-2575.
35. P.N. Naik, S.A. Chimatadar, S.T. Nandibewoor, "Kinetics and Oxidation of Fluoroquinoline Antibacterial Agent, Norfloxacin, by Alkaline Permanganate: A Mechanistic Study", *Ind. Eng. Chem. Res.* Vol. 48 2009, pp. 2548-2555.




Ag-TiO₂ nanoparticles for photocatalytic degradation of lomefloxacin

Raviraj M. Kulkarni, Ramesh S. Malladi, Manjunath S. Hanagadakar, Mrityunjay R. Doddamani & Udaya K. Bhat

To cite this article: Raviraj M. Kulkarni, Ramesh S. Malladi, Manjunath S. Hanagadakar, Mrityunjay R. Doddamani & Udaya K. Bhat (2016) Ag-TiO₂ nanoparticles for photocatalytic degradation of lomefloxacin, Desalination and Water Treatment, 57:34, 16111-16118, DOI: [10.1080/19443994.2015.1076352](https://doi.org/10.1080/19443994.2015.1076352)

To link to this article: <http://dx.doi.org/10.1080/19443994.2015.1076352>

 Published online: 06 Aug 2015.

 Submit your article to this journal [↗](#)

 Article views: 74

 View related articles [↗](#)

 View Crossmark data [↗](#)

 Citing articles: 1 View citing articles [↗](#)



Ag-TiO₂ nanoparticles for photocatalytic degradation of lomefloxacin

Raviraj M. Kulkarni^{a,*}, Ramesh S. Malladi^a, Manjunath S. Hanagadakar^a,
Mrityunjay R. Doddamani^b, Udaya K. Bhat^c

^aDepartment of Chemistry, KLS Gogte Institute of Technology, (Affiliated to Visvesvaraya Technological University), Belagavi 590008, Karnataka, India, Tel. +91 8312498511; Fax: +91 8312441909; emails: ravirajmk@git.edu (R.M. Kulkarni), rameshmalladi7@gmail.com (R.S. Malladi), manju.hanagadakar@gmail.com (M.S. Hanagadakar)

^bMechanical Engineering, National Institute of Technology Karnataka, Surathkal, India, Tel. +91 8242473678; email: Mrd1978@rediffmail.com

^cMetallurgical and Materials Engineering, National Institute of Technology Karnataka, Surathkal, India, Tel. +91 8242474000; email: udayabhatk@gmail.com

Received 5 January 2015; Accepted 21 July 2015

ABSTRACT

The photocatalytic activity of silver-doped TiO₂ (Ag-TiO₂) nanoparticles was studied by photocatalytic degradation of lomefloxacin (LMF) using a photoreactor with a mercury lamp (PHILIPS, TUV 8 W T5, E_{max} = 254 nm). The 1 and 2% silver-doped TiO₂ nanoparticles were synthesized by liquid impregnation (LI) method. The resulting nanoparticles were characterized by surface analytical methods such as X-ray diffraction (XRD), scanning electron microscope (SEM), energy dispersive X-ray analysis and transmission electron microscope (TEM). The study shows 2% Ag-TiO₂ nanoparticles exhibited better results (95% degradation) in 1 h for the degradation of lomeofloxacin compared to 1% Ag-TiO₂ and pure TiO₂. XRD analysis indicated that the crystallite size of TiO₂ was 17.00 nm, while the crystallite size of 1% Ag-TiO₂ and 2% Ag-TiO₂ was 13.07 to 14.17 nm. TEM images show the particle size of Ag-TiO₂ nanoparticles were in the range 40–45 nm in length and 10–15 nm in breadth. Pseudo-first-order rate constants were found to decrease with increase in pH. The effect of UV intensity, catalyst dosage and initial concentration of LMF on the degradation rate were also studied and elaborately discussed.

Keywords: Titanium dioxide; Liquid impregnation; Photocatalysis; Lomeofloxacin; AOP

1. Introduction

Advanced oxidation processes (AOPs) are techniques designed for the degradation of harmful organic contaminants which are resistant to conventional and biological treatment methods. AOPs depend on the generation of highly reactive radical species such as OH· that decompose a number of

organic contaminants without being selective [1–3] using chemical or light energy. The AOPs normally involve a semiconductor photocatalyst activated by UV or visible light resulting in partial or complete mineralization of the organic molecules [4,5].

There are several studies related to the use of TiO₂ in the photomineralization of pharmaceutical compounds [6,7].

Titanium dioxide (TiO₂), a metal oxide semiconductor has been found to be one of the most

*Corresponding author.

effective photocatalysts due to its chemical structure, biocompatibility, high efficiency low cost and optical and electrical properties [8,9]. TiO_2 has a band gap of 3.2 eV that allows UV light to excite the valance electrons into the conduction band leaving holes in the valance band [10]. The high rate of electron–hole recombination in TiO_2 , however, limits the efficiency of the photocatalyst which can be prevented, to some extent, by doping with noble metals such as silver, gold, platinum [11]. The most important advantage of the doping of silver on TiO_2 is improving the charge separation efficiency of the TiO_2 . Moreover, the antibacterial action of silver, particularly in the colloidal form, is also well reported [12].

Lomefloxacin (LMF) is an antibacterial agent which belongs to the fluoroquinolone family, it is used to treat various bacterial infections, such as urinary tract, bronchitis etc. Now-a-days, antibacterial agents have been used in large amount for last few decades; these agents enter in to the environment through domestic sewage due to partial metabolism in the human body [13]. The chemical structure of LMF is given in Fig. 1.

However, no significant efforts have been made to investigate the detailed degradation kinetics, which is essential for the application point of view. Hence, we have carried out a detailed study on the photocatalytic degradation of LMF by Ag- TiO_2 nanoparticles in aqueous medium examining various reaction parameters such as pH, substrate and catalyst concentration, intensity of UV light. In the present work, TiO_2 nanoparticles were doped with silver using liquid impregnation (LI) technique. These nanoparticles were characterized by the techniques such as X-ray diffraction (XRD), scanning electron microscope (SEM), energy dispersive X-ray analysis (EDX) and transmission electron microscope (TEM).

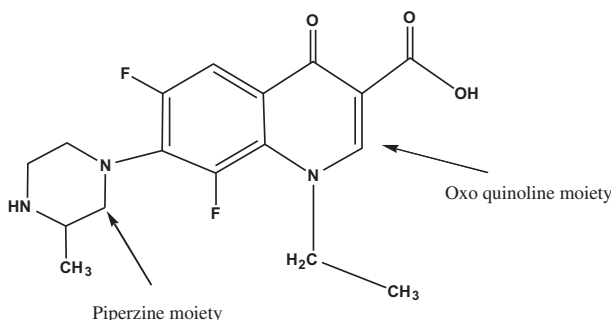


Fig. 1. Chemical structure of lomefloxacin.

2. Experimental

2.1. Materials and methods

A stock solution of LMF (Gift sample from Dr Reddy's laboratories) was prepared by dissolving appropriate amount of sample in double distilled water. The TiO_2 sample was purchased from Sisco Research Pvt. Ltd, Mumbai 93, India (TiO_2 -Anatase). AgNO_3 purchased from HIMEDIA. The analytical grade chemicals were used to prepare acetate (pH 4–5), phosphate (pH 6.0–8.5) and borate (pH 9) buffers.

2.1.1. Instruments used

- (1) For kinetic measurements, a CARY 50 Bio UV–vis spectrophotometer (Varian BV, The Netherlands) with temperature controller and HPLC system (Agilent 1100 series, USA) were used.
- (2) For degradation study, a photoreactor with mercury lamp (PHILIPS, TUV 8 W T5, $E_{\text{max}} = 254 \text{ nm}$) was used. The typical light intensity illuminated on the surface of reaction mixture was 4 mW/cm^2 .
- (3) For UV light intensity measurements, an optical power metre (Newport 2936-C) and for pH measurements, Elico pH metre models LI 120 were used.
- (4) For characterization of nanoparticles, a Siemens X-ray diffractometer (Cu source) (XRD) AXS D5005 was used to identify the particle size of the doped TiO_2 . The surface morphologies were examined using a scanning electron microscope (SEM) JEOL JSM 6360.
- (5) The topography and particle size of Ag- TiO_2 was measured using JEOL JEM-2010 TEM.

2.2. Photo catalyst preparation

2.2.1. LI method

500 mg of TiO_2 was added to 100 ml deionized water in a 500 ml Pyrex beaker. For silver doping 1 and 2% (molar ratio) of AgNO_3 was also added to the suspension. The resulting slurry was thoroughly mixed by vigorous stirring and allowed to settle at room temperature overnight. The liquid so obtained was dried in an oven at 100°C for 12 h to get rid of any remaining moisture. The solid material resulting from this step was calcined at 500°C for 3 h in a muffle furnace. This resulted in fine particles of Ag- TiO_2 nanoparticles [14,15].

2.3. The photocatalysis process

To investigate the photocatalytic degradation, a known concentration of LMF solution and buffer was taken in a Pyrex beaker. A dose of 100 mg/l 2% Ag-TiO₂ nanoparticles was added. Then, it was transferred in to the photoreactor and then kept under 8 W UV lamps (Philips) with a wavelength peak at 254 nm and of 4 mW/cm² intensity with continuous stirring. After every 15 min interval, the solution was taken out and centrifuged at 2,000 rpm for 5 min. The degradation of centrifuged solution was measured at 287 nm ($\epsilon = 27,209 \text{ L M}^{-1} \text{ cm}^{-1}$) using visible spectrophotometer (a CARY 50 Bio UV-vis spectrophotometer (Varian BV, The Netherlands)) and the degree of mineralization was studied.

3. Results and discussion

3.1. Comparison of different photocatalysts

The rate of photo catalytic degradation of LMF with UV, UV/TiO₂, UV/(1%) Ag-TiO₂ and UV/(2%) Ag-TiO₂ was studied. It is observed that the degradation effect of LMF treatment with UV/Ag-TiO₂ was more efficient than other two treatments namely UV and UV/TiO₂.

Effect of silver doping on anatase TiO₂ was studied by changing the percentage of silver from 1 to 2% (mole ratio) an increase in the content of silver leads to decrease in the particle size and increase in the photocatalytic activity as shown in Fig. 2. Smaller particle size increases surface area and higher content silver may also favour separating charge carriers efficiently, inhibiting the recombination of electron-hole pairs, and thus increasing the photocatalytic activity

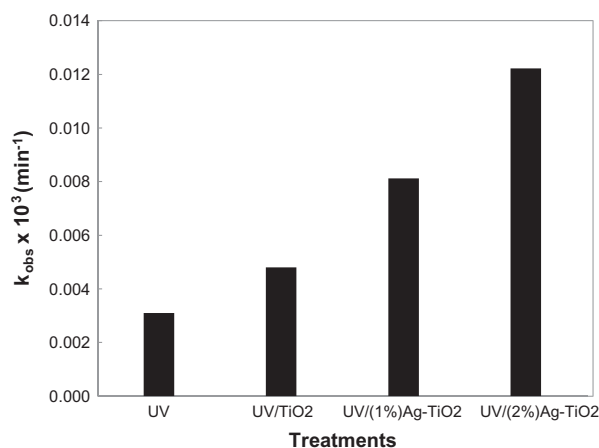


Fig. 2. Rate constants for the photocatalytic degradation of LMF by various treatments.

[16]. The photodegradation rate was highest with 2% Ag-TiO₂; hence, further studies were carried out with 2% Ag-TiO₂.

3.2. Characterization of TiO₂ and Ag-TiO₂

The crystal phase of prepared nanoparticles was identified using X-ray diffractometer as shown in Fig. 3. The data indicates that the major phase of all the prepared nanoparticles is anatase. The average crystalline size of prepared nanoparticles was determined from the broadening of the anatase main intense peak (1 0 1), using Scherrer equation (1), which is shown in Table 1. Crystallite size of pure TiO₂ is of 17.00 nm, while the crystallite size of Ag-TiO₂ 1% is 14.17 nm, Ag-TiO₂ 2% 13.07. Our results are in accordance with earlier report [7], where Ag-TiO₂ nanoparticles dimensions were reported in between 15 and 37 nm.

$$D = \frac{0.94\lambda}{\beta_{1/2} \cos \theta} \quad (1)$$

where D is the average crystalline diameter, λ is the wavelength in angstrom, β is the line width at half-maximum and θ is the Bragg angle.

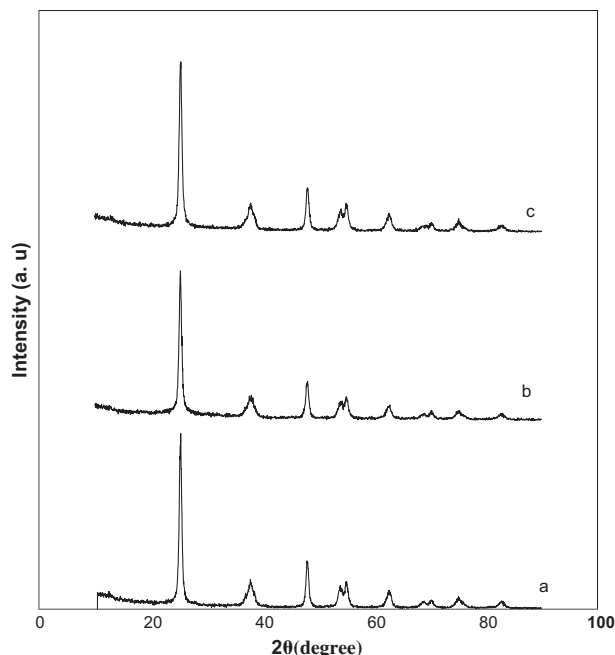


Fig. 3. XRD patterns of (a) undoped TiO₂, (b) 1% and (c) 2% Ag-TiO₂.

Table 1
Crystal size of undoped and Ag doped TiO₂ nanoparticles from Scherrer equation

Sl. no.	Particles	Particle size (nm)
1	Un doped TiO ₂	17.00
2	1% Ag-TiO ₂	14.17
3	2% Ag-TiO ₂	13.07

3.3. Surface morphology study

3.3.1. Scanning electron microscope

The SEM images have been used to characterize the size, shape and morphologies of formed nanoparticle clusters. It shows the non-uniform aggregates of the Ag-TiO₂ nanoparticles, which results in a high surface area. (Fig. 4(a)–(c)) represents the SEM images of the undoped and prepared Ag-TiO₂ nanoparticles [12].

3.3.2. Transmission electron microscope

TEM images show the heterogeneously dispersed aggregates of Ag-TiO₂ nanoparticles having cylindrical shape crystalline structures which can be clearly observed in (Fig. 5(a) and (b)). Dispersion of small dark spots seen were presumed as Ag particles on TiO₂ nanoparticles with a particle size of approximately 10–15 nm in breadth and 40–45 nm in length. It is revealed that the crystallite size of the synthesized nanoparticles is close to that of TiO₂ nanoparticles obtained from XRD values.

3.3.3. Electron diffraction X-ray spectroscopy

EDX examination provides information on chemical composition of samples. Fig. 6(a) and (b) shows that the prepared sample is mainly composed of Ti and O with small amount of Ag that increases with increase number of loading. Ag L peak was found, but peak of Ag K cannot be detected because low electron accelerating voltage was applied [17].

3.4. Effect of photocatalyst loading

To study the effect of catalyst loading, different amounts of catalyst were used from 50 to 250 mg/l while keeping [LMF] and pH 4 constant. It has been observed that initially the rate of photo degradation increases up to 100 mg/l, beyond 100 mg/l the rate of reaction almost constant (Fig. 7). This may be due to the fact that as the amount of semiconductor was increased in the initial state, the exposed surface area

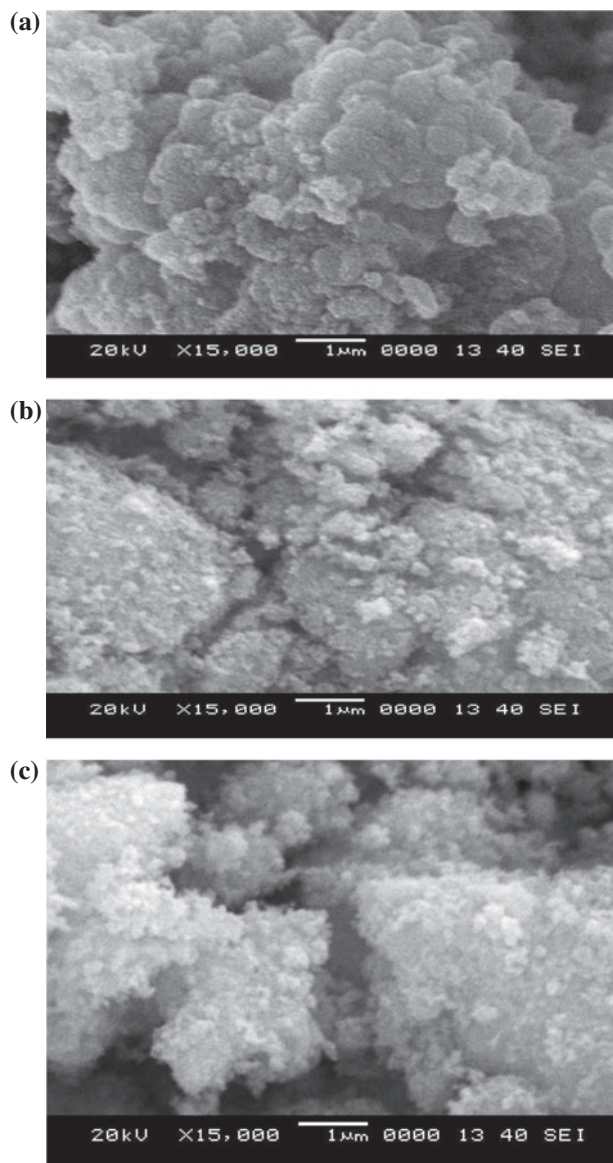


Fig. 4. SEM micrographs of (a) undoped TiO₂, (b) 1% Ag-TiO₂ and (c) 2% Ag-TiO₂.

of the semiconductor also increases, but after this limiting value (100 mg/l) any increase in the amount of semiconductor increases the turbidity of the solution and thus blocks UV irradiation for the reaction to proceed, and therefore degradation starts decreasing [18].

3.5. Effect of substrate concentration

The effect of variation of LMF concentration was studied by taking different concentration of LMF from 8×10^{-5} to 28×10^{-5} mol dm³ by keeping other condition constant. It has been observed that with the initial

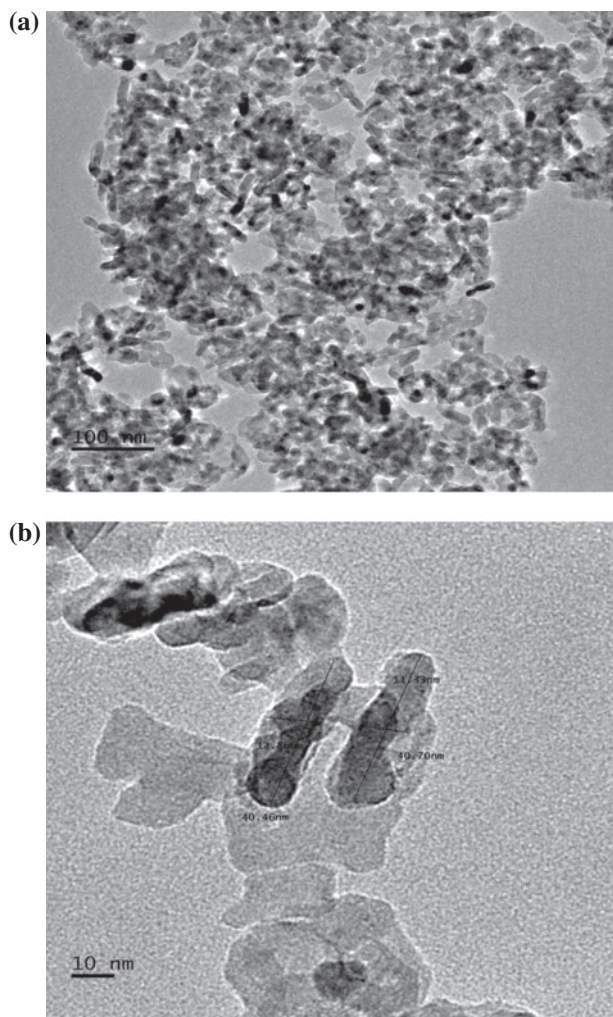


Fig. 5. TEM micrographs of 0.2% Ag/TiO₂.

increase in the concentration of LMF, the rate of photocatalytic degradation increases, reaching maximum value [LMF] = 20×10^{-5} mol dm³; further increase in concentration resulted in decrease in the rate of photocatalytic degradation as shown in Fig. 8. It may be due to the fact that, as the concentration of the drug increased, more number of drug molecules are excited and consequently available for degradation, and hence the rate of degradation increases. But at concentration above 20×10^{-5} mol dm³, the drug itself acts as a filter for the incident light. This reduces the formation of OH⁻ ions, due to which, the rate of photocatalytic degradation decreases [19].

3.6. Effect of pH

The pH normally influences the adsorption capacity of the adsorbent in aqueous medium by altering

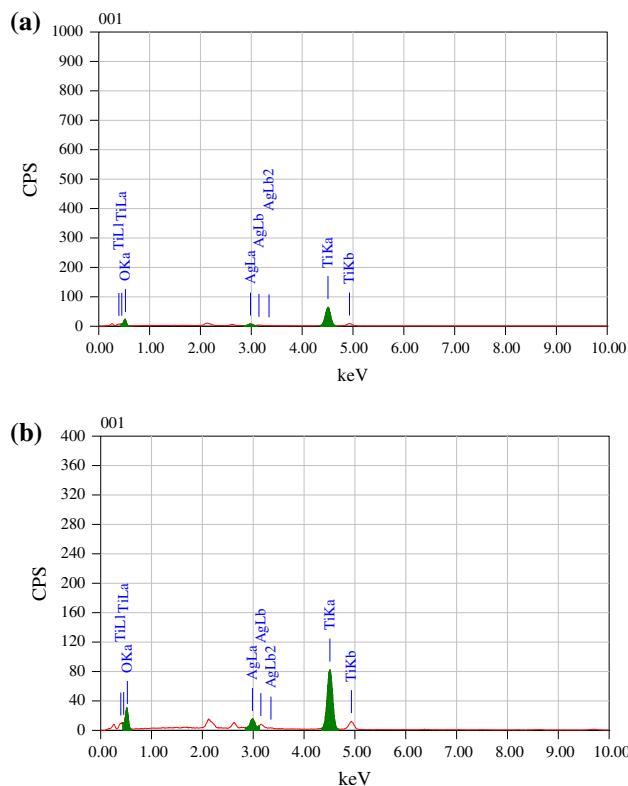


Fig. 6. (a) EDX analysis of 1% Ag-TiO₂ and (b) EDX analysis of 2% Ag-TiO₂.

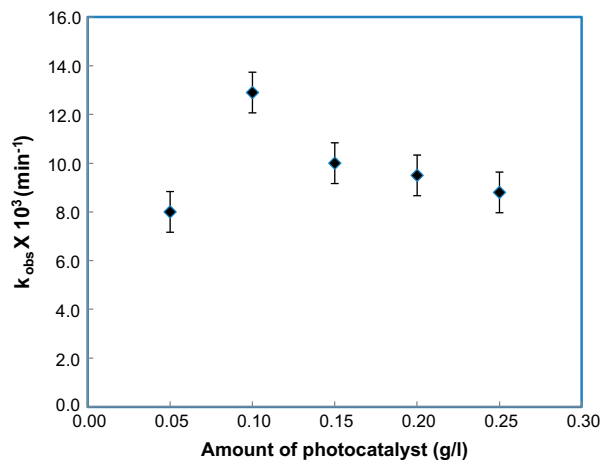


Fig. 7. Effect of different amounts of photocatalyst [LMF] = 20×10^{-5} M, at pH 4.

the surface properties of adsorbent. The effect of pH on the rate of photo degradation of LMF was studied by varying the pH from 4 to 8, while keeping other conditions constant. The rate of photocatalytic degradation of LMF was slightly higher in the pH

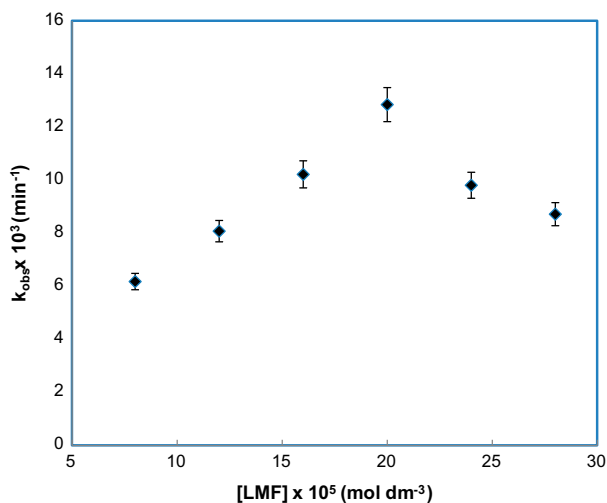


Fig. 8. Effect of variation of [LMF] on photocatalytic rate constants of photocatalytic process with 2% Ag-TiO₂ at 25 °C, [Ag-TiO₂] = 100 mg/l, at pH 4.

range 4–5 and slightly lower in the pH range 7–8 as shown in Fig. 9. This behaviour may be explained on the basis that an increase in the rate of photocatalytic degradation may be due to the increased availability of OH⁻ ions at acidic pH value. OH⁻ ions will generate more hydroxyl radicals (·OH) by combining with holes, which are considered responsible for the photocatalytic degradation. The adsorption on Ag-TiO₂ primarily depends on its surface properties and surface

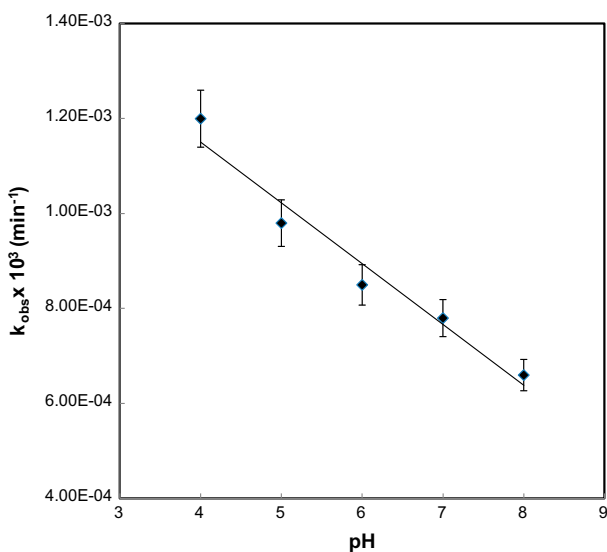


Fig. 9. Effect of pH on the rate constant of photocatalytic degradation of LMF with 2% Ag-TiO₂ at 25 °C, [Ag-TiO₂] = 100 mg/l, [LMF] = 20 × 10⁻⁵ M.

reactivity largely related to surface hydroxyl groups. It is evident from Table 2 that the adsorption capacity decreases with increase in the pH from 4 to 8. The LMF contains >NH and carboxyl functional groups in its molecular structure. This enables LMF to react with the H⁺ and OH⁻ in solution to form three different LMF species viz., LMFH⁺ (cation), LMF⁰ (neutral) and LMF⁻ (anion). The pK_a values of LMF were computed by using Chem axon calculator and they were found to be pK_{a1} (5.64) and pK_{a2} (8.7) [20]. The proportion of LMF in different forms can be calculated from the pK_a values of LMF. The speciation pattern of LMF at different pH is shown in Fig. 10. LMF forms about 98% LMFH⁺ at pH 4 by combining with H⁺ ions from the solution, which favours the LMF adsorption on the negatively charged surface of Ag-TiO₂ photocatalyst. The proportion of LMFH⁺ decreases to 81% at pH 5, reduces to 30% at pH 6 and further reduces to 4% (negligible) at pH 7. LMF neutral species dominates in the pH range 6–8. With the proportional decrease in the concentration of LMFH⁺ and proportional increase in the concentration of LMF neutral, the adsorption capacity of LMF on Ag-TiO₂ decreases. The adsorption of LMFH⁺ is due to the combination of cation with negatively charged surface of Ag-TiO₂, whereas the adsorption of LMF neutral is due to weak Van der Waals forces of attraction. This observation is in line with the earlier report [21].

3.7. Effect of UV lamp distance

To examine the effects of UV light intensity on the degradation of lomefloxacin was studied by varying the distance of UV lamp from the target. The results are reported in Fig. 11. It is seen that an increase in light intensity increase the rate of photocatalytic degradation, and it is due to the fact that as the intensity increases the more number of Ag-TiO₂ nanoparticles excite to generate more electron hole pairs. The holes decompose the lomefloxacin molecules adsorbed on the surface of Ag-TiO₂ particles and oxidize it to water resulting in their efficient degradation [22].

3.8. Mechanism of photocatalytic degradation

On the basis of the experimental data the following tentative mechanism may be given for photocatalytic degradation of LMF.

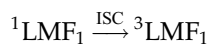
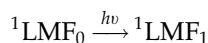


Table 2
Adsorption capacity at different pH (Langmuir isotherm)

Sl. no.	pH	Adsorption capacity (Langmuir isotherm) (mol/g)
1	4	0.00110
2	5	0.00091
3	6	0.00085
4	7	0.00072
5	8	0.00062

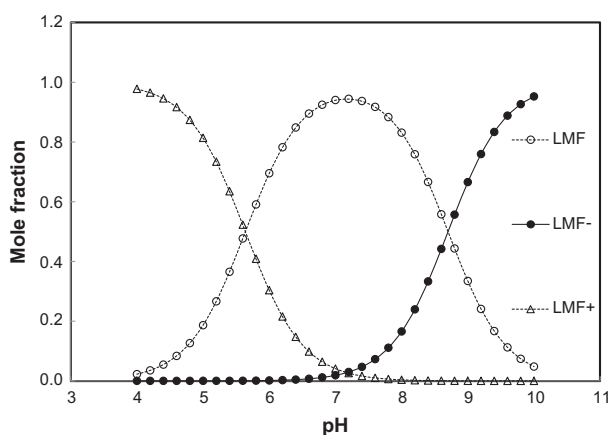


Fig. 10. Speciation of LMF at different pH.

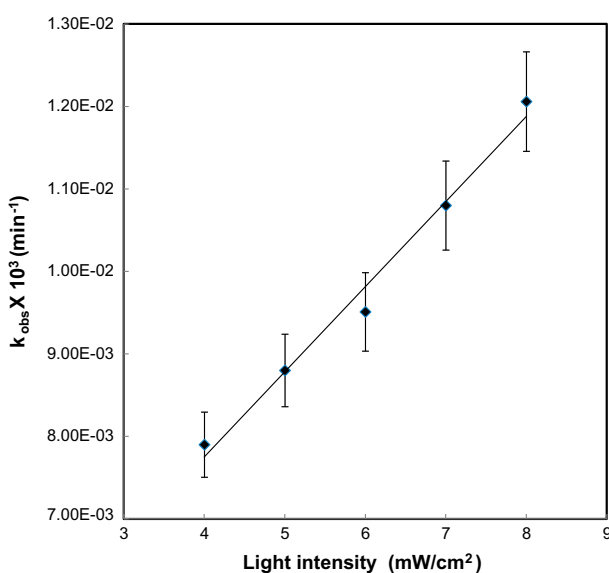
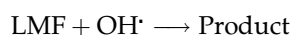
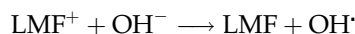
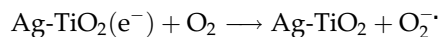
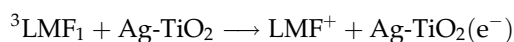


Fig. 11. LMF degradation under different UV intensities LMF with 2% Ag-TiO₂ at 25°C, [Ag-TiO₂] = 100 mg l⁻¹, [LMF] = 20 × 10⁻⁵ M, at pH 4.



When the LMF solution is exposed to UV light, in the presence of Ag-TiO₂, initially LMF molecules are excited to first singlet state (¹LMF₁). Then these excited molecules are moved to the triplet state through inter system crossing (ISC). The triplet drug (³LMF₁) may provide its electron to the photocatalyst and become positively charged. The dissolved oxygen of the solution will pull an electron from the conduction band of the photocatalyst, thus generating the photocatalyst. The positively charged molecules of the drug (LMF) will immediately reacts with ⁻OH ions to form OH[·] radicals, which will convert the drug molecules in to products.

In undoped TiO₂, molecular oxygen is the only one electron trapping entity, whereas in Ag-TiO₂, two other electron trapping entities are set up, viz., Ag⁺ ions and Ag⁰. Since the Fermi level of TiO₂ is higher, hence electrons will move from TiO₂ nanoparticles to the metallic silver nanoparticles resulting in a space charge between Ag and TiO₂. The electric field finally force the electrons to the interfacial space of the TiO₂ nanoparticles. Here, silver particles act as electron traps [23]. This leads to an increase in the charge separation efficiency and slows down electron-hole recombination. Silver metal on the catalyst surface improves the quantum yields by increasing the removal and the transfer of electrons from catalyst to molecular oxygen [24]. Therefore, molecular oxygen can trap photogenerated electrons to form superoxide radicals and consequently enhance the oxidation of LMF.

4. Conclusion

1 and 2% silver doped TiO₂ nanoparticles were synthesized successfully by LI method. The XRD patterns of synthesized Ag-TiO₂ nanoparticles indicate anatase crystal structure. The EDX analysis and TEM topograph show the doping of silver in TiO₂. In acidic environment at pH 4, the prepared Ag-TiO₂ nanoparticles (17.00–13.07 nm) exhibit good potential for the photocatalytic degradation of LMF. It is evident from the results that over 95% degradation of LMF could be achieved in 1 h using 2% Ag-TiO₂ photocatalyst.

References

- [1] T. Kudo, Y. Nakamura, A. Ruke, The design of highly active rectangular column structured titanium oxide photocatalysts and their application in purification systems, *J. Catal. Today* 122 (2003) 14–19.
- [2] G. Zayani, L. Bousselmi, F. Mhenni, A. Ghrabi, Solar photocatalytic degradation of commercial textile azo dyes: Performance of pilot plant scale thin film fixed-bed reactor, *Desalination* 246 (2009) 344–352.
- [3] U.I. Gaya, A.H. Abdullah, Heterogeneous photocatalytic degradation of organic contaminants over titanium dioxide: A review of fundamentals, progress and problems, *J. Photochem. Photobiol. C* 9(1) (2008) 1–12.
- [4] C. Guillard, J. Disdier, J.M. Herrmann, C. Lehaut, T. Chopin, S. Malato, J. Blanco, Comparison of various titania samples of industrial origin in the solar photocatalytic detoxification of water containing 4-chlorophenol, *Catal. Today* 54 (1999) 217–228.
- [5] P. Bansal, N. Bhullar, D. Sud, Studies on photodegradation of malachite green using TiO₂/ZnO photocatalyst, *Desalin. Water Treat.* 12(1–3) (2009) 108–113.
- [6] A. Jodat, A. Jodat, Photocatalytic degradation of chloramphenicol and tartrazine using Ag/TiO₂ nanoparticles, *Desalin. Water Treat.* 52(13–15) (2014) 2668–2677.
- [7] A. Verma, I.D. Chhikara Photocatalytic treatment of pharmaceutical industry wastewater over TiO₂ using immersion well reactor: Synergistic effect coupling with ultrasound, *Desalin. Water Treat.* 52(34–36) (2014) 6591–6597.
- [8] Y. Yang, X.J. Li, J.T. Chen, L.Y. Wang, Effect of doping mode on the photocatalytic activities of Mo/TiO₂, *J. Photochem. Photobiol., A* 163(3) (2004) 517–522.
- [9] K.V. Baiju, C.P. Sibin, K. Rajesh, P.K. Pillai, P. Mukundan, K.G.K. Warriar, W. Wunderlich, An aqueous sol-gel route to synthesize nanosized lanthanadoped titania having an increased anatase phase stability for photocatalytic application, *Mater. Chem. Phys.* 90 (2005) 123–127.
- [10] C. Kormann, D.W. Bahnemann, M.R. Hoffmann, Preparation and characterization of quantum-size titanium dioxide, *J. Phys. Chem.* 92 (1988) 5196–5201.
- [11] M.S. Lee, S.S. Hong, M. Mohseni, Synthesis of photocatalytic nanosized TiO₂-Ag particles with sol-gel method using reduction agent, *J. Mol. Catal. A* 242 (2005) 135–140.
- [12] D. Guin, S.V. Manorama, J.N.L. Latha, S. Singh, Photoreduction of Silver on Bare and Colloidal TiO₂ nanoparticles/nanotubes: Synthesis, characterization, and tested for antibacterial outcome, *J. Phys. Chem. C* 111 (2007) 13393–13397.
- [13] B. Halling-Sørensen, S.N. Nielsen, P.F. Lanzky, F. Ingerslev, H.C. Holten Lützhøft, S.E. Jørgensen, Occurrence, fate and effects of pharmaceutical substances in the environment—A review, *Chemosphere* 36(2) (1998) 357–393.
- [14] M.A. Behnajady, N. Modirshahla, M. Shokri, B. Rad, Enhancement of photocatalytic activity of TiO₂ nanoparticles by silver doping: Photodeposition versus liquid impregnation methods, *Global NEST J.* 10(1) (2008) 1–7.
- [15] H. Ilyas, I.A. Qazi, W. Asgar, M.A. Awan, Z. Khan, Photocatalytic degradation of nitro and chlorophenols using doped and undoped titanium dioxide nanoparticles, *J. Nanomater.* 2011 (2011) 1–8.
- [16] U.S. Ozkan, M.W. Kumthekar, G. Karakas, Characterization and temperature-programmed studies over Pd/TiO₂ catalysts for NO reduction with methane, *Catal. Today* 40(1) (1998) 3–14.
- [17] K. Wetchakun, S. Phanichphant, Effect of Ru on photocatalytic activity of TiO₂ nanoparticles, *J. Microsc. Soc. Thailand* 22 (2008) 11–14.
- [18] J. Sun, L. Qiao, S. Sun, G. Wang, Photocatalytic degradation of Orange G on nitrogen-doped TiO₂ catalysts under visible light and sunlight irradiation, *J. Hazard. Mater.* 155 (2008) 312–319.
- [19] C.C. Wang, C.K. Lee, M.D. Lyu, L.C. Juang, Photocatalytic degradation of C.I. Basic Violet using TiO₂ catalysts supported by Y. Zeolite an investigation of the effects of operational parameters, *Dyes Pigm.* 76 (2008) 312–319.
- [20] Marvin 5.10.1, 2012, ChemAxon. Available from: <<http://www.chemaxon.com>>.
- [21] I.T. Horvath, Heterogeneous photocatalytic degradation of organic contaminants over titanium dioxide: A review of fundamentals, progress and problems, *J. Encycl. Catal.* 5 (2003) 577–599.
- [22] Z. Guo, R. Ma, G. Li, Degradation of phenol by nanomaterial TiO₂ in wastewater, *Chem. Eng. J.* 119 (2006) 55–59.
- [23] C. He, Y. Yu, X. Hu, A. Larbot, Influence of silver doping on the photocatalytic activity of titania films, *Appl. Surf. Sci.* 200 (2002) 239–247.
- [24] H. Gerischer, A. Heller, Photocatalytic oxidation of organic molecules at TiO₂ particles by sunlight in aerated water, *J. Electrochem. Soc.* 139 (1992) 113–118.

Ru–TiO₂ semiconducting nanoparticles for the photo-catalytic degradation of bromothymol blue

R. M. Kulkarni¹ · R. S. Malladi¹ · M. S. Hanagadakar¹ · M. R. Doddamani² ·
B. Santhakumari³ · S. D. Kulkarni⁴

Received: 6 June 2016 / Accepted: 25 July 2016 / Published online: 2 August 2016
© Springer Science+Business Media New York 2016

Abstract Photo-catalytic degradation of bromothymol blue (BTB) in an aqueous medium by Ru–TiO₂ using UVC (254 nm) irradiation was investigated for a pH range of 4.0–8.0. The liquid impregnation method was used to synthesize 0.2, 0.4 and 0.8 % ruthenium doped TiO₂ (Ru–TiO₂) nanoparticles. The characterizations of resulting nanoparticles were done using X-ray diffraction, scanning electron microscopy, fourier transform infrared spectroscopy, transmission electron microscopy (TEM) and energy dispersive X-ray spectroscopy analysis. The crystallite sizes of doped and undoped nanoparticles were determined from X-ray diffraction spectra using Scherrer equation. The average crystallite size of undoped TiO₂ was found to be 17.00 nm, whereas the crystallite sizes of 0.2, 0.4 and 0.8 % Ru–TiO₂ were 16.67, 15.70 and 14.40 nm respectively. The TEM images confirm the particle sizes to be 10–40 nm. Pseudo-first order rate constants (k_{obs}) determined were found to decrease with increase in pH. The effect of BTB Concentration, catalyst dosage, a percentage of doping of photo catalyst, pH and UV light

intensity of BTB on the degradation rate were also examined.

1 Introduction

A wide variety of organic contaminants has been detected in the aquatic environment which are discharged through municipal waste-water, industrial effluents, commercial operations, runoff from agricultural lands, chemical spills etc [1]. Till now, the conventional and biological methods have not been able to get rid of these persistent organic contaminants from the environment [2].

Dye effluent generated from textile and dye industries has to be treated due to its impact on flora and fauna and growing public concern over the toxicity and carcinogenicity [3–5]. This fact compels elimination of dyes in the effluent treatment plants [6].

Advanced oxidation processes (AOPs) have been used extensively for the degradation of harmful organic contaminants [7], which are resistant to biological and conventional treatment methods. AOPs depend on the generation of highly reactive radical species such as OH[•] by chemical or photochemical methods, which decomposes a number of organic contaminants without being selective [8–10]. The technique primarily focuses on the usage of semiconductor particles activated by UV or visible light for degradation of environmental contaminants yielding to partial or complete mineralization of the organic contaminants [11, 12].

Metal oxide semiconductor Titanium dioxide (TiO₂) nanoparticles have attracted much interest due to their low cost, greater efficiency and stability [13, 14]. It allows UV light to excite the valence electrons as it has a band gap of 3.2 eV [15], the valence electrons jump into the conduction

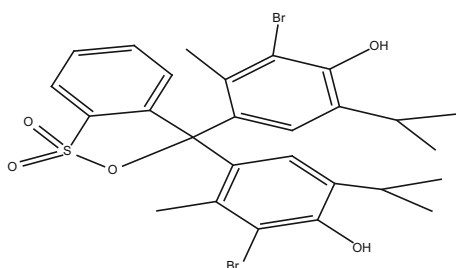
✉ R. M. Kulkarni
ravirajmk@git.edu

¹ Department of Chemistry, KLS Gogte Institute of Technology (Autonomous) Affiliated to Visvesvaraya Technological University, Belagavi, Karnataka 590 008, India
² Mechanical Engineering, National Institute of Technology Karnataka, Surathkal, India
³ Center for Materials Characterization Division, CSIR-National Chemical Laboratory, Pune, Maharashtra 411008, India
⁴ Department of Atomic and Molecular Physics, MIT Campus, Manipal University, Manipal 576104, India

band generating positive holes in the valence band [16]. The efficacy of the photo catalyst depends on the rate of electron–hole recombination in TiO_2 [17, 18]. This rate of recombination can be minimized by doping the TiO_2 with metals such as silver, ruthenium, copper, iron, chromium, nickel etc [19–21].

These doped cations reduce the band gap and shift the threshold for photonic excitation of the TiO_2 towards the visible range [22]. Ruthenium might act as a suitable element for doping of TiO_2 , because of its closeness in atomic radius with TiO_2 (Ru—0.056 nm, Ti—0.060 nm) [23].

The model compound used for study bromothymol blue (BTB) is a textile dye derivative. The photo-catalytic degradation of bromothymol blue by TiO_2 has been investigated earlier [24]. From the application point of view, kinetics of degradation of textile dye derivatives by doped nanostructure is essential. Therefore, in the present work, we have undertaken a detailed study on the photo-catalytic degradation of bromothymol blue by prepared Ru- TiO_2 nanoparticles in an aqueous medium by varying reaction parameters namely pH of the reaction, substrate concentration, catalyst concentration, percentage of doping of photo-catalyst and intensity of UV-light.



Chemical structure of Bromothymol blue (BTB) $\text{C}_{27}\text{H}_{23}\text{Br}_2\text{O}_5\text{S}$

2 Materials and methods

2.1 Reagents and chemicals

A stock solution of bromothymol blue (Sigma-Aldrich) was prepared by dissolving appropriate amount of sample in double distilled water. The TiO_2 (anatase) (SRL) and $\text{RuCl}_3 \cdot 3\text{H}_2\text{O}$ (SRL) samples were directly used to prepare Ru doped TiO_2 without any further purification. The chemicals and reagents used to carry out the degradation study were of analytical grade.

2.1.1 Instruments used

1. For kinetic measurements, a CARY 50 Bio UV–Vis Spectrophotometer (Varian BV, The Netherlands) with

a temperature controller and HPLC system (Agilent 1100 series, USA) were used.

2. For degradation study, a mercury lamp (PHILIPS, TUV 8W T5, $E_{\text{max}} = 254 \text{ nm}$) mounted inside the UV cabinet was used. The typical light intensity illuminated on the surface of the reaction mixture was 4 mW cm^{-2} .
3. For intensity measurement an optical power meter (Newport 2936—C) and for pH measurements, Elico pH meter models LI 120 were used.
4. For characterization of nanoparticles, a Siemens X-ray Diffractometer (Cu source) (XRD) AXS D5005 was used to identify the particle size of the doped TiO_2 . The surface morphology was studied using a Scanning electron microscope (SEM) JEOL JSM 6360.
5. FTIR Perkin Elmer model-spectrum 100 was used for the characterization.
6. The topography and particle size of Ru-doped TiO_2 were measured using JEOL JEM-2010 transmission electron microscopy (TEM). Before the analysis, the catalyst sample ultrasonically dispersed in a solvent and dropped on a copper grid. The sample was allowed to dry before TEM analysis.

2.2 Photo-catalyst preparation

Ruthenium (Ru) doped anatase TiO_2 nanoparticles were prepared by liquid impregnation method. For ruthenium doping, 0.2, 0.4 and 0.8 % (mole ratio) of $\text{RuCl}_3 \cdot 3\text{H}_2\text{O}$ was dissolved in 100 ml of 0.2 M HCl solution. Further, 1.0 g of Anatase nanoparticles TiO_2 was added to the solution. The resultant slurry was thoroughly stirred for 3 h and allowed to settle at room temperature for 24 h. Afterward, the slurry was dried out in an oven at $80 \text{ }^\circ\text{C}$ for further 24 h. The dried solids were ground in a mortar and calcined at $400 \text{ }^\circ\text{C}$ for 3 h in a muffle furnace because the Anatase to Rutile phase transformation takes place above $400 \text{ }^\circ\text{C}$ [25, 26].

2.3 The photo-catalysis process

To investigate the photo-catalytic degradation, a known concentration of BTB solution and the buffer was taken in a Pyrex beaker, and then a dosage of 100 mg l^{-1} Ru- TiO_2 nanoparticles was added. Before illumination, the suspensions were stirred at a dark place for 1 h to reach adsorption and desorption equilibrium between the BTB and photo-catalyst. Then, the beaker was placed in a photo-catalytic chamber under 8W UV-lamp (Phillips) with a wavelength peak at 254 nm with continuous stirring for adsorption–desorption equilibrium and then exposed to UV light. At the interval of every 15 min, the solution was

taken out and centrifuged at 5000 rpm for 10 min. The decrease in the concentration of bromothymol blue was monitored at 429 nm ($\epsilon = 10,860 \text{ l M}^{-1} \text{ cm}^{-1}$) using UV–Vis spectrophotometer (Varian CARY 50 Bio UV–Vis Spectrophotometer).

3 Results and discussion

3.1 Comparison of different photo-catalysts

The rate of photo-catalytic degradation of BTB with UV, UV/TiO₂, UV/0.2 % Ru–TiO₂, UV/0.4 % Ru–TiO₂ and UV/0.8 % Ru–TiO₂ was studied. It was observed that the degradation effect of BTB treatment with UV/Ru–TiO₂ was more efficient than other two treatments namely UV and UV/TiO₂ (Fig. 1).

Effect of ruthenium doping on anatase TiO₂ was studied by varying the percentage of ruthenium from 0.2 to 0.8 % (mole ratio) an increase in the content of ruthenium leads to decrease in the particle size and increase in the photo-catalytic activity [27] as shown in Fig. 1. Smaller particle size increases surface area and higher content ruthenium may also favour separating charge carriers efficiently, inhibiting the recombination of electron–hole pairs, and thus increase the photo-catalytic activity [28]. The photo-catalytic degradation rate was highest with 0.8 % Ru–TiO₂; hence, further studies were carried out with 0.8 % Ru–TiO₂. Increasing the percentage of ruthenium above 0.8 % resulted in the deposition of ruthenium on the surface of the TiO₂ but not in the crystal lattice.

The % degradation efficiency of BTB was studied under same conditions with UV, UV/TiO₂, UV/0.2 % Ru–TiO₂, UV/0.4 % Ru–TiO₂, UV/0.8 % Ru–TiO₂ and percentage

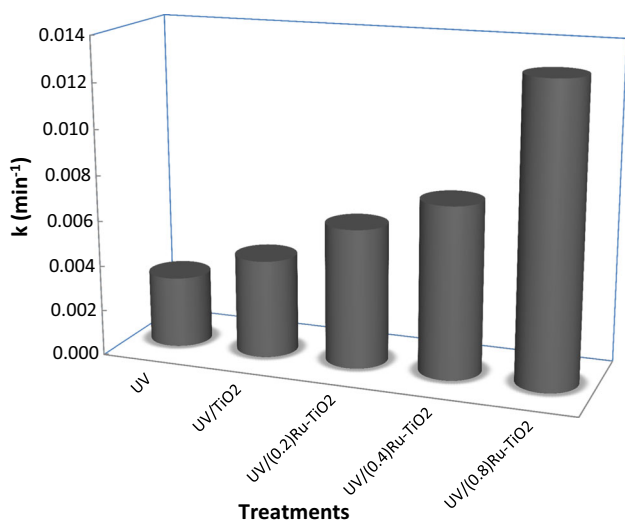


Fig. 1 Rate constants for the photo catalytic degradation of BTB by various treatments

adsorption in dark was also determined. The percentage degradation efficiency of BTB was found to be 48, 60, 75, 82 and 95 % with UV, UV/TiO₂, UV/0.2 % Ru–TiO₂, UV/0.4 % Ru–TiO₂ and UV/0.8 % Ru–TiO₂ respectively within 100 min as shown in Fig. 2. The % degradation efficiency of UV/0.8 % Ru–TiO₂ is about 35 % higher than UV/TiO₂ report by Haque et al. under our experimental conditions with [Photocatalyst] = 100 mg l⁻¹, [BTB] = 5 × 10⁻⁵ mol dm⁻³ at pH 4 and light intensity 4 mW cm⁻².

3.2 Characterization of TiO₂ and Ruthenium doped TiO₂

3.2.1 X-ray diffraction studies (XRD)

X-ray diffraction pattern of pure TiO₂ and Ru–TiO₂ were obtained from an X-ray diffractometer using Cu K_α radiation over a scan range of 2θ (10°–90°). XRD patterns of pure and 0.2, 0.4 and 0.8 % Ru–TiO₂ were shown in Fig. 3. Several well defined diffraction reflections were appeared in the pattern 25.2, 38.0, 48.2, 53.9, 55.0, 62.5, 70.2, 70.8, and 78.5, 82.9, which corresponds to the XRD pattern of all the ten peaks of anatase TiO₂ with lattice planes of (101), (004), (200), (105), (211), (204), (116), (220), and (215), (224), respectively. The absence of metal peaks is due to the ultrafine dispersion of TiO₂ nanoparticles and or due to very low metal concentration. The average particle sizes of prepared nanoparticles were determined from a full width half maximum of A (101) peak of anatase TiO₂ by applying Scherrer Eq. (1) [29]

$$D = \frac{k\lambda}{\beta \cos\theta} \tag{1}$$

where k is a constantly called shape factor is equal to 0.94, λ is the X-ray wavelength is equal 0.154 nm, β, is the full width at half maximum and θ is the half diffraction angle.

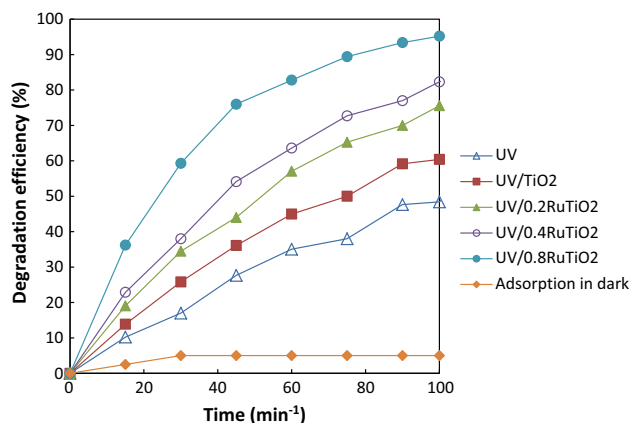


Fig. 2 % degradation efficiencies of various treatment methods with time

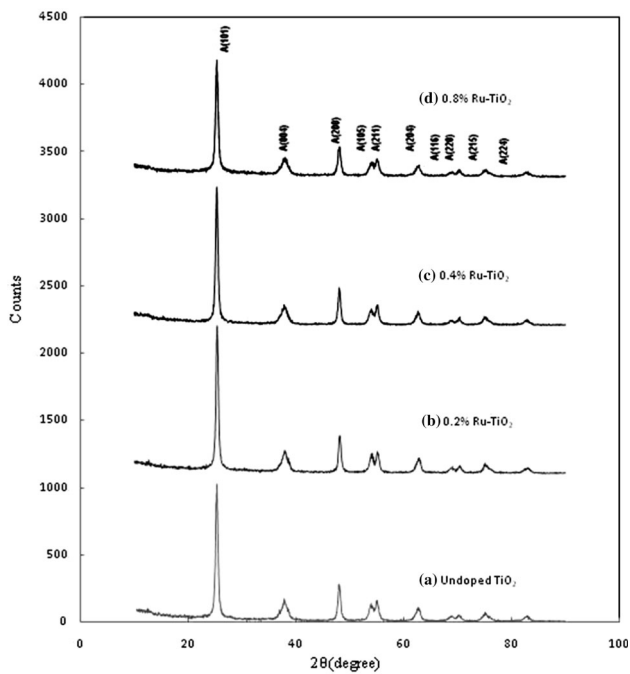


Fig. 3 X-ray diffraction patterns of **a** undoped TiO₂, **b** 0.2 % Ru-TiO₂, **c** 0.4 % Ru-TiO₂, **d** 0.8 % Ru-TiO₂

The average particle size of TiO₂, 0.2 % Ru-TiO₂, 0.4 % Ru-TiO₂, 0.8 % Ru-TiO₂ were found to be 17.00, 16.67, 15.70 and 14.40 nm respectively.

3.2.2 Scanning electron microscope

The SEM images of undoped and Ru-doped TiO₂ nanoparticles obtained at the high magnification 15000× using JEOL JSM-6360 are presented in Fig. 4a, b. Thin films of the sample were prepared on a carbon coated copper grid by just dropping a very small amount of the sample on the grid, extra solution was removed using a blotting paper and then the film on the SEM grid were allowed to dry by putting it under a mercury lamp for 5 min which reveal that synthesized nanoparticles possess a porous and spongy network of unequal shapes resulting in the high surface area. SEM images show that ruthenium is not equally deposited on the surface of TiO₂ nanoparticles; this is in agreement with the earlier literature [12].

3.2.3 Energy dispersive X-ray spectroscopy

The EDX pattern of Ru-TiO₂ (Fig. 5) was obtained using the JEOL JED-2300 equipment. The EDX shows the presence of three different X-ray patterns linked with O K α , Ru K α , and Ti K α [30]. The peaks from the spectrum reveal the presence of Ti, O and Ru at 4.508, 0.525 and 2.558 keV respectively. The atomic % of Ti, O and Ru is 36.40, 62.79 and 0.81 respectively. This composition of Ti,

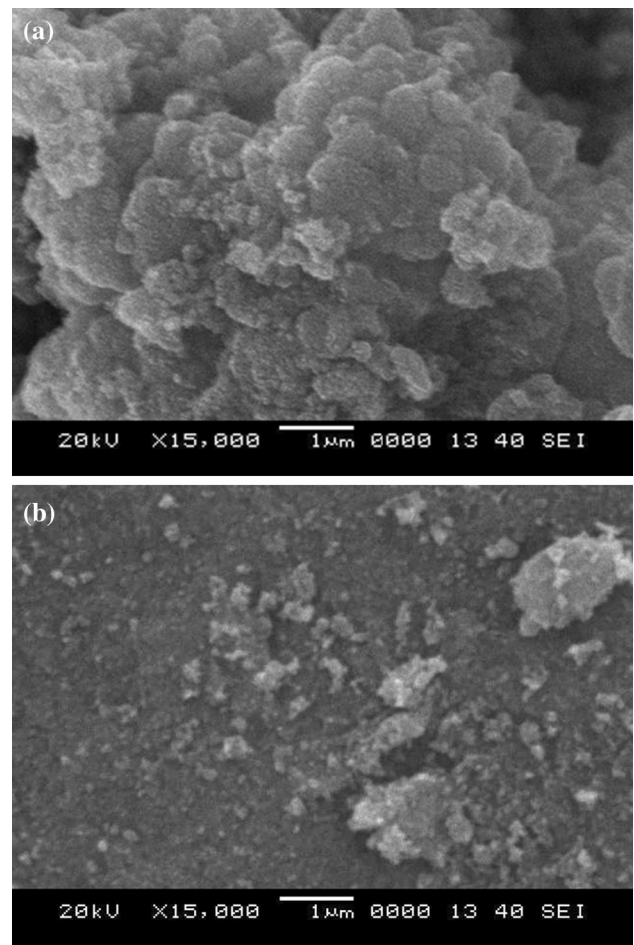
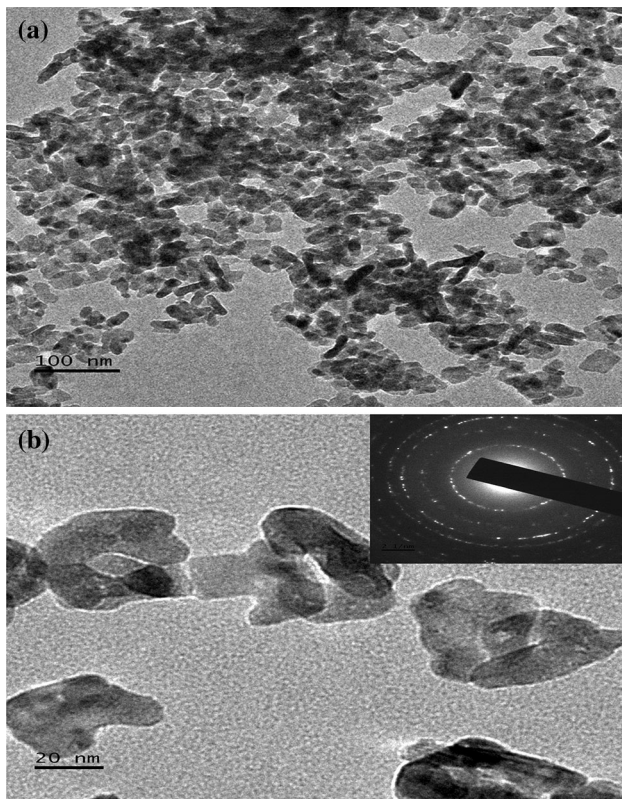
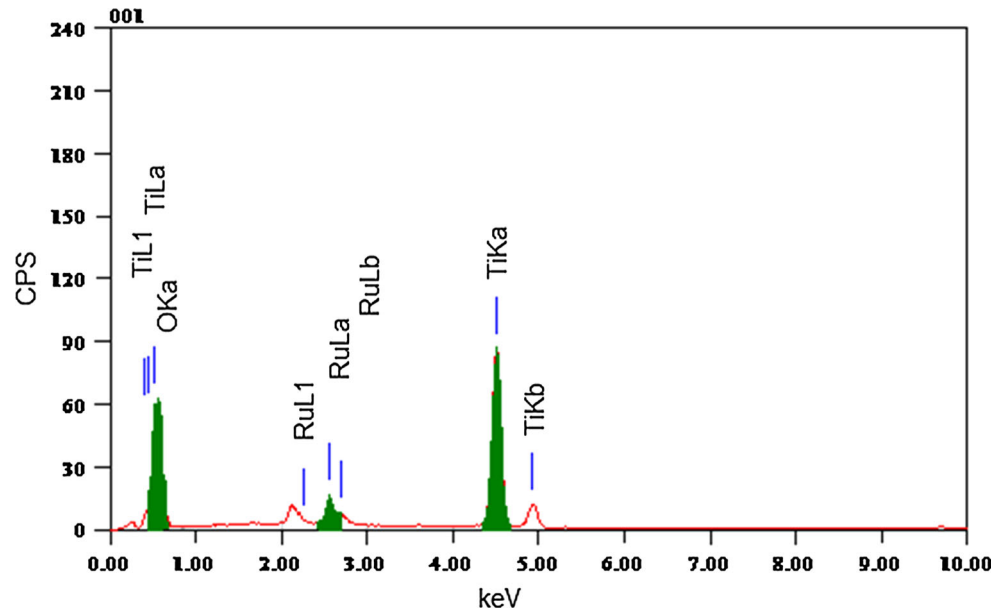


Fig. 4 SEM micrographs of **a** undoped TiO₂, **b** 0.8 % Ru-TiO₂ nano particles

O and trace amount of Ru revealed that the formation of non-stoichiometric TiO₂ with oxygen vacancy, which leads to better photo-catalytic activity [31].

3.2.4 Transmission electron microscope

A typical TEM image of Ru-TiO₂ powders synthesized by Liquid Impregnation method is presented in Fig. 6a, b, which reveals that the synthesized Ru-TiO₂ nanoparticles is well crystallized uniformly dispersed aggregates having the spherical rod in shape without defects. The average particle size of the nanoparticles was found to be 15–20 nm. These results are in good agreement with that of calculated particle size by Scherrer equation. The selected area electron diffraction pattern (SAED) is shown in inset of Fig. 6b. The D values of diffractions were obtained from the rings which can be assigned [101], [004], [200], and [211] (Table 1) and these values are in agreement with the D values obtained from XRD. In SAED, the small spots making up rings, each spot arising from Bragg reflection from an individual crystallite indicates our sample is poly-

Fig. 5 EDX analysis of 0.8 % Ru/TiO₂**Fig. 6** TEM micrographs of 0.8 % Ru/TiO₂ at **a** 100 nm resolution and **b** 20 nm resolution (*inset* SAED pattern)

nano-crystalline in nature. In poly-nano-crystalline samples, if more than one crystal contributes to the selected area diffraction pattern, it can be difficult or impossible to analyze. SAED is similar to XRD but unique in that areas as small as several hundred nanometers in size can be examined, whereas XRD typically samples areas several

centimetres in size due to that we could observe small difference in the D values of SAED and XRD [32, 33].

3.2.5 Fourier transform infrared (FTIR) spectra analysis

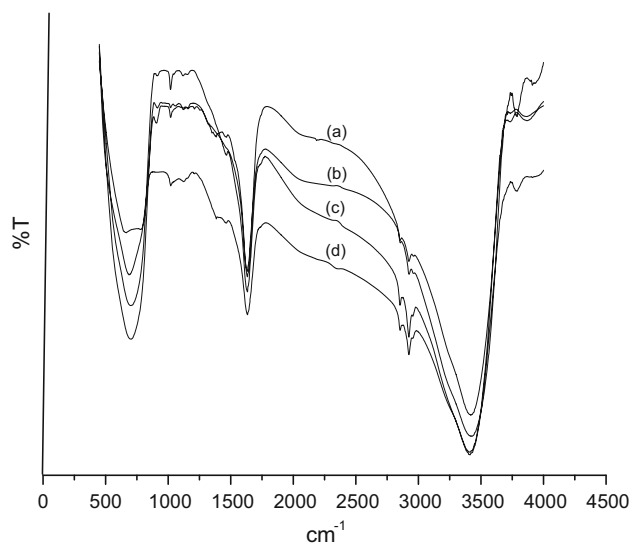
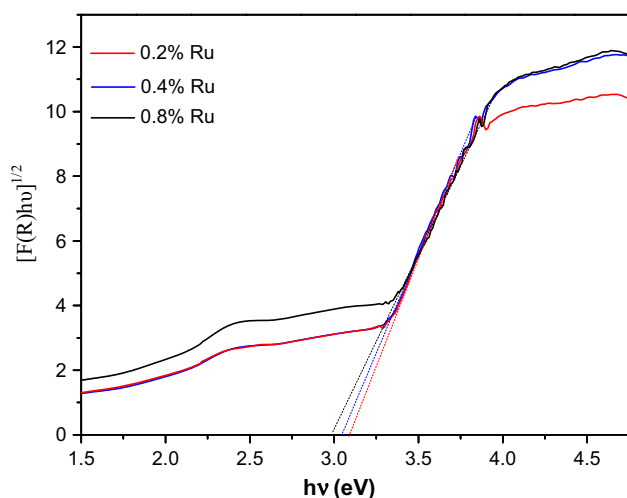
The FT-IR spectra of pure TiO₂ and Ru–TiO₂ nanoparticles were shown in Fig. 7. The FT-IR spectra of TiO₂ and Ru–TiO₂ show a broad band between 3500–3000 cm⁻¹, which is a characteristic band of associated hydroxyl groups. The other peaks at 1635 cm⁻¹ correspond to the stretching vibration of a hydroxyl group and representing the water as moisture [34]. The peak observed between 750 and 500 cm⁻¹ indicates the Ti–O stretching bands. Calcination of TiO₂ and Ru–TiO₂ sample at 600 °C leaves a strong band between 800 and 450 cm⁻¹, which can be attributed to the formed of TiO₂ nanoparticles [35].

3.2.6 Band gap measurement

The bandgap measurements of nanoparticles were made from the diffuse reflectance spectra collected using a Perkin Elmer Lambda 950 UV/Vis/NIR spectrophotometer with a 150 mm integrating sphere attachment. Diffuse reflectance measurements were made between 800 and 200 nm using BaSO₄ as a reflectance standard. The optical bandgaps (E_g) of the nanoparticles were determined from the Tauc plot of the Kubelka–Munk function obtained from the diffuse reflectance spectra. The Kubelka–Munk function is given by the equation $F(R) = (1 - R)^2/2R$, where R is the diffuse reflectance of the sample. Extrapolation of the linear portion of the modified Kubelka–Munk function, $[F(R)h\nu]^{1/2}$ vs the photon energy ($h\nu$) curve on the zero ordinate gives the E_g (Fig. 8). The band gap of

Table 1 Selected area electron diffraction data

2R [1/nm]	R [1/nm]	SAED D [nm]	XRD D [nm]	Difference SAED and XRD	D [\AA^0]	h k l	2-theta
5.92	2.96	0.3378	0.3496	0.0118	3.38	101	25.45
8.87	4.43	0.2254	0.2352	0.0098	2.25	004	38.22
10.6	5.30	0.1886	0.1882	0.0004	1.89	200	48.28
12.6	6.30	0.1587	0.1667	0.0080	1.59	201	55.00

**Fig. 7** FT-IR spectra of **a** pure TiO₂, **b** 0.2 % Ru-TiO₂, **c** 0.4 % Ru-TiO₂, **d** 0.8 % Ru-TiO₂ nanoparticles**Fig. 8** Plot of $[F(R)h\nu]^{1/2}$ versus the photon energy ($h\nu$)

0.2, 0.4 and 0.8 % Ru-TiO₂ was found to be 3.10, 3.04 and 2.96 eV respectively. However, in the literature it is reported that the pure anatase TiO₂ nanoparticles shows the band gap 3.2 eV. This red shift is due to the localized energy level introduced by the Ru in the forbidden energy range of TiO₂ [36]. From the decrease in the value of band

gap it is confirmed that ruthenium is successfully doped in TiO₂ lattice [31].

3.2.7 Surface area measurement

Photo-catalytic activity of Ru-doped TiO₂ also depends on the surface area of the particles. Hence, it would be interesting to determine the surface area of Ru-doped TiO₂ nanoparticles. The specific surface area of the nanoparticles was measured by the BET nitrogen gas adsorption method using Smart Instruments Surface Area Analyser (Smart-Sorb 92/93).

Our studies indicate that synthesized nanoparticles showed a surface area of 85.23, 88.79, 92.91 and 94.28 m²/g for pure TiO₂, 0.2 % Ru-TiO₂, 0.4 % Ru-TiO₂ and 0.8 % Ru-TiO₂ nanoparticles respectively. The decrease in particle size can be explained on the basis of Nae-Lih Wu's theory [37]. According to Nae-Lih Wu's theory, the motion of the crystallites is restricted due to the interaction on the boundaries between TiO₂ and Ru [38–40], which results in the reduction of particle size of TiO₂. Hence, the specific surface area increases with decrease in particle size. The very high surface area of 0.8 % Ru-TiO₂ nanoparticles is responsible for the enhanced photo-catalytic degradation of BTB.

3.3 Variation of BTB concentration

The effect of initial of dye concentration on the rate of photo-catalytic degradation of bromothymol blue at pH 4 was studied at different concentrations varying from 2.0–20.0 × 10⁻⁵ mol dm⁻³. Initially, the rate constant, k_{obs} , was found to increase with the increase in substrate concentration from 2.0–12.0 × 10⁻⁵ mol dm⁻³. A further increase in BTB concentration above 12.0 × 10⁻⁵ mol dm⁻³ resulted in a decrease in the rate constant (Fig. 9). This trend can be attributed to the fact that as initial concentrations of the dye increase, the colour of the irradiating mixture progressively becomes intense which prevents the penetration of light photons to reach the surface of the catalyst. Hence, the generation of a relative amount of OH[·] and O₂^{·-} on the surface of a catalyst does not

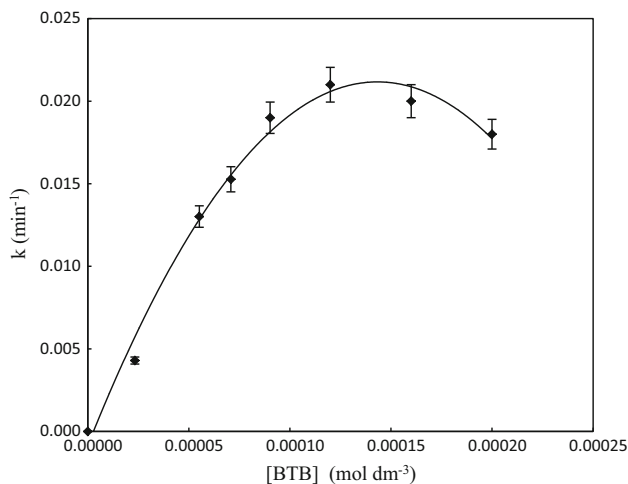


Fig. 9 Effect of variation of [BTB] on the degradation of BTB by Ru-TiO₂ at 25 °C. [Ru-TiO₂] = 100 mg l⁻¹ pH = 4.0

increase, as the intensity of the light and the irradiation time are constant. Consequently, the rate of photo-catalytic degradation decreases with increase in a concentration of BTB [24].

3.4 Effect of catalyst dosage

The effect variation in the photo-catalyst dosage on the degradation kinetics of bromothymol blue was studied using a different concentration of 0.8 % Ru-TiO₂ varying from 0–250 mg dm⁻³ and keeping other conditions constant. The rate constant, *k*_{obs}, was found to increase with an increase in the dosage of a catalyst as shown in Fig. 10. This can be attributed to the fact that, as the dosage of Ru-TiO₂ increases, the exposed surface area of the photo-catalyst also increases. The results are in agreement with the earlier reports [24, 41, 42].

3.5 Adsorption experiment

The adsorption experiment was carried by varying the BTB concentration from 2.0–20 × 10⁻⁵ mol dm⁻³. The appropriate amount of BTB solution was taken in 100 ml beaker and 10 mg of Ru-TiO₂ nano particles was added. The pH value of the each set was adjusted to 4, 5, 6, 7 and 8 respectively. The solution was sealed and stirred at 25 °C for overnight in the absence of UV light. The solution was centrifuged and the BTB concentration of the supernatant was measured by UV spectrophotometer. The adsorption amount (Capacity) was calculated using the following equation (Table 2).

$$S = \frac{(C_0 - C)V}{m}$$

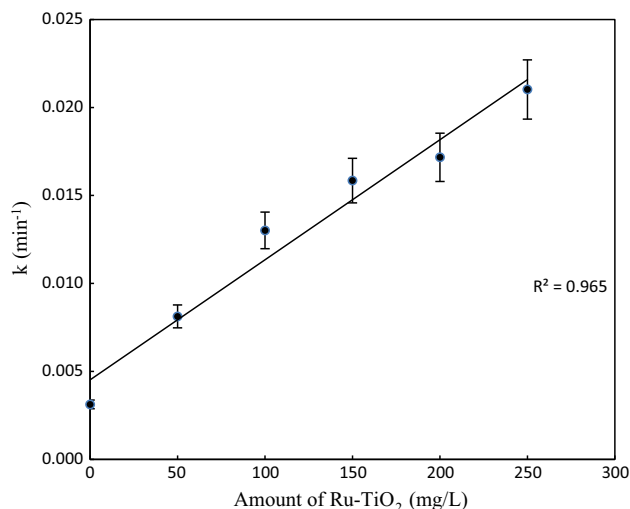


Fig. 10 Effect of variation of Ru-TiO₂ dosage on the degradation of BTB at [BTB] = 5.0 × 10⁻⁵ mol dm⁻³

where *S* basically represents efficiency of adsorption (mol g⁻¹), *C*₀ is the initial concentration of BTB, *C* is the BTB is the equilibrium concentration (mol dm⁻³), *V* is the volume (dm³) of the solution, and *m* is the mass of added Ru-TiO₂ (g).

The adsorption of the BTB on the surface of Ru-TiO₂ photo-catalyst was studied by continuous stirring the aqueous solution of BTB in the dark for 24 h in a flask containing varying amounts of Ru-TiO₂. The analysis of BTB concentration after centrifugation shows no observable loss of the dye. Hence, adsorption has no significant effect on the degradation rate.

3.6 Effect of pH

pH is an important parameter in photo-catalytic reactions, it gives information pertaining to the surface properties of the photo-catalyst and adsorption behaviour of pollutants. Effect of pH on the degradation of BTB in water medium of Ru-TiO₂ was studied between pH 4.0–8.0 under UV-light. Whilst maintaining other reaction conditions constant. The photo-catalytic degradation of BTB was higher

Table 2 Adsorption capacities at different pH, [BTB] = 5 × 10⁻⁵, (0.8 %) Ru-TiO₂ = 100 mg l⁻¹

Sl. No	pH	Adsorption capacity (mol g ⁻¹)
1	4	0.00091
2	5	0.00083
3	6	0.00074
4	7	0.00067
5	8	0.00060

in the pH range 4.0–6.0 and slightly lower in the pH range 7.0–8.0 as shown in Fig. 11. This performance possibly elucidated on the bases that increase in the rate of photo-catalytic degradation was due to the surface activity of photo-catalyst. The adsorption at pH 4.0–6.0 is favoured by attractive electrostatic forces existing between BTB anion and as Ru-TiOH_2^+ , where Ru-TiOH_2^+ is a major active species in this pH range. Whereas in basic medium, i.e. pH 7.0–8.0 Ru-TiO^- is a major active species, Hence electrostatic repulsion between two negatively charged species, Ru-TiO^- and BTB anion disfavours photo-catalytic degradation [43, 44]. The adsorption capacity decreases with increase in the pH from 4.0 to 8.0. The BTB react with the H^+ and OH^- in solution to form two different BTB species viz., BTB^0 (neutral) and BTB^- (anion). The proportion of BTB in different forms can be calculated from the pK_a (7.1) [45] as shown in Fig. 12. BTB neutral species dominates in the pH range 4.0–7.0 and are adsorbed at a higher degree than highly ionised species. Whereas BTB^- dominates in the pH range above 7.0 and are less adsorbed due to electrostatic repulsion forces. Whereas above pH 7 the adsorption of BTB neutral is due to weak van der Waals forces of attraction. This observation is in line with the earlier report [46].

3.7 Effect of UV lamp distance

The variation of UV light intensity on the rate constant of photo-catalytic degradation of BTB was studied by altering the distance of UV lamp from the reaction mixture as shown in Fig. 13. It is observed that the rate constant increased with increase in the light intensity. This can be attributed due to the fact that as the intensity of light

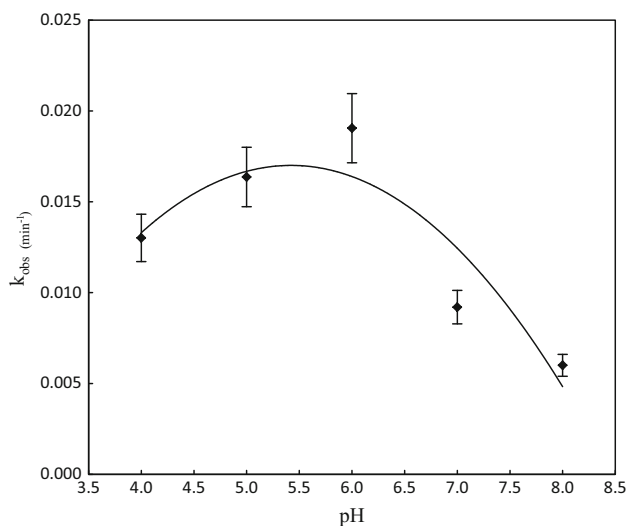


Fig. 11 Effect of pH on the rate constant of photo catalytic degradation of Bromothymol blue with Ru-TiO_2 at 25 °C, $[\text{Ru-TiO}_2] = 100 \text{ mg l}^{-1}$ $[\text{BTB}] = 5 \times 10^{-5} \text{ mol dm}^{-3}$

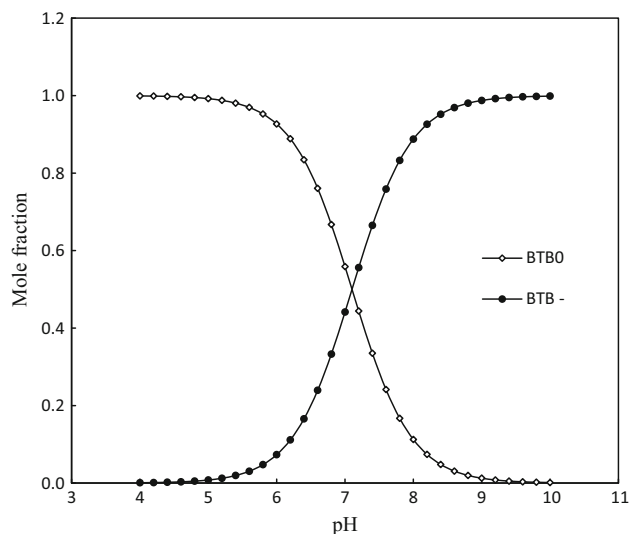


Fig. 12 Speciation of BTB at different pH

increases, the number of photons reaching the surface of photo-catalyst (Ru-TiO_2) also increases, consequently, increasing the number of electron-hole pairs. The holes decompose the BTB molecules adsorbed on the surface of Ru-TiO_2 particles and oxidize it to water resulting in their efficient degradation [10].

3.8 The mechanism of photo-catalytic degradation of BTB with Ru-TiO_2

When UV light was allowed fall on the photo-catalyst, electrons in the valence band were to the conduction band. Consequently, an electron-hole-pair is generated [47].

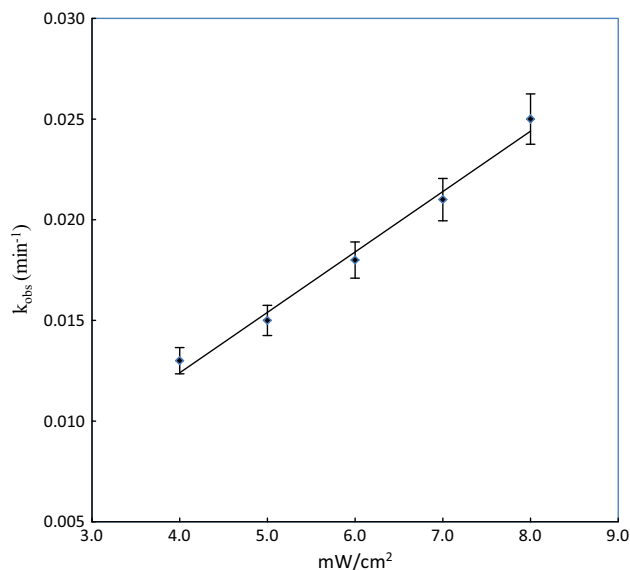


Fig. 13 BTB degradation under different UV intensities Bromothymol blue with Ru-TiO_2 at 25 °C, $[\text{Ru-TiO}_2] = 100 \text{ mg l}^{-1}$ $[\text{BTB}] = 5 \times 10^{-5} \text{ mol dm}^{-3}$

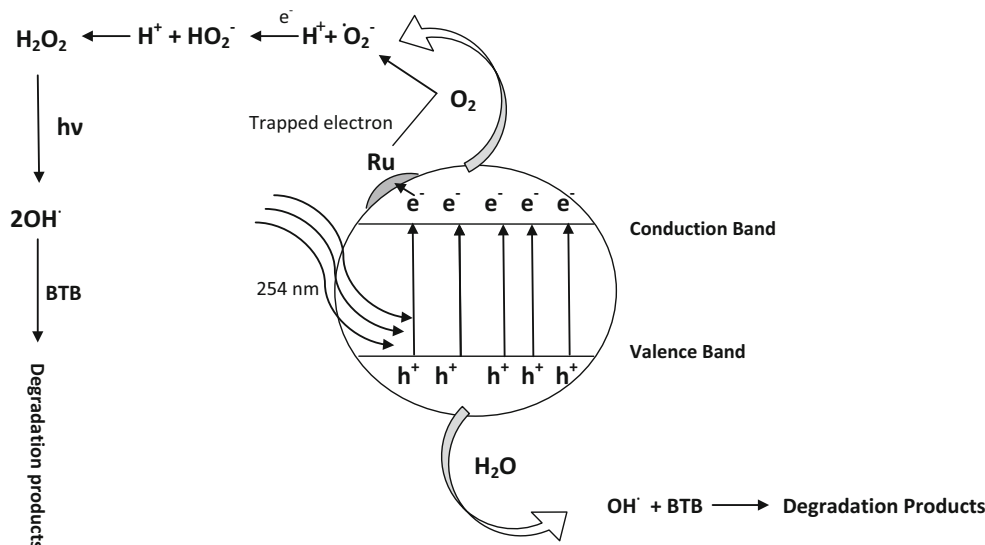
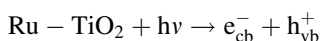
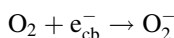
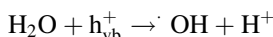


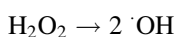
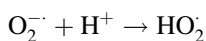
Fig. 14 Mechanism of photo catalytic degradation of BTB with Ru-TiO₂



Here e_{cb}^- represents electrons in the conduction band and h_{vb}^+ represents the holes in the valence band. The positive hole of the valence band reacts with a water molecule to produce hydroxide free radicals, where the superoxide anion radical is formed as a result of oxygen reduction by transfer of trapped electrons from Ru metal to oxygen as shown in Fig. 14 [48].



The above reaction eliminates the possibility of electron-hole recombination. The $\cdot\text{OH}$ and O_2^- produced in the above manner can then react with the BTB to yield degradation products.



It may be noted that all these reactions in photo-catalysis are possible due to the presence of both dissolved oxygen and water molecules. Without the presence of water molecules, the high hydroxyl radicals ($\cdot\text{OH}$) could not be formed and inhibit the photo-catalytic degradation of liquid phase organic molecules.

4 Conclusions

The experimental results lead to following conclusions:

- Liquid impregnation method was used to synthesize Ru-TiO₂ nanoparticles.
- The particle size of TiO₂ decreases with increasing percentage of ruthenium doping.
- 0.8 % Ru-TiO₂ nanoparticles exhibited a better potential compared to UV and UV/TiO₂ techniques for the effective photo-catalytic degradation of bromothymol blue in acidic medium (pH 4–6).
- Photo-catalytic degradation of Bromothymol blue could be achieved in 100 min with 100 mg l⁻¹ dosage of 0.8 % Ru-TiO₂.

References

1. S.A. Hosseini, P. Moalemzade, *J. Mater. Sci. Mater. Electron.* **27**, 8802–8806 (2016)
2. O.E. Ligrini, A. Oliveros, A.M. Braun, *Chem. Rev.* **93**, 671–698 (1993)
3. N.S. Arul, D. Mangalaraj, P.C. Chen, N. Ponpandian, P. Meena, Y. Masuda, *J. Sol-Gel Sci. Technol.* **64**, 515 (2012)
4. S.K. Kansal, P. Kundu, S. Sood, R. Lamba, A. Umar, S.K. Mehta, *New J. Chem.* **38**, 3220 (2014)
5. D. Chen, Z. Jiang, J. Geng, Q. Wang, D. Yang, *Ind. Eng. Chem. Res.* **46**, 2741 (2007)
6. Q. Sun, Y. Xu, *J. Phys. Chem. C* **114**, 18911 (2010)
7. M.M. Momeni, M. Mirhosseini, Z. Nazari, A. Kazempour, M. Hakimiyan, *J. Mater. Sci. Mater. Electron.* **27**, 8131–8137 (2016)
8. T. Kudo, Y. Kudo, A. Riuke, *Catal. Today* **122**, 14–19 (2007)
9. G. Zayani, L. Bousselmi, F. Mhenni, A. Ghrabi, *Desalination* **248**, 23–31 (2009)
10. U.I. Gaya, A.H. Abdullah, *J. Photochem. Photobiol. C* **9**, 1–12 (2008)
11. M. Mousavi-Kamazani, M. Salavati-Niasari, M. Sadeghinia, *Mater. Lett.* **142**, 145–149 (2015)
12. M. Panahi-Kalamuei, M. Mousavi-Kamazani, M. Salavati-Niasari, S.M. Hosseinpour-Mashkani, *Ultrason. Sonochem.* **23**, 246–256 (2015)

13. J. Li, L. Yan, Y. Wang, Y. Kang, C. Wang, S. Yang, *J. Mater. Sci. Mater. Electron.* **27**, 7834–7838 (2016)
14. A. Taicheng, H. Yang, W. Song, G. Li, H. Luo, J.C. William, *J. Phys. Chem. A* **114**, 2569–2575 (2010)
15. Z. Zarghami, M. Maddahfar, M. Ramezani, *J. Mater. Sci. Mater. Electron.* **26**, 6339–6343 (2015)
16. X. Jiang, Z. Li, Q. Lin, K. Dong, Y. Zhang, Z. Sun, *J. Mater. Sci. Mater. Electron.* **27**, 8856–8861 (2016)
17. L. Man, S.H. Seong, M. Mohseni, *J. Mol. Catal. A* **242**, 135–140 (2005)
18. X. Shu, J. He, D. Chen, *Ind. Eng. Chem. Res.* **47**, 4750–4753 (2005)
19. P. Govindhan, C. Pragathiswaran, *J. Mater. Sci. Mater. Electron.* **27**, 8778–8785 (2016)
20. L. Kumaresan, M. Mahalakshmi, M. Palanichamy, V. Murugesan, *Ind. Eng. Chem. Res.* **49**, 1480–1485 (2010)
21. N. Sasirekha, S.J.S. Basha, K. Shanti, *Appl. Catal. B Environ.* **62**, 169–180 (2006)
22. S.G. Ansari, F. Tuz-Zehra, H. Fouad, A.S. Hassenein, Z.A. Ansari, *J. Mater. Sci. Mater. Electron.* **26**, 5170–5174 (2015)
23. S.I. Shah, W. Li, C.P. Huang, O. Jung, C. Ni, *Proc. Natl. Acad. Sci. USA PNAS* **99**, 6482–6486 (2002)
24. M.M. Haque, M. Muneer, *Dyes Pigments* **75**, 443–448 (2007)
25. J. Choi, H. Park, M.R. Hoffmann, *J. Phys. Chem. C* **114**(2), 783–792 (2009)
26. K. Wetchakun, N. Wetchakun, S. Phanichphant, *Adv. Mater. Res.* **55–57**, 853–856 (2008)
27. V. Marinova, S.H. Lin, K.Y. Hsu, M.L. Hsieh, M.M. Gospodinov, V. Sainov, *J. Mater. Sci. Mater. Electron.* **14**, 857–858 (2003)
28. S. Ozkan, M.W. Kumthekar, G. Karakas, *Catal. Today* **40**, 3–14 (1998)
29. T. An, H. Yang, W. Song, G. Li, H. Luo, W.J. Cooper, *J. Phys. Chem. A* **114**(7), 2569–2575 (2010)
30. M.S. Lee, S.S. Hong, M. Mohseni, *J. Mol. Catal. A* **242**(1–2), 135–140 (2005)
31. A.N. Kadam, R.S. Dhabbe, M.R. Kokate, Y.B. Gaikwad, K.M. Garadkar, *Spectrochim. Acta A Mol. Biomol. Spectrosc.* **133**, 669–676 (2014)
32. S. Ullah, E.P. Ferreira-Neto, A.A. Pasa, C.C.J. Alcantara, J.J.S. Acuna, S.A. Bilmes, M.L.M. Ricci, R. Landers, T.Z. Fermino, U.P. Rodrigues-Filho, *Appl. Catal. B Environ.* **179**, 333–343 (2015)
33. D. Williams, C. Carter, *Transmission electron microscopy: a textbook for material science* (Springer, New York, 2009), p. 35
34. M.M. Ba-Abbad, A.H. Kadhun, A.B. Mohamad, M.S. Takriff, K. Sopian, *Int. J. Electrochem. Sci.* **7**, 4871–4888 (2012)
35. M. Hema, A. Yelil Arasi, P. Tamilselvi, R. Anbarasan, *Chem. Sci. Trans.* **2**(1), 239–245 (2013)
36. L. Liu, S. Chen, W. Sun, J. Xin, *J. Mol. Struct.* **1001**, 23–28 (2011)
37. C.N. Xu, J. Tamaki, N. Miura, N. Yamazoe, *Sens. Actuators B Chem.* **3**, 147–155 (1991)
38. B.K. Min, S.D. Choi, *Sens. Actuators B Chem.* **108**, 119–124 (2005)
39. G. Neri, A. Bonavita, G. Micali, N. Donato, F.A. Deorsola, P. Mossino, I. Amato, B. de Benedetti, *Sens. Actuators B Chem.* **117**, 196–204 (2006)
40. N.L. Wu, S.Y. Wang, I.A. Rusakova, *Science* **285**, 1375–1377 (1999)
41. M.M. Haque, M. Muneer, *J. Environ. Manag.* **69**, 169–176 (2003)
42. M. Qamar, M. Saquib, *Desalination* **171**, 185–193 (2004)
43. H. Chun, W. Yizhong, T. Hongxiao, *Chemosphere* **41**, 1205–1209 (2000)
44. C. Hu, Y. Tang, J.C. Yu, P.K. Wong, *Appl. Catal. B Environ.* **40**, 131–140 (2003)
45. E. Klotz, R. Doyle, E. Gross, B.J. Mattson, *J. Chem. Educ.* **88**, 637–639 (2011)
46. A. Verma, M. Sheoran, A.P. Toor, *Indian J. Chem. Technol.* **20**, 46–51 (2013)
47. I.K. Konstantinou, T.A. Albanis, *Appl. Catal. B Environ.* **49**, 1–14 (2004)
48. N.M. Mahmoodi, M. Arami, N.Y. Limaee, N.S. Tabrizi, *J. Colloid, Interface Sci.* **295**, 159–164 (2006)